

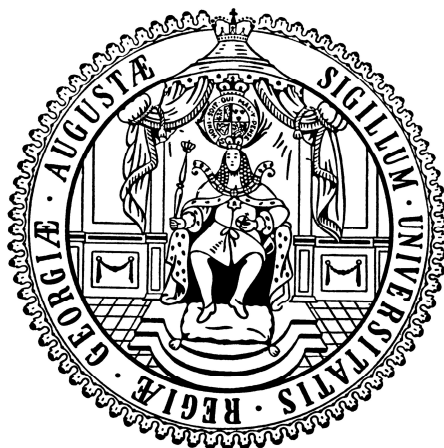
Ammonia stabilized Carbanions

Dissertation

zur Erlangung des mathematisch-naturwissenschaftlichen Doktorgrades

„Doctor rerum naturalium“

der Georg-August-Universität Göttingen



Im Promotionsprogramm Chemie
der Georg August University School of Science (GAUSS)

Vorgelegt von
Reent Michel
aus Wilhelmshaven.

Göttingen, 2016

Betreuungsausschuss

Professor Dr. Dietmar Stalke, Institut für Anorganische Chemie der Georg-August-Universität Göttingen

Professor Dr. Oliver Wenger, Institut für Anorganische Chemie der Georg-August-Universität Göttingen

Mitglieder der Prüfungskommission

Referent: Professor Dr. Dietmar Stalke, Institut für Anorganische Chemie der Georg-August-Universität Göttingen

Korreferent: Professor Dr. Franc Meyer, Institut für Anorganische Chemie der Georg-August-Universität Göttingen

Dr. Heidrun Sowa, Fakultät für Geowissenschaften und Geographie der Georg-August-Universität Göttingen

Professor Dr. Thomas Waitz, Institut für Anorganische Chemie der Georg-August-Universität Göttingen

Professor Dr. Konrad Koszinowski, Institut für Organische und Biomolekulare Chemie der Georg-August-Universität Göttingen

Professor Dr. Manuel Alcarazo, Institut für Organische und Biomolekulare Chemie der Georg-August-Universität Göttingen

Tag der mündlichen Prüfung: **18. Januar 2017**

This work is dedicated to Fei Luo

Table of Content

| | |
|---|-----|
| Abbreviations | i |
| 1. Introduction | 1 |
| 1.1. Cyclopentadiene and its Derivatives | 1 |
| 1.2. Solvent free Alkali metal Compounds of Cp and its Derivatives | 6 |
| 1.3. Solvated Alkali Metal Cyclopentadienyl Compounds | 11 |
| 1.4. Hydrogen Bonding | 27 |
| 1.5. Ammonia as a Donor-Solvent | 31 |
| 2. Scope | 37 |
| 3. Results | 39 |
| 3.1. Lithium Derivatives | 39 |
| 3.2. Sodium Derivatives | 48 |
| 3.3. Potassium Derivatives | 64 |
| 3.4. Rubidium Derivatives | 73 |
| 3.5. Caesium Derivatives | 80 |
| 3.6. Compound Overview | 89 |
| 4. Discussion | 91 |
| 4.1. Lithium Ammoniacates | 91 |
| 4.2. Sodium Ammoniacates | 99 |
| 4.3. Cp- and Cp ⁺ -Ammoniacates of the Higher Alkali Metal Cations | 104 |
| 4.4. Indenyl and Fluorenyl Ammoniacates of Potassium, Rubidium and Caesium | 109 |
| 5. Summary | 117 |
| 6. Experimental Section | 119 |
| 6.1. General procedures | 119 |
| 6.2. Synthesis | 119 |
| 7. Crystal Structure Determination | 125 |
| 7.1. Crystal Selection | 125 |

| | |
|---|-----|
| 7.2. Data Acquisition and Processing..... | 129 |
| 7.3. General Remarks on Disorder Refinement | 129 |
| 7.4. Treatment of the Modulated Structures 9 and 11 | 135 |
| 7.5. Treatment of the Twinned Structure CpK(NH ₃) ₂ (12) | 138 |
| 7.6. Lithium Ammoniacates | 140 |
| 7.7. Sodium Ammoniacates..... | 144 |
| 7.8. Potassium Ammoniacates..... | 151 |
| 7.9. Rubidium Ammoniacates | 155 |
| 7.10. Caesium Ammoniacates | 159 |
| 7.11. Structures determined for Aurelia Falcichio (Prof. Dr. Vito Capriati) | 164 |
| 7.12. Structures determined for the work group of Prof. Dr. Guido Clever..... | 167 |
| 7.13. Structures determined for Shabana Khan (Prof. Dr. Herbert W. Roesky) | 170 |
| 7.14. Structures determined for Tamal K. Sen..... | 182 |
| 8. Bibliography | 185 |
| Danksagung | 195 |
| Curriculum vitae..... | 197 |

Abbreviations

| | |
|-------------------|---|
| BuLi | Butyllithium |
| Cp | Cyclopentadienyl |
| Cp' | Methylcyclopentadienyl |
| Cp* | Pentamethylcyclopentadienyl |
| CIP | Contact ion pair |
| CSD | Cambridge Crystallographic Database |
| DME | Dimethoxyethane |
| Diglyme | 1-Methoxy-2-(2-methoxyethoxy)ethane |
| Et ₂ O | Diethylether |
| Flu | Fluorenyl |
| GooF | Goodness of Fit |
| HSAB | Hard acid soft base |
| HMDS | Hexamethyldisilazane |
| Ind | Indenyl |
| LDA | Lithiumdiisopropylamine |
| MTBE | Methyl <i>tert</i> -butyl ether |
| PMDETA | <i>N,N,N',N'',N'''</i> -pentamethyldiethylenetriamine |
| Py | Pyridine |
| SSIP | Solvent separated ion pair |
| THF | Tetrahydrofuran |
| TMEDA | Tetramethylethylenediamine |
| TMPDA | <i>N,N,N',N'</i> -tetramethyl-1,3propanediamine |
| TMS | Tetramethylsilyl |
| Tol | Toluene |

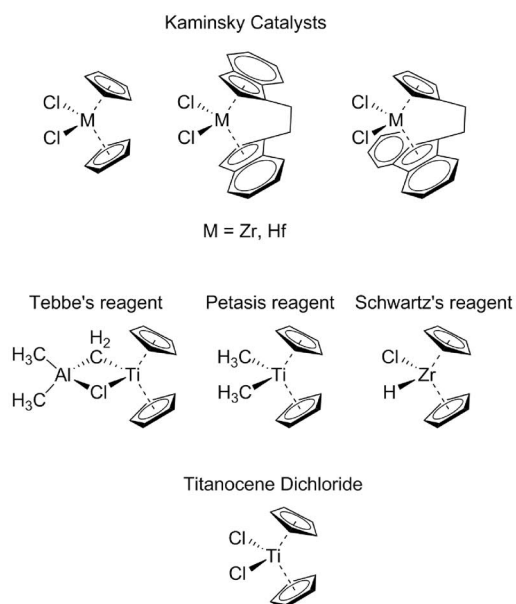
1. Introduction

1.1. Cyclopentadiene and its Derivatives

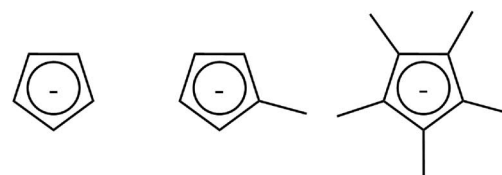
Cyclopentadiene (CpH) and its derivatives are very important ligands in organometallic chemistry. Their metallocene and ansa-type complexes play an important role in homogeneous Ziegler-Natta polymerization of α -olefins to produce isotactic and syndiotactic polymers (Scheme 1).^[1] Compounds like Tebbe's reagent^[2], Petasis reagent^[3], and Schwartz's reagent^[4] are useful in specific organic synthesis. Titanocene dichloride even shows anti-cancer potency.^[5] The main feature of cyclopentadiene and its derivatives is the anionic π -system obtained by deprotonation of the respective cyclopentadiene derivative.^[6] Due to the anionic charge of the aromatic system, the ligand is highly attracted to metal cations of all types. The prevalent type of interaction is η^5 -coordination with the cation placed on top of the ring center. This type of coordination effectively shields huge parts of the cation. More bulky derivatives of Cp, like pentamethylcyclopentyl, indenyl, and fluorenyl enhance this effect which is, for instance, crucial for the design of narrow paths for monomers in Ziegler-Natta polymerization to create the isotactic and syndiotactic polymers.

1.1.1. Cp, Cp', and Cp*

The cyclopentadienyl anion (Cp) is the most prominent ligand in the class of cyclopentadiene derivatives (Scheme 2). It is obtained by deprotonation of the relatively acidic cyclopentadiene ($pK_a = 16.0$ ^[7] in dmsO) by alkali-metal hydrides, organolithium- or Grignard reagents, or directly by alkali metals. The ligand has a high affinity to metal cations due to its various features in coordination, benefitting all types of metal ions. Three types of complexes are formed: π -



Scheme 1: Metallocene complexes used in olefin polymerization (upper row), used in organic synthesis (middle row), and as a potential anti-cancer drug (bottom).



Scheme 2: The Cyclopentadienyl anion (Cp) and the methylated derivatives Methylcyclopentadienyl (Cp') and Pentamethylcyclopentadienyl (Cp*).

Introduction

Cyclopentadiene and its Derivatives

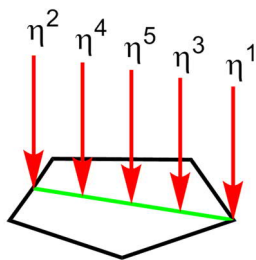
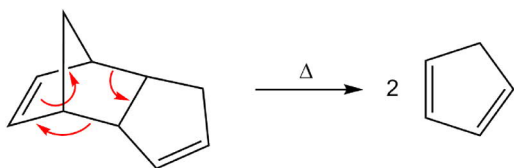


Figure 1: Modes of metal coordination to Cp.

complexes, σ -complexes and ionic complexes. The most prevalent is the π -complex formed with transition metals. The π -electrons act as a $6e^-$ -donor ligand with their molecule orbitals overlapping with d-orbitals of the transition metals. These complexes exhibit η^5 -coordination. Depending on the electron configuration of the metal ion, the Cp anion can also act as a $4e^-$ -allylic ligand with η^3 -coordination. σ -Complexes with a η^1 -coordination are rare in comparison to the dominant η^5 -coordination. Typically, σ -bonds are formed with main group metals as in $\text{Al}(\text{Cp})_3$ ^[8], $\text{Ga}(\text{Cp})_3$ ^[9], $\text{Sn}(\text{Cp})_4$ ^[10], $\text{Sb}(\text{Cp})_3$ ^[11], PbCp_2 ^[12], and $\text{Bi}(\text{Cp})_3$ ^[13]. But main group metals also form complexes with η^5 -coordination. Ionic complexes are formed with alkali metals and alkali earth metals. For these metals, η^5 -Coordination is prevalently found as well, but the solely ionic attraction gives rise to more flexibility in coordination. Depending on the cation and the environment in the crystal, all types of coordination from η^1 to η^5 (Figure 1) are possible. A prominent example is beryllocene with one Cp ligand coordinating η^5 , the other one η^1 .^[6] A detailed description of the alkali metal compound will be given in section 1.2 and 1.3. The anion is a soft Lewis-anion and its affinity towards cations increases with the ionic radius.



Scheme 3: Heat induced Retro-Diels-Alder reaction of dicyclopentadiene.

The precursor, cyclopentadiene, was first encountered in 1886 by *H. E. Roscoe* as a low temperature fraction in coal tar distillation.^[14] Today's main sources of cyclopentadiene are still coal tar and cracking of naphtha. *Kraemer* et al. discovered in 1896 the reversible dimerization of cyclopentadiene to dicyclopentadiene.^[15] Cyclopentadiene dimerizes in a Diels-Alder reaction to dicyclopentadiene. For lab use, cyclopentadiene is obtained by the retro-Diels-Alder reaction of dicyclopentadiene through heating and direct distillation (Scheme 3). When stored at low temperatures, monomeric cyclopentadiene can be used for a couple of days.

By direct metallation with sodium, the first metal-cyclopentadienyl compound was discovered by *Thiele et al.* in 1900.^[16] One year after the discovery of NaCp, the analogous synthetic route with potassium led to KCp.^[17] The major breakthrough in the study of cyclopentadienyl complexes was the discovery of ferrocene by *Pauson* and *Kealy* in 1951.^[18] The unexpected stability of the complex attracted the attention of other scientist. *Robert Burns Woodward* together with *Geoffrey Wilkinson* and independently *Ernst Otto Fischer* discovered the sandwich structure of the complex in 1952.^[19] Soon after the discovery, the number of Cp-complexes rose rapidly (Figure 2).

The vast majority of the complexes contain transition metal complexes. A search in the *Cambridge Structural Database*^[20] (CSD, 5.37 Nov. 2015, last update Feb. 2016) yields 24717 structures containing Cp and any metal atom. In 23816 structures, Cp is connected to a transition metal, in 743 structures to lanthanides/actinides, in 191 structures to alkali/alkaline earth metals, and in 63 structures to main group metals (some structures combine different metal ions).

The prevalence of η^5 -coordination can be rationalized by comparing the distance of the metal to the ring center and the distance to the plane (Figure 3). For this analysis, only aromatic Cp anions are involved (20418 structures including 34165 independent metal–Cp coordinations). If the metal is η^5 -coordinated, both distances match up. Therefore, the bulk of the anions lie on a line. If the cation shifts from the center, the distance from the ring center increases compared with the distance to the ring plane. Only a minor fraction of the 34165 data points deviate from the linear correlation. These points correspond to different coordination motifs.

The Cp-derivative methylcyclopentadiene (Cp'H) is very similar to CpH. Just like CpH, it is obtained by cracking of naphtha. It also forms methylcyclopentadiene dimers and it coordinates metal ions in the same way as Cp. The methyl group enhances the solubility of formed complexes in organic solvents. However, known complexes containing Cp' are far less numerous than those containing Cp. A CSD search gives only 1250 hits, 19 times less than for Cp.

Cp* is in many ways different to Cp and Cp'. Cp* is not available from coal tar or naphtha cracking, but has to be synthesized. There-

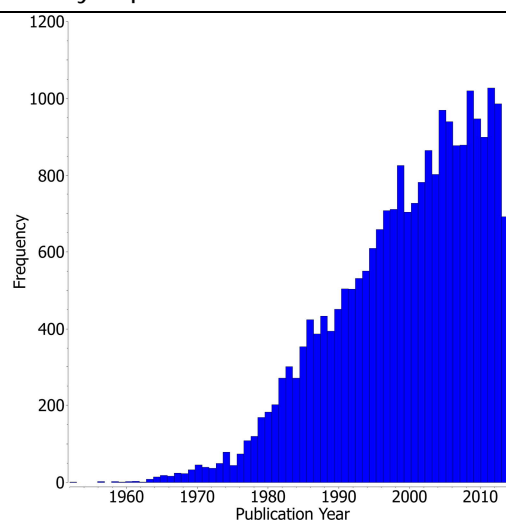


Figure 2: Published crystal structures of Cp-metal compounds per year according to deposited structures in the *Cambridge Crystallographic Database* (v. 5.37, Nov.2015). Total number: 24717.

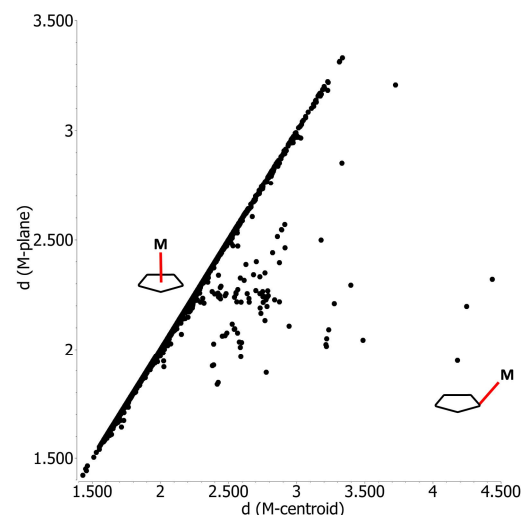


Figure 3: Distance of the metal ion from the Cp-ring centre vs. distance from the Cp-ring plane (in Å) for 20418 crystal structures (CSD v. 5.37, Nov.2015) with 34165 data points. Linear relation indicates η^5 -coordination.

Introduction

Cyclopentadiene and its Derivatives

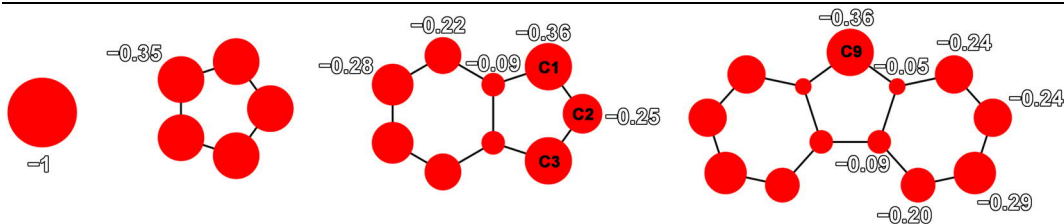
fore, Cp*H is much more expensive than CpH and Cp'H. It also does not undergo Diels–Alder dimerization. The five methyl groups exert two main effects: they have a very high steric demand and increase the electron density in the π -system. As a stronger electron donor and by shielding a huge part of the sphere around the cation, Cp* forms more stable complexes, reduces intermolecular interactions, and prevents the formation of polymeric structures. Also the solubility of the complexes in unpolar solvents is increased. These beneficial properties are reflected in the presence of the comparably high number of 14419 structures listed in the CSD.

1.1.2. *Indenyl and Fluorenyl*



Scheme 4: The indenyl (left) and fluorenyl anion (right).

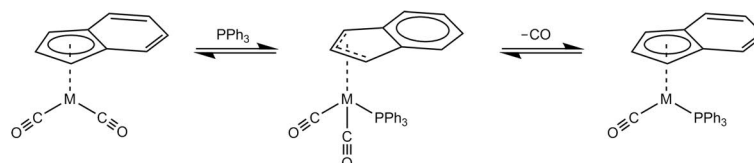
Indene and fluorene are cyclopentadiene derivatives with annellated aromatic six-membered rings (Scheme 4). They serve as ligands in organometallic chemistry and their ansa-derivatives serve as ligands in homogenous Ziegler-Natta polymerization (Scheme 1). The annellated phenyl rings narrow the reaction path for the monomer and therefore enhance regular tacticity. Both compounds are mainly obtained from coal tar. The expansion of the anionic π -system leads to a dilution of the negative charge compared to Cp, lowering the attraction of the anions indenyl and fluorenyl to cations. On the other hand, the expanded π -system gives much more possibilities for coordination. Not only η^5 - and η^6 -coordination positions at the corresponding rings are available, but also flexible coordination at the ring peripheries. The asymmetric shape of the anions also leads to an uneven distribution of the negative charge. Scheme 5 presents the calculated atomic charges of Cp, indenyl, and fluorenyl.^[21] While the carbon atoms in Cp all bear the same negative charge due to the five-fold symmetry of the anion, the indenyl anion experiences a charge accumulation at the carbon atoms C1 and C3 (numbering according to IUPAC). Fluorenyl has a distinct charge accumulation at C9 (the top of the five membered ring). These charge accumulations are consistent with the chemistry of these two anions. The positions of the charge accumulation are also the positions of protonation in indene and fluorene. The protonation of indenyl at C1 and C3 is favored due to the formation of a double bond within the five-membered ring. Protonation at C2 leads to the unstable *2H*-indene, which polymerizes under normal conditions when exposed to air or radiation.^[22] In fluorene, protonation at C9 is directed by the annellated phenyl-rings. A 1,5-sigmatropic shift of the protons, as in cyclopentadiene, is therefore not observed in the cases of indene and fluorene. The carbon atoms C1 and C3 of indenyl and C9 of fluorenyl are also main targets for substitution reactions.



Scheme 5: Charge density for the Cp, indenyl, and fluorenyl anions, as calculated from NBO (B3LYP/6-311G**). The area of the spheres represents the negative charge, relative to the sphere on the left.

The indenyl anion, just as Cp and fluorenyl, serves as a ligand in organometallic chemistry. It coordinates metal ions mostly with the five-membered ring. Of 665 structures listed in the CSD, only 24 structures are coordinated at the six-membered ring. In 23 of these 24 structures, both η^5 - and η^6 -coordination is present at the same time. Just in [Ru(ind)(Cp*)], only the six-membered ring is coordinated.^[23] Also some examples of σ -coordination of transition metals to indenyl have been reported, especially for Pd, Zn, Ti and with at least one example for Mn, W, Rh, Ir. Only three structures of indenyl and main group metals like Ge and Sn are known. In all three structures, the metal is σ -bonded to the ligand. An interesting feature found for the indenyl anion is the allylic η^3 -coordination where a cation coordinates the carbon atoms C1, C2, and C3. This type of coordination is formed with transition-metal complexes if the valence shell of the cation does not require six electrons which would be obtained from η^5 -coordination. η^3 -Coordination to the allylic part of the anion provides four electrons. This type of coordination is stabilized by the remaining phenyl ring – an effect which is commonly referred to as ‘indenyl-effect’.^[24] In solution, an 18- e^- indenyl–transition metal complex can undergo a much faster associative substitution than the corresponding Cp-complex (Scheme 6). The arene stabilizes a shift of the cation to η^3 -coordination after addition of a ligand. From this intermediate state, a ligand dissociates and the metal shifts back to η^5 -coordination. The exchange rate can be up to 10^8 times faster compared with the corresponding Cp complex.

The effect of a higher ligand substitution rate can be even more pronounced for the fluorenyl ligand. The haptotropic shift in the fluorenyl compound $\text{Mn}(\eta^5\text{-flu})(\text{CO})_3$ is about 60 times faster than in the respective indenyl compound $\text{Mn}(\eta^5\text{-ind})(\text{CO})_3$.^[24f]



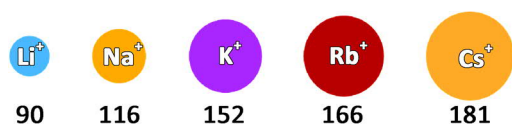
Scheme 6: Proposed mechanism of the indenyl effect by Hart-Davis and Murdy.

Introduction

Solvent free Alkali metal Compounds of Cp and its Derivatives

The fluorenyl anion as a ligand is with only 126 structures much less prominent in the CSD. With a number of 37, all main group metal complexes (Al, Ga, Ge, In, Sn) are σ -bonded to the top of the five membered ring. The coordination of transition metals is much more variable compared to indenyl and Cp, although 33 structures hardly give the whole picture. With only 13 out of 33 structures, η^5 -coordination is not overwhelmingly favored as was the case for indenyl and Cp, but only four structures are η^6 -coordinated. 13 structures contain σ -bonding and some structures also combine these two types of coordination like $[\text{Ti}(\eta^5\text{-flu})(9\text{-flu})(i\text{-PrO})_2]$ and $[\text{Zr}(\eta^5\text{-flu})(9\text{-flu})(\text{Cl})(\text{Cp})]$.^[25] The η^5 -coordination can easily shift to σ -coordination by addition of ligands to the cation as in $[\text{Mn}(\eta^5\text{-flu})(\text{CO})_3]$ and $[\text{Mn}(9\text{-flu})(\text{CO})_5]$ or $[\text{Re}(\eta^5\text{-flu})(\text{CO})_3]$ and $[\text{Re}(9\text{-flu})(\text{CO})_5]$.^[26]

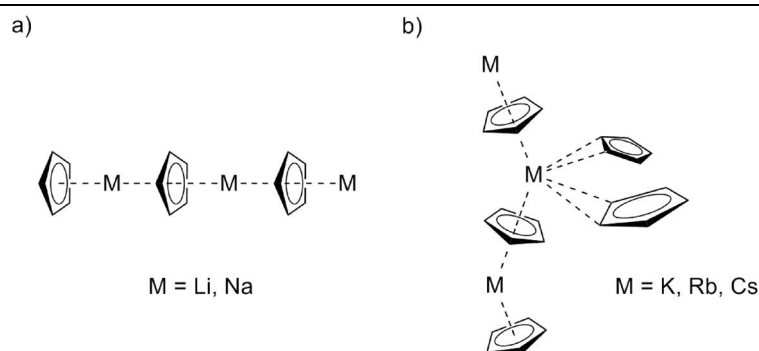
1.2. Solvent free Alkali metal Compounds of Cp and its Derivatives



Scheme 7: Crystal ionic radii of the alkali metals in pm.^[35] The ratio of the spheres represents their size difference. The presented colours are used throughout the work.

Alkali metal compounds of cyclopentadienyl derivatives play an important role as precursors in organometallic chemistry. Via transmetalation and salt elimination, a huge variety of sandwich and half-sandwich compounds can be created. Salt-elimination reactions are widely used to introduce functional groups and side-arms to the respective cyclopentadienyl derivative.^[27]

Alkali-metal–cyclopentadienyl compounds have a salt-like character.^[28] They are soluble only in aprotic, polar and donating solvents like THF and DME. The nature of the Cp–alkali-metal bond is almost entirely ionic.^[29] Before crystallographic data became available, IR^[30], NMR^[31], and theoretical calculations^[28, 32] had already clearly indicated a η^5 -coordination, which was supported by the first crystal structures of solvated Cp-compounds (section 0). Due to the powder nature of the compounds, the crystal structures from solvent-free CpLi up to CpCs had been unknown until 1997. *Dinnebier et al.* revealed the respective crystal structures using powder diffraction.^[33] They found 1-dimensional coordination polymers for all alkali-metal–cyclopentadienyl compounds with the anions being η^5 -coordinated from both sides by cations. Two different motifs are present (Scheme 8). LiCp and NaCp are isostructural and form linear chains with coplanar anion rings (Figure 4). The anions are syn-arranged in relation to each other. KCp, RbCp, and CsCp, on the other hand, exhibit a zig-zag arrangement with significant inter-chain attractions.^[34] Li⁺ and Na⁺ have ionic radii of 90 pm and 116 pm (Scheme 7), compared to 152 pm, 166 pm, and 181 pm for K⁺, Rb⁺, and Cs⁺.^[35] Therefore, the attraction to the ring is stronger with cation–anion plane distances of 1.97 Å for LiCp and 2.36 Å for



Scheme 8: a) Structural motif of CpLi and CpNa. b) Structural motif of CpK, CpRb, and CpCs. Side-on interactions with adjacent chains are present.

CpNa. The distances for the higher alkali-metal ions are 2.81 Å (KCp), 2.96 Å (RbCp), and 3.12 Å (CsCp). The strong attraction leads to LiCp and NaCp featuring a straight linear arrangement. The different strands are shifted towards each other by the M–anionic plane distance. The dense tongue-and-groove type arrangement also forces the anions into a syn-staggered arrangement in contrast to the anti-staggered arrangement in lithocene, sodocene, and other metallocenes. The larger size and polarizability of the higher alkali metal ions allow them to interact with adjacent anions. The larger distances now facilitate bending of the anions and additional interaction of the cation with anions of adjacent CpM strands. With that side-on attraction taking place, the coordinated anions incline in the opposing direction of the side-on interactions.

The types of side-on attraction diverge for the three higher alkali-metal cations. The distance of the cations to the closest carbon atom of a neighbored strand shall be used as a measure. Although KCp, RbCp, and CsCp look very similar, their ionic radii have an impact on the crystal packing. The strands in KCp are ordered in a distorted square grid (Figure 5). RbCp can assume two polymorphs (Figure 6, Figure 7). Polymorph 1 is built up by monolayers of parallel strands. These layers alternate in their orientation by 90°. The strands in polymorph 2 are ordered

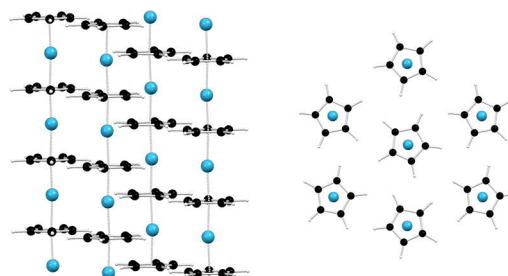


Figure 4: Crystal structure of LiCp viewed perpendicular from the strands and along the strands. The structure of NaCp is isostructural.

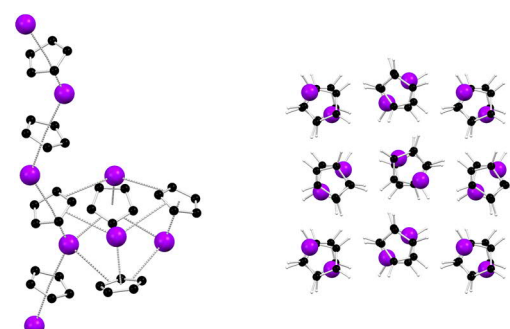


Figure 5: Left: Section of the KCp crystal structure depicting the mutual attractions between four KCp-strands. Right: Arrangement of the stands in the crystal packing.

Introduction

Solvent free Alkali metal Compounds of Cp and its Derivatives

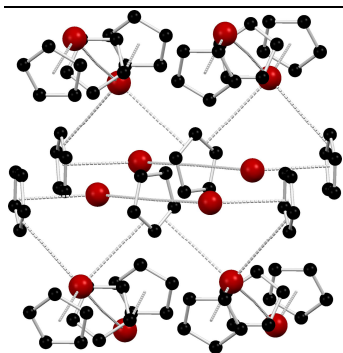


Figure 6: Polymorph 1 of RbCp in which the polymeric strands of each layer are oriented perpendicular to the strands of the next layer. Significant interaction only takes place between perpendicular oriented strands.

in a distorted hexagonal grid, isostructural to CsCp (Figure 7).

The KCp strands form the distorted square grid due to stronger side-on attractions compared with CsCp and the isostructural polymorph of RbCp. The K–C distance to a neighboring strand is 3.33 Å short. These distances increase to 3.73 Å in polymorph 2 of RbCp and to 3.77 Å in CsCp. The stronger attraction in KCp leads to a clustering of four adjacent KCp units to a substructure of two intertwined distorted tetrahedra of potassium and Cp. The clear leap in M–C side-on distances from potassium and the two isostructural Cs and Rb structures is undercut by the other polymorph of RbCp with the shortest Rb–C side-on distance being 3.48 Å. Placed between potassium and caesium in the alkali metal group, rubidium has an ambivalent nature in the way the side-on attractions can form the general structural pattern.

Substituents to the Cp-ring have naturally a disrupting effect on the arrangement by steric repulsion and by shielding parts of the anion from coordination or side-on attractions. Larger substituents are supposedly having a bigger effect on the crystal packing. The methylcyclopentadienyl compounds of lithium and sodium are unknown to date, but the impact of non-donating substituents on Li^+ can be observed in $\text{LiCp}(\text{TMS})^{[36]}$ and $\text{LiCp}(\text{Bz})^{[37]}$ (Figure 8). The motif of a linear coordination polymer remains, but the angles between the anionic planes incline from coplanarity by 5.14° to 8.28° in $\text{LiCp}(\text{TMS})$ and by 10.80° in $\text{LiCp}(\text{Bz})$. The same bending occurs with substituents like menthyl, $\text{Si}(\text{Me})_2(\text{Flu})$, and ethylene-1-dimethylamine.^[38] The only sodium derivative reported yet is

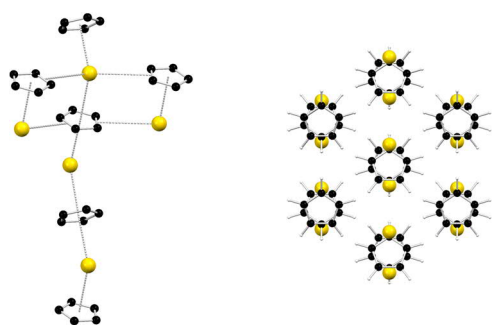


Figure 7: Crystal structure of CsCp (isostructural with polymorph 2 of RbCp). Left: Section of the crystal packing depicting mutual side-on attractions. Right: View along the direction of the strands.

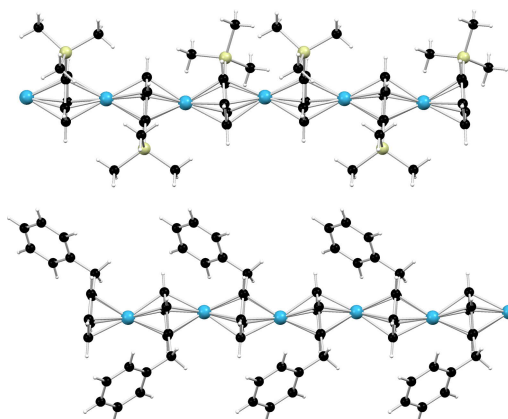


Figure 8: Sections of the crystal structures of $\text{LiCp}(\text{TMS})$ (above) and $\text{LiCp}(\text{Bz})$ (below).

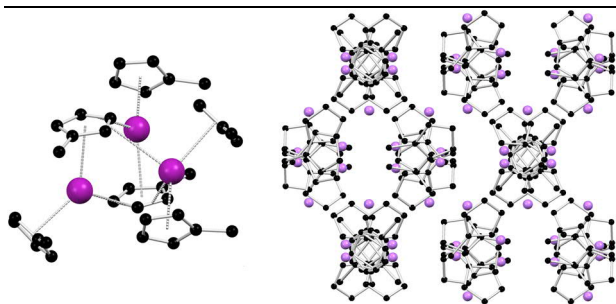


Figure 9: Left: segment of KCp' resembling the interactions between three KCp' -strands. Right: View along the helical strands of KCp' . Coordination bonds have been removed for clarity.

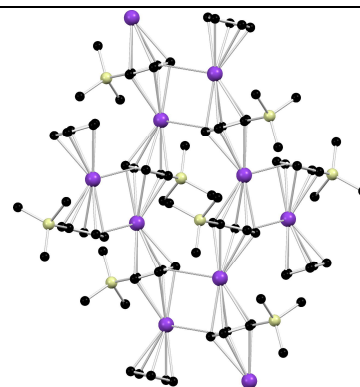


Figure 10: Section on the crystal structure of $\text{KCp}(\text{TMS})$.

(menthyl) CpNa with analogous bending.^[38a]

Substituents on KCp have a large impact on crystal packing due to the preference of potassium for strong side-on coordination. The methyl group in KCp' (Figure 10) shields part of the anion from side-on interaction.^[39] While in KCp , segments of four adjacent strands exhibit mutual attraction, this number is reduced to three strands for KCp' . As a result, the crystal packing is far more complicated as in KCp . The impact of the TMS-group in $\text{KCp}(\text{TMS})$ reduces the interaction even further (Figure 9).^[40] Only segments of two adjacent strands can interact with each other. Due to the increasing steric demand of the two TMS-substituents in $(\text{TMS})_2\text{CpK}$, no side-on interaction occurs anymore and the anions are less inclined. In $(\text{TMS})_3\text{CpK}$ and with very bulky substituents as in $((4\text{-Bu})\text{Ph})_5\text{CpK}$, the anions become almost coplanar.^[41] Analogous structures of RbCp have not been reported to date.

The crystal structure of CsCp' (Figure 11) is much less complex compared to KCp' .^[42] The strands are linear with the methyl groups pointing in various directions. The caesium cation is less attracted to side-on coordination than potassium and forms attractive interaction locally only between two strands. This allows CsCp' to form a crystal packing very similar to CsCp . Derivatives with different substituents have not been reported yet.

Solvent-free structures of Cp^* include LiCp^* , NaCp^* , RbCp^* , and CsCp^* (Figure 12).^[43] The structures look similar to those of the analogous Cp compounds. The lithium and sodium compounds form linear coordination polymers with parallel arranged ani-

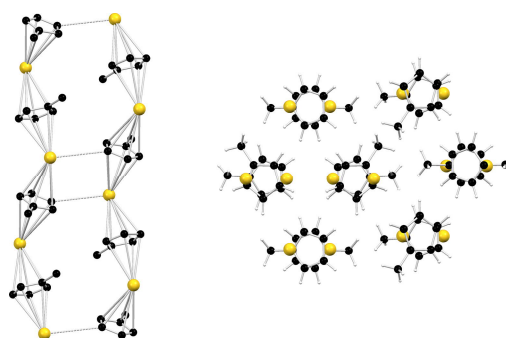


Figure 11: Left: section of the crystal structure of CsCp' resembling interstrand attractions. Right: View along the strands of CsCp' .

Introduction

Solvent free Alkali metal Compounds of Cp and its Derivatives

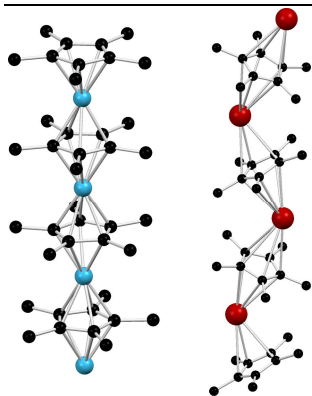


Figure 12: Crystal structures of LiCp^* (left), isostructural to NaCp^* , and RbCp^* (right), isostructural to CsCp^* .

ons. Also RbCp^* and CsCp^* form zig-zag structures just as their Cp-counterparts. The major difference is clearly the absence of metal–Cp* side-on interactions, which are blocked by the methyl groups.

Only a few crystal structures of unsolvated indenyl and fluorenyl alkali metal compounds are known: indenyllithium, fluorenyllithium, and fluorenylsodium.^[44] Indenyllithium forms 1-dimensional coordination polymers like for example LiCp (Figure 13). The anions are coplanar and the six-membered rings are packed one above the other. Substituents like $-\text{N}(\text{Et})(2\text{-propylene})$ at the five membered ring result in a rippled coordination polymer as observed in the substituted

LiCp -compounds.^[45] Fluorenyllithium looks very different. It is not a coordination polymer but rather a double metallocene. Two lithium cations coordinate the six-membered rings of two fluorenyl-anions. Fluorenylsodium looks entirely different from fluorenyllithium (Figure 13). The structure is a 2-dimensional coordination polymer with two different coordination motifs. In one motif, a single sodium cation coordinates three anions at the top of the five-membered ring. The second motif has some similarity to fluorenyllithium and consists of two sodium cations coordinating three anions at the region of the top of the six-membered rings. Both motifs are present on the two sides of the anion.

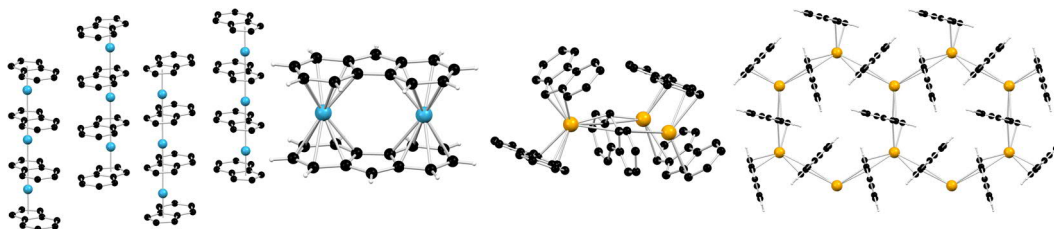
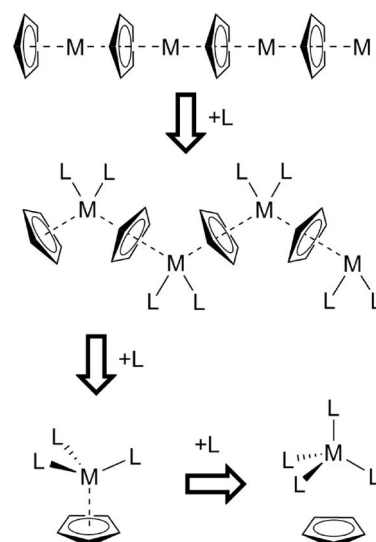


Figure 13: On the left: Crystal structures of indenyllithium and fluorenyllithium. On the right: Sections of the formed 2-dimensional coordination polymer formed by fluorenylsodium.

1.3. Solvated Alkali Metal Cyclopentadienyl Compounds

Alkali metal cyclopentadienyl compounds can be solvated by aprotic donating solvents to enable them to undergo transmetalation or salt-elimination reactions. The disaggregation by solvent molecules in the solid phase can go through several modes (Scheme 9): Solvation of the metal ions under preservation of the polymeric nature and subsequent formation of CIPs and SSIPs. Depending on the used compounds, also 2- or 3-dimensional coordination polymers are possible as well as solvent-separated chain fragments.

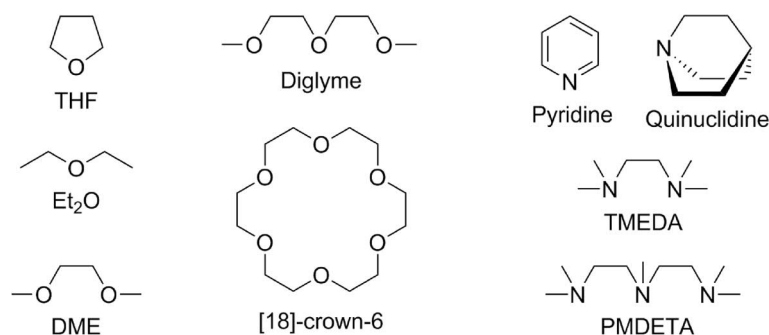


Scheme 9: Stepwise disaggregation by solvation of alkali metal cyclopentadienyl compounds in the solid phase.

Three factors determine the state of aggregation: the nature of the anion, the cation, and the donor solvent. Anions without annellated phenyl rings have a higher charge concentration and are more attractive to metal ions. Methyl groups increase that attraction, but possibly hinder certain types of aggregation due to their steric demand. Anions with annellated benzene rings have a lower attraction to the metal ion, but are far more flexible in coordination, ranging from η^1 to η^6 . The size of the cation dictates the affinity to the ring system. With a growing cationic radius, the coordination of the alkali metal ion to the anions grows more and more stable according to the Pearson–HSAB concept.

The size of the cation also determines the attraction to donor solvents and adjacent anions. Hard cations like Li^+ and Na^+ tend to interact more strongly to O- and N-based donor ligands due to their similar size. Side-on coordination is more important for the higher alkali metal cations K^+ , Rb^+ , and Cs^+ .

The donor solvent (Scheme 10) can influence the aggregation in multiple ways. Generally,



Scheme 10: Selection of O- and N-based aprotic donor solvents.

Introduction

Solvated Alkali Metal Cyclopentadienyl Compounds

the ability for disaggregation increases from monodentate ligands to cryptands. Steric demand of the donor solvent can have different effects depending on the denticity of the ligand. In monodentate solvents, the ability to disaggregate decreases with growing steric demand. THF for example is able to dissolve LiCp, but not Et₂O. The multidentate donor solvents show a more complex picture. Due to the chelate effect, multidentate solvents have a higher affinity to metal cations as monodentate solvents. The steric demand of the solvent can have the opposite effect. DME and diglyme have one methyl group attached to the donor atoms in the side-arms, whereas the nitrogen counterparts TMEDA and PMDETA have two attached methyl groups, as well as an additional methyl group at the central nitrogen atom for PMDETA. This added steric demand has two effects: the cation gets effectively shielded from further interaction and the solvent molecule itself has a reduced tendency to coordinate two or more cations at the same time. The closed ring systems of crown ethers maximize this effect and therefore lead to systems with the highest tendency to disaggregate.

In the following, the crystal structures of solvated alkali-metal-cyclopentadienyl compounds and their derivatives will be discussed to elucidate the influence of the donor ligand.

1.3.1. Solvated Lithium Cyclopentadienyl Compounds

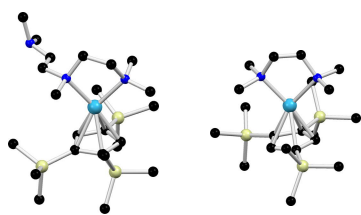


Figure 14: The first solvated CpLi-derivatives (TMS)₃CpLi·PMDETA and (TMS)₃CpLi·TMEDA by *Jutzi et al.*^[46]

No solvated polymeric strands of LiCp or with other Cp-derivatives have been reported to date. The strong attraction of Li⁺ to the ring system (Li⁺–Cp_{plane} distance: 1.97 Å) does not allow for a coordination to the lithium cations in the coordination polymer strands. The coordination polymers break up directly into solvated contact-ion pairs. The first structures to demonstrate this effect, which also were the first proofs of a η⁵-coordination, were the adducts Cp(TMS)₃Li·PMDETA and Cp(TMS)₃Li·TMEDA by *Jutzi et al.* (Figure 14).^[46] While the high steric demand of the three TMS-groups in *Jutzi's* compounds makes a breakup of the polymeric chains far more likely, the later discovered solvated LiCp-based CIPs (Table 1) show the same pattern regardless of the presence of substituents on the ring

Table 1 lists all solvated structures of CpLi, Cp'Li, indenyllithium, fluorenyllithium known as of now. No structure of solvated Cp*Li has been reported yet. Table 2 additionally lists all reported solvated derivatives of CpLi, indenyllithium, and fluorenyllithium. The list only includes derivatives with non-donating substituents and also excludes structures

with additionally substituted Cp, indenyl, or fluorenyl moieties. Table 1 shows a preference for the formation of contact-ion pairs for Cp-derivatives. Ligands like DME, TMEDA, PMDETA, and 12-crown-4 form monomeric contact-ion pairs with Cp, Cp', and a broad variety of other Cp-derivatives.^[47] Most of the monomeric contact-ion pairs in Table 2 contain TMEDA as donating solvent. In all cases, the lithium cation is η^5 -coordinated to the ring plane. Both ligands and substituents have a significant effect on the distance of the lithium cation to the ring plane, which is a measure of the strength of attraction between cation and anion. Generally, the more electron density is supplied from the donor atoms, the lower is the attraction of Li^+ to the π -density of the anion. Twofold coordination of TMEDA and threefold coordination of PMDETA to LiCp results in a $\text{Li}^+ - \text{Cp}_{\text{plane}}$ distance of almost 0.15 Å.^[47a] Onefold coordination of for example THF in $(\text{TMS})_3\text{CpLi} \cdot \text{THF}$ leads to an average $\text{Li}^+ - \text{Cp}_{\text{plane}}$ distance of 1.794 Å compared to an average of 1.930 Å in $\text{CpLi} \cdot \text{TMEDA}$.^[48] It is noteworthy that fourfold coordination of 12-crown-4 in $\text{CpLi} \cdot (12\text{-crown-4})$ does not lead to an increased $\text{Li}^+ - \text{Cp}_{\text{plane}}$ distance compared with $\text{CpLi} \cdot \text{PMDETA}$.^[47c] With 2.061 Å, the distance is even shorter for 12-crown-4 than the distance of 2.083 Å for PMDETA. One reason is the rigid nature of the crown ethers. Unlike the two sidearms of PMDETA, crown ethers cannot coordinate as flexibly due to the restraint of the ring-shaped hydrocarbon backbone. Another conceivable reason for the shorter distance is the type of donor atom. The electron pairs of oxygen are more contracted than those of nitrogen due to the higher effective nuclear charge and the higher electronegativity. Therefore, oxygen supplies less charge to the cation than the electron pair of nitrogen. This effect is visible in the structures of $\text{CpLi} \cdot \text{DME}$ and $\text{CpLi} \cdot \text{TMEDA}$.^[47a] The former has a $\text{Li}^+ - \text{Cp}_{\text{plane}}$ distance of 1.909 Å and the latter a distance average of 1.930 Å.

Also substituents on the ring have an effect on the $\text{Li}^+ - \text{Cp}_{\text{plane}}$ distance. Substituents can increase the charge of the π -system through the inductive effect, visible for example in the structures of $\text{Cp}'\text{Li} \cdot \text{TMEDA}$ and $\text{CpLi} \cdot \text{TMEDA}$.^[47b] The $\text{Li}^+ - \text{Cp}_{\text{plane}}$ distance of 1.930 Å is about 0.013 Å shorter than the $\text{Li}^+ - \text{Cp}'_{\text{plane}}$ distance due to the slightly higher attraction of the lithium cation to the π -system of Cp'. This value can even further decrease to 1.907 Å in $(\text{isodicyclopentadienyl})\text{Li} \cdot \text{TMEDA}$, where Cp is carbon-substituted at the 1,2-position.^[49] At the same time, if the steric demand of the substituents is too high, the $\text{Li}^+ - \text{Cp}_{\text{plane}}$ distance increases again as in $(t\text{Bu})_2\text{CpLi} \cdot \text{TMEDA}$ (1.952 Å).^[50]

The second categorically different type of complexes formed consists in . Instead of forming a contact-ion pair as PMDETA, two molecules of diglyme encapsulate a lithium cation and shield it from any further interaction.^[47a] The resulting counterion in LiCp is lithocene. In this case, the lower steric demand of the ligand is crucial. The methyl groups of

Introduction

Solvated Alkali Metal Cyclopentadienyl Compounds

PMDETA hinder such a complexation. 12-crown-4 is another potent agent for solvent separation, which is promoted by bulky substituents on Cp. In $[\text{Li}(12\text{-crown-4})_2][(\text{isodicyclopentadienyl})_2\text{Li}]$, the counteranion is also a lithocene-derivative, whereas in $[\text{Li}(12\text{-crown-4})_2][(\text{TMS})_3\text{Cp}]$, the counteranion is naked.^[47c, 49] The three TMS groups hinder the formation of lithocene. In addition to the method of solvent separation, lithocene has been previously synthesized by salt elimination in the cases of $[\text{PPh}_4][\text{Cp}_2\text{Li}]$ and $[\text{Me}_2\text{PPh}_2][(\text{tBu-Cp})_2\text{Li}]$, as well as using ligand transfer in the case of $[\text{S}(\text{NMe}_2)_3][\text{Cp}_2\text{Li}]$.^[51]

Table 1: Solvated Cp-, Cp⁻-, indenyl-, and fluorenyllithium structures. Under the picture are listed: Name, CCDC-code, reference, and Li – anion plane distance in Å.

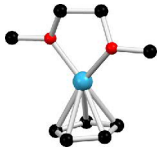
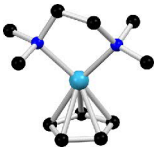
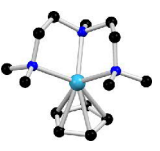

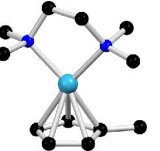
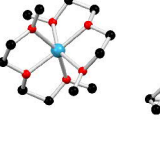

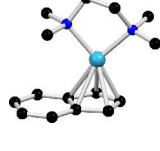
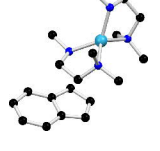
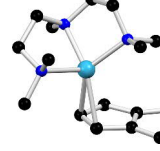
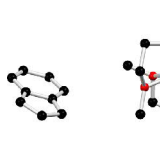

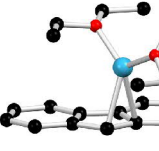
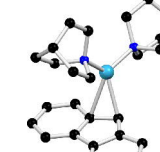


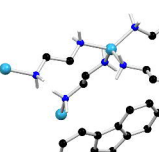
| | | | | |
|--|---|---|---|---|
|  |  |  |  |  |
| CpLi-DME OBABIE [47a] 1.909 | CpLi-TMEDA OBABEA [47a] 1.929/1.931 | CpLi-PMDETA OBABAW [47a] 2.083 | CpLi-(12-crown-4) VITKAK [47c] 2.061 | Cp'Li-TMEDA SIJNII [47b] 1.917 |
|  |  |  |  | |
| $[\text{Li}(\text{Diglyme})_2][\text{Cp}_2\text{Li}]$ OBABOK [47a] 1.974/1.995 | $\text{Ind}_2\text{Li}_2(\text{DME})_2(\mu\text{-DME})$ OBACAX [47a] 2.111 | IndLi-TMEDA INDYLI [52] 2.001 | $[\text{Li}(\text{TMEDA})_2][\text{Ind}]$ CABRAZ [53] | |
|  |  |  |  | |
| IndLi-PMDETA OBABUQ [47a] 2.236-2.314 | $[\text{Li}(\text{Diglyme})_2][\text{Ind}]$ OBACEB [47a] | $\{\text{FluLi-Et}_2\text{O}\}$ NUWDEO [54] 2.242/2.239 | FluLi-2Et ₂ O SANNUQ [55] 2.165 | |
|  |  |  |  | |
| FluLi-2Quinuclidine FULIAO10 [56] 2.054 | FluLi-3THF VABFOU [57] 2.257 | $[\text{Li}(\text{Diglyme})_2][\text{Flu}]$ VUZWIW [58] | $[\text{Li}(\text{en})_2][\text{Flu}]$ JALTUL [59] | |

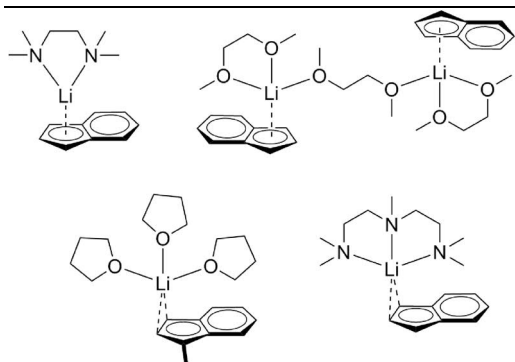
Table 2: List of solvated Cp-, indenyl-, and fluorenyllithium derivatives with non-donating substituents. Listed are name, Li – anion plane distance in Å, type of aggregation, CCDC-code, and reference. The structures are sorted by type of aggregation and Li – anion plane distance.

| | | | | |
|--|-------------|-----------------|----------|-------|
| [Li(12-crown-4) ₂][Cp(TMS) ₃] | | Monomeric, SSIP | VITJUD | [47c] |
| [Li(THF) ₄][((TMS) ₂ Cp) ₂ Li] | 1.982/1.992 | Dimeric, SSIP | EHEHEE | [60] |
| [Li(12-crown-4) ₂][(Isodicyclopentadienyl) ₂ Li] | 1.986/2.006 | Dimeric, SSIP | YEHTOU | [49] |
| [(((Me) ₂ Ph) ₅ Cp) ₂ Li ₃ ·(THF) ₂][(((Me) ₂ Ph) ₅ Cp) ₂ Li ₂] | 1.872-2.118 | Dimeric, SSIP | OHUCUP | [61] |
| [Li(TMEDA) ₂][(((Me) ₂ Ph) ₅ Cp) ₂ Li] | 2.086/2.095 | Dimeric, SSIP | OHUCOJ | [61] |
| (TMS) ₃ CpLi·Quinuclidine | 1.775/1.813 | Monomeric, CIP | DECPOQ | [46c] |
| (TMS) ₃ CpLi·THF | 1.794/1.803 | Monomeric, CIP | SEBHUC | [48] |
| (SiHMe ₂) ₅ CpLi·(O=CPh ₂) | 1.820 | Monomeric, CIP | PAVMEE | [62] |
| (TMS) ₃ CpLi·(tBu-Imidazol-2-ylidene) | 1.901 | Monomeric, CIP | MALRAS | [63] |
| (Isodicyclopentadienyl)Li·TMEDA | 1.907 | Monomeric, CIP | YEHTIO | [49] |
| (Menthyl)CpLi·TMEDA | 1.910 | Monomeric, CIP | NUPYIG | [38a] |
| (C(Me) ₂ P(Ph) ₂)CpLi·TMEDA | 1.914 | Monomeric, CIP | QAKPEX | [64] |
| (Propylene)CpLi·TMEDA | 1.914 | Monomeric, CIP | QAKPIB | [64] |
| (C(Me) ₂ P(Me) ₂)CpLi·TMEDA | 1.920 | Monomeric, CIP | QAKPOH | [64] |
| (TMS)CpLi·TMEDA | 1.929 | Monomeric, CIP | CEZTIK | [65] |
| (tBu)(propylene)CpLi·TMEDA | 1.940 | Monomeric, CIP | YEGFAS | [66] |
| (Phenyl-Isotricyclopentadienyl)Li·(THF) ₂ | 1.944 | Monomeric, CIP | OHUXUK | [67] |
| ((Mesityl) ₂ -diazaphosphenyl)CpLi·DME | 1.946 | Monomeric, CIP | SIFLID | [68] |
| (tBu) ₂ Cp·TMEDA | 1.952 | Monomeric, CIP | GISCEQ | [50] |
| (TMS) ₃ CpLi·PMDETA | 1.980 | Monomeric, CIP | COJROI | [46b] |
| (TMS) ₃ CpLi·TMEDA | 1.980 | Monomeric, CIP | COJRUO10 | [46c] |
| (B(pinacol))CpLi·(12-crown-4) | 2.080 | Monomeric, CIP | ZOOMEX | [69] |
| ((Bz) ₅ Cp) ₂ Li ₂ ·Benzene | 1.769-2.019 | Dimeric, CIP | RAQWUB | [70] |
| [Li(DME) ₃][P(C ₂ B ₁₀)(N(<i>i</i> Pr) ₂)Ind] | | Monomeric, SSIP | ETAGIP | [71] |
| (B(NMe ₂) ₂)IndLi·(Me) ₃ -triazacyclohexane | 1.942 | Monomeric, CIP | GOSNIL | [72] |
| (TMS) ₂ IndLi·(THF) ₂ | 1.992 | Monomeric, CIP | YALJOL | [73] |
| (Menthyl)(Me) ₂ IndLi·(THF) ₂ | 1.996 | Monomeric, CIP | FABQAB | [74] |
| Bu-IndLi·Sparteine | 2.092 | Monomeric, CIP | SUPYIL | [75] |
| Br-IndLi·Sparteine | 2.096 | Monomeric, CIP | LESLOL | [76] |
| Me-IndLi·(THF) ₃ | 2.285 | Monomeric, CIP | SUPYEH | [75] |
| [Li(DME) ₃][P(Ph(<i>t</i> -Bu) ₃)(<i>t</i> -Bu) ₂ Flu] | | Monomeric, SSIP | XUPJOJ | [77] |
| [Li(THF) ₄][1-(P(C(SiMe ₃) ₂) ₂)Flu] | | Monomeric, SSIP | DIBYES | [78] |
| (Si(Me) ₂ (N <i>t</i> Bu))(tBu) ₂ FluLi·DME | 1.981 | Monomeric, CIP | IMEPOF | [79] |
| (Si(TMS) ₃)FluLi·(THF) ₂ | 2.080 | Monomeric, CIP | OLEXUY | [80] |
| (TMS)FluLi·(Et ₂ O)(tBu-NH ₂) | 2.106 | Monomeric, CIP | IPIKIC | [81] |

As mentioned before, the indenyl and fluorenyl anions are less attractive to the lithium cation. The electron density provided by the ligands therefore has a much stronger effect on coordination than in the Cp-structures. In the case of indenyl, twofold coordination results in η^5 -coordination, as can be evidenced in IndLi·TMEDA.^[47a] Threefold coordination leads to η^5 -coordination in the case of Ind₂Li₂·(DME)₂(μ -DME) and to η^2 -coordination in Me-IndLi·(THF)₃ and IndLi·PMDETA (vgl, Scheme 11).^[47a, 75b] The electron density supplied by THF and PMDETA allows the cation to shift to the periphery of

Introduction

Solvated Alkali Metal Cyclopentadienyl Compounds



Scheme II: Coordination of Li to indenyl depending on coordinated donor solvent.

the five-membered ring where the highest charge density is located. The threefold coordination of DME, however, does not give rise to this shift. The steric strain of the hydrocarbon backbone hinders effective coordination to the cation and less electron density is supplied. Solvent separation has also been observed with diglyme and TMEDA.^[47a, 53] In each case, the lithium cation is encapsulated by two donor molecules

with a naked indenyl anion as the counterion. The lower attraction of indenyl to Li^+ prevents the formation of an indenyl-based lithocene.

In the even larger extended π -system of unsubstituted fluorenyl, no η^5 -coordination of Li^+ is present. With one equivalent of Et_2O , $\text{Li}(\text{Flu})$ even forms the 1-dimensional linear coordination polymer $\{(\text{Flu})\text{Li}\cdot\text{Et}_2\text{O}\}$.^[54] This is achieved by η^1 -coordination to the top of the five-membered ring, the position with the highest local charge density. Twofold coordination with Et_2O and quinuclidine leads to η^2 -coordination, whereas threefold coordination from THF leads to η^1 -coordination of the lithium cation.^[55-56] Fluorenyl also forms SSIPs with diglyme, analogous to indenyl.^[58] Ethylenediamine (en) forms a three-dimensional framework.^[59b] Each lithium cation is fourfold coordinated by the en ligand and the resulting cavities are filled with fluorenyl anions.

1.3.2. Solvated Sodium Cyclopentadienyl Compounds

With its higher radius and lower charge concentration, sodium shows a solvation pattern which is significantly different from the one with lithium. The sodium cation has a higher ionic radius and is therefore more attracted to the Pearson-soft π -systems of the various anions than is the case with lithium. In general, sodium forms larger aggregates than lithium. In general, sodium forms larger aggregates than lithium. Table 3 lists all known solvated monomeric and polymeric NaCp , NaCp' , NaCp^* , $\text{Na}(\text{Ind})$, and $\text{Na}(\text{Flu})$ -based compounds. Table 4 lists all solvated derivatives of NaCp and $\text{Na}(\text{Ind})$ with non-donating substituents. Derivatives of fluorenylsodium with non-donating substituents have not been reported yet.

Although solvent free NaCp is isostructural to LiCp with syn-staggered and coplanar Cp-rings, solvated NaCp -derivatives tend to form higher aggregates than LiCp -derivatives. Monomeric CIPs are formed with shielding ligands like 15-crown-5 as in the case of $\text{CpNa}\cdot(15\text{-crown-5})$, and 18-crown-6 as in the case of $\text{Cp}'\text{Na}\cdot(18\text{-crown-6})$.^[82] Surprisingly,

18-crown-6 does not form monomeric CIPs with NaCp, but a sodocene moiety which is η^2 -co-coordinated by a $\text{Na}(18\text{-crown-6})^+$ -fragment.^[83] The methyl group increases the attraction of the sodium cation and probably hinders the formation of dimethyl-sodocene due to steric restraint. Bulky substituents also lead to the formation of monomeric CIPs as in $\text{Cp}^*\text{Na}\cdot(\text{Py})_3$, $\text{Ph}_4\text{CpNa}\cdot(\text{THF})_3$, and $(\text{TMS})_3\text{CpNa}\cdot\text{PMDETA}$.^[50, 84] Without substituents and fewer shielding donor ligands, the resulting structures are generally 1-dimensional coordination polymers, just as $\{\text{CpNa}\cdot\text{THF}\}$, $\{\text{CpNa}\cdot\text{DME}\}$, and $\{\text{CpNa}\cdot\text{TMEDA}\}$.^[82, 85] $\{\text{CpNa}\cdot\text{THF}\}$ and $\{\text{CpNa}\cdot\text{DME}\}$ are linear zig-zag coordination polymers; $\{\text{CpNa}\cdot\text{TMEDA}\}$ has a helical arrangement. Onefold coordination with THF in $\{\text{CpNa}\cdot\text{THF}\}$ generated – unlike what one would probably expect – a dense crystal packing with the $\text{Na}(\text{THF})$ -moieties packed like a zipper. In other words, here, the crystal packing wins over coordination. NaCp-derivatives with a single bulky substituent generally form a coordination polymer with a onefold coordinated sodium cation as in $\{(\text{Me}_2\text{N})_2\text{BCpNa}\cdot\text{THF}\}$, $\{(\text{Cyclopentyl})\text{CpNa}\cdot\text{THF}\}$, or $\{(\text{Me}_2\text{N})_2\text{BCpNa}\cdot\text{THF}\}$.^[69, 86]

But also solvent separation has been reported. 12-crown-4 forms a SSIP with NaCp.^[87] Two ligands encapsulate one sodium cation with a naked anion as the counterion. DME, diglyme, and 18-crown-6 also form SSIPs with the following bulky anions: Ph_5Cp in $[\text{Na}(\text{DME})_3][\text{Ph}_5\text{Cp}]$, Ph_4Cp in $[\text{Na}(\text{diglyme})_2][\text{Ph}_4\text{Cp}]$, as well as 18-crown-6 in $[\text{Na}_2(18\text{-crown-6})_3][\text{Ph}_4\text{Cp}]_2$. In the last structure, three 18-crown-6 units form a dicationic complex with two sodium cations.^[84b, 88] The formation of naked anions in this case is clearly due to the difficulty to form sodocene or other oligomers through steric repulsion. Sodocene itself has been synthesized not by solvent separation but via ligand transfer in $[(\text{Me}_2\text{N})_3\text{S}]_2\text{Cp}][\text{Na}_2\text{Cp}]$ and via salt elimination in $[\text{PPh}_4][\text{Na}_2\text{Cp}]$.^[51d, 51e, 89]

While an almost same amount of indenyllithium and fluorenyllithium compounds and their derivatives have been reported, fluorenylsodium compounds largely outnumber indenylsodium compounds. Also only one indenylsodium derivative without donating substituents has been reported, the monomeric CIP $(\text{TMS})_2\text{IndNa}\cdot(\text{Et}_2\text{O})(\text{Bipyridine})$, but none for fluorenylsodium.^[90] SSIPs of fluorenylsodium are formed with [2.2.1]cryptand, diglyme, and 18-crown-6 together with two molecules of THF.^[58, 91] The complexation of the sodium cation in $[\text{Na}(\text{diglyme})_2][\text{Flu}]$ is analogous to the complexation in $[\text{Li}(\text{diglyme})_2][\text{Cp}_2\text{Li}]$, $[\text{Li}(\text{diglyme})_2][\text{Ind}]$, and $[\text{Li}(\text{diglyme})_2][\text{Flu}]$, but diglyme forms a second aggregate with fluorenylsodium, a dimeric structure with two fluorenylsodium moieties connected by two molecules of diglyme.^[58] The structure of $\text{Flu}_2\text{Na}_2\cdot(\text{diglyme})_2$ resembles the DME-solvated indenyllithium structure $\text{Ind}_2\text{Li}_2\cdot(\text{DME})_3$.

Introduction

Solvated Alkali Metal Cyclopentadienyl Compounds

Table 3: Crystal structures of solvated NaCp, NaCp', NaCp*, Na(Ind) and Na(Flu)-based compounds. Under the pictures are listed: Name, CCDC-code, reference, Na – anion plane distance in Å.

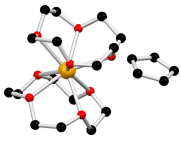

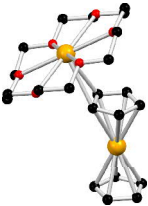


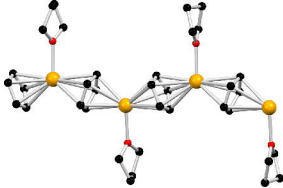
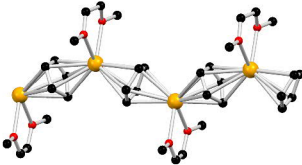
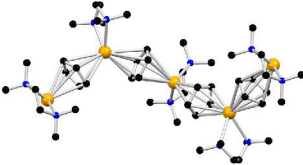
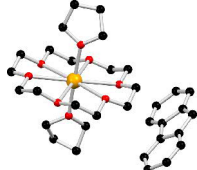
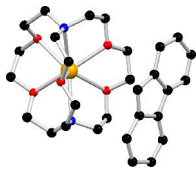
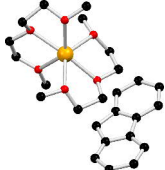
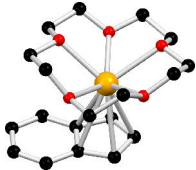
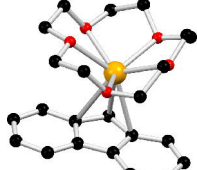
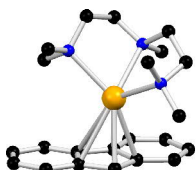
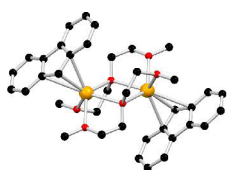
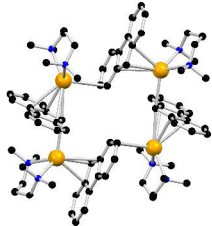
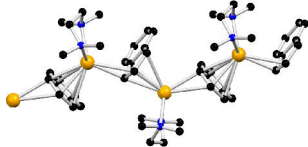
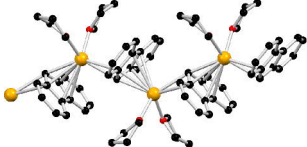
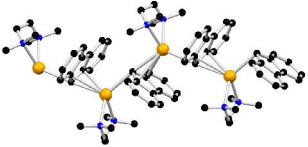
| | | | | |
|---|---|---|---|---|
|  |  |  |  |  |
| [Na(12-crown-4) ₂] [Cp] MIVVIW ^[87] | CpNa-(15-crown-5) AFEQOR ^[82] 2.543 | Cp ₂ Na ₂ -(18-crown-6) MIVVAO ^[83] 2.345/2.448 | Cp'Na-(18-crown-6) AFEQUX ^[82] 2.555 | Cp*Na-(Py) ₃ KOHZOW ^[84a] 2.398 |
|  |  |  | | |
| {CpNa-THF} QODGEW ^[85a] 2.453 | {CpNa-DME} AFEQEH ^[82] 2.541/2.551 | {CpNa-TMEDA} CPNATM10 ^[85b] 2.664/2.677 | | |
|  |  |  |  | |
| [Na(18-crown-6)(THF) ₂][Flu] BADPUS ^[91c] | [Na(2.2.1-cryptand)][Flu] HEDXOD ^[91a, 91b] | [Na(Diglyme) ₂][Flu] VUZWOC ^[58] | IndNa-15-crown-5 OFUNIM ^[92] 2.602 | |
|  |  |  |  | |
| FluNa-15-crown-5 OFUNOS ^[92] 2.599 | FluNa-PMDETA VOKPUG ^[93] 2.512 | Flu ₂ Na ₂ -(Diglyme) ₂ VUZXOD ^[58] 2.582 | Flu ₄ Na ₄ -(TMPDA) ₄ VOKRES ^[93] 2.569-2.864 | |
|  |  |  | | |
| {IndNa-TMEDA} GABHAS ^[94] 2.496/2.536 | {FluNa-(THF) ₂ } XACSID ^[44a] 2.573/2.605 | {FluNa-TMEDA} VOKRAO ^[93] 2.582/2.675 | | |

Table 4: List of solvated Cp- and indenylsodium derivatives with non-donating substituents. Listed are name, Na – anion plane distance in Å, type of aggregation, CCDC-code, and reference. The structures are sorted by type of aggregation and Na – anion plane distance.

| | | | | |
|---|-------------|-----------------|---------------|------------|
| [Na(Diglyme) ₂][Ph ₄ Cp] | | Monomeric, SSIP | RATNOP | [84b] |
| [Na(DME) ₃][Ph ₃ Cp] | | Monomeric, SSIP | XAVXOH | [88a] |
| [Na ₂ (18-crown-6) ₃][Ph ₄ Cp] ₂ | | Dimeric, SSIP | TUQWOR | [88b, 88c] |
| (<i>t</i> Bu-Isotricyclopentadienyl)Na·(THF) ₃ | 2.444 | Monomeric, CIP | OHUYEV | [67] |
| (Phenyl-Isotricyclopentadienyl)Na·(THF) ₃ | 2.477 | Monomeric, CIP | OHUYAR | [67] |
| Ph ₄ CpNa·(THF) ₃ | 2.481 | Monomeric, CIP | RATNIJ | [84b] |
| (TMS) ₃ CpNa·PMDETA | 2.501 | Monomeric, CIP | GISCAM | [50] |
| (Isodicyclopentadienyl)Na·(15-crown-5) | 2.499/2.519 | Monomeric, CIP | PULTUL | [95] |
| Ph ₄ CpNa·(DME) ₂ | 2.577 | Monomeric, CIP | ZOZHOL | [96] |
| {((Me ₂ N) ₂ B)CpNa·THF} | 2.436/2.453 | 1D-Coord. Pol. | ZOQMAT | [69] |
| {(Cyclopentyl)CpNa·THF} | 2.449/2.473 | 1D-Coord. Pol. | SUDWET | [86] |
| {(Menthyl)CpNa·THF} | 2.481/2.484 | 1D-Coord. Pol. | NUPYUS | [38a] |
| {BzCpNa·THF} | 2.488/2.512 | 1D-Coord. Pol. | SUDWAP | [86] |
| {(Me ₂ N) ₂ BCpNa·THF} | 2.497/2.476 | 1D-Coord. Pol. | ZOQLUM | [69] |
| {(Si(Me) ₂ (Flu))CpNa·THF} | 2.547/2.554 | 1D-Coord. Pol. | UDOBAQ | [38b] |
| {Me ₂ BCpNa·(THP) ₂ } | 2.566/2.597 | 1D-Coord. Pol. | ZOQMIB | [69] |
| (TMS) ₂ IndNa·(Et ₂ O)(Bipyridine) | 2.423/2.476 | Monomeric, CIP | MIGBUB | [90] |

15-crown-5 and PMDETA create monomeric CIPs with indenyl and fluorenyl.^[92-93] In IndNa·(15-crown-5), the sodium cation is η^5 -coordinated. The lithium cation in analogous indenyllithium compounds containing THF and PMDETA is shifted to the periphery of the five-membered ring due to the high amount of supplied charge density from the ligands. The softer sodium cation in IndNa·(15-crown-5), in contrast, stays between the two centres of highest charge of the indenyl anion. In FluNa·(15-crown-5) and FluNa·PMDETA, the sodium cation shifts significantly towards the area of the highest charge concentration at the top of the five-membered ring.

Coordination polymers are mainly formed with mono- and bidentate ligands. {IndNa·TMEDA}, {FluNa·(THF)₂}, and {FluNa·TMEDA} form very similar patterns.^[44a, 93-94] Each anion is η^5 -coordinated from one side. From the other side, the anions are coordinated at the ring periphery with a high charge concentration. The TMPDA-ligand, with its size lying between the sizes of TMEDA and PMDETA, creates the tetramer (Flu)₄Na₄·(TMPDA)₄.^[93] Similar to the coordination polymers, the anions of the tetramer are coordinated from one side to the five-membered ring and from the other side to the ring periphery of both the six- and five-membered rings.

1.3.3. Solvated Potassium Cyclopentadienyl Compounds

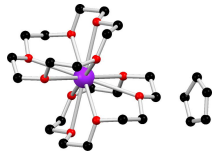
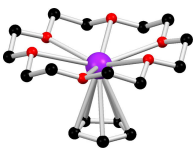
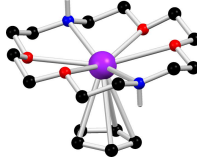
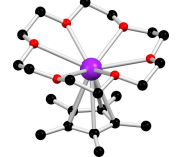
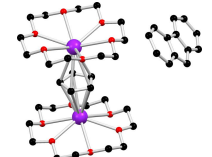
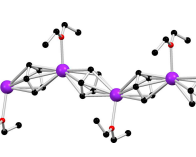
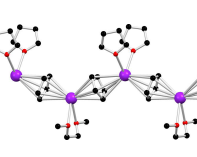
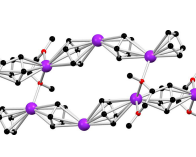
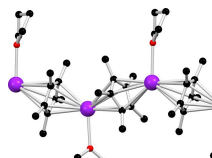
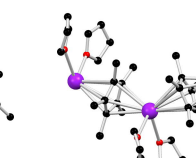
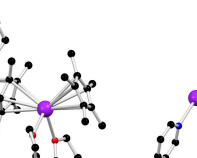
From lithium to sodium, the size of the formed aggregates increases. This tendency continues with potassium. Table 5 shows crystal structures of solvated Cp, and Cp* compounds containing potassium (solvated KCp' structures have not been reported), Table 7

Introduction

Solvated Alkali Metal Cyclopentadienyl Compounds

contains all known solvated indenylpotassium and fluorenylpotassium compounds, and Table 6 lists all Cp- and fluorenylpotassium derivatives with non-donating substituents. Similar to $[\text{Na}(12\text{-crown-}4)_2][\text{Cp}]$, a SSIP of KCp emerges with the use of 15-crown-5: the compound $[\text{K}(15\text{-crown-}5)_2][\text{Cp}]$.^[82] SSIPs with naked anions are also formed with the [2.2.2]cryptand together with isocyclopentadienylpotassium or $(\text{TMS})\text{CpK}$.^[95, 97] 18-crown-6 and two molecules of THF also create a SSIP with the very bulky Ph_4CpK .^[98] Crown ethers are generally not suitable for coordination polymers. They effectively shield large parts of the cationic coordination sphere without any flexibility in their conformation as in diglyme and PMDETA. Monomeric CIPs of KCp and KCp^* are formed with 18-crown-6 and diaza-18-crown-6, whereas more bulky anions as in $(t\text{Bu})(\text{homoadamanto})_2\text{CpK}$, $(\text{Ph})(\text{homoadamanto})_2\text{CpK}$, and $(\text{Bz})_5\text{CpK}$ form monomeric CIPs with three molecules of THF.^[99] When both Cp and fluorenyl are present when using 18-crown-6, a SSIP emerges with a cationic $\text{CpK}_2 \cdot (18\text{-crown-}6)_2^+$ complex and a naked fluorenyl anion as a counterion.^[100]

Table 5: Crystal structures of solvated KCp-based compounds. Under the pictures are listed: Name, CCDC-code, reference, K – anion plane distance in Å.

| | | | |
|--|---|--|--|
|  |  |  |  |
| $[\text{K}(15\text{-crown-}5)_2][\text{Cp}]$ AFERAE ^[82] 2.811 | $\text{CpK} \cdot (18\text{-crown-}6)$ BIQMIX ^[99a] 2.811 | $\text{CpK} \cdot (\text{diaza-}18\text{-crown-}6)$ QOTQIB ^[99b, 99c] 2.933/2.935 | $\text{Cp}^* \text{K} \cdot (18\text{-crown-}6)$ BIQMOD ^[99a] 2.850 |
|  |  |  |  |
| $[\text{K}_2(18\text{-crown-}6)_2\text{Cp}][\text{Flu}]$ HOJJOF ^[100] 2.849/2.854 | $\{\text{CpK} \cdot \text{Et}_2\text{O}\}$ NAGSUJ ^[101] 2.767/2.768 | $\{\text{CpK} \cdot (\text{THF}) (\text{DME})_{0.5}\}$ XUMKEW ^[102] 2.813/2.849 | $\{\text{CpK} \cdot (\mu\text{-DME})_{0.5}\}$ AFEQIL ^[82] 2.675-2.965 |
|  |  |  | |
| $\{\text{Cp}^* \text{K} \cdot \text{THF}\}$ CAKTEO ^[103] 2.758/2.768 | $\{\text{Cp}^* \text{K} \cdot (\text{THF})_2\}$ CAKTIS ^[103] 2.810/2.820 | $\{\text{Cp}^* \text{K} \cdot (\text{Py})_2\}$ KOHZUC ^[84a] 2.777/2.787 | |

Solvated Alkali Metal Cyclopentadienyl Compounds

Table 6: List of solvated Cp- and fluorenylpotassium derivatives with non-donating substituents. Listed are name, Na – anion plane distance in Å, type of aggregation, CCDC-code, and reference. The structures are sorted by type of aggregation and K – anion plane distance.

| | | | | |
|---|-------------|-----------------|--------|------------|
| [K([2.2.2]cryptand)][isodicyclopentadienyl] | | Monomeric, SSIP | PULVAT | [95] |
| [K([2.2.2]cryptand)][(TMS)Cp] | | Monomeric, SSIP | CUKMAY | [97] |
| [K(18-crown-6)(THF) ₂][Ph ₄ Cp] | | Monomeric, SSIP | CUKBIV | [98] |
| (<i>t</i> Bu)(homoadamanto) ₂ CpK·(THF) ₃ | 2.739 | Monomeric, CIP | SAGMAP | [99d] |
| (Ph)(homoadamanto) ₂ CpK·(THF) ₃ | 2.749 | Monomeric, CIP | XANRAH | [99e] |
| (Bz) ₅ CpK·(THF) ₃ | 2.784 | Monomeric, CIP | SAXRAK | [99f, 99g] |
| (<i>t</i> Bu) ₂ CpK·(18-crown-6) | 2.829 | Monomeric, CIP | CAHCOF | [104] |
| {(Pentyl)(Me) ₄ CpK·THF} | 2.713/2.719 | 1D-Coord. Pol. | REZMAM | [105] |
| {(5-CH ₂ -1-phenyl-1-azafluorenyl)(Me) ₄ CpK·THF} | 2.741/2.757 | 1D-Coord. Pol. | OJEQIE | [106] |
| {(Naphtyl)(Me) ₄ CpK·THF} | 2.755/2.763 | 1D-Coord. Pol. | FANBED | [107] |
| {Me ₄ CpK·DME} | 2.762/2.766 | 1D-Coord. Pol. | ALUYAH | [108] |
| {(Si(Et) ₃ CpK·Py)} | 2.774/2.778 | 1D-Coord. Pol. | WOZDIY | [109] |
| {(Si(Me) ₂ (Pr))(Me) ₄ CpK·THF} | 2.764/2.795 | 1D-Coord. Pol. | CAKTOY | [103] |
| {(Me) ₄ (<i>t</i> BuNSiMe ₂)CpK·THF} | 2.780/2.805 | 1D-Coord. Pol. | HACYOZ | [110] |
| {(Si(Me) ₂ (C≡CPh))CpK·THF} | 2.806/2.820 | 1D-Coord. Pol. | MACVAP | [111] |
| {(TMS) ₂ CpK·THF} | 2.825/2.827 | 1D-Coord. Pol. | LUJHEF | [112] |
| {(Menthyl)CpK·DME} | 2.827/2.861 | 1D-Coord. Pol. | NUPZAZ | [38a] |
| (P(Mesityl))(<i>t</i> Bu) ₂ FluK·(THF) ₃ | 2.822 | Monomeric, CIP | XUPJID | [77] |
| (TMS)FluK·(18-crown-6) | 3.113 | Monomeric, CIP | ISASEA | [113] |
| {(Si(TMS) ₃)FluK·THF} | 2.822/2.848 | 1D-Coord. Pol. | OLEYIN | [80] |
| { <i>t</i> Bu-FluK·(THF) ₂ (TMEDA)} | 2.878-2.945 | 1D-Coord. Pol. | PEPWAI | [114] |

Monodentate ligands like pyridine, THF, Et₂O, and the bidentate ligand DME create 1-dimensional coordination polymers both with Cp and Cp*, as well as with a variety of Cp-derivatives with moderate steric demand. In the DME adduct {CpK·DME}, the KCp-strands are interconnected by one sidearm of DME with the oxygen atom coordinating two potassium cations. Bulky substituents of Cp-derivatives in Table 6 generally only allow the coordination of one monodentate ligand. The coordination patterns of KCp and KCp* also show some flexibility. KCp* can be coordinated by either one or two molecules of THF per potassium cation.^[103]

The coordination polymers of Cp*K·(Py)₂ demonstrates the tendency of potassium to form higher aggregates than sodium.^[84a] The analogous sodium compound is the CIP Cp*Na·(Py)₃. The larger distance of potassium to the ring plane leaves enough space to coordinate the cation without interfering with the Cp*-methyl groups.

Introduction

Solvated Alkali Metal Cyclopentadienyl Compounds

Table 7: Crystal structures of solvated indenyl- and fluorenylpotassium compounds. Under the pictures are listed: Name, CCDC-code, reference, K – anion plane distance in Å.

| | | | |
|--|--|---|--|
| IndK·(18-crown-6) BIQMUI [99a] 2.857 | [K(18-crown-6)(THF) ₂][Flu] ULOWAT [113] | (Flu)K·(18-crown-6)(Tol) BIQNAQ [99a] 2.992 | (Flu)K·(18-crown-6)(Py) BIFMOT [113] 3.043 |
| FluK·(18-crown-6)(THF) BIQNEU [99a] 3.091 | FluK·(TMEDA) ₂ PEPVUB [114] 2.936 | Flu ₂ K ₂ ·(18-crown-6) ₂ (μ-DME) BIQNIY [99a] 3.081 | Flu ₃ K ₃ ·(Diglyme) ₃ VUZWUI [58] 2.358-2.950 |
| {IndK·TMEDA} NAGTEV01 [101] 2.814/2.828 | {IndK·PMDETA} NAGTEU [101] 2.684-2.881 | {Flu ₂ K ₂ ·Diglyme} VUZXIX [58] 2.894-3.008 | |
| {FluK·PMDETA} XIQNUH [115] 2.764-2.950 | {FluK·(μ-TMEDA) ₂ } FLMENK [116] 2.972/3.053 | {Flu ₂ K ₂ ·(μ-THF) ₂ } XACSAV [44a] 2.915-2.947 | |

Many more solvated fluorenylpotassium structures (11) than indenylpotassium structures (3) have been reported (Table 7). There are no reports of indenylpotassium derivatives with non-donating substituents at all. Similar to the Cp-derivatives, 18-crown-6 generates mostly monomeric CIPs with indenylpotassium and fluorenylpotassium, but the presence of six-membered rings leads to a variety of coordination patterns. In $\text{IndK}\cdot(18\text{-crown-6})$, the potassium cation coordinates the five-membered ring.^[99a] In the three monomeric CIPs of fluorenylpotassium, co-coordinated by either toluene, pyridine, and THF, the cation coordinates the six-membered ring.^[99a, 113] The subtle influence of the three molecules leads to a shift from strictly η^6 (toluene) to a position closer to the five-membered ring (pyridine, THF). In contrast to pyridine and THF as the ligands, the cation shifts to the periphery of the six-membered ring when the $\text{FluK}\cdot(18\text{-crown-6})$ -fragment is co-coordinated by DME in the dimeric CIP $\text{Flu}_2\text{K}_2\cdot(18\text{-crown-6})(\mu\text{-DME})$.^[99a] 18-crown-6 also creates aSSIP with two molecules of THF in $[\text{K}(18\text{-crown-6})(\text{THF})_2][\text{Flu}]$.^[113]

The bi- and tridentate ligands TMEDA, PMDETA and diglyme reveal more of the flexible coordination nature of fluorenylpotassium. PMDETA forms 1-dimensional coordination polymers with both indenylpotassium and fluorenylpotassium.^[101, 115] In both cases, the anion is η^5 -coordinated from one side and coordinated from the other side at the periphery of the five-membered ring. Both areas of coordination have a high charge accumulation. In contrast to $\{\text{FluK}\cdot\text{PMDETA}\}$, fluorenylsodium and PMDETA form the CIP $\text{FluNa}\cdot\text{PMDETA}$, making $\{(\text{Flu})\text{K}\cdot\text{PMDETA}\}$ an example for the tendency of potassium to form higher aggregates. TMEDA forms a 1-dimensional coordination polymer as well, but with both cations η^5 -coordinated to the five-membered ring in contrast to $\{\text{IndNa}\cdot\text{TMEDA}\}$, where one side of the anion is η^5 -coordinated and side-on coordinated from the other side.

TMEDA forms two different aggregates with fluorenylpotassium. Two molecules of TMEDA form a CIP with $\text{K}(\text{Flu})$ with the cation coordinating the five-membered ring.^[114] TMEDA also forms a coordination polymer with $\text{K}(\text{Flu})$.^[116] Instead of TMEDA coordinating one cation, two TMEDA molecules bridge two cations of neighboring $\text{K}(\text{Flu})$ -strands. The result is a 2-dimensional coordination polymer with TMEDA-interlinked strands of fluorenylpotassium. Also diglyme forms two polymorphs: a solvated $\text{K}(\text{Flu})$ -trimer and a coordination polymer.^[58] The trimer is an expansion of the corresponding sodium compound $(\text{Flu})_2\text{Na}_2\cdot(\mu\text{-diglyme})_2$. The coordination polymer $\{(\text{Flu})\text{K}\cdot\text{diglyme}\}$ has a very compact coordination pattern. Each anion is either coordinated by four cations at the six-membered rings. Or it is coordinated from one side by two cations at the six-membered rings and from the other side by one cation at the five-membered ring. This compact packing increases when using THF. $\{(\text{Flu})_2\text{K}_2\cdot(\mu\text{-THF})\}$ is a three-dimensional

coordination polymer.^[44a] Each cation coordinates to the six-membered rings of three anions. Two cations are in close proximity and bridged by a molecule of THF.

1.3.4. *Solvated Rubidium Cyclopentadienyl Compounds*

Table 8 lists all known solvated structures of Cp, Cp', Cp*, indenyl-, and fluorenyl rubidium. No other derivatives with non-donating substituents have been reported. Like KCp, also RbCp forms aSSIP with 15-crown-5 containing a naked Cp-anion as counterion in the form of [Rb(15-crown-5)₂][Cp].^[117] The same SSIP is formed with indenylrubidium in the form of [Rb(15-crown-5)₂][Ind].^[118] One noteworthy observation is the large variety of solvated RbCp-compounds with 18-crown-6. It is known to either form the monomeric CIP CpRb·(18-crown-6), a SSIP with the inverse sandwich complex CpRb₂·(18-crown-6)₂⁺ as cation and naked Cp as anion. Or it forms the oligomeric Cp₄Rb₄·(18-crown-6)₂.^[100, 119]

The Cp₄Rb₄·(18-crown-6)₂ oligomer demonstrates the influence of the increasing ionic radius of rubidium compared with potassium. One rubidium cation in the oligomer is coordinated by three Cp-anions of two CpRb·(18-crown-6)-moieties and a rubidocene-fragment. A similar structure arises when both Cp and Cp* are present. The structure itself is a SSIP with the inverse sandwich structure Cp*Rb₂·(18-crown-6)⁺ as cation and the oligomer Cp₃Cp*₂Rb₄·(18-crown-6)₂ as anion.^[100] Two rubidium cations in the oligomeric anion are threefold coordinated as well. The cations of the linear Cp₃Rb₂-fragment are both coordinated to a Cp*Rb·(18-crown-6)-moiety.

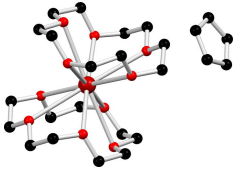
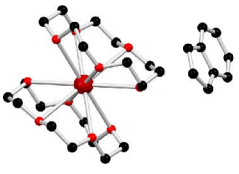
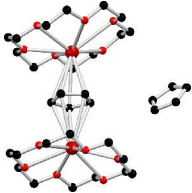

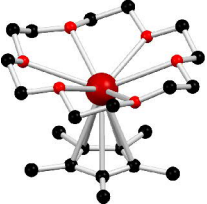

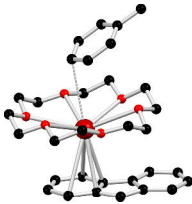
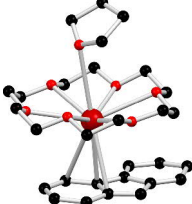
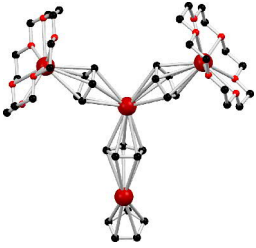
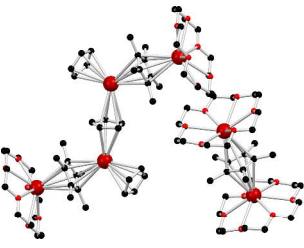
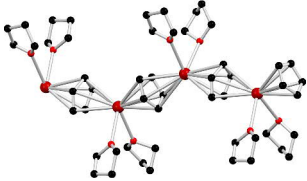
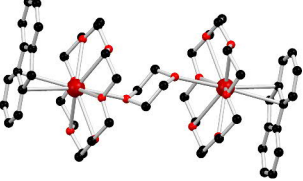
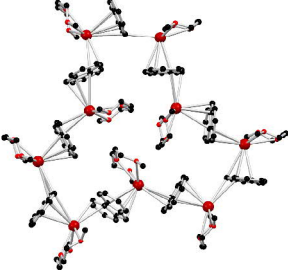
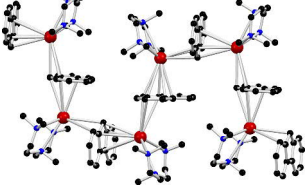
18-crown-6 also forms monomeric CIPs with RbCp*, indenylrubidium, and fluorenylrubidium.^[99a] The 18-crown-6 adducts of fluorenylrubidium are similar to those of potassium. The rubidium cation is either co-coordinated by toluene, THF, or two FluRb·(18-crown-6) are linked together by a molecule of 1,4-dioxane. The rubidium cation shifts in the structures from a position closer to the six-membered ring (toluene) to a position between the five- and six-membered ring (1,4-dioxane).

A distinct increase in oligomerization can be observed in the diglyme-solvated structure (Flu)₉Rb₉·(diglyme)₉.^[58] While fluorenylpotassium forms a trimer, fluorenylrubidium forms a closed nonameric ring. The space inside this array is occupied by diglyme. A similar pattern can be observed in the coordination polymer {(Flu)Rb·PMDETA} with its meandering progression like an opened version of the nonameric diglyme structure.^[120] In this arrangement, the cation can coordinate the anions more efficiently at the five-membered rings. In the linear {(Flu)K·PMDETA}, the cation only coordinates to one five-membered ring. It coordinates to the next anion only at the periphery. The only reported 1-dimensional coordination polymer is the THF-adduct {CpRb·(THF)₂}.^[121]

Introduction

Solvated Alkali Metal Cyclopentadienyl Compounds

Table 8: Crystal structures of solvated cyclopentadienyl-, indenyl-, and fluorenylrubidium compounds. Under the pictures are listed: Name, CCDC-code, reference, Rb – anion plane distance in Å.

| | | | |
|---|---|---|---|
|  |  |  |  |
| [Rb(15-crown-5) ₂][Cp] PUYJOI [117] | [Rb(15-crown-5) ₂][Ind] XUSQOR [118] | [Rb ₂ (18-crown-6) ₂ Cp][Cp] QIRFIG [119b] 2.961/2.974 | CpRb-(18-crown-6) QEXTIW [119a] 2.984 |
|  |  |  |  |
| Cp*Rb-(18-crown-6) QEXTUI [119a] 2.936 | (Ind)Rb-18-crown-6 QEXVEU [119a] 2.955 | (Flu)Rb-(18-crown-6)(Tol) QEXVOE [119a] 3.027 | (Flu)Rb-(18-crown-6)(THF) QEXVUK [119a] 3.075 |
|  |  |  | |
| Cp ₄ Rb ₄ -(18-crown-6) ₂ VABGIP [100] 2.937-3.059 | [Cp*Rb ₂ -(18-crown-6) ₂] [Cp ₃ Cp* ₂ Rb ₄ -(18-crown-6) ₂] PUYGUL [100] 2.918-3.172 | CpRb-(THF) ₂ SOKTOC [121] 2.893/3.0131 | |
|  |  |  | |
| (Flu) ₂ Rb ₂ -(18-crown-6) ₂ (μ-dioxane) QEXWEV [119a] 3.159 | (Flu) ₉ Rb ₉ -(Diglyme) ₉ VUZXP [58] 2.703-3.232 | ((Flu)Rb-PMDTA) LAWPEE [120] 3.020-3.164 | |

Introduction

Solvated Alkali Metal Cyclopentadienyl Compounds

1.3.5. Solvated Caesium Cyclopentadienyl Compounds

Similar to the rubidium structures, not many solvated compounds of Cp, Cp', Cp*, indenyl-, and fluorenylcaesium have been reported. Table 9 lists the known structures. There are also no reported derivatives of solvated Cp-, indenyl-, or fluorenylcaesium with non-donating substituents. The caesium structures are very similar to those of rubidium, but the tendency to form higher aggregates can be observed here as well.

Table 9: Crystal structures of solvated cyclopentadienyl-, indenyl-, and fluorenylcaesium compounds. Under the pictures are listed: Name, CCDC-code, reference, Cs – anion plane distance in Å.

| | | | |
|---|--|--|--|
| CpCs·(18-crown-6) QEXTOC [119a] 3.039 | Cp*Cs·(18-crown-6) QEXVAQ [119a] 3.039 | (Ind)Cs·18-crown-6 QEXVIY [119a] 3.196 | (Flu)Cs·18-crown-6 QEXWIZ [119a] 3.186 |
| (Flu)Cs·(18-crown-6)·(Tol) QEXWOF [119a] 3.115 | (Flu)Cs·(18-crown-6) (THF) QEXWUL [119a] 3.089 | {Cp ₂ Cs ₂ ·(18-crown-6)} VABGOV [100] 2.845-3.507 | {Cp' ₂ Cs ₂ ·(18-crown-6)} IFUGEV [42] 3.124-3.173 |
| [Cp*Cs·(18-crown-6) ₂] [Cp* ₂ Cp ₃ Cs ₄ ·(18-crown-6) ₂] HOJJUL [100] 3.027-3.188 | Flu ₉ Cs ₉ ·(Diglyme) ₉ VUZXET [58] 2.836-3.358 | {Flu ₂ Cs ₂ ·THF} XACSEZ [44a] 2.730-3.316 | |

As in the case of rubidium, the 18-crown-6 ligand forms a variety of different structures with CsCp. A monomeric CIP is formed and also the mixed aggregate with Cp and Cp* is equally built as in the complex with rubidium.^[100, 119a] The $\text{Cp}_4\text{Rb}_4\cdot(18\text{-crown-6})_2$ oligomer is expanded to a 1-dimensional coordination polymer with side-branches.^[100] $\{\text{Cp}_2\text{Cs}_2\cdot(18\text{-crown-6})\}$ consists of a linear CsCp-strand with each cation within the strand coordinated by a CpCs(18-crown-6) moiety. The Cp'-derivative $\{\text{Cp}'_2\text{Cs}_2\cdot(18\text{-crown-6})\}$ is similarly built, but the methyl groups create meandering CsCp'-strands and the Cp'Cs(18-crown-6) moieties arrange askew.^[42]

18-crown-6 also creates monomeric CIPs with CsCp*, indenylcaesium, and fluorenylcaesium.^[119a] In the case of FluCs(18-crown-6), three structures have been reported: one without an additional ligand, a toluene adduct and a THF adduct. Toluene and THF seem to have only a weak interaction with the caesium cation, and the cation does not significantly shift from its position between the five- and the six-membered ring in contrast to the analogous potassium- and rubidium structures. The influence of the co-ordination has already been weaker for rubidium compared to potassium and is almost irrelevant for caesium.

The diglyme structure of fluorenylcaesium Flu_9Cs_9 is built equally to the analogous rubidium structure.^[58] Also the THF adduct of fluorenylcaesium $\{\text{Flu}_2\text{Cs}_2\cdot\text{THF}\}$ is built analogously to the corresponding potassium structure: a 3-dimensional coordination polymer with THF bridging two caesium cations.^[44a] In contrast to the potassium structure, the caesium cations do not coordinate at the periphery of the six-membered rings, but are fully η^6 -coordinated due to their larger size.

1.4. Hydrogen Bonding

Crystallization is driven by intermolecular interactions. In minerals, only covalent and ionic bonding are present in the crystal. The interactions in organometallic crystals are mostly ligand-to-metal coordination, electrostatic cation–anion interactions, hydrogen bonding, and dispersive forces.^[122] In crystal engineering, the synthesis of metal–organic frameworks (MOFs), materials for catalysis or hydrogen storage, can be based on building blocks like cations, clusters, and ligands to create 1-, 2-, or 3-dimensional frameworks (Figure 15) that contain cavities or contain a catalyst.^[123] *Gautam Desiraju* compares the design of supermolecular crystals to the synthesis of an organic molecule.^[124] He coined the term “supramolecular synthon” in the world of supermolecular chemistry in analogy to the term “synthon” in organic chemistry, a structural unit of a molecule in retrosynthesis which can be employed for synthetic operations. Supramolecular synthons are specific intermolecular interactions between functional groups of molecules or between lig-

Introduction

Hydrogen Bonding

ands and cations/organometallic clusters. With the right choice of functional groups attached to a molecule or cluster, the self-assembly of the crystal can be directed. Hydrogen bonding not only plays a crucial role in supramolecular chemistry and crystal engineering, but is the most important intermolecular interaction generally in life.

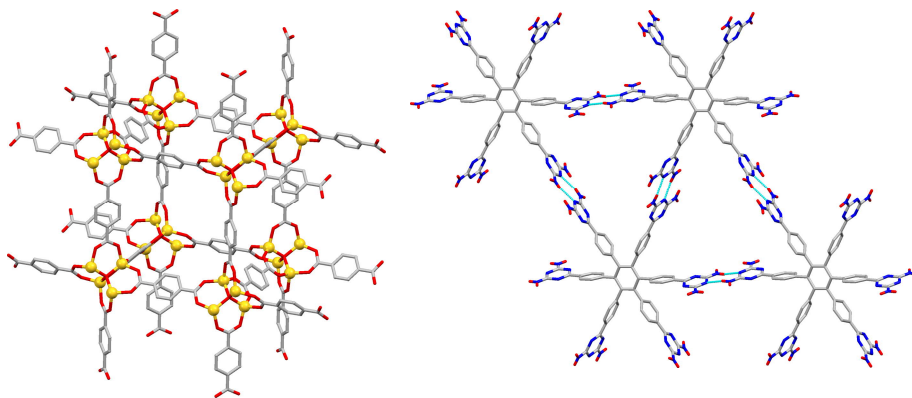


Figure 15: Examples of crystal engineering using supramolecular synthons. Left: MOF-5, Zn_4O -clusters complexed by the dianion of terephthalic acid.^[125] Right: Molecular self-assembly by N–H hydrogen bonding.^[126]

Hydrogen bonding is the basis of the life-donating properties of water; it plays a crucial role in the structural organization of proteins and DNA, and helps forming structures of cellulose, just to name a few.^[127]

Hydrogen bonds require a hydrogen donor and a hydrogen acceptor. The stronger the donating and accepting properties, the stronger is the hydrogen bond. The hydrogen donor is a highly electronegative atom like nitrogen, oxygen, or fluorine connected to a hydrogen atom where it creates a positive partial charge by withdrawing electron density. The hydrogen acceptor bonds to the hydrogen atom with a lone pair. The hydrogen bond is described as an electrostatic dipole–dipole interaction with features of a covalent bond.

HF is the strongest hydrogen donor with fluorine being the most electronegative element, followed by oxygen and nitrogen. But not only electronegativity determines the quality as a donor, but also the number of bonded atoms. In HF, only one hydrogen atom is attached to fluorine and the whole intramolecular force is applied to a single H–F bond. In H_2O or alcohols, the already weaker electronegativity works on two bonds, either O–H or O–heteroatom, making water and alcohols significantly weaker hydrogen donors. In ammonia or any amine, the yet already weaker electronegativity is shared between three bonds, making amines weaker hydrogen donors than water and alcohols. The interactions between hydrogen bound to fluorine, oxygen, and nitrogen represent the strongest type of

hydrogen interaction, but the strength of hydrogen bonds also highly depends on other bonded atoms and the geometry.

Table 10 lists hydrogen bonds with calculated energies of a variety of dimers.^[128] The energies range from very strong as for the [F–H–F][–]-dimer to very weak as for the CH₄...F–CH₃-dimer. The idealized energies have to be taken as guiding values to compare different types of interactions, since the real environment in practice has a huge influence on geometry and energy. Traditionally, the HOH...OH₂-dimer with an energy of 4.7/5.0 kcal/mol is regarded as a moderately strong hydrogen bond and interactions of lower energy are regarded as weak hydrogen bonds. According to Table 11, weak hydrogen interactions are characterized by a relatively long distance of over 3.2 Å, a low energy of under 4 kcal/mol, as well as no significant detachment of the hydrogen atom from the donor atom.^[127] Weak hydrogen interactions play a significant role in the crystallography of organic and organometallic compounds. The vast majority of molecules contain saturated carbon atoms with 1–3 bonded hydrogen atoms and many molecules possess aro-

Table 10: Calculated hydrogen bond energies (kcal/mol) in some gas-phase dimers.^[128]

| Dimer | Energy |
|---|--------------------|
| [F–H–F] [–] | 39 |
| [H ₂ O–H–OH ₂] ⁺ | 33 |
| [H ₃ N–H–NH ₃] ⁺ | 24 |
| [HO–O–OH] [–] | 23 |
| NH ₄ ⁺ ...OH ₂ | 19 |
| NH ₄ ⁺ ...Bz | 17 |
| HOH...Cl [–] | 13.5 |
| O=C–OH...O=C–OH | 7.4 |
| HOH...OH ₂ | 4.7; 5.0 |
| N≡C–H...OH ₂ | 3.8 |
| HOH...Bz | 3.2 |
| F ₃ C–H...OH ₂ | 3.1 |
| Me–OH...Bz | 2.8 |
| F ₂ HC–H...OH ₂ | 2.1; 2.5 |
| NH ₃ ...Bz | 2.2 |
| HC≡CH...OH ₂ | 2.2 |
| CH ₄ ...Bz | 1.4 |
| FH ₂ C–H...OH ₂ | 1.3 |
| HC≡CH...C≡CH [–] | 1.2 |
| HSH...SH ₂ | 1.1 |
| H ₂ C=CH ₂ ...OH ₂ | 1.0 |
| CH ₄ ...OH ₂ | 0.3; 0.5; 0.6; 0.8 |
| C=CH ₂ ...C=C | 0.5 |
| CH ₄ ...F–CH ₃ | 0.2 |

matic carbon atoms with 1–3 bonded hydrogen atoms and many molecules possess aro-

Table 11: Strong, moderate and weak hydrogen bonds following the classification of Jeffrey. The numerical data are guiding values only.^[127].

| | Strong | Moderate | Weak |
|--|-------------------|----------------------|--------------------------|
| Interaction type | Strongly covalent | Mostly electrostatic | Electrostatic/dispersive |
| bond length [Å] | | | |
| H...A | 1.2–1.5 | 1.5–2.2 | >2.2 |
| lengthening of X–H | 0.08–0.25 | 0.02–0.08 | <0.02 |
| X–H versus H...A | X–H ≈ H...A | X–H < H...A | X–H ≪ H...A |
| X...A | 2.2–2.5 | 2.5–3.2 | >3.2 |
| Directionality | strong | moderate | weak |
| bond angles [°] | 170–180 | >130 | >90 |
| bond energy [kcal/mol] | 15–40 | 4–15 | <4 |
| relative IR shift Δν _{XH} [cm ^{–1}] | 25% | 10–25% | <10% |
| ¹ H downfield shift | 14–22 | <14 | |

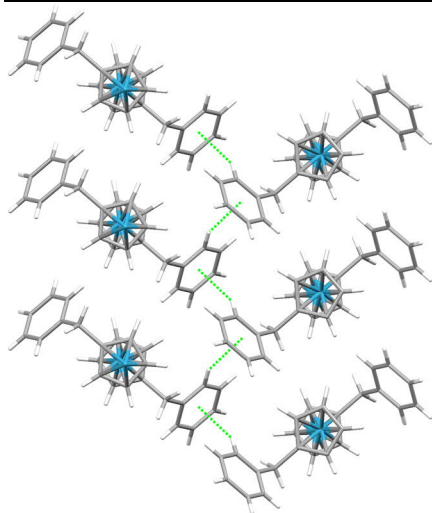


Figure 16: Polymeric LiCp(Bz), aligned by intermolecular hydrogen bonding between the benzyl-groups.^[37]

matic moieties. The aromatic π -system is a good hydrogen acceptor, demonstrated by the dimers $\text{HOH}\cdots\text{Bz}$, $\text{NH}_3\cdots\text{Bz}$, and $\text{CH}_4\cdots\text{Bz}$. Together with $\text{CH}\cdots\text{O}$ -interactions, aromatic hydrogen bonding can have important effects on both crystal packing and conformation of the molecule. The unsolvated coordination polymer LiCp(Bz) (Figure 16, see section 1.2.1) is an example.^[37] The packing of the polymeric strands is organized around intermolecular $\text{Bz-H}\cdots\text{Bz}$ hydrogen bonding with the hydrogen atom at the position C2 pointing towards the center of an adjacent benzyl ring. Hydrogen bonding connects the polymeric strands like a zipper.

Solvated indenyllithium is a good example for both intermolecular and intramolecular hydrogen bonding.^[52] Figure 17 depicts IndLi-TMEDA. Hydrogen bonding is indicated by cyan-colored lines between the hydrogen atoms and the aromatic carbon atoms. The legend below the picture contains a color code in different shades of cyan. The shade is relative to a simple indicator of interaction in crystallography:

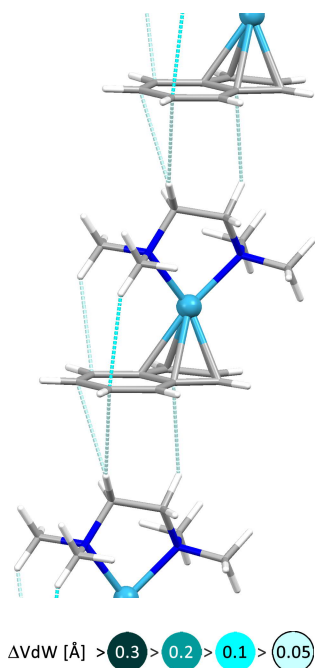


Figure 17: Intra- and intermolecular interactions of IndLi-TMEDA. The colour of the dashed contact lines indicates their relative length.

if the actual distance of two atoms is shorter than the sum of the Van-der-Waals (VdW) radii, in by far most cases an attractive interaction takes place. The color code further graduates the weak hydrogen bonding in steps of 0.1 Å. Stronger interactions with a VdW difference greater than 0.3 Å are depicted in dark cyan, very weak interactions with a VdW difference limit of 0.05 Å are depicted in light cyan. Below that internal mark, hydrogen bonding is most likely still present, but cannot be distinguished from arbitrary close contacts and gives little value in the analysis of the multitude of hydrogen-bond interactions. This depiction of $\text{H}\cdots\pi$ hydrogen bonding will be used throughout this work. It can serve as a guidance for analysis, since it is not possible without heavy efforts in computational methods or, if available, high-resolution XRD data, to reveal the true nature and strength of each interaction of each hydrogen atom with the indistinct π -cloud.

The hydrogen bonds of IndLi·TMEDA take place both intra- and intermolecularly. The lithium cation coordinates to the five-membered ring and allows the methyl groups to interact with the unoccupied six-membered ring of the anion. The interaction is most likely the reason for the orientation of the TMEDA ligand towards the six-membered ring in contrast to the sterically more beneficial arrangement askew to the anion. This motif is repeated in IndLi·PMDETA, (Me)IndLi·(THF)₃, and (Bu)IndLi·sparteine.^[75] The intermolecular interactions between the ethylene moiety and the uncoordinated side of the anion lead to a stacking of the complexes on top of each other. This stacking motif is apparent in all monomeric solvated CpLi and IndLi compounds and their derivatives. This demonstrates the significant impact of weak hydrogen bonds in the formation of crystal structures. In the mentioned examples, both intramolecular conformation and the pattern of the packing is affected by hydrogen bonds. The CH-hydrogen atoms are poor hydrogen donors and the flexibility in the orientation of the hydrogen atoms is very limited due to the hydrocarbon skeleton. A molecule that has both higher flexibility and hydrogen donor properties, is ammonia.

1.5. Ammonia as a Donor-Solvent

Ammonia is a key molecule of the modern world and one of the most produced chemicals. It plays the most important role in the production of fertilizers and is also the starting point in the industrial synthesis of all other nitrogen-containing chemicals.^[129] Fritz Haber and Carl Bosch developed the revolutionary Haber–Bosch process with research by Haber beginning in 1904 to the first commercial plant in 1913.^[130] The process consists in the direct reduction of gaseous nitrogen with gaseous hydrogen to ammonia with the use of α -iron as catalyst.

At room temperature, ammonia is a gas. It has a boiling point of $-33\text{ }^{\circ}\text{C}$ and a freezing point of $-77.7\text{ }^{\circ}\text{C}$ at 1 bar.^[131] In the liquid phase it has many similarities with water. H₂O is a good proton donor and has two lone pairs accessible for hydrogen bonding resulting in an effective interaction network. This makes water the showcase for hydrogen bonding.^[132] Ammonia, on the other hand, is a poorer hydrogen donor and has only one unoccupied lone pair for interaction and thus creates a weaker network of hydrogen bonds in the liquid phase, resulting in lower boiling and freezing points. However, regarding the size of the molecule, ammonia has a high vaporization enthalpy of $\Delta H_V = 23.35\text{ kJmol}^{-1}$ (H₂O: $\Delta H_V = 40.65\text{ kJmol}^{-1}$).^[133] Due to its physical properties, ammonia is also used as a refrigerant for industrial cooling systems known as R-717.

As a solvent in chemical synthesis, ammonia is of minor importance although it has many advantages. Its relative permittivity is lower than that of other polar solvents like H₂O,

Introduction

Ammonia as a Donor-Solvent

acetonitrile, and MeOH, but higher than that of THF (Table 12).^[134] Ammonia also has a high dipole moment and strong electron donating properties due to the lone pair and its small size. This allows ammonia to both dissolve a variety of organic compounds and electrolytes.^[135] As a solvent, it is particularly interesting for organometallic chemistry, especially for salt-like compounds such as the higher homologues of alkali-metal-cyclopentadienyl compounds, which are insoluble in THF. Ammonia is almost completely aprotic with a pK_a -value^[136] of 40 in DMSO and is deprotonated only by strong bases such as *n*-BuLi and LDA, but not by weaker bases like Li(HMDS). Ammonia can replace solvation-enhancing donor solvents like DME, TMEDA, PMDETA, and diglyme, which could possibly shield cations from reactions. The very high reduction barrier allows for the dissolution of highly potent reductants. Ammonia is well-known for its ability to dissolve alkali metals and higher alkaline earth metals from calcium to barium. In these solutions, electrons are solvated and cause a deep blue color, which remains stable for a reasonable amount of time. This feature is used for example in the *Birch*-reduction, the reduction of aromatic compounds with a benzene ring to 1,4-cyclohexadienes.

Table 12: Relative permittivity, dipole moments, and pK_a -values of various solvents.^[134, 136-137]

| | H ₂ O | Acetonitrile | MeOH | NH ₃ | THF | Toluene |
|--------------|-------------------------|--------------|-------------------------|-----------------------|-------------|-----------------------|
| ϵ_r | 80.10 (20°C) | 36.64 (20°C) | 32.0 (20°C) | 16.61 (20°C) | 7.52 (22°C) | 2.379 (24°C) |
| Dipole [D] | 1.85 | 3.92 | 1.70 | 1.47 | 1.75 | 0.38 |
| pK_a | 15.7 (H ₂ O) | 31.3 (dmsO) | 15.5 (H ₂ O) | 38 (H ₂ O) | | 41 (H ₂ O) |
| | 32 (dmsO) | | 27.9 (dmsO) | 41 (dmsO) | | 43 (dmsO) |

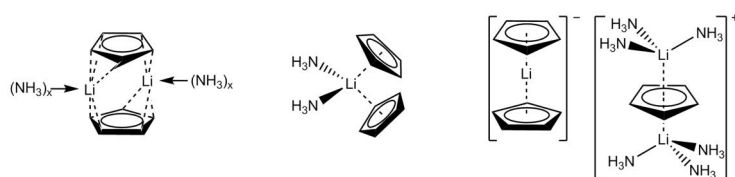
Gaseous ammonia can be bought in different purity grades ranging from $\geq 99.98\%$ to $\geq 99.9999\%$.^[138] Therefore, it is suitable for the work with highly moisture-sensitive compounds. Other solvents with similar beneficial properties like acetonitrile are difficult to dry from moisture. After evaporation of ammonia, the product is solvent-free, an advantageous feature.

Table 13: Solubility of gaseous ammonia in a range of non-aqueous solvents.^[140]

| Solvent | T [K] | Mole fraction |
|-------------------|-------|---------------|
| Hexane | 293.2 | 0.0233 |
| | 298.2 | 0.0146 |
| Benzene | 293.2 | 0.0359 |
| Methanol | 298.2 | 0.304 |
| Ethanol | 298.2 | 0.179 |
| Trichloromethane | 298.2 | 0.125 |
| THF | 298.2 | 0.140 |
| Et ₂ O | 288.2 | 0.125 |

The reason for the only marginal role as a solvent in industry and academia is the small employable temperature range between $-77.7\text{ }^\circ\text{C}$ and $-33\text{ }^\circ\text{C}$, the high energy costs for liquefaction and evaporation, and its corrosive and hazardous properties.^[139] To make use of the strong donating properties of ammonia without being limited to the inconvenient temperature range, gaseous ammonia can be dissolved up to a considerable mole fraction in THF or Et₂O (Table 13).^[140]

1.5.1. Ammoniacates of LiCp



Scheme 12: Structural suggestions of LiCp in liquid ammonia by Brandsma et al. derived from cryoscopy.

Brandsma et al. were the first to analyze organolithium compounds in liquid ammonia.^[141] Via cryoscopy, they analyzed the aggregation of $\text{PhC}\equiv\text{CLi}$, PhOLi , PhSLi , $\text{H}_2\text{C}=\text{C}(\text{OLi})\text{Ph}$, and LiCp. They determined the presence of a dimeric structure or a higher aggregate and suggested different structures (Scheme 12) including a sandwich complex of two lithium cations, a titanocene–dichloride-type complex, and a lithocene-containing SSIP.

LiCp is an excellent case to study the effects of solvation with ammonia. LiCp and most of other alkali-metal–cyclopentadienyl derivatives are exclusively soluble in THF due to their salt-like character.^[28, 142] In preceding research to this work, two ammonia-solvated structures of LiCp were observed: the co-coordinated lithocene $\text{Cp}_2\text{Li}_2(\text{NH}_3)_3$ (**1**) and the SSIP $[\text{Li}(\text{NH}_3)_4][\text{Cp}]\cdot\text{NH}_3$ (**2**) (Figure 18).^[143] $\text{Cp}_2\text{Li}_2(\text{NH}_3)_3$ (**1**) was synthesized by saturating a solution of LiCp in THF with gaseous ammonia at $-15\text{ }^\circ\text{C}$ and crystallization at $-23\text{ }^\circ\text{C}$, whereas $[\text{Li}(\text{NH}_3)_4][\text{Cp}]\cdot\text{NH}_3$ (**2**) was synthesized by highly oversaturating a solution of LiCp in THF by condensation of a large amount of ammonia at $-78\text{ }^\circ\text{C}$ and subsequent crystallization at $-45\text{ }^\circ\text{C}$. The two structures are very different, but both are strongly modeled by $\text{NH}\text{-}\pi$ hydrogen bonding.

Structure **1** is a lithocene fragment with a co-coordinated $\text{Li}(\text{NH}_3)_3$ moiety and structure **2** is a SSIP with a naked Cp anion, a $\text{Li}(\text{NH}_3)_4^+$ cation, and lattice ammonia. Structures **1** and **2** represent the stepwise solvation of LiCp with ammonia as presented in Scheme 13. In the first step of solvation, every second lithium cation of a LiCp strand is solvated by ammonia, thus fragmenting the LiCp-strands into complexes of **1**. Thereby, the complexes remain in a linear arrange-

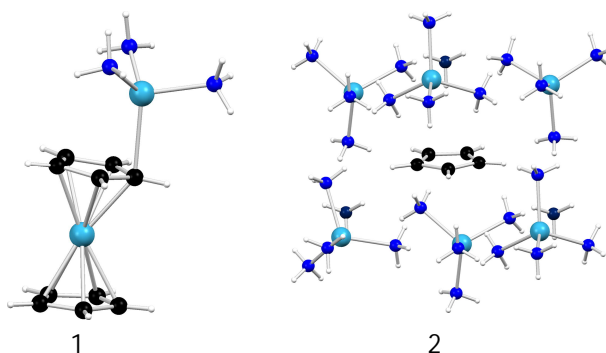
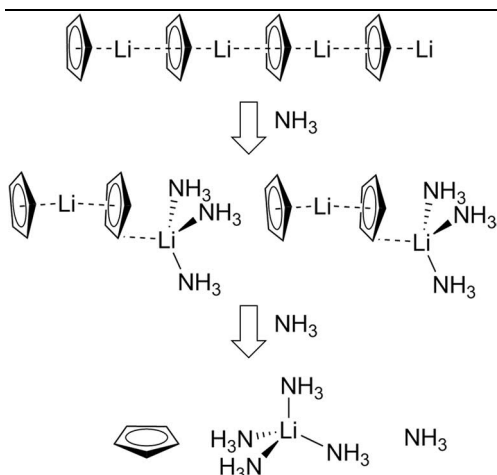


Figure 18: First published LiCp-ammoniacates by Michel et al.: the co-coordinated lithocene $\text{Cp}_2\text{Li}_2(\text{NH}_3)_3$ (**1**) and the SSIP $[\text{Li}(\text{NH}_3)_4][\text{Cp}]\cdot\text{NH}_3$ (**2**). The lattice ammonia of **2** is highlighted in dark blue.

Introduction

Ammonia as a Donor-Solvent



Scheme 13: Subsequent breakup of LiCp-strands into **1** and **2** by solvation of ammonia.

by $\text{Li}(\text{NH}_3)_4^+$ cations and lattice ammonia. Cations and lattice ammonia interact via NH–N hydrogen bonding and form channels perfectly suiting the Cp anions. The formation of naked Cp is extremely remarkable since the next anticipated step of solvation would have rather been a monomeric CIP like $\text{CpLi}\cdot(\text{NH}_3)_3$, resembling the LiCp adduct of DME, TMEDA, and PMDETA. Free Cp by solvation has only been achieved by crown ethers as in $[\text{Na}(\text{12-crown-4})_2][\text{Cp}]$, $[\text{K}(\text{15-crown-5})_2][\text{Cp}]$, and $[\text{K}(\text{15-crown-5})_2][\text{Cp}]$. Through chelation, crown ethers have a very high affinity for cations overcoming the affinity of the cation for the Cp anions. Although 12-crown-4 is able to solvent-separate NaCp, it forms the monomeric CIP $\text{CpLi}\cdot(\text{12-crown-4})$ with LiCp. Diglyme is able to solvent-separate LiCp under formation of lithocene in $[\text{Li}(\text{diglyme})_2][\text{Cp}_2\text{Li}]$. Thus, not even 12-crown-4

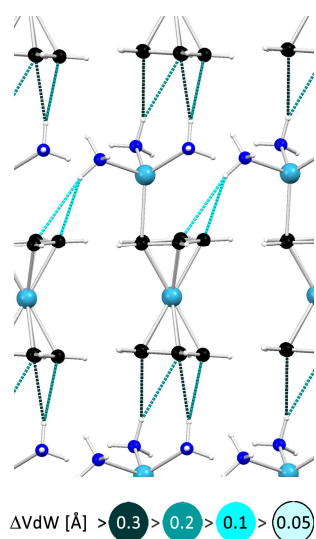


Figure 19: Intermolecular NH- π hydrogen bonding in **1**.

and diglyme are able to overcome the attraction of the lithium cation to the Cp anion. The fourfold complexation with ammonia cannot explain the formation of naked Cp alone. And if the reason was an extremely high donor quality of ammonia alone, the formation of the much less solvated structure **1** could not be explained with that argumentation.

Subsequent solvation with more molecules of ammonia leads to a total disassembling of the LiCp strands to naked Cp anions, surrounded

by $\text{Li}(\text{NH}_3)_4^+$ cations and lattice ammonia. Cations and lattice ammonia interact via NH–N hydrogen bonding and form channels perfectly suiting the Cp anions. The formation of naked Cp is extremely remarkable since the next anticipated step of solvation would have rather been a monomeric CIP like $\text{CpLi}\cdot(\text{NH}_3)_3$, resembling the LiCp adduct of DME, TMEDA, and PMDETA. Free Cp by solvation has only been achieved by crown ethers as in $[\text{Na}(\text{12-crown-4})_2][\text{Cp}]$, $[\text{K}(\text{15-crown-5})_2][\text{Cp}]$, and $[\text{K}(\text{15-crown-5})_2][\text{Cp}]$. Through chelation, crown ethers have a very high affinity for cations overcoming the affinity of the cation for the Cp anions. Although 12-crown-4 is able to solvent-separate NaCp, it forms the monomeric CIP $\text{CpLi}\cdot(\text{12-crown-4})$ with LiCp. Diglyme is able to solvent-separate LiCp under formation of lithocene in $[\text{Li}(\text{diglyme})_2][\text{Cp}_2\text{Li}]$. Thus, not even 12-crown-4

and diglyme are able to overcome the attraction of the lithium cation to the Cp anion. The fourfold complexation with ammonia cannot explain the formation of naked Cp alone. And if the reason was an extremely high donor quality of ammonia alone, the formation of the much less solvated structure **1** could not be explained with that argumentation. The major role in the formation of **1** and **2** is played by NH- π hydrogen bonding. In structure **1**, the $\text{Li}(\text{NH}_3)_3$ -moiety is involved in NH- π hydrogen bonding with both sides of the lithocene fragment (Figure 19). Comparatively strong interactions take place between the complexes having the original linear LiCp-like arrangement. Two molecules of ammonia point towards the single coordinated Cp anion of the next complex and lock the complexes in their linear arrangement.

Another weak interaction takes place between the third ammonia molecule and the unoccupied space at the twofold coordinated Cp-anion of the next complex outside the linear arrangement. This interaction contributes to the stabilization of the η^1 -coordination of the $\text{Li}(\text{NH}_3)_3$ moiety.

In the case of **2** (Figure 20), the $\text{Li}(\text{NH}_3)_4^+$ cations and the lattice ammonia molecules, interconnected by NH–N hydrogen bonding, form a matrix of channels filled with Cp anions. Various NH- π hydrogen bonds fix the anions within the channels. The average strength of the hydrogen bonds is weaker than in **1**, but they are far more numerous.

Seven to eight hydrogen atoms form hydrogen bonds to the Cp anion and thus stabilize the uncoordinated form of Cp. This kind of self-assembly is unique to ammonia. It combines the flexible coordination, its small size, and its ability for hydrogen bonding to create an efficient network overcoming the attraction of the lithium cation to the Cp anion.

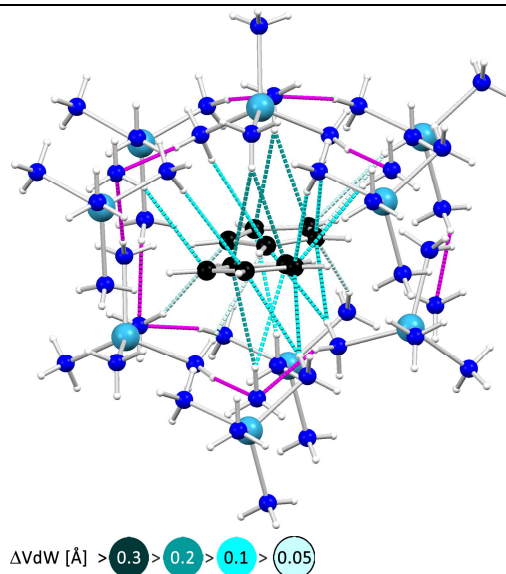


Figure 20: Intermolecular NH-N (magenta) and NH- π interactions in **2**.

2. Scope

Despite the aforementioned powerful properties of ammonia as a donor solvent in organometallic chemistry, only relatively little attention has been drawn to research on this subject. Thanks to its small size, its sterically unrestrained donating center, its high dipole moment and its relative permittivity, the ammonia molecule exhibits high potential in solvation, aggregation, and enhancing the reactivity of organometallic compounds. The high reduction barrier strongly benefits sensitive reactions and the easy, residual-free removal of the solvent has the potential to both save time and increase the yield. The limited temperature range of applicability in pure form can even be expanded by dissolving ammonia in aprotic polar solvents.

In order to explore the potential and properties of ammonia as solvent, alkali-metallated cyclopentadienyl derivatives are the compounds of choice. Alkali-metallated organic compounds require strong donating aprotic solvents for stabilization and their typical temperature of application matches the temperature range of ammonia being liquid. Alkali-metal cations are inert and have a flexible coordination sphere, both features rendering them compatible to ammonia. The solvation of alkali metals constitutes the most prominent reaction in liquid ammonia.

The cyclopentadienyl derivatives Cp', Cp*, indenyl, and fluorenyl are widely used in coordination chemistry as ligands and scaffolds of important catalysts and reagents (e.g. Kaminsky catalysts, and Tebbe's reagent). Their anionic nature and molecular size place their complexes with alkali metals between salt-like compounds and larger organic molecules. They can therefore be considered model systems for a huge variety of organometallic compounds. The chosen cyclopentadienyl derivatives are easily available and practical in application. The π -system of the anions enables the investigation of an important property of ammonia in solvation and stabilization: the ability to form hydrogen bonds. This property distinguishes ammonia from most other aprotic solvents.

This work will shed light on the respective roles of the cation, the anion, and the ammonia molecules in solid-state aggregation of ammonia-solvated complexes of alkali metals and cyclopentadienyl derivatives. X-ray diffraction and computational methods will be applied to elucidate the distinct features and common themes found in these systems as well as the particular role of hydrogen bonding.

3. Results

3.1. Lithium Derivatives

3.1.1. $[\text{Li}(\text{NH}_3)_4][\text{Cp}']$ (3): A Solvent-Separated Ion Pair

$[\text{Li}(\text{NH}_3)_4][\text{Cp}']$ (3) was synthesized by saturating a solution of $\text{Cp}'\text{Li}$ in THF with gaseous ammonia and subsequent crystallization at -83°C . The crystals are very thin, colorless plates of high sensitivity to moisture and elevated temperatures. Sample preparation and mounting on the diffractometer proved very difficult. Compound 3 crystallizes in the triclinic space group $P\bar{1}$ as a SSIP with two $\text{Li}(\text{NH}_3)_4^+$ -cations and two Cp' -anions in the asymmetric unit (Figure 21).

Both cations show a significant distortion from the ideal tetrahedral angle (Figure 22). One N–Li–N angle in the Li1-cation is widely opened ($125.0(1)^\circ$, N1–Li1–N2). The opposite angle N3–Li1–N4 is reduced to $98.20(9)^\circ$. The equivalent angles at Li2 are N5–Li2–N6 with $125.8(2)^\circ$ and N7–Li2–N8 with $98.29(9)^\circ$. The cause of the distortions is the NH– π attraction of the ammonia molecules to the neighboring anions in the crystal. Figure 22 displays the short contacts of the ammonia hydrogen atoms of the cation containing Li1 with the π -system of two adjacent anions. Each Li cation faces two anions on two of its four tetrahedral faces. Two ammonia units interact with both anions via NH– π bonding, the other two NH_3 -molecules interact with only one of the two adjacent anions each. The shortest NH–C contacts marked with the darkest color code lie between $2.40(2) \text{ \AA}$ and $2.58(2) \text{ \AA}$. They are more than 0.3 \AA shorter than the sum of the respective van-der-Waals (VdW) radii which amounts to 2.9 \AA . Together with the contacts between 2.60 \AA and 2.70 \AA

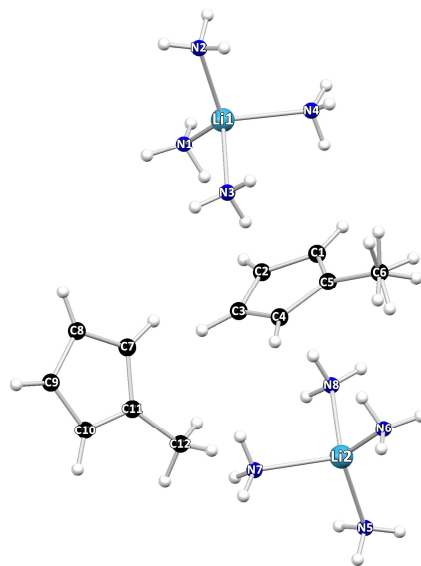


Figure 21: Asymmetric unit of $[\text{Li}(\text{NH}_3)_4][\text{Cp}']$ (3). The hydrogen atoms of C6 are disordered by 72%(14). Li–N distances range from $2.036(2) \text{ \AA}$ to $2.085(2) \text{ \AA}$.

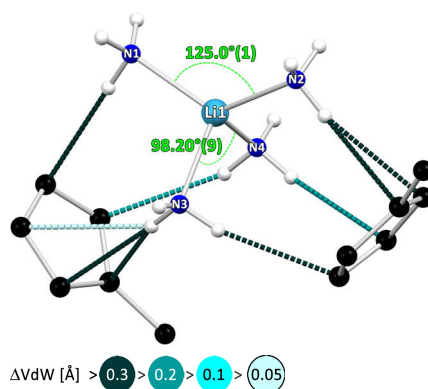


Figure 22: NH– π interactions of the Li1-cation with two adjacent anions. All other N–Li–N angles range from $106.0^\circ(1)$ to $110.3^\circ(1)$. The Li2-cation has a similar interaction pattern.

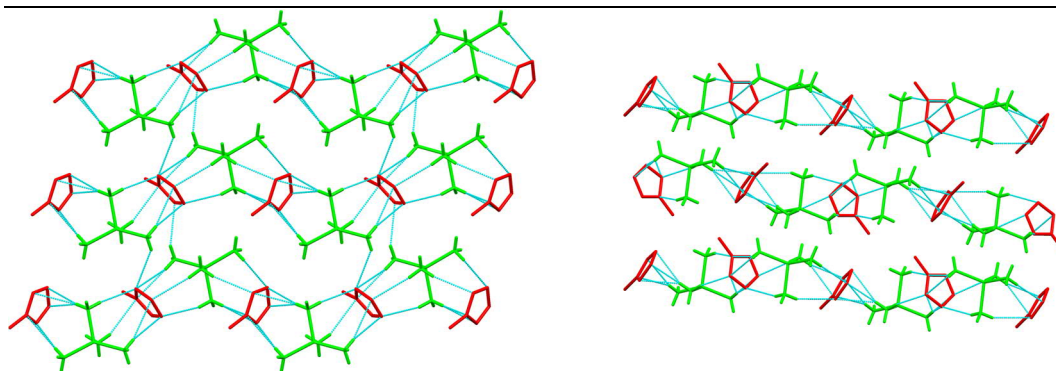


Figure 23: Packing plot of **3**. Anions are drawn in red, cations in green, and NH- π interactions in cyan. CH hydrogen atoms have been omitted. Left: view along the b-axis; cations and anions are forced into a zig zag arrangement; the zig zag strands are interconnected by additional NH- π interactions. Right: view along a; the interactions form layers that are not interconnected.

(drawn in dark cyan, 0.2 Å shorter than the sum of the VdW radii) they reflect the strongest interactions of the ammonia hydrogen atoms with the π -system of the anion. The two NH₃ molecules which interact with only one anion are pulled apart from each other, resulting in a stretched angle.

Each cation strongly interacts with two adjacent anions and vice versa. The packing in **3** can therefore be described as a zig zag arrangement of cations and anions induced by NH- π hydrogen bonding (Figure 23). The zig-zag strands are packed on top of each other and are interconnected by weaker NH- π bonding (distances 2.65(2) Å and 2.73 (2) Å), resulting in a layered structure. No notable NH- π bonding can be observed between the layers.

3.1.2. [Li(NH₃)₄][Cp*₂Li]·(NH₃)_{0.87} (**4**): A Lithocene-Derivative

[Li(NH₃)₄][Cp*₂Li]·(NH₃)_{0.87} (**4**) was synthesized by adding Cp*H to a solution of Li(HMDS) in liquid NH₃. Subsequent crystallization at -45 °C generated colorless needle-shaped crystals. Compound **4** crystallizes in the orthorhombic space group *Pccn* and the asymmetric unit (Figure 24) consists of a Cp* anion η^5 -coordinated by a lithium cation, on its part coordinated by two molecules of ammonia and a single molecule of lattice-ammonia. The site occupation is 86.7(6) %. The Cp* fragment is part of a lithocene anion, completed by inversion in the position of Li2. The lithium cation Li1 with the two molecules of ammonia is part of a Li(NH₃)₄⁺-cation, which is completed by rotation around a twofold axis laying on the position of Li1. Several parts of the structure are disordered: all hydrogen atoms of the Cp*-methyl groups are disordered by rotation about the C-C bond (not depicted in the shown figures), the ammonia molecule containing N2 is disordered at a second position (N2A) by 50(4) %, also the hydrogen atoms bound to N3 exhibit symmetry induced disorder. The types of disorder of N2/N2A and N3 are related to each other, driven by NH-N hydrogen bonding (Figure 25).

The NH_3 -molecules with N2/N2A and N3 are close to each other. The molecule containing N3 faces the ammonia molecule containing N2/N2A either with the nitrogen atom or with its hydrogen atoms. When the molecule containing N3 faces N2/N2A with its nitrogen atom, NH–N hydrogen bonding occurs. When it faces N2/N2A with its hydrogen atoms, steric repulsion pushes the ammonia molecules apart. The hydrogen atom H2E connected to N2A points directly towards N3 with a distance of 2.52(2) Å. The interplay of NH–N hydrogen bonding and steric repulsion explains the 50 %-ratio of the N2/N2A-disorder.

The N–Li1–N-angles between the two disordered N2-moieties are widely bent with 132.9(2)° for N2–Li1–N2, 133.0(2)° for N2–Li1–N2A, and 135.1(2)° for N2A–Li1–N2A. The opposite angle of N1–Li2–N1 is diminished to 99.0(2)°. The bending is caused by hydrogen bonding of the ammonia molecules with the π -system of the Cp-derivative in a similar way as in **3**. The cation in **4** faces the ring planes of two anions. Two molecules of ammonia—N1 and its symmetry equivalent—interact with two anions (Figure 25). The ammonia molecules containing N2 and N2A interact with one single anion. Similar to the structure of **3**, the angle between the singly-interacting molecules is widened and the angle between the bridged molecules is reduced.

Possible explanations for the stronger bending in **4** than in **3** are the slightly different orientation of the C_5 -perimeters towards the $\text{Li}(\text{NH}_3)_4^+$ -cation and the different environment in the crystal. The positions of the C_5 -perimeters in **3** and **4** are pretty similar, although the steric de-

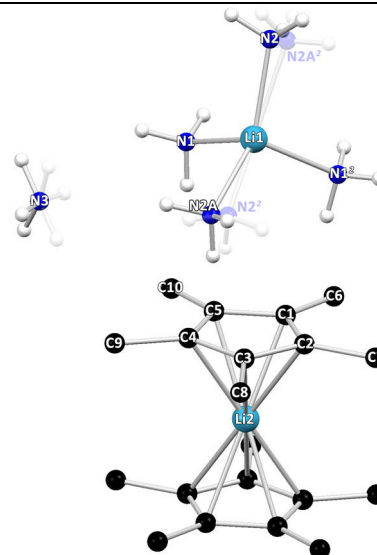


Figure 24: $[\text{Li}(\text{NH}_3)_4][\text{Cp}^*_2\text{Li}]\cdot(\text{NH}_3)_{0.87}$ (**4**). CH-hydrogen atoms have been omitted for clarity. The two anions of lithocene are symmetry related by inversion in the position of Li2. Superscript '2' indicates symmetry generation by a twofold axis. The ammonia molecules of N2 is disordered (N2A) by 50(4)%. The hydrogen atoms of N3 are disordered by rotation around a twofold axis.

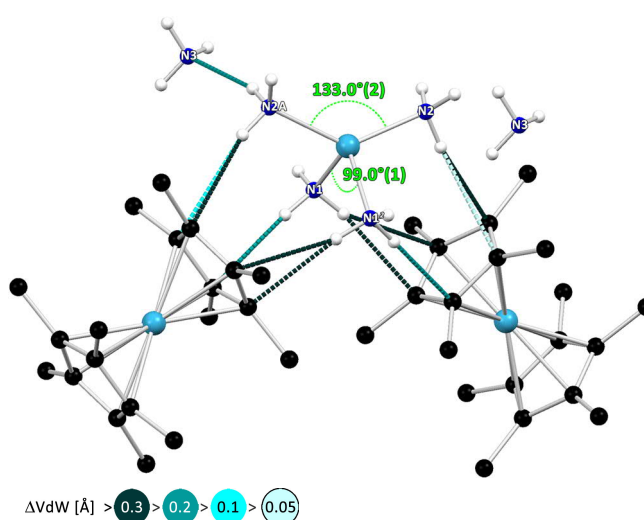


Figure 25: Interactions of the $\text{Li}(\text{NH}_3)_4^+$ -cation with the environment: The two assumed positions of the cation, the lattice- NH_3 , and the related interactions are drawn full and transparent as well as the second Cp* of the lithocene.

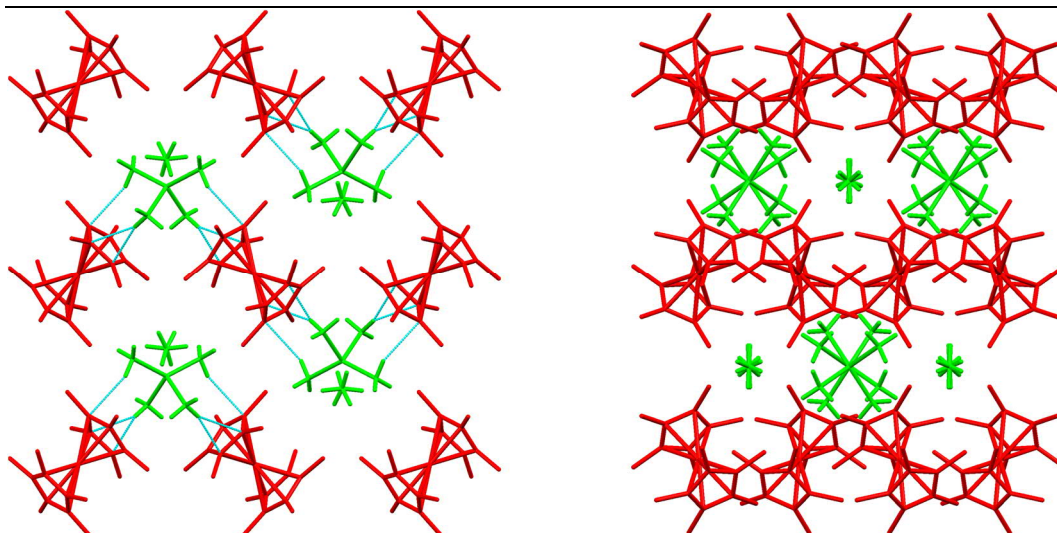


Figure 26: Crystal packing of **4** along *a* (left) and *c* (right). Lithocene (red) and $\text{Li}(\text{NH}_3)_4^+$ form a zig zag pattern forced by $\text{NH}-\pi$ interactions (cyan). These strands have two alternating directions, leaving a void partially filled with lattice- NH_3 .

mand of Cp^* is much higher than that of Cp' . The angles between the anionic planes facing the cations are similar in both **3** ($77.25(5)^\circ$) and **4** ($80.71(3)^\circ$). The ranges of the $\text{NH}-\text{C}$ interactions are also similar, the distances being $2.40 \text{ \AA}-2.88 \text{ \AA}$ in **3** and $2.51 \text{ \AA}-2.81 \text{ \AA}$ in **4**. The stronger bending in **4** might be caused by push-pull effects of the surrounding fragments. In **3**, the cations exhibit strong $\text{NH}-\pi$ bonding with the two closest anions, but also weaker interactions with other anions in their close proximity. These attractive forces possibly narrow the bent $\text{N}-\text{Li}-\text{N}$ -angles in **3** compared with **4**. In **4**, the close environment of $\text{Li}(\text{NH}_3)_4^+$ consists of methyl groups of Cp^* anions in close proximity resulting in steric repulsion.

The anions and cations form a zig-zag pattern in the crystal similar to **3** (Figure 26) due to a similar interaction pattern. The lithocene anion is much larger and bulkier than the Cp' anion and cannot be packed as efficiently as the cations and anions in **3**. The zig zag strands leave larger voids in the crystal packing, which are partially filled with lattice ammonia molecules.

The most prominent structural feature of **4** is arguably the Cp^* -lithocene anion. According to the CSD (CSD, v. 5.37, Nov.2015, last Update Feb. 2016) it is to this day the first of its kind and only the third structure with lithium coordinating Cp^* . The first compound is the base-free Cp^*Li characterized by *Dinnebier* et al. via powder diffraction. Here, linear ‘multidecker’ contact polymers are found, similar to the structure of base-free CpLi .^[43a] The second one is a tri-phosphaferrocene by *Nixon* et al., co-coordinated by lithium.^[144] In the CSD, base-free Cp^* metallocenes (297 hits) are listed which are dominated by metals of the first transition series (232 hits), especially iron (127 hits) and cobalt (60 hits). No

Cp^{*}-metallocenes of alkali metals have been observed yet, and only seven Cp^{*}-metallocenes of alkaline earth metals. Compared with the already known base-free and non-co-ordinated Cp lithocenes found by *Harder et al.*, *Mews et al.*, and *Stalke et al.* there is no significant difference in the structure.^[47a, 51a, 51b, 51d, 51e] The lithium cation is η⁵-coordinated and the ligands are orientated in a parallel and staggered way. Notably, the distance of the lithium cation to the ring plane, at 1.899(6) Å, is significantly shorter than the Cp–lithocene distance, at 1.968 Å–2.006 Å. This is due to the higher negative charge in the aromatic ring induced by the methyl groups.

The formation of the Cp^{*}-lithocene complex can be explained by the high steric demand of the methyl groups. The π-density can be approached by ammonia hydrogen atoms only from directly above. In the case of Cp and Cp', nearby ammonia hydrogen atoms can interact with the π-density from more directions. The smaller size of Cp and Cp' also allows them to be incorporated in a framework of NH–π bonding. Therefore, the η⁵-coordination is preferred and the ammonia molecules play the same role as diglyme in [Li(diglyme)₂][Cp₂Li], in which two molecules of diglyme coordinate a lithium ion with lithocene as the counterion.

3.1.3. [Li(NH₃)₄][Ind] (5): A zig zag -Pattern

[Li(NH₃)₄][Ind] (5) was synthesized by saturating a solution of Li(HMDS) and indene in a mixture of THF and Et₂O with ammonia at –15 °C and subsequent crystallization at –16 °C. **4** crystallizes in the orthorhombic space group *P*2₁2₁2₁ as a SSIP consisting of uncoordinated ind[–] and Li(NH₃)₄⁺ (Figure 27). The interactions between cations and anions are similar to those in **3** and **4** (Figure 29). But compared to the previous Cp derivatives, the additional six-membered ring of ind[–] exerts two effects: the negative charge is distributed over a larger π-system and the anion provides more access to NH–π interactions. The general patterns of interaction and crystal packing are similar to **3** and **4**. Two anions face two tetrahedral faces of a cation and vice versa. The interactions are also similar, but with some notable differences: In **3** and **4**, bridging interactions between two NH₃-molecules of each cation and the adjacent anions can be found as well as single interactions between these partners. This binding scheme is different in **5**. Here, the ammonia molecule with N1 bridges a five- and a six-membered ring, whereby the binding to the five-membered ring is particularly strong. The other

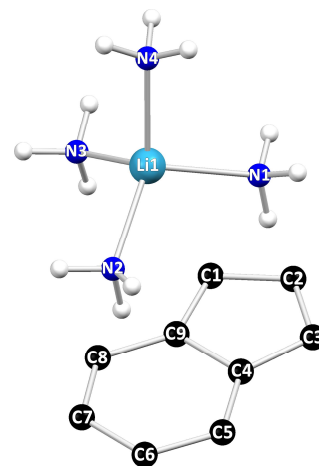


Figure 27: Asymmetric unit of [Li(NH₃)₄][Ind] (5). CH-hydrogen atoms have been omitted for clarity.

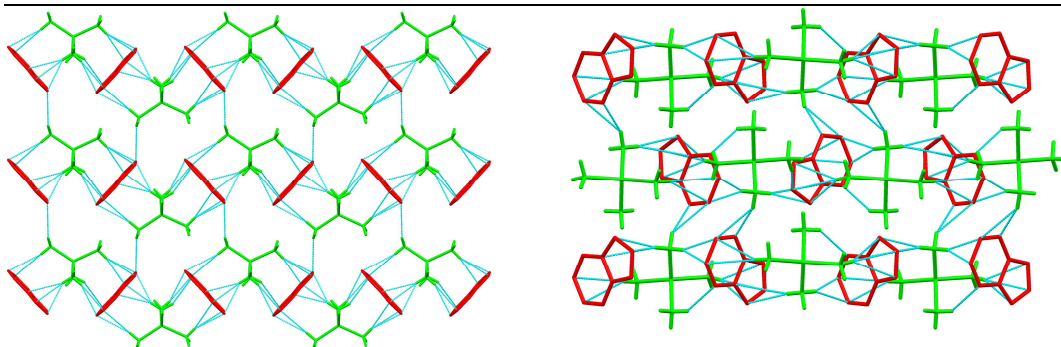


Figure 28: Crystal packing of $[\text{Li}(\text{NH}_3)_4][\text{Ind}]$. Cations are drawn in green, anions in red. Left: View along the b-axis (only one layer of molecules); Right: View along the a-axis; interactions are present between the zig zag strands in all directions.

three ammonia molecules interact with only one of the two adjacent anions. The ammonia molecules containing N2 and N3 show weak interactions with the six-membered rings and N4 is strongly attracted to the five-membered ring. NH- π bonding to the five-membered ring is preferred over bonding to the six-membered ring because the higher charge concentration in the five-membered ring induces a stronger attraction. The strong association with the five-membered ring is also reflected in the angles of the planes facing

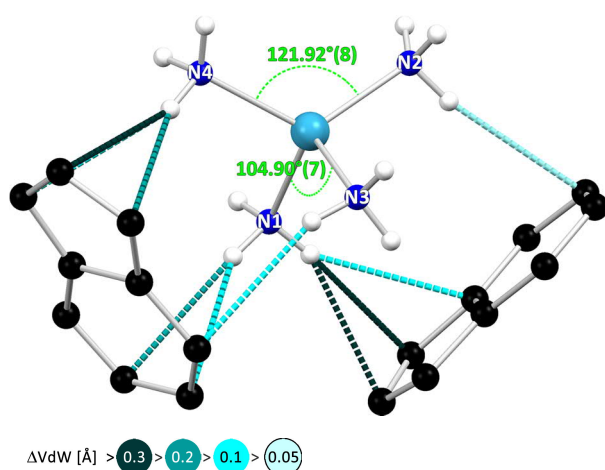


Figure 29: NH- π interactions of the $\text{Li}(\text{NH}_3)_4^+$ -cation with the adjacent ind⁻-fragments.

the cation. The planes of the two indenyl anions facing one cation have an angle of $87.47(3)^\circ$, whereas the angle between the two tetrahedral faces of the cation (N1/N2/N3 and N1/N3/N4) is $69.40(4)^\circ$.

The cation itself is not as distorted as in **3** and **4**. The N2-Li-N4-angle is widened to $121.92(8)^\circ$, similar to the corresponding widened N-Li-N-angles in **3** ($125.0(2)^\circ$ – $125.8(2)^\circ$) and **4**, ($132.9(2)^\circ$ – $135.1(2)^\circ$), but the N1-Li-N3-

angle, at $104.90(7)^\circ$, is not as reduced as in the previous structures.

The resulting crystal packing is similar to the zig-zag arrangement (Figure 28) in **3**. Cations and anions form zig-zag strands, which are stacked upon and next to each other. NH- π bonding connect each zig-zag strand with the two horizontally neighboring and the two vertically neighboring strands.

3.1.4. $[\text{Li}(\text{NH}_3)_4][\text{Flu}]\cdot(\text{NH}_3)_2$ (**6**): Anionic Channel

$[\text{Li}(\text{NH}_3)_4][\text{Flu}]\cdot(\text{NH}_3)_2$ (**6**) was synthesized by adding *n*-butyllithium to a solution of fluorene in *t*-BuOMe and subsequent condensation of ammonia until the solution turned clear. Crystallization at -76°C yielded orange crystals. **6** crystallizes in the monoclinic space group *Pn*. The asymmetric unit consists of two

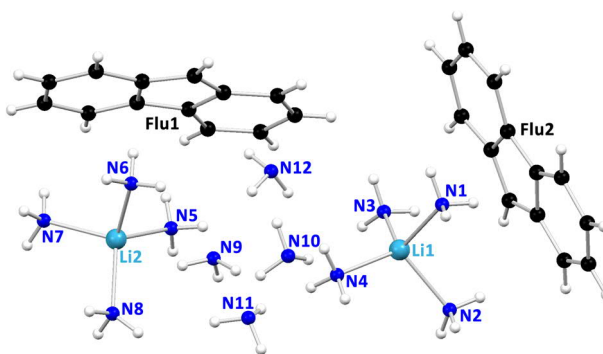


Figure 30: Asymmetric unit of $[\text{Li}(\text{NH}_3)_4][\text{Flu}]\cdot(\text{NH}_3)_2$. CH-hydrogen atoms have been omitted for clarity. Carbon atoms with letter 'A' indicate disordered moieties with an occupation below 7%.

$\text{Li}(\text{NH}_3)_4^+$ cations, two uncoordinated fluorenyl anions, and four lattice- NH_3 molecules (Figure 30). 6.5(3) % and 2.6(4) % of the two types of fluorenyl anions are disordered. Since the disordered fractions are small, they will not be discussed in this section. The fluorenyl anions form rhomboid-shaped channels along the *b*-axis (Figure 31). Hereby, the anions are not arranged in a co-parallel way to each other, but are inclined by 15.7° and 18.7° (values calculated by XP without error consideration) with respect to the direction of the channel. Within the channel segments of four anions, the $\text{Li}(\text{NH}_3)_4^+$ cations are located in the corners and the voids between the cations are filled with four molecules of lattice ammonia. Two types of hydrogen bonds are present: $\text{NH}-\pi$ bonding and $\text{NH}-\text{N}$ bonding. Both cations and lattice- NH_3 molecules interact with the π -system of the anion and form a network of $\text{NH}-\text{N}$ hydrogen bonds with each other.

The cations interact with two adjacent anions via three hydrogen atoms each (Figure 32). Two ammonia molecules in each cation bridge two anions mostly at the C_6 -perimeter. The other two ammonia molecules interact solely with the C_5 -ring.

The ammonia molecule with N5 interacts with one five-membered ring only and the one with N8 stacks to a six-membered ring. The lattice- NH_3 molecules interact with the area not occupied by the cations.

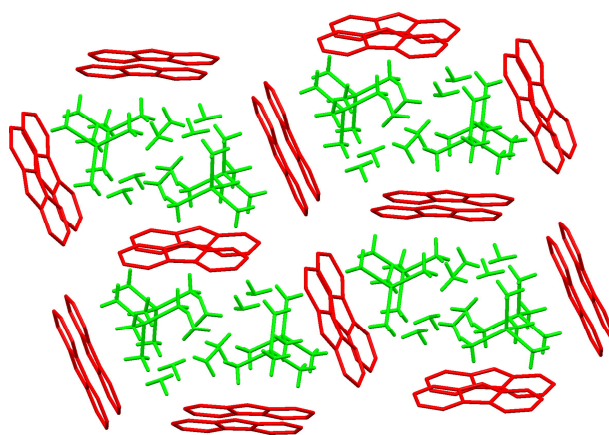


Figure 31: Packing plot of $[\text{Li}(\text{NH}_3)_4][\text{Flu}]\cdot(\text{NH}_3)_2$ (**6**). Anions are drawn in red, cations and lattice- NH_3 in green.

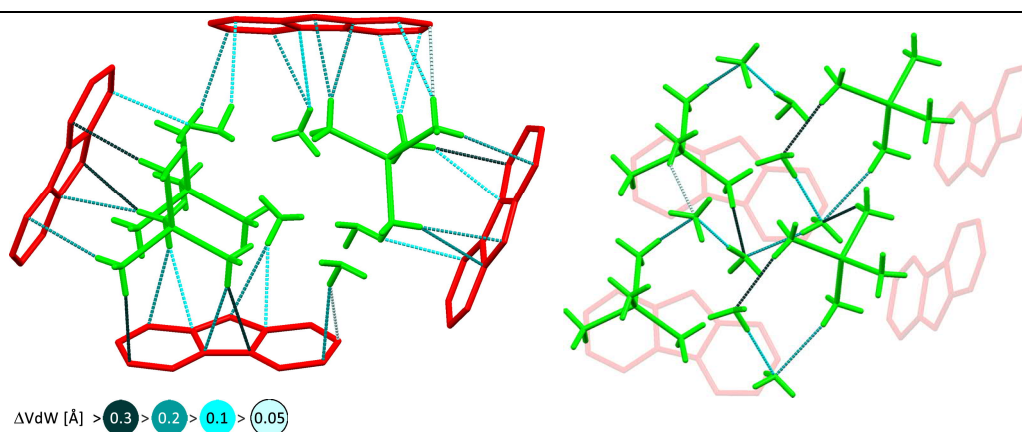


Figure 32: Display of the various NH- π interactions of $\text{Li}(\text{NH}_3)_4^+$ -cations and lattice ammonia with the anions (left) and NH-N interactions between lattice ammonia itself and the cations.

The fluorenyl anion containing C1–C13 is associated with four hydrogen atoms on each side of the π -system, the fluorenyl anion containing C14–C26 is associated with five hydrogen atoms from one side and six hydrogen atoms from the other side of the π -system.

The lattice- NH_3 molecules between the cations form a network with ten distinct NH-N hydrogen bonds all along the direction of the channel with the N-H distances ranging from 2.32(2) Å to 2.72(2) Å. The ammonia molecules containing N9 and N10 interact with three adjacent hydrogen atoms and provide one hydrogen atom for association with other lattice- NH_3 molecules. The NH_3 molecules containing N11 and N12 interact with two adjacent hydrogen atoms and also provide one hydrogen atom for NH-N bonding. Strong attractive interactions are present between the lattice NH_3 molecules and the hydrogen atoms of the cations.

A distortion of the $\text{Li}(\text{NH}_3)_4^+$ cations similar to the one seen in the structures 3-5 can be observed in **6** as well, but on a smaller scale. As in the previous structures, the N-Li-N angles in the non-anion-bridging ammonia molecules are widened. The respective angles in **6** are N3-Li1-N4, at 116.6(2)°, and N5-Li2-N8, at 114.5(2)°. Therefore, the cations in **6** are not as distorted as in 3-5 with bending angles ranging from 122.0(1)° to 135.1(2)°.

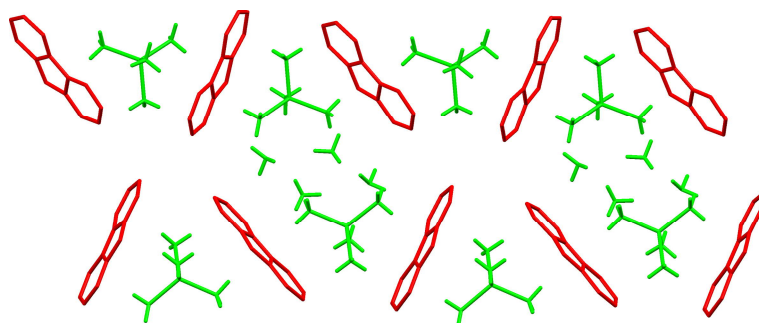


Figure 33: Zig zag arrangement of cations and anions in **6**.

The small bending can be explained by the presence of the lattice solvent. It flexibly fills the gap between the two cations and allows an optimized arrangement of both cations and anions. The geometry of the anions fits the geometry of the cations very well. The angle between the planes of the anions that face both the cation containing Li1 and the cation containing Li2 is $72.60(4)^\circ$. The angle between the two sides of the cation facing the anions are $72.85(6)^\circ$ for the cation with Li1 (N1/N2/N3 and N1/N2/N4) and $71.98(6)^\circ$ for the cation with Li2 (N5/N6/N7 and N6/N7/N8).

The previously observed (3–5) zig-zag arrangement of cations and anions can also be identified in **6** (Figure 33). The larger steric demand of the anions compared with Cp' and indenyl creates voids which are filled with lattice NH_3 .

3.2. Sodium Derivatives

3.2.1. $\text{CpNa}(\text{NH}_3)_3$ (7): A Piano-Stool Cation

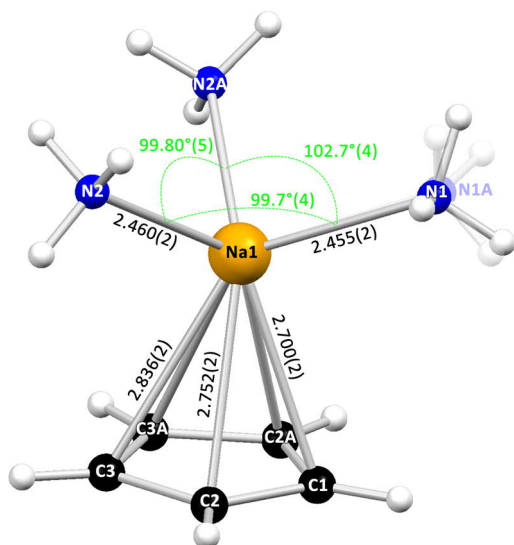


Figure 34: Crystal structure of $\text{CpNa}(\text{NH}_3)_3$ (7). The letter 'A' indicates symmetry generation by the mirror plane lying on C1, Na1, and the C3–C3A-bond centre. Contact-distances are given in Å. The symmetry induced disorder of N1 is depicted transparently.

$\text{CpNa}(\text{NH}_3)_3$ (7) has been synthesized by saturating a solution of cyclopentadiene and $\text{Na}(\text{hmds})$ in THF with gaseous NH_3 at -15°C and subsequent crystallization at -30°C . 7 crystallizes in the orthorhombic space group $Pnma$; the asymmetric unit comprises half a Cp anion together with half a sodium cation and two molecules of ammonia attached to it (Figure 34). The whole molecule consists of a Cp anion η^5 -coordinated by a sodium cation, which itself is coordinated by three molecules of ammonia. It constitutes a so-called piano-stool complex. Piano stool complexes are half sandwich complexes of a metal ion, normally of a transition metal, with a cyclic polyhaptic ligand (Cp, benzene, cyclooctatriene,

etc.) as the seat, and single donating ligands (here: NH_3) as the legs of the stool. Prominent examples are $\text{Cp}^*\text{Mn}(\text{CO})_3$ as an anti-knock agent, $\text{CpCo}(\text{CO})_2$ as a catalyst for the synthesis of pyridines, and $(\text{C}_4\text{H}_4)\text{Fe}(\text{CO})_3$ as a precursor for cyclobutadiene.^[145]

7 is generated from the asymmetric unit by a mirror plane located at C1, Na1, and the center of the C3–C3A bond. The ammonia molecule of N1 shows symmetry-induced disorder related to the mirror plane. With a distance of $0.17(4)$ Å the positions of N1 and N1A are very close to each other and could alternatively be described with N1 placed on the mirror plane with a pronounced vibration perpendicular to the plane. However, the refinement of N1 outside the mirror plane results in a more spherical vibration (for more information see crystallographic section). From previously observed structures of solvated NaCp , the formation of a piano-stool complex cannot be directly anticipated, because they generally form 1-dimensional coordination polymer strands. The bi-dentate solvents TMEDA and DME as well as the mono-dentate THF form 1-dimensional zig zag-shaped coordination-polymers with the donor-solvent filling up the coordination sphere of Na^+ .^[82, 85] A piano-stool-complex like 7 could be obtained using [15]-crown-5, effectively shielding the coordination sphere of the sodium cation.^[82] Using the next larger crown-

ether [18]-crown-6 instead leads to solvent separation and formation of sodocene anions linked by side-on-coordination of Na^+ , itself sitting in the centre of the crown-ether.^[83] Therefore, ammonia has the ability to coordinate the cation more effectively than THF because of its smaller size and higher donor strength, but is not able to form solvent-separated species as in the case of the CpLi ammoniacates **2** and **3**. The higher ionic radius of Na^+ compared to Li^+ is reflected in the longer Na–N distances of 2.455(2) Å and 2.460(2) Å in **7** compared to the average of 2.06 Å between Li^+ and N.

The higher radius renders Na^+ more attracted to the soft Cp anion according to the HSAB-concept.

The molecule is extensively embedded in NH- π bonding (Figure 35). The ammonia molecule of N2 and the symmetry-related N2A form bridging attraction with two adjacent Cp anions each while N1 forms a weaker attraction with another Cp anion. On the other side, each Cp anion exhibits hydrogen bonding with five molecules of ammonia.

As the overall structure of **7** shows some remarkable features, a more detailed study was conducted by *Jakob Hey* et al.^[146] The cation, with a distance of 2.497(2) Å to the ring plane, is significantly shifted from the ideal position above the ring center toward C1. The Na1–C1 distance of 2.700(2) Å is significantly shorter than Na1–C3 with 2.836(2) Å. This shift is not unusual for alkali metal cations, since the coordination with Cp is dominated by *Coulomb* attractions. This makes the position of the cation far more dependent to electronic and steric influences of the close environment than for the *d*-orbital-controlled coordination of transition metals. However, the ligands do not impose any steric restraint on the structure and should allow Na^+ to occupy the minimum of the energy hypersurface, which is anticipated to be the η^5 -coordination for the isolated molecule. The Na1–N1 contact and the C1–H1 bond are also almost perfectly eclipsed toward each other, which is sterically less beneficial. A close look into the structure by *Jakob Hey* using high resolution SCXRD data revealed an unusual bending of the CH-hydrogen atoms toward Na1, especially for the bond of C1–H1. The sophisticated and careful treatment of high resolution data and the use of the SHADE server for anisotropic thermal motion allowed him to refine the positions of the hydrogen atoms without using classical constraints.^[147] In theo-

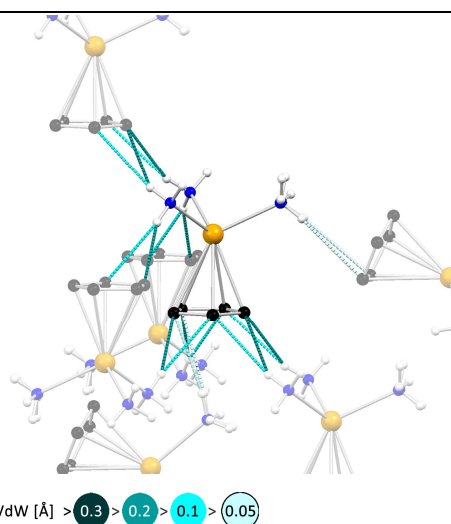


Figure 35: NH- π interactions of $\text{CpNa}(\text{NH}_3)_3$ (**7**) with the environment.

ry, the hydrogen atoms are supposed to bend away from the cation. The attraction of Na^+ creates a charge concentration of the π -density toward the cation and a depletion in the opposite direction. As a result, the C–H bonds bend away from the cation. A gas-phase-geometry optimization of the complex endorses this theoretical prediction. In this optimization, the position of the sodium cation is above the centre of the ring and the NH_3 umbrella is considerably wider opened than in the solid state structure. By charge-density analysis and further calculation regarding the larger environment of the complex, NH- π bonding could be identified as the forces that shape the complex distinctly. Charge-density analysis refers to an in-depth analysis of the electron density in crystal structures using high-resolution X-ray data to investigate chemical bonding and electrostatic properties.^[148] From the typology of the *Laplacian* around C1, a significant shift of the electron density away from the cation was found, which explains the bending of C1–H1. Using the *Source-Function*^[149] on the experimental data—a measure of the contribution of single-atom basins of a molecule to the charge density $\rho(\mathbf{r})$ at any given point \mathbf{r} in the molecule—revealed a significant contribution of the interacting NH-hydrogen atoms to bond and ring critical points of the Cp ring. A geometry optimization of the complex placed in growing shells of 13, 57, 153, 345, and 587 complexes as point charges showed an increasing similarity of the complex to the experimental data with growing shells. The most dominant NH- π bonding is present between H1C and C1 as well as H2B and C3 with VdW differences of 0.22 Å.

3.2.2. $\text{Cp}'\text{Na}(\text{NH}_3)_3$ (**8**): Contact ion pair

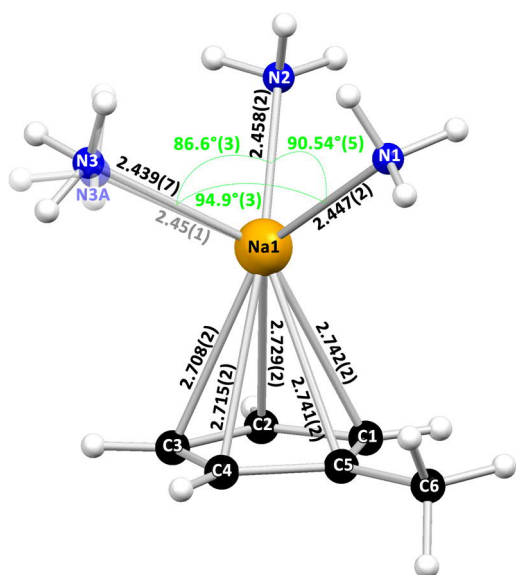


Figure 36: Crystal structure of $\text{Cp}'\text{Na}(\text{NH}_3)_3$ (**8**). Contact-distances are given in Å. Disorder of N3 is depicted transparently.

$\text{Cp}'\text{Na}(\text{NH}_3)_3$ (**8**) has been synthesized by saturating a solution of $\text{Cp}'\text{H}$ and $\text{Na}(\text{hmds})$ in THF with gaseous ammonia at -15°C and subsequent crystallization at -45°C . **8** crystallizes in the triclinic space group $P\bar{1}$ with a sodium cation η^5 -coordinated by Cp' and three molecules of ammonia (Figure 36). At first sight, the complex looks similar to **7**, but important features are different. In **8**, the sodium cation is located rather centrally in relation to the five-membered ring with only a very slight shift toward the C1–C5 bond. The distance of the cation in **8** to the anionic plane of 2.449(2) Å is slightly closer

than in **7** (2.497(2) Å). The distances of the three Na–N contacts vary only slightly. As in **7**, one molecule of ammonia is disordered. The ammonia molecule shows positional disorder in fractions of 59(3) % to 41(3) %. The N–Na–N angles are more acute compared to **7** with the smallest angle of 86.6°(3) and the largest angle of 94.9°(3) compared to 99.7°(4) and 102.7°(4) in **7**. A feature the structure of **8** shares with **7** is the almost eclipsed conformation of the Na1–N1 contact and the C5–C6 bond with a conformation angle of 4.33°(8). In the solid state, the steric restraint of the methyl group creates a different packing and differences in NH– π bonding (Figure 37). The packing in **7** allows the complex to interact with six other adjacent molecules. The packing in **8** only allows an effective hydrogen bonding with two neighboring complexes. **8** forms strands of linearly arranged complexes with translational symmetry. The ammonia molecules face the uncoordinated side of the next Cp'-anion and significant NH– π bonding is only formed within these strands. Strong interactions between neighboring strands are not present. Only two molecules interact with adjacent Cp'. Stronger hydrogen bonding is gained with the disordered NH₃ molecule of N3/N3A. NH– π bonding of the N1 molecule is weaker and the molecule of N2 is not significantly involved in any NH– π bonding, although the molecule is bent toward the next anion. This focus of interactions to only one anion is most likely the reason for the more acute N–Na–N-angles compared to **7** and the lacking shift of the sodium cation.

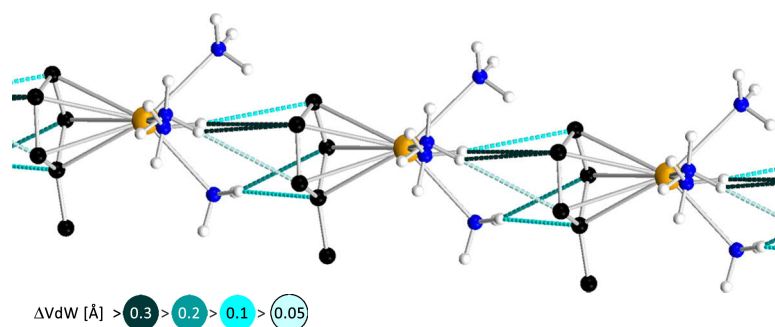


Figure 37: Linear packing of **8** induced by NH– π interactions.

3.2.3. $\text{Cp}^*\text{Na}(\text{NH}_3)_3 \cdot (\text{HN}(\text{SiMe}_3)_2)_{0.8}$ (**9**)

$\text{Cp}^*\text{Na}(\text{NH}_3)_3 \cdot (\text{HN}(\text{SiMe}_3)_2)_{0.8}$ (**9**) has been synthesized by adding Cp*H to a solution of Na(hmde) in liquid NH₃ at –78°C. The reaction mixture was warmed up to –33°C and stirred until the mixture turned clear. The crystallization temperature was –45°C. **9** is a rather complicated crystallographic problem. The compound crystallizes in a trigonal crystal system and the structure is twinned and modulated.^[150] A detailed description of the solution and subsequent refinement is given in the crystallographic section. In modu-

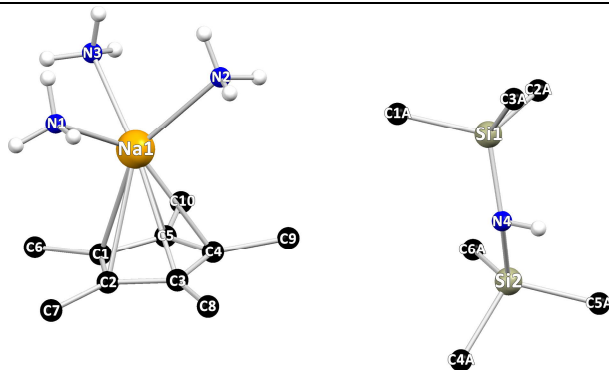


Figure 38: Crystal structure of $\text{Cp}^*\text{Na}(\text{NH}_3)_3 \cdot (0.8)\text{HN}(\text{SiMe}_3)_2$ (**9**). CH-hydrogen atoms have been omitted. No distances are given due to the overall disorder of the structure.

lated structures each reflection has a new set of weak satellite reflections. These satellite reflections appear when the atoms are not any longer fixed points in the 3-dimensional lattice, but when their position varies up to three additional dimensions. It can be roughly described as *ordered disorder*, meaning that there is additional symmetry in the shift of the atomic positions. Modulation under con-

sideration of the satellite reflections cannot be refined with the SHELX-program package.^[151]

A workaround to this problem is either a refinement of the structure disregarding the satellite reflections or the *supercell* approach, where the satellite reflections are indexed and integrated as normal reflections resulting in a larger cell. This *supercell* contains many more molecules, which roughly mirror the different positions of the atoms or molecules because of the modulation. Both approaches have been undertaken, but only give a rough image of the content. The ratio of data to refined parameters is low in both cases and the accuracy of the electron density map is less precise. However, both ways give a good image of the crystal content. The refinement using only the main reflections gives cell parameters of $a = b = 12.3369(9)$ Å and $c = 7.0334(6)$ Å and the space group $P\bar{3}1c$. The

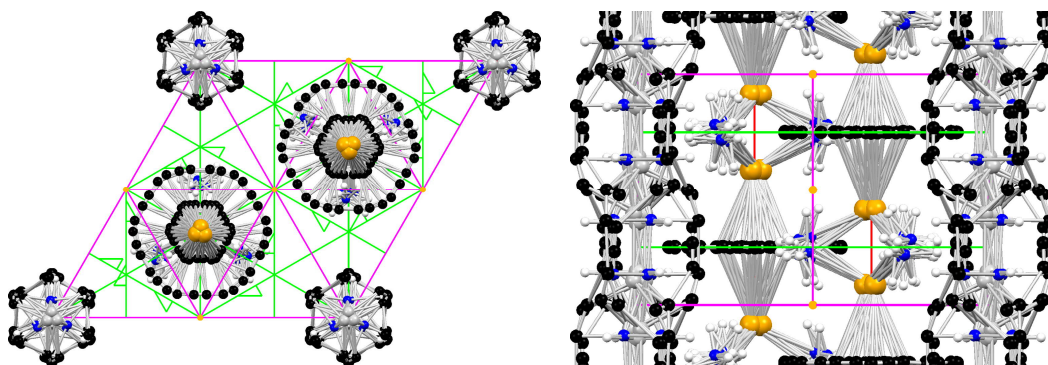


Figure 39: Crystal packing of **9** in the small cell. CH-hydrogen atoms have been omitted for clarity. Multiple bonds drawn by Mercury 3.6 between symmetry related atoms need to be ignored. 2_i-axes are drawn in green, glides planes in magenta (edges only), centre of inversion in orange, and threefold axis in red (not visible along the c-direction). Left: view along the c-axis; $\text{Cp}^*\text{Na}(\text{NH}_3)_3$ and $\text{HN}(\text{SiMe}_3)_2$ are disordered around threefold axes. Right: View along the a-axis; the $\text{Na}(\text{NH}_3)_3$ -units are disordered on both sides of the anion.

asymmetric unit contains a Cp^{*}-anion η^5 -coordinated by a Na(NH₃)₃⁺ fragment (Figure 38) as in the case of **7** and **8**, and a molecule of HN(SiMe₃)₂ as a byproduct of the reaction (Figure 18). The ratio of Cp^{*}Na(NH₃)₃ and HN(SiMe₃)₂ is 5 : 4, which has been concluded from the *supercell* approach, which will be discussed later. The modulation is reflected by the high amount of disorder in the structure. The complex is placed on a threefold axis perpendicular to the plane of the anion, which results in symmetry-induced disorder (Figure 39). Additional twofold screw axes lying in the anion plane induce symmetry-side disorder of the ammonia molecule. The same is true for the HN(SiMe₃)₂ fragment. Together with the poor data-to-parameter ratio this prevents a meaningful detailed description of atomic distances and angles.

In the crystal packing, the complexes form linear NH- π -connected strands along the *c*-axis, similar to those in **8**. The strands have two different orientations, in which all Na(NH₃)₃⁺ fragments are placed above or below the anion, respectively. Those two orientations overlap in the crystal packing (Figure 39) and give a merged picture of the two orientations.

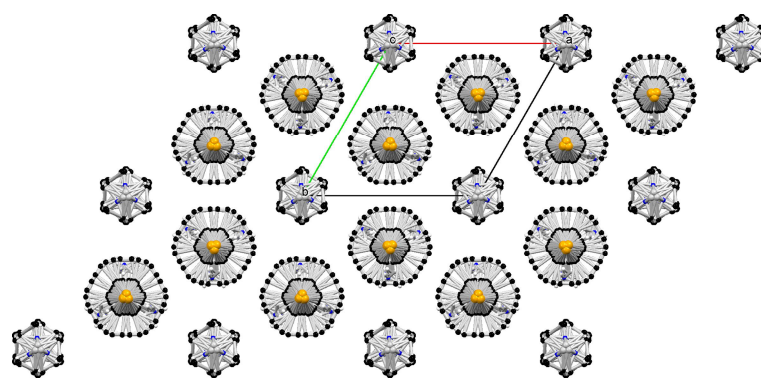


Figure 40: Expanded crystal packing of **9** along the *c*-axis. Each strand of HN(SiMe₃)₂ is surrounded by six strands of Cp^{*}Na(NH₃)₃.

Six of those strands surround a void filled with HN(SiMe₃)₂ (Figure 40). The same picture is coming up with the *supercell* approach (Figure 41). The integrated unit cell is with $a = b = 21.362(2)$ Å and $c = 35.160(2)$ Å fifteen times larger than the smaller cell. The space group changes to $P\bar{3}c1$ with five molecules of Cp^{*}Na(NH₃)₃ and six molecules of HN(SiMe₃)₂ in the asymmetric unit. The ratio of Cp^{*}Na(NH₃)₃ and HN(SiMe₃)₂ in the cell is 5 : 4. This information was used to determine the right occupation of HN(SiMe₃)₂ in the refinement of the previously discussed basic cell. In contrast to the basic cell, the complexes do not lie on threefold axes. However, positional disorder is present. Each Cp^{*} anion has been refined on two positions as well as on the ammonia molecules. The picture is the same as in the basic cell. The five complexes are arranged in a strand that propagates along the *c*-axis.

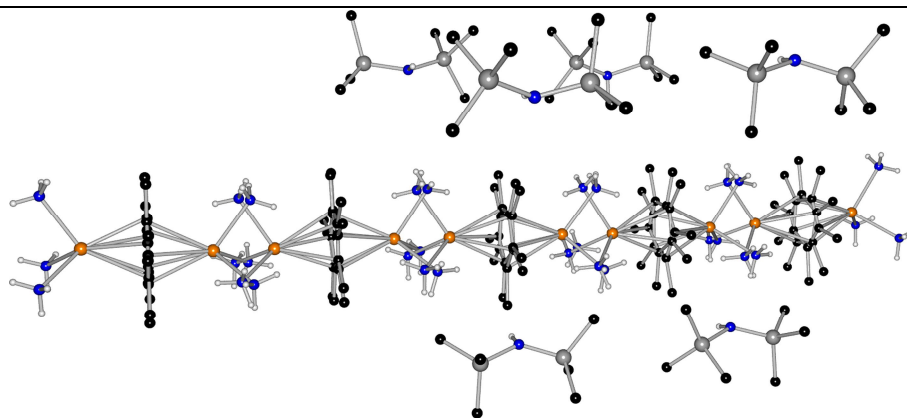


Figure 41: Asymmetric unit of **9** in the supercell.

Although both refinements only give a rough image of the structure, distinct conclusions can be drawn out of it. For the discussion of the structural features, the solution and refinement of the small cell will be used. Compared to **7** and **8**, the sodium cation is closer to the plane of the anion with a distance of 2.37(2) Å. Corresponding values are 2.497(2) Å in **7** and 2.449(2) Å in **8**. The complexes in **9** are perfectly stacked upon each other. Whereas in **8** the complexes are slightly offset toward each other in the linear strands and only two molecules of ammonia interact with the adjacent anion, the anions in **9** are arranged perpendicular to the orientation of the strand and are stacked perfectly upon each other. This allows all the molecules of ammonia to interact with the π -system of the next anion (Figure 42). The disorder of the ammonia molecules and the anion do not allow a detailed view on the NH- π bonding, but a look on the most likely attractions

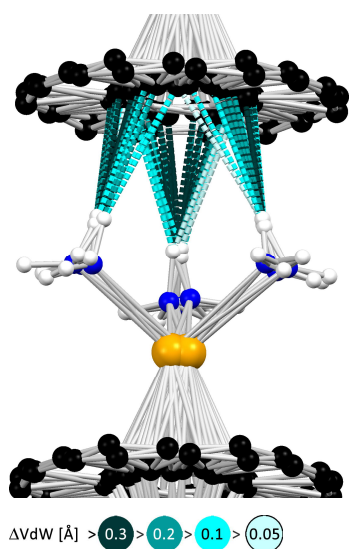


Figure 42: All possible NH- π interactions between the both disordered Na(NH₃)-moiety and the next anion.

is insightful. The distance range of hydrogen bonding reaches roughly from 2.85 Å to 2.41 Å. In figure 42, all possible hydrogen bonding with a minimum of $\Delta V_{dW} > 0.05$ Å between the disordered ammonia molecules and the C₅-perimeter of the disordered Cp* anion are drawn. From a total number of 87 possible hydrogen bonding, 39 have a distance below 2.60 Å. Any hydrogen atom of any symmetry operation pointing to the C₅-perimeter has at least one strong attraction to a central carbon atom of the Cp* anion of any symmetry operation. This makes **9** the most strongly interacting species of the CpNa derivatives.

An interesting feature of the structure is the co-crystallization of $\text{HN}(\text{SiMe}_3)_2$. In Figure 40, it is not directly obvious, how the void filled with $\text{HN}(\text{SiMe}_3)_2$ is formed. Figure 43 shows a strand of $\text{HN}(\text{SiMe}_3)_2$ depicted in a ball and stick model, surrounded by six complexes (no hydrogen atoms omitted) in a spacefilling presentation. The complexes in red and green are shifted along the c -axis with a Cp^* anion facing neighboring $\text{Na}(\text{NH}_3)_3$ moieties and vice versa. This zip arrangement of six complex strands leaves naturally no space for another strand of complexes. However, the void is big enough to fit $\text{HN}(\text{SiMe}_3)_2$, a byproduct of the reaction, in a non-stoichiometric way.

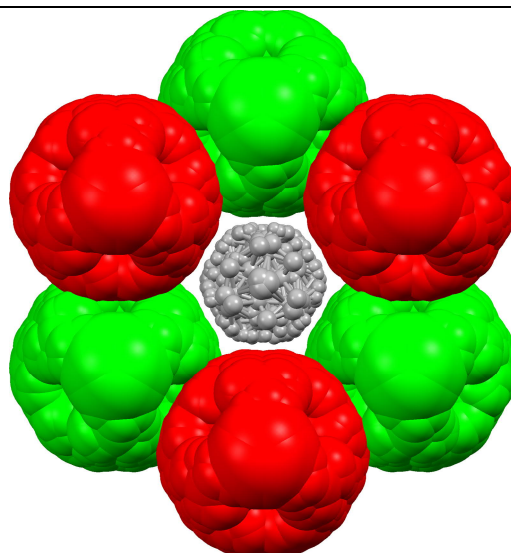


Figure 43: Stacking of the $\text{Cp}^*\text{Na}(\text{NH}_3)_3$ -strands (spacefill) and the formation of the void filled with $\text{HN}(\text{SiMe}_3)_2$ (ball and stick); cations in red and green are on the same level along the c -axis, respectively.

3.2.4. $[\text{Na}(\text{NH}_3)_4][\text{Ind}]$ (**10**): A Square Planar Cation

$\text{Na}(\text{NH}_3)_4[\text{Ind}]$ (**10**) was synthesized by saturating a solution of indene and $\text{Na}(\text{hmds})$ in Et_2O with gaseous ammonia at -15°C and subsequent crystallization at -16°C . **10** crystallizes in the monoclinic space group $P2_1$ with an indenyl anion and a square planar $\text{Na}(\text{NH}_3)_4^+$ cation in the asymmetric unit (Figure 44).

The crystal packing is a layered structure with sheets of indenyl anions and $\text{Na}(\text{NH}_3)_4^+$ cations (Figure 45). The layers of cations and anions are rippled and the interlayer distance between the anions is 6.04 \AA . The $\text{N}-\text{Na1}-\text{N}$ *cis*-angles are close to 90° . The $\text{N}-\text{Na1}-\text{N}$ *trans*-angles are $174.67^\circ(6)$ for $\text{N1}-\text{Na1}-\text{N3}$ and $175.47^\circ(6)$ for $\text{N2}-\text{Na1}-\text{N4}$, both bending in the same direction. The plane through the four nitrogen atoms of the cation has a *root mean square* deviation of only 0.0250 \AA , roughly double the value of the deviation of the carbon atoms of a plane through the indenyl anion of 0.0113 \AA . The deviation from a

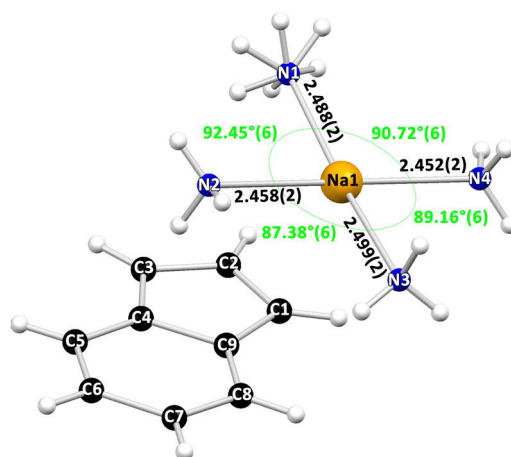


Figure 44: Asymmetric unit of $[\text{Na}(\text{NH}_3)_4][\text{Ind}]$ (**10**). Distances are given in \AA .

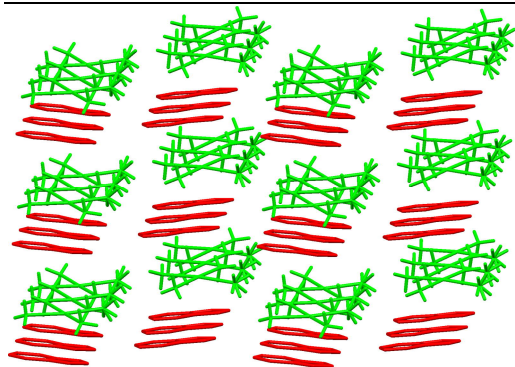


Figure 45: Crystal packing of **10**. Anions are depicted in red, cations in green.

perfect plane is remarkably small for these small sterically unhindered ligands. The sodium cation slightly shifts out of the plane by 0.091(2) Å.

Fourfold coordination of a sodium cation is not unusual itself, but together with a square planar configuration it is an unusual result. A CSD-search for a sodium cation, fourfold coordinated by oxygen and/or nitrogen as donor atoms, gives 482 structures. A search

for sixfold coordination reveals 1141 structures, making it the dominant form of coordination. It has to be mentioned that some of the fourfold coordinated structures in the search have remarkably short distances to two additional donor atoms, making them almost sixfold coordinated as well. This is especially true for more or less square planar coordinated species. In general, planarity is either a result of ligand design of larger organic molecules or additional interactions. The most prominent example is the $\text{Na}(\text{TMEDA})_2^+$ species. **10** almost square planar species are present in the CSD database. This is counterintuitive due to the steric demand of the ligand. In the crystal packing of these structures, the vacant axial positions are occupied by tellurium, iodine, methyl groups and other functional groups/anions. They either interact with the sodium cation or block the tetrahedral arrangement of the cation. The sodium cation seems to be more flexible in responding to its environment in contrast to the previously discussed lithium species, where in any case $\text{Li}(\text{NH}_3)_4^+$ tetrahedra are formed. This is easy to understand due to the larger ionic radius of Na^+ . A closer look into the structure of **10** indicates attraction of the sodium cation to the indenyl anions as well. The distances of the sodium cation to the next carbon atoms of the two adjacent indenyl anions are 3.047(2) Å to C1 and 3.238(2) Å to C3. The distances of the sodium cation to the two indenyl planes are 2.956(2) Å and 3.085(2) Å. The C–Na distances in the previous sodium containing structures **7** to **9** range from 2.57(3) Å to 2.836(2) Å. A CSD search for a sodium cation attached to an aromatic five membered ring (76 hits) reveals a maximum distance to the ring plane of 2.763 Å and a maximum distance of 3.106 Å to the closest coordinating carbon atom. Five structures are reported with Na–C distances longer than 3 Å. The mean and median Na–C distances in the CSD search are 2.765 Å and 2.778 Å, respectively. For aromatic six-membered rings (192 hits), the maximum distance to the plane is 3.062 Å, the maximum Na–C distance is 3.477 Å, 102 structures have Na–C distances higher than 3 Å, and the mean and median Na–C dis-

tances are 2.851 Å and 2.841 Å, respectively. Therefore, the structure of **10** can be seen as at the boundaries of a CIP and aSSIP.

NH- π bonding plays a crucial role in the formation of the shape of the cation. The ammonia molecules of N2, N3, and N4 are involved in NH- π bonding, the ammonia molecule of N1 does not interact with the environment (Figure 46). It therefore shows positional disorder in fractions of 68(3) % and 32(3) %.

All interacting ammonia molecules have short contacts to two indenyl anions. The ammonia molecules containing N2 and N3 point toward the six-membered rings of the central $\text{ind}^- \cdots \text{Na}(\text{NH}_3)_4^+ \cdots \text{ind}^-$ fragment. The contacts to the carbon atoms are not very strong but multiple. This indicates an interaction with the whole π -cloud of the anion. The ammonia molecule containing N2 is also attracted to C1 of an adjacent five-membered ring and the ammonia molecule with N3 has a contact to an adjacent six-membered ring. The ammonia molecule containing N4 interacts with the same anions as the one of N3 and bridges C1 and C2 of the central fragment with C3 of the other adjacent anion. The strength of the additional attractions places the cation in a position that excludes N1 from interacting with any anion in the surrounding.

3.2.5. Theoretical calculations on $[\text{Li}(\text{NH}_3)_4][\text{Ind}]$ (**5**) and $[\text{Na}(\text{NH}_3)_4][\text{Ind}]$ (**10**)

In order to elucidate the influence of the NH- π bonding in the formation of **10**, theoretical calculations have been conducted in collaboration with *Dr. Johannes M. Dieterich* and *Jun.-Prof. Ricardo A. Mata*.^[152] The structure of **5** was used to compare the influence of the cation. At first, the relative stability of the cations of $\text{Li}(\text{NH}_3)_4^+$ and $\text{Na}(\text{NH}_3)_4^+$ have been compared. Calculations were performed by density fitted local second order Møller Plesset perturbation theory (DF-LMP2). The tetrahedral configuration is the most stable for both cations with a Li-N distance of 2.119 Å and a Na-N distance of 2.490 Å (Figure 47). The cations and nitrogen atoms have been subsequently forced into a plane, which results in a D_{2d} symmetry of the cations with each ammonia molecule rotated by 180° to its neighbor, respectively. The Li-N distance shifts to 2.218 Å and the Na-N distance to

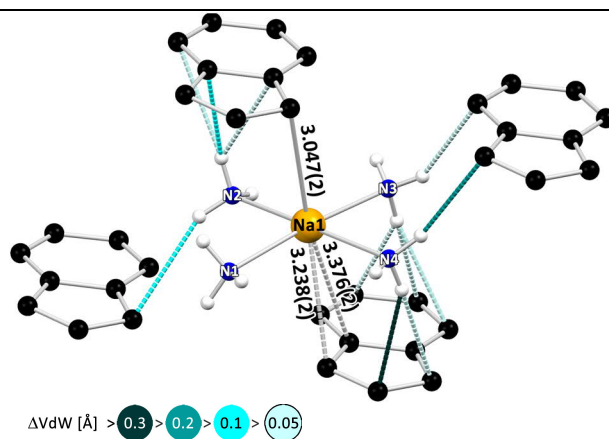


Figure 46: NH- π interactions of the $\text{Na}(\text{NH}_3)_4^+$ -cation with surrounding anions. CH-hydrogen atoms and the minor fraction of the N1-disorder of the hydrogen atoms have been omitted. Distances are given in [Å].

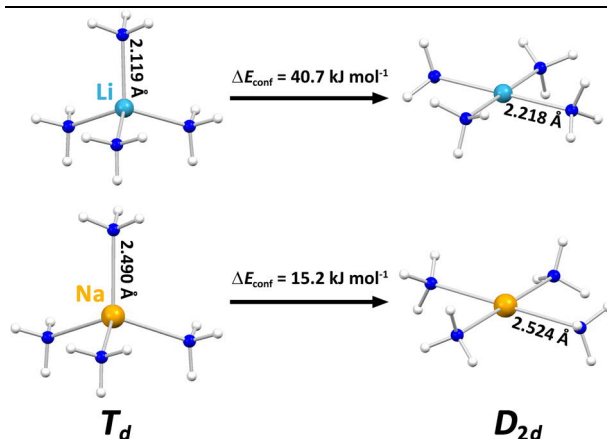


Figure 47: Energy differences between optimised tetrahedral and square planar $\text{Li}(\text{NH}_3)_4^+$ and $\text{Na}(\text{NH}_3)_4^+$.

2.524 Å. The larger shift of the Li–N distance correlates with the differences in energy of $\Delta E_{\text{conf}} = 40.7 \text{ kJ mol}^{-1}$ for $\text{Li}(\text{NH}_3)_4^+$ and $\Delta E_{\text{conf}} = 15.2 \text{ kJ mol}^{-1}$ for $\text{Na}(\text{NH}_3)_4^+$.

This can be understood by examining the potential curves of the single $\text{Na}^+ - \text{NH}_3$ and $\text{Li}^+ - \text{NH}_3$ coordination (Figure 48). They have been calculated by a relaxed distance scan with frozen Na–N and Li–N interatomic distances.

The potential curve of $\text{Li}^+ - \text{NH}_3$ is lower in energy and, most importantly, the potential curve of $\text{Na}^+ - \text{NH}_3$ is very shallow. The energy difference in the $\text{Li}^+ - \text{NH}_3$ potential curve is 6.7 kJ mol^{-1} for the Li–N distances in the tetrahedral and square planar configuration. The according difference in the $\text{Na}^+ - \text{NH}_3$ potential curve is only 0.7 kJ mol^{-1} . The values derived from the potential curves reflect only one cation and one molecule of NH_3 , the combined energy penalty of the whole $\text{Li}(\text{NH}_3)_4^+$ cation for the change in conformation from T_d to D_{2d} is therefore 24.0 kJ mol^{-1} larger than of the $\text{Na}(\text{NH}_3)_4^+$ cation. The flat energy profile for Na^+ makes the cation more flexible whereas the small changes in geometry have a larger penalty for $\text{Li}(\text{NH}_3)_4^+$ cations.

To elucidate the influence of the indenyl anions, calculations were carried out on $\text{ind}^- \cdots \text{X}(\text{NH}_3)_4^+ \cdots \text{ind}^-$ fragments ($\text{X} = \text{Li}, \text{Na}$). The indenyl anions were optimized and placed on the crystallographic positions by a root mean square fit. The cations were relaxed between the anions, where they shift slightly from the position in the crystal structure (Figure 49). Especially in the case of **10**, the former uninvolved ammonia molecule shifts to a position where it interacts with one of the indenyl anions as well. This underlines the preference of the cation for NH– π bonding.

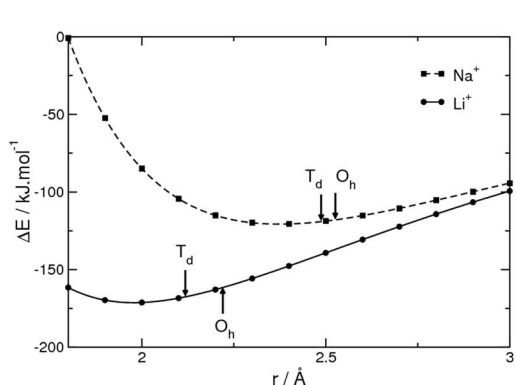


Figure 48: Potential energy curves for a Li– NH_3 and a Na– NH_3 system with regard to the metal–nitrogen distance. The distances for the free cations are marked with arrows.

For the lithium cation, the deformation energy from the optimized T_d conformation to the shape between the cations is 15.9 kJ mol^{-1} (Figure 50). The deformation energy from the optimized T_d conformation to the shape between the cations is 15.9 kJ mol^{-1} (Figure 50). The deformation energy from the optimized T_d conformation to the shape between the cations is 15.9 kJ mol^{-1} (Figure 50).

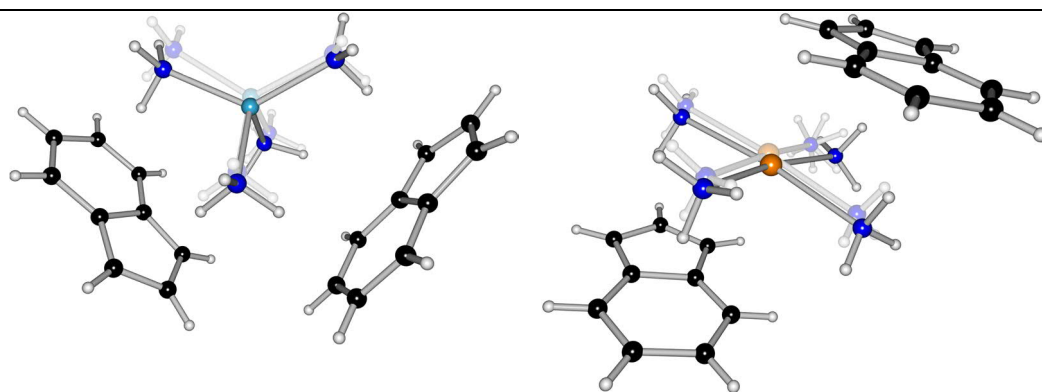


Figure 49: Overlay of the crystallographic position (transparent) and the theoretical position of the cations between the indenyl-anions. The CH-protons are on the crystallographic positions.

mation energy for the square planar sodium cation with D_{2d} -symmetry is 12.1 kJ mol^{-1} .

The optimized model of $\text{ind}^- \cdots \text{Na}(\text{NH}_3)_4^+ \cdots \text{ind}^-$ was used to further analyze the $\text{NH} \cdots \pi$ bonding. The energy profiles for the rotation of the ammonia molecules along the $\text{Na}-\text{N}$ bond were calculated to get an idea of the energy differences when the interacting hydrogen atoms move away from their favored positions. The rotation was set out by varying the $\text{H}-\text{N}-\text{Na}-\text{H}'$ dihedral angle stepwise for 360° for all hydrogen atoms in a single molecule, where H' is a non-rotating hydrogen atom of another ammonia molecule. Therefore, the $\text{H}-\text{N}-\text{Na}$ angles of the rotating ammonia molecule are kept constant resulting in a tumbling motion of the ammonia molecule. Figure 51 shows the potential energy curves for the rotation of the $\text{Na}-\text{NH}_3$ bond for the square planar cation with (dashed) and without (bold) indenyl planes. Because of the undertaken rigid scan, the energy profiles are not 120° -symmetric as they would be in a relaxed scan. Rotation of the free square planar cation has a barrier of only 0.5 kJ mol^{-1} . The situation changes dramatically with the indenyl planes. N1 and N4 stand for the two ammonia molecules that interact with the five membered rings.

The rotational barrier is about 16 kJ mol^{-1} and thus much higher than the rotational barrier of N2 and N3 with 6 kJ mol^{-1} interacting with the six-membered ring. The difference in the rotational barrier is reflected in the difference in distance of the closest carbon atom to the interacting hydrogen atom of about 0.1 \AA . The rotational barriers reflect the

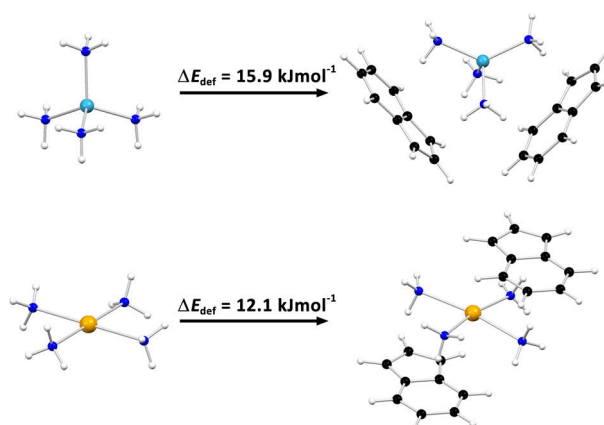


Figure 50: Energy differences of the free cations and between the indenyl-anions.

Results

Sodium Derivatives

strength of the NH- π bonding. Those attractions alone can compensate the deformation energies for the sodium cation from tetrahedral to square planar configuration (15.2 kJ mol^{-1}) and stacking between two indenyl planes (12.1 kJ mol^{-1}). The coordination of the sodium cation to the indenyl planes has not even been incorporated into that estimation. The examined types of NH- π bonding are clearly not able to deform a lithium cation the same way as sodium.

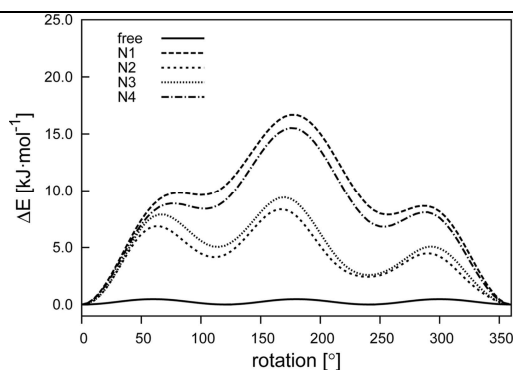


Figure 51: Potential energy curves for the individual rotation of the ammonia molecules along the Na-N bonds. The rotation is tumbling in contrast to a symmetric rotation along the C_3 -axis of ammonia.

A further analysis was done by calculating the DF-LMP2 density difference of the whole $\text{ind}^- \cdots \text{Na}^+ \cdots \text{ind}^-$ fragment and the constituting elements. The density of the full system has been computed as well as the density of the indenyl anions and the cation separately by keeping the internal geometry and basis sets constant. The values of the whole system and the constituting parts were then added or subtracted, respectively. Figure 52 is a density-difference plot where red color indicates charge-density depletion and grey color charge-density gain. The charge reorganization is clearly oriented toward the five-membered rings. The charge accumulation at the five-membered ring is somewhat stronger than at the six-membered ring, which is in good agreement with the higher rotational barriers for the five-membered ring. At both five-membered rings, two regions of charge accumulation are visible. One is at the top of the five-membered ring and close to the interacting ammonia molecule. The other accumulation at the side of the five-membered ring points toward the sodium cation and reflects the attraction toward it.

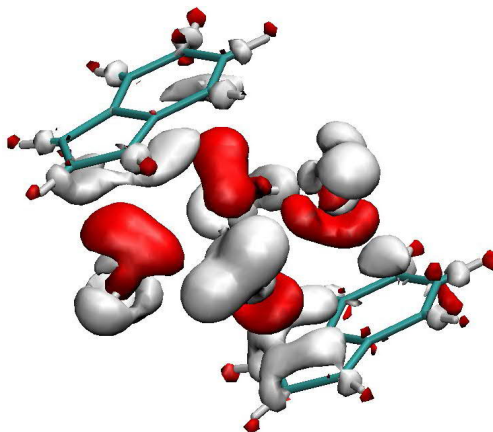


Figure 52: Isodensity plot of the DF-LMP2 density difference for the $[\text{Na}(\text{NH}_3)_4 2\text{Ind}]^-$ system and the respective interacting elements (ind^- and $\text{Na}(\text{NH}_3)_4^+$). Red colour indicates density depletion and grey colour density gain.

Altogether, the calculations show that the energy penalty from tetrahedral to square planar configuration is much smaller for $\text{Na}(\text{NH}_3)_3^+$ compared to $\text{Li}(\text{NH}_3)_3^+$. Additional deformation energy is needed for the alignment of the cations between the indenyl anions. NH- π bonding has been proven to be a major force in the formation of the square planar

configuration of the cation in **10**, shown by the energy profile of the NH_3 rotation and in the density differences of the $\text{ind}^- \cdots \text{Na}(\text{NH}_3)_4^+ \cdots \text{ind}^-$ model.

3.2.6. $[\text{Na}(\text{NH}_3)_{4/6}][\text{Flu}]$ (**11**): An Anionic Channel filled with $\text{Na}(\text{NH}_3)_6^+$ and $\text{Na}(\text{NH}_3)_4^+$

$[\text{Na}(\text{NH}_3)_{4/6}][\text{Flu}]$ (**11**) was synthesized by condensation of ammonia into a solution of $\text{Na}(\text{hmds})$ and fluorene in methyl-tert-butylether. Ammonia was added at -78°C until the solution turned clear. Crystallization took place at -45°C . **11** is a modulated structure and crystallizes in a monoclinic crystal lattice. Unlike the modulated structure of **9**, the apparent structure is *incommensurate* (for more information see crystallographic section). This fact makes an evaluation of the structure more difficult. Attempts to solve and refine the structure with the *JANA 2006* program package^[153] and the help of *Andreas Schönleber* from the University of Bayreuth have yet been unsuccessful.

However, a similar approach as in the case of **9** also reveals some insights into the structure. An integration, solution, and refinement of a basis cell and a *supercell* have been undertaken. The basis cell has the parameters $a = 22.095(3) \text{ \AA}$, $b = 11.569(2) \text{ \AA}$, $c = 14.929(2) \text{ \AA}$, $\beta = 120.870^\circ(2)$ and the space group is $C2/c$. After solution with *ShelXT*^[154], a fluorenyl anion is clearly visible in the asymmetric unit (Figure 53).

The fluorenyl anions form rhombic channels in the crystal packing (Figure 54). Within these channels, strands of electron density are allocated toward the corners, in the center, and some density is located also between the corners and the center. The electron-density strands indicate a distribution of the content within the channel, which explains the observed modulation.

Concluding from the shape of the channels, the arrangement of the strands, and the tendency for

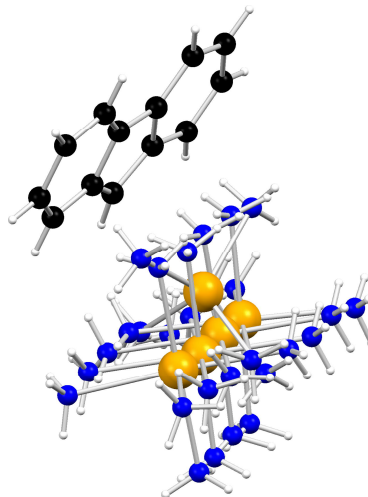


Figure 53: Asymmetric unit of $[\text{Na}(\text{NH}_3)_{4/6}][\text{Flu}]$ (**11**) in the basic cell.

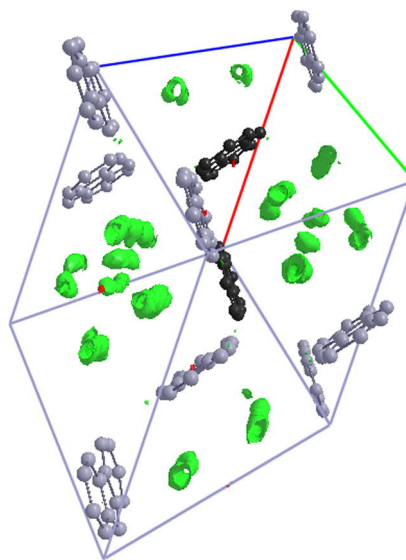


Figure 54: A packing plot of **11** in the basic cell without $\text{Na}(\text{NH}_3)_6^+$ and $\text{Na}(\text{NH}_3)_4^+$. Strands of electron density are distributed within channels of fluorenyl anions along the c -axis.

Results

Sodium Derivatives

sixfold coordination of sodium, $\text{Na}(\text{NH}_3)_6^+$ cations were anticipated to be the major content within the anionic channels. The refinement of the $\text{Na}(\text{NH}_3)_6^+$ octahedra was achieved by treating the density strands as disorder of the cations along the direction of the channel. The octahedral needed to be modelled into the strands: All Na–N distances have been set to 2.46 Å, all distances between *cis*-arranged nitrogen atoms were restrained to be equal as well as all isotropic thermal motion parameters within one cation. Five of these octahedra can be modelled into the strands with occupations roughly between 5 % and 17 %.

It should be mentioned that a modulation generally affects the whole structure, meaning that also the fluorenyl anions are modulated. In this refinement, the displacement of the anions seems to be low and therefore, the modulation consists predominantly of a small variation of the atomic positions. As a result, the disorder could not be deconvoluted successfully.

The charge density accumulation between the sodium cations and the *axial* ammonia molecules have been interpreted as a $\text{Na}(\text{NH}_3)_4^+$ species with the ammonia molecules being allocated in the density strands as well.

To get an additional approach to the content of the anionic channels, a larger cell incorporating the satellite reflections has been integrated. The cell parameters of the *supercell* are $a = 11.537(2)$ Å, $b = 14.370(3)$ Å, $c = 53.057(7)$ Å, $\alpha = 91.01^\circ(3)$ $\beta = 90.20^\circ(2)$ $\gamma = 113.66^\circ(2)$. The cell has been integrated in the triclinic lattice system. The structure has

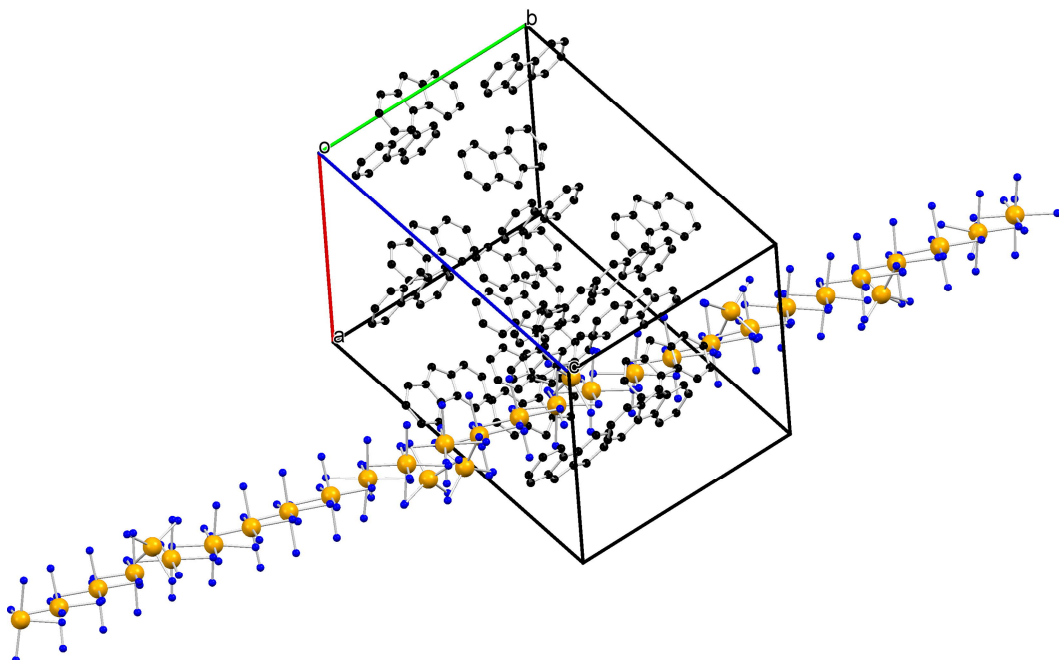


Figure 55: Asymmetric unit of **11** in the *supercell*. Hydrogen atoms have been omitted for clarity.

been solved and refined in the space group $P1$ to refine the whole content of the unit cell independently. The accuracy of this approach is pretty poor, but nonetheless, all previously observed elements become visible in the *supercell* as well. 20 fluorenyl anions have been identified, 27 $\text{Na}(\text{NH}_3)_6^+$ octahedra, and 6 $\text{Na}(\text{NH}_3)_4^+$ tetrahedra (Figure 55). The occupation of the cations has been restrained to sum up to the amount of fluorenyl anions with one sodium cation per fluorenyl anion. The fluorenyl anions form the same channel like structure as in the basic cell (Figure 56). The R_1 -value of 30% is far worse for this approach compared to the basic cell (R_1 : 16%), but the advantage of this approach is the appearance of the individual cations, which proves the ideas for the basic cell to be correct.

The reason for the high variability in the position of the cations within the channels clearly lies in the arrangement and properties of the fluorenyl anion. A channel-like arrangement of the fluorenyl anions has been previously observed in the structure of $[\text{Li}(\text{NH}_3)_4][\text{Flu}] \cdot (\text{NH}_3)_2$ (**6**). In **6**, the anions form rhomboid-shaped channels with the anions arranged transversal to the direction of channel. They form multiple $\text{NH}-\pi$ bondings with $\text{Li}(\text{NH}_3)_4^+$ cations and lattice ammonia with their large π -system. The two fluorenyl anions in the asymmetric unit together form 19 hydrogen bonds with adjacent ammonia hydrogen atoms. However, the system in **6** is rigid because of the inflexible nature of the $\text{Li}(\text{NH}_3)_4^+$ cation and the ordering effect of $\text{NH}-\text{N}$ bonding with the lattice ammonia molecules. The position of the anions is strongly guided by the tetrahedral shape of the cations with the angles between the anions being close to those of the interacting tetrahedral sides. The plane of the anions is also inclined by 15.7° and 18.7° along the direction of the channel. In **11**, the anions are arranged along the direction of the channel and do not incline, thus providing a more continuous arrangement of π -clouds. The sodium cations most likely interact with this π -density as well and the shape of the channels also seems to reflect the shape of the octahedral cations. The previously observed flexible nature of the sodium cations makes different positions of the cations and even differences in coordination understandable.

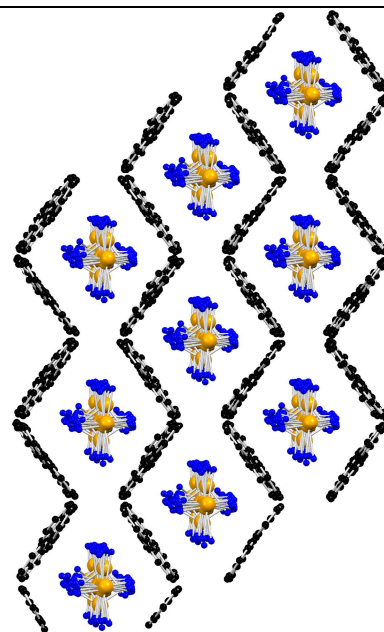


Figure 56: Packing plot of **11** in the supercell. Hydrogen atoms have been omitted for clarity.

3.3. Potassium Derivatives

3.3.1. $\text{CpK}(\text{NH}_3)_2$ (12): A 1-Dimensional Coordination Polymer

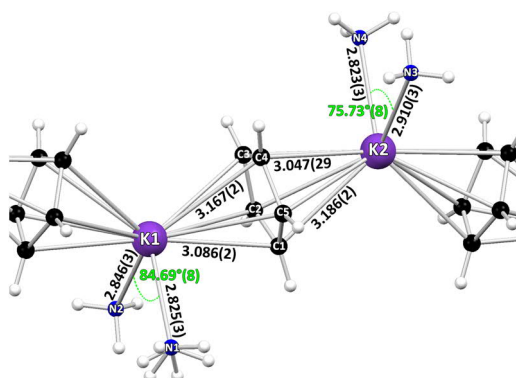


Figure 57: Crystal structure of $\text{CpK}(\text{NH}_3)_2$ (12). The atoms of the asymmetric unit within the 1-dimensional coordination polymer are labelled. Atomic distances are given in Å. The hydrogen atoms of N1 are symmetry-site disordered by a mirror plane along N1, N2, and K1. Distances are given in Å.

$\text{K}(\text{Cp})(\text{NH}_3)_2$ (12) was synthesized by condensation of ammonia in a mixture of CpH and $\text{K}(\text{hmds})$ at -78°C until the solution turned clear. The reaction mixture was stored for crystallization at -45°C . The crystals turned out to be highly twinned. A detailed description can be found in the crystallographic section. The structure crystallizes in the orthorhombic space group $Pnma$ with one Cp anion, two half occupied potassium cations and four half occupied molecules of ammonia in the asymmetric unit (Figure 57).

The whole structure is a 1-dimensional coordination polymer of Cp anions which are η^5 -coordinated by potassium cations (Figure 58). Each cation is coordinated by two molecules of ammonia. The distances of the potassium cations to the Cp plane are $2.889(2)$ Å for K1 and $2.876(2)$ Å for K2. The coordination polymer is zigzag shaped with an angle of $34.20(5)^\circ$ between the planes of the Cp anions. The potassium cations are slightly shifted from the ideal position facing the ring centre towards the open side of the tilted anions. K1 is shifted towards C1 ($3.086(2)$ Å) and away from C4 ($3.167(2)$ Å), and K2 is shifted towards C4 ($3.047(2)$ Å) and away from C1 ($3.186(2)$ Å). The N–K distances between the ammonia molecules and the potassium atoms range from $2.824(3)$ Å for N4 to $2.910(3)$ Å for N3. The N–K–N angles differ moderately with $84.69(8)^\circ$ for K1 and $75.72(9)^\circ$ for K2. The potassium cations and the nitrogen atoms of each $\text{K}(\text{NH}_3)_2^+$ unit are located on mirror planes. The hydrogen atoms attached to N1 are disordered by the mirror plane. Symmetry induced disorder of the other ammonia hydrogen atoms can be refined as well, but does not lead to significant improvements and has therefore not been included in the final model. For the following discussion of NH- π bonding, a disorder

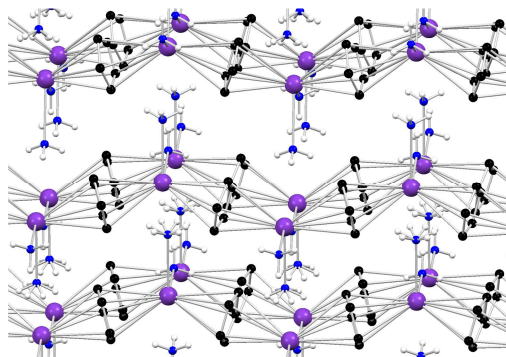


Figure 58: Packing plot of $\text{CpK}(\text{NH}_3)_2$ (12).

refinement of N2, N3, and N4 does not change the picture significantly.

Analogous to the previously discussed lithium and sodium structures, NH- π bonding is present in **12** as well, but seems to have a far lower impact on the structure. The hydrogen atoms of the ammonia molecules have short contacts to Cp anions of adjacent coordination polymer strands (Figure 59). In the crystal packing, the neighboring coordination polymers have a parallel orientation to each other. The strands are not shifted towards each other. The $K(NH_3)_2$ moieties are surrounded by other $K(NH_3)_2$ moieties of the neighboring strands. The same holds true for the Cp anions. The $K(NH_3)_2$ moieties are located on mirror planes perpendicular to the direction of the coordination polymers. In proximity to each molecule of ammonia, two tilted Cp anions of a potassocene fragment can be found in an adjacent polymer strand. The ammonia molecules containing N2, N3, and N4 form bridging hydrogen bonds with these two anions with distances to the next carbon atoms ranging from 2.749(8) Å to 2.796(9) Å (ΔVdW -range: 0.104 Å–0.151 Å). The ammonia molecule with N1 shows a significant attraction to only one of the adjacent Cp anions of a potassocene fragment with a distance of 2.84(2) Å (ΔVdW : 0.06 Å) to the closest carbon atom of the anion (the distance has a one order of magnitude higher stand-

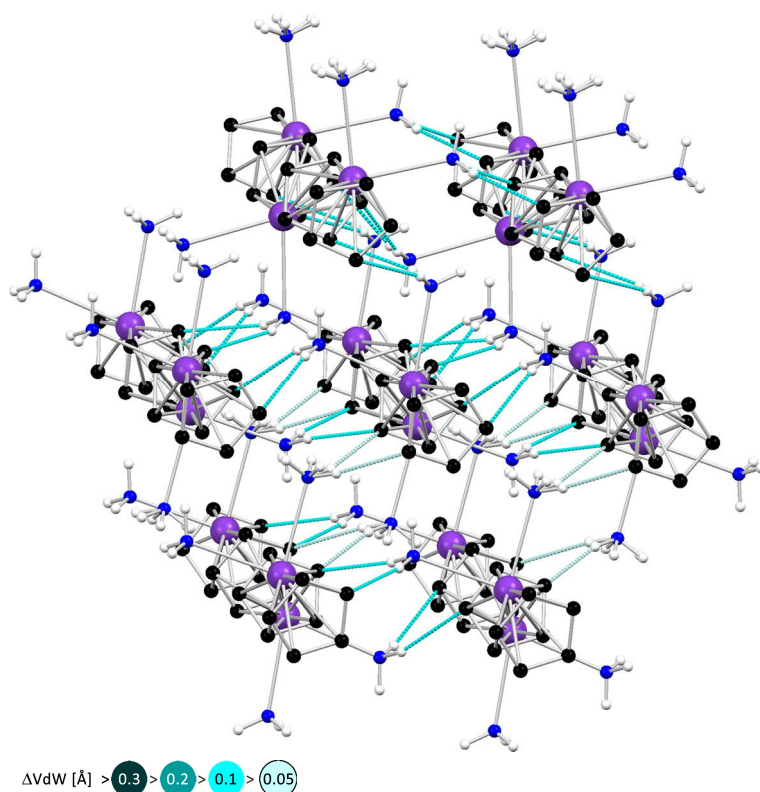


Figure 59: NH- π contacts in $CpK(NH_3)_2$ (**12**). CH-hydrogen atoms have been omitted. The disordered ammonia molecule has weaker interaction to the adjacent anions than the other molecules of ammonia.

ard deviation than the previous ones).

In comparison with already known solvated K–Cp coordination polymer chains, the impact of the ammonia coordination is only clearly visible in the distance of the cation-to-anion plane. Analogous structures to **12** are K(Cp)(Et₂O) by *Weiss et al.*, K(Cp)(THF)(DME)_{0.5} by *Wagner et al.*, and also solvent free KCp by *Olbrich et al.* (Table 14).^[33a, 101-102] In all these structures, a zigzag arrangement is present and the cations are coordinated by a donating solvent or side-on coordinated to adjacent anions as in the case of KCp. The distance of the cation to the ring plane is governed by the amount of charge density provided by the coordination sphere. The more charge density the cation receives by donation or side-on coordination, the less it attracts the Cp anion. In contrast to what could be expected, side-on coordination has a greater impact on the K–Cp distance than coordination of Et₂O. In **12**, the cations are coordinated with less steric restraint and with the more beneficial donor atom nitrogen. Therefore, the longer distance to the anion could already be predicted. Another structural factor that could be affected is the angle between the anion planes, but no clear picture is present. Uncoordinated KCp and highly coordinated K(Cp)(THF)(DME)_{0.5} have relatively wide angles and K(Cp)(Et₂O) and **12** have smaller angles. It has thus to be concluded that the different types of interaction between the polymeric chains and steric repulsion of the donating molecules are rather individual for each structure.

Table 14: Selected structural parameters for KCp-compounds.

| | KCp | K(Cp)(Et ₂ O) | K(Cp)(THF)(DME) _{0.5} | 12 |
|-----------------------------------|------------------|--------------------------|--------------------------------|-----------------|
| CSD-code | NIBSOG | NAGSUJ | XUMKEW | |
| d(K-plane) [Å] | 2.805, 2.816 | 2.767, 2.768 | 2.813, 2.849 | 2.889, 2.876 |
| Cp-K-Cp-angle^a | 137.95° | 145.24° | 136.12°/137.02° | 138.31°/141.38° |
| Density [g/cm³] | 1.325 | 1.068 | 1.148 | 1.192 |
| Reference | ^[33a] | ^[101] | ^[102] | |

^a Calculated with the centroids of the Cp-anions.

3.3.2. Cp'K(NH₃) (**13**): Between a 1- and 2-dimensional Coordination Polymer

Cp'K(NH₃) (**13**) was synthesized by saturating a solution of K(hmds) and Cp'H in Et₂O with gaseous ammonia at –15 °C and subsequent crystallization at –45 °C. **13** crystallizes in the monoclinic space group *P2₁/c* with an asymmetric unit consisting of a Cp' anion which is η⁵-coordinated by a potassium cation (Figure 60). The cation is additionally coordinated by one molecule of ammonia. Both the hydrogen atoms of the methyl group and the hydrogen atoms of the ammonia molecule are disordered on two positions, the methyl group by 29(11)% and the ammonia molecule by 49(5)%. Coordination in **13** forms zigzag-shaped 1-dimensional polymeric chains, similar to the structure of **12**. The distances of K1 to the two coordinating ring planes are 2.819(2) Å and 2.837(2) Å, about 0.05 Å

shorter than in **12**. The Cp–K–Cp angle of $128.70(3^\circ)$ between the two planes is more bent than in **12** and the methyl groups point in alternating directions. The reason for this strong bending and for the absence of an additional molecule of ammonia is the side-on attraction of the potassium cation to a Cp anion of a neighboring coordination polymer chain (Figure 61).

The distances between K1 and the η^5 -coordinated carbon atoms range from

$2.930(2)$ Å to $3.268(2)$ Å. The potassium cation has short contacts to C3 and C5 of an adjacent chain with the shortest distances of $3.284(2)$ Å and $3.530(2)$ Å. This side-on coordination is similar to unsolvated KCp', where contact distances range from 3.255 Å to 3.404 Å. It is stronger than in unsolvated KCp where the corresponding distances are 3.331 Å and 3.661 Å. The attractions in KCp are weaker, because the potassium cation interacts with two anions at the same time instead of just one as in the case of KCp' and

13. The side-on attraction in **13** also causes the strong bending of the angle ($56.21(3)^\circ$) between the two anion planes. These angles are relatively similar in unsolvated KCp', where they range from 50.98° to 57.50° .

In **13**, the strands are arranged like a zipper. Each fragment consists of Cp', K1, and ammonia with the methyl group and the ammonia molecule pointing in opposite directions. This unit faces an inverted, equally build fragment in the adjacent strand. K–Cp side-on attractions between these two fragments bind them together.

The ammonia molecules fill up the coordination sphere of the potassium atoms. Together with the methyl group they are located on the open side of

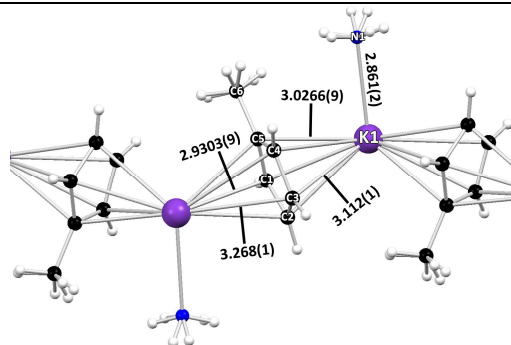


Figure 60: Crystal structure of CpK(NH₃) (**13**). The asymmetric unit is labelled. Distances are given in [Å]. The presented K–C distances are the shortest and longest, respectively. NH₃ is disordered by 49(5)% and the methyl-group by 29(11)%.

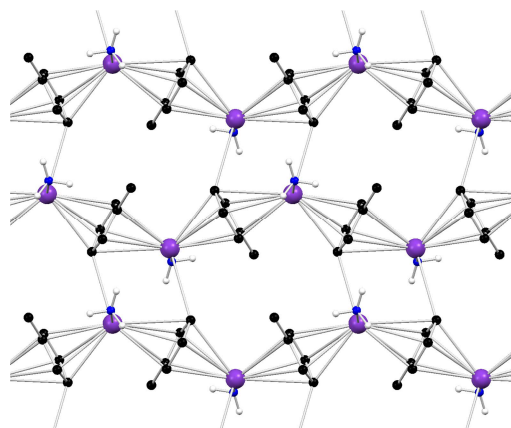


Figure 61: Layer formed of zig zag strands of **13** interconnected by K–Cp' side-on interactions.

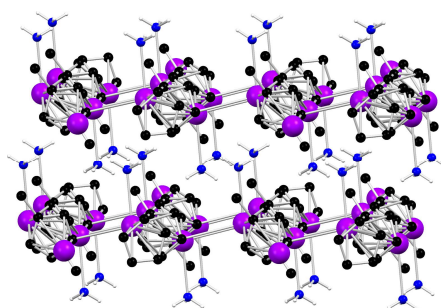


Figure 62: Stacking of layers in **13**

Results

Potassium Derivatives

the bent KCp' strands (Figure 62). The disorder of 49(5)% does not suggest any presence of hydrogen bonding. However, close contacts to the adjacent aromatic carbon atoms with distances between 2.806 Å and 2.850 Å are observed, but only for one fraction of the two disordered moieties. Therefore, they do not seem to be strong enough to lock the ammonia molecule into position and the ammonia molecule does not seem to be involved in $\text{NH}-\pi$ bonding.

3.3.3. $(\text{Ind})\text{K}(\text{NH}_3)_2$ (**14**): A Helical Coordination Polymer

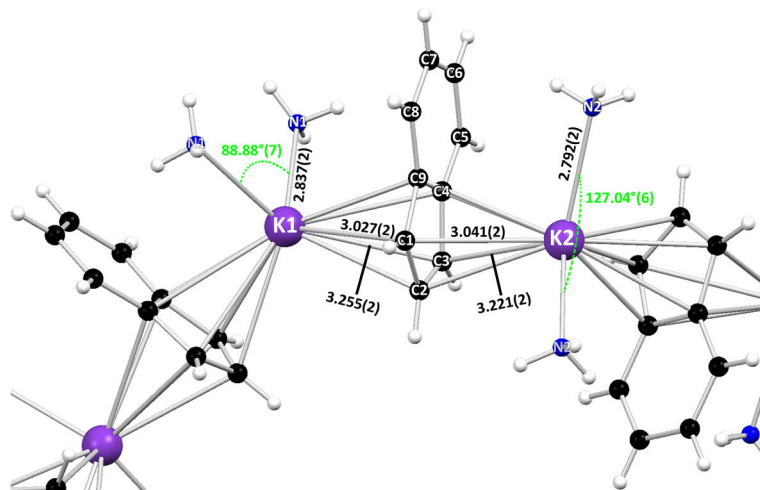


Figure 63: Crystal structure of $(\text{Ind})\text{K}(\text{NH}_3)_2$ (**14**). The asymmetric unit is labelled. Transparent labels reflect symmetry equivalent atoms. Bond distances are given in [Å]. The shortest and longest K-ind distances are depicted.

$(\text{Ind})\text{K}(\text{NH}_3)_2$ (**14**) was synthesized by saturating a solution of $\text{K}(\text{hmds})$ and indene in Et_2O with gaseous ammonia at -15°C . Crystallization took place at -45°C and **14** crystallizes in the orthorhombic space group $Fddd$. The asymmetric unit contains an indenyl anion, from both sides of the five-membered ring η^5 -coordinated by potassium cations (Figure 63). The potassium cations are half occupied and two molecules of ammonia are attached to each cation. In the crystal packing, **14** forms a coordination polymer as in the

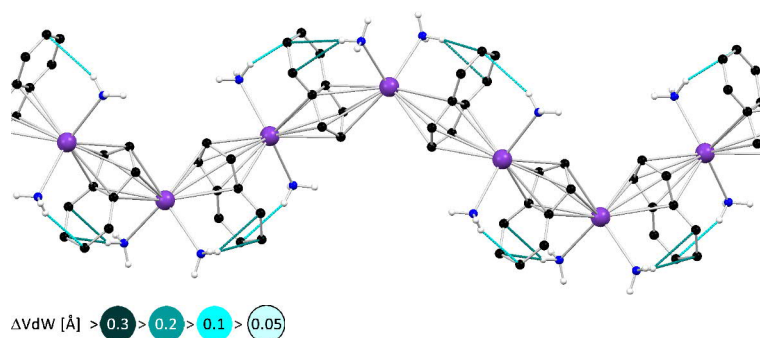


Figure 64: Polymeric chain of **14** and intramolecular $\text{NH}-\pi$ interaction between ammonia and the indenyl anions.

previously discussed structures **12** and **13**. Each cation is coordinated by two indenyl anions and two molecules of ammonia.

The structural pattern of the coordination polymer **14** is different from the previously discussed analogues containing Cp. Instead of a linear zigzag arrangement, a helical arrangement is observed with one

'rotation' of the indenyl anion every four K–ind units (Figure 64, Figure 66). K1 and K2 are each coordinated by the indenyl anions in a slightly different way: While both cations coordinate the indenyl anions exclusively at the five-membered ring with distances from the ring plane of 2.88(2) Å for K1 and 2.87(2) for K2, the angle of the two indenyl planes coordinating K1 is 50.87°(3) and the angle at K2 is 63.71°(2). Moreover, the two indenyl anions coordinating K1 have a *cis*-arrangement and the two indenyl anions coordinating K2 have a *trans*-arrangement, meaning that the six-membered rings in the coordination sphere of K1 point in the same direction and the six-membered rings in the coordination sphere of K2 point in opposite directions.

The ammonia molecules adapt to this arrangement following the position of the six-membered rings. At the potassium cation with the *cis*-arrangement, the N1–K1–N1 angle of 88.88°(7°) is comparable to and even wider than the corresponding angles in **12** (84.69°(8°) and 75.72°(9°)). At the potassium cation with the *trans*-arrangement, the N2–K2–N2-angle is widened to 127.04°(6°). This effect is directed by NH- π bonding (Figure 64). In the *cis*-arrangement, the ammonia molecule containing N1 forms strong hydrogen bonds to the six-membered ring, whereas in the *trans*-arrangement, the ammonia molecule containing N2 forms weaker hydrogen bonds to the six-membered ring. The weaker hydrogen bonds of the ammonia molecule containing N2 are caused by additional hydrogen bonds of the same ammonia molecule with anions of adjacent coordination polymer chains (Figure 65).

Similar structures to **14** are (Ind)K(TMEDA) and (Ind)K(PMDETA) by Weiss *et al.*^[101] In contrast to ammonia as donor ligand, TMEDA and PMDETA are multidentate and

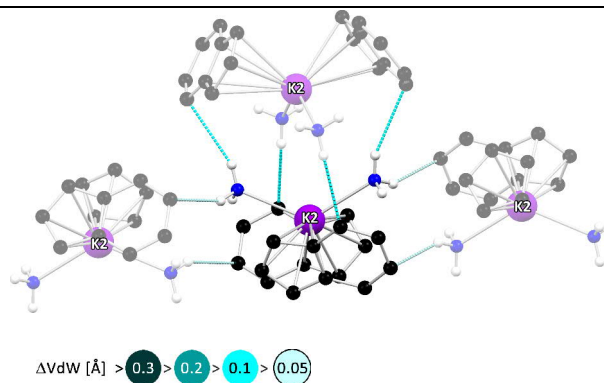


Figure 65: NH- π interactions of the H₃N–K–NH₃ unit with three adjacent coordination polymer strands.

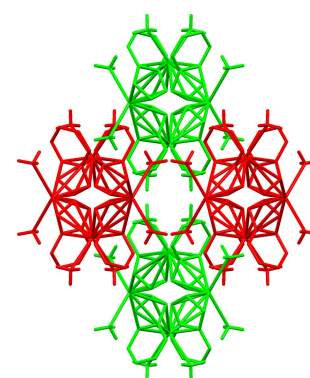


Figure 66: Packing plot of **14** along the a-axis. Colours red and green are only used for visualisation.

Results

Potassium Derivatives

possess a bulky hydrocarbon backbone. The increased steric demand forces the anions into an arrangement which is different from that in **14**. Both structures form linear zigzag-shaped coordination polymers. In the structure with of TMEDA as the ligand, the cation coordinates the anion at the five-membered ring in the same way as in **14**. The six-membered ring is pointing in alternating directions; the configuration around any cation is therefore always *trans*. The six-membered rings are aligned with the K(TMEDA) moieties and form a compact strand. In the structure with PMDETA, the by far bulkier ligand forces the six-membered ring to align in a transversal orientation with respect to the K(PMDETA) moiety, and the cation coordinates the anion from one side at the five-membered ring and from the other side in a side-on fashion at the connection of the five- and six-membered rings. In both structures from literature, NH- π bonding between the ligands and the anion does not play an important role in the formation of the strands. In **14**, coordination of ammonia on the other side of the cations creates an arrangement where every NH₃ molecule is involved in NH- π bonding. Comparing the spatial arrangement of the anions in the TMEDA and PMDETA structures, interactions like in **14** would not be possible. Therefore, NH- π bonding seems to be the driving force in the formation of the helical structure.

3.3.4. (Flu)K(NH₃)₂ (**15**): A 2-dimensional Coordination Polymer

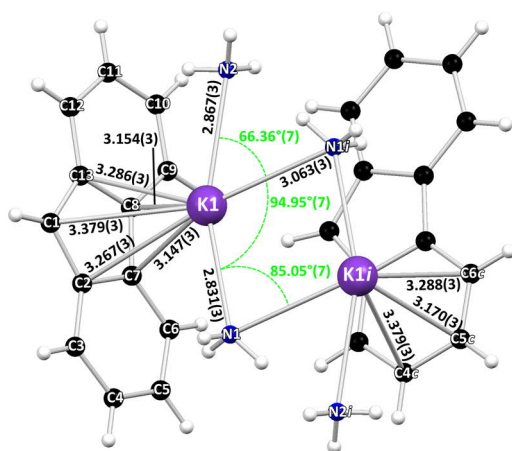


Figure 67: Section of the crystal structure of (Flu)K(NH₃)₂ (**15**). Distances are given in [Å]. Label 'i' and 'c' indicates symmetry generation by inversion and c-glide planes, respectively. The other labelled atoms are part of the asymmetric unit. A structural identical second fragment part of the asymmetric unit has been omitted for clarity.

(Flu)K(NH₃)₂ (**15**) was synthesized by condensation of ammonia in a solution of K(hmde) and fluorene in methyl-*tert*-butylether at -78 °C until the solution turned clear. Crystallization was achieved at -76 °C. **15** crystallizes in the monoclinic space group *P*₂₁/*c* with two identically built fragments in the asymmetric unit. Each fragment consists of a fluorenyl anion which is η^5 -coordinated by a potassium cation having two molecules of ammonia attached to it (Figure 67).

The crystal packing reveals a new structural motif: a 2-dimensional coordination polymer with a building block consisting of a

K₂(μ -NH₃)₂(NH₃)₂²⁺ unit corralled by four fluorenyl anions (Figure 68). Each fragment in the asymmetric unit forms an independent layer without any significant structural differ-

ence between them. Within the building block, two cations are bridged by two molecules of ammonia. The distances of the bridging ammonia molecule to the two cations are different with 2.831(3) Å for K1–N1 and 3.063(3) Å for K1*i*–N1 (*i* : symmetry-related by inversion in a central point between the two bridged cations). For the second fragment, the distances are 2.822(3) Å for K2–N4 and 3.023(3) Å for K2*i*–N4. The distances of the single-coordinated ammonia molecules to the cations are 2.867(3) Å for K1–N2 and 2.840(3) Å for K2–N3. The angles between the connections of the potassium cations and the bridging ammonia molecules are 85.07°(7°) for K1–N1–K1*i* and 87.73°(7°) for K2–N4–K2*i*. The angles between the connections from the potassium centers to the single-coordinating ammonia molecules and to the bridging ammonia molecules next to them are comparably narrow with 66.36°(7°) for N2–K1–N1*i* and 68.58°(7°) for N3–K2–N4*i*. Each cation in the building block interacts with three adjacent fluorenyl anions. The strongest attraction is achieved by coordination of the five-membered ring with a distance of the cation to the fluorenyl plane of 2.97(3) Å for K1 and 2.98(2) Å for K2. The cations are significantly shifted away from the center of the five-membered ring towards C7 and C8 with distances of 3.379(3) Å to C1, 3.147(3) Å to C7, and 3.154(3) Å to C8. K2 is slightly less shifted than K1 and points towards C21 with distances of 3.176(3) Å, 3.237(3) Å to C15, and 3.257(3) Å to C14. In addition to the coordination to the five-membered ring, the potassium cations also coordinate to a six-membered ring of an adjacent fluorenyl anion. The distance to this fluorenyl plane is 3.05(3) Å for K1 and 3.07(2) Å for K2. The coordination to the six-membered ring can be described as a η^3 -coordination of K1 around C5 with distances of 3.170(3) Å to C5, 3.288(3) Å to C6, and 3.302(3) Å to C4 (Figure 67). The coordination of K2 is lying between a η^3 - and a η^4 -coordination around C23 and C22 with distances of 3.201(3) Å to C23, 3.276(3) Å to C22, 3.346(3) Å to C24, and 3.484(3) Å to C21. A third – but even weaker – attraction is also present: a third adjacent anion is located at the top of the five-membered ring with distances of 3.420(3) Å for K1 to C1 and 3.552(3) Å for K2 to C14.

Within the building blocks, strong NH- π bonding is present. Each molecule of ammonia interacts with at least two fluo-

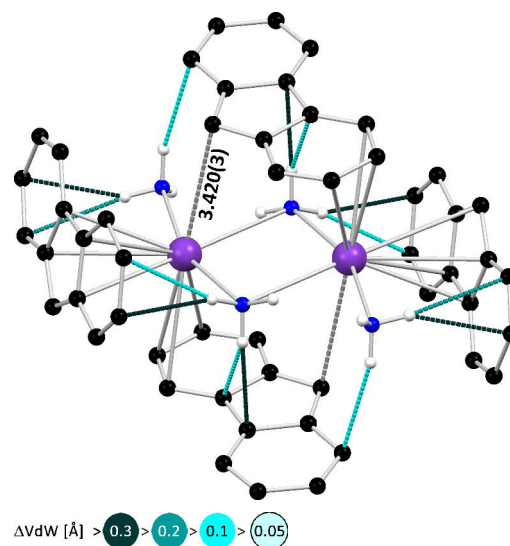


Figure 68: Central structural element of the 2-dimensional coordination polymer and NH- π interactions involved of the fragment involving K1. The fragment of K2 shows a similar pattern. Distance is given in [Å].

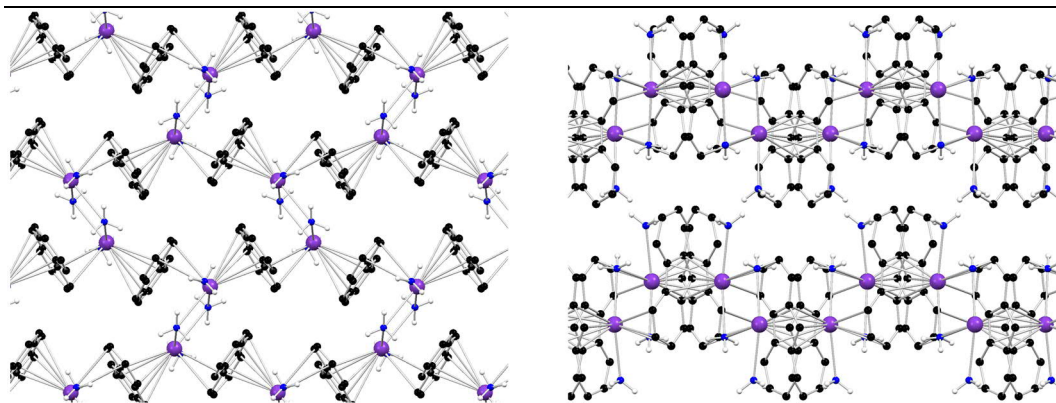


Figure 69: Packing plots of 15. Left: Single layer of 15 along the b-axis. Right: Stacking of the 2-dimensional layers along the c-axis.

renyl anions. The distances of the ammonia hydrogen atoms to the closest carbon atoms range from 2.46(2) Å to 2.71(2) Å ($\Delta\text{VdW} = 0.44(2)$ Å to 0.19(2) Å) and are therefore comparably strong for almost all involved hydrogen atoms. The single coordinating ammonia molecules containing N2 and N3 interact at the periphery of the six-membered ring of the anions, whereas the bridging ammonia molecules with N1 and N4 interact at the periphery of the five-membered ring. The ammonia molecule containing N3 is also involved in a weak hydrogen bonding with an anion of the next layer.

In the crystal packing the building blocks are arranged in a herringbone pattern and form a layer along the *c*- and *b*-axes (Figure 69). Viewed along the *c*-axis, the layers have a zig-zag shape and are packed accordingly.

3.4. Rubidium Derivatives

3.4.1. $\text{CpRb}(\text{NH}_3)_2$ (**16**): Isostructural to $\text{K}(\text{Cp})(\text{NH}_3)_2$

$\text{CpRb}(\text{NH}_3)_2$ (**16**) was synthesized by condensation of ammonia at -78°C to RbCp until the solution turned clear. Crystallization took place at -76°C and gave **16** in the orthorhombic space group $Pnma$. The asymmetric unit consists of a Cp-anion that is η^5 -coordinated from both sides by half-occupied rubidium cations (Figure 70). Each rubidium cation is coordinated by two molecules of ammonia. The nitrogen atoms of the ammonia

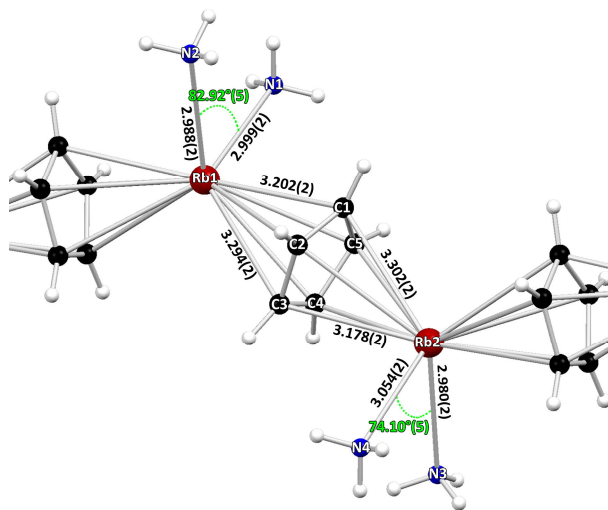


Figure 70: Crystal structure of $\text{CpRb}(\text{NH}_3)_2$ (**16**). The asymmetric unit is labelled. Distances are given in [Å].

molecules are half-occupied as well and are lying on the same mirror plane as the rubidium cations. In the crystal packing, **16** forms 1-dimensional-coordination polymers like the previously discussed $\text{CpK}(\text{NH}_3)_2$ (**12**). This is not the only similarity to **12**. Also the content of the asymmetric unit is equally structured, the space group is the same and even the cell parameters only differ slightly with $a = 22.279(5)$, $b = 10.843(3)$, $c = 6.381(2)$ for **12** and $a = 22.571(6)$, $b = 11.234(2)$, $c = 6.400(2)$ for **16**. The cell volume of **16** is $1622.9(8) \text{ \AA}^3$ and about 5% larger than the cell volume of **12** with $1541.3(7) \text{ \AA}^3$. No significant disorder of the hydrogen atoms of the ammonia molecules as in **12** has been observed in **16**. Disorder along the mirror planes could possibly be present, but a refinement does not result in a significantly better model. The ammonia molecules have been refined with one hydrogen atom of each ammonia molecule placed on a mirror planes and one hydrogen atom placed outside the mirror plane. The whole molecule is completed by the symmetry operation of the mirror. Slight differences between **12** and **16** are the coordination distances, which range from $3.047(2) \text{ \AA}$ to $3.187(2) \text{ \AA}$ for $\text{K}-\text{C}$ in **12** and from $3.178(2) \text{ \AA}$ to $3.302(2) \text{ \AA}$ for $\text{Rb}-\text{C}$ in **16**, and the in average about 0.023 \AA weaker $\text{NH}-\pi$ interaction in **16**.

3.4.2. $\text{Cp}'\text{Rb}(\text{NH}_3)_2$ (**17**): 1-Dimensional Coordination Polymer

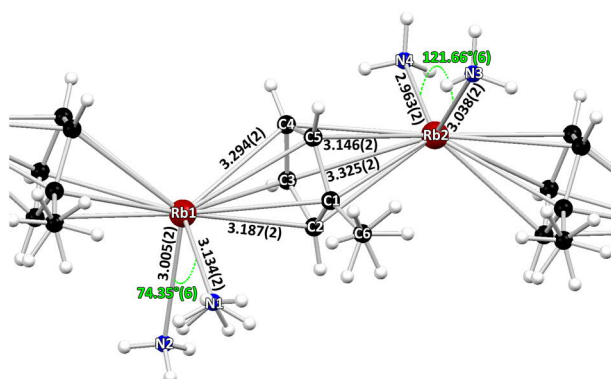


Figure 71: Crystal structure of $\text{Cp}'\text{Rb}(\text{NH}_3)_2$ (**17**). The asymmetric unit is labelled. Distances are given in [Å]. The methyl group is disordered by 39(3)% and the ammonia molecule of N1 is disordered by symmetry and a mirror plane.

molecules, the rubidium cations are placed on mirror planes. The hydrogen atoms of the methyl group and the ammonia molecule of N1 are disordered: the methyl group by 39(3)% and the ammonia molecule is symmetry-site disordered (Figure 71). The distances of the cations to the anion plane are 3.01(2) Å for Rb1 and 3.00(2) Å for Rb2 and the angle between two anion planes is 33.65°(4).

The structural motif of **17** (Figure 72) is a 1-dimensional coordination polymer like the 'zig-zag' arrangement in **12** and **16**. Within one strand the methyl groups point in the same direction as in **13**, but no Rb-Cp' side-on coordination is present. A significant difference to both **12** and **16** is the strong bending of the N3-Rb2-N4-angle of 121.66°(6). The N1-Rb1-N2-angle of 74.35°(6) lies within the expected range. The angles in **12** and **16** range from 74.35°(6) to 84.69°(8). The ammonia molecule of N3 deviates from the anticipated configuration as observed in

12 and **16**.

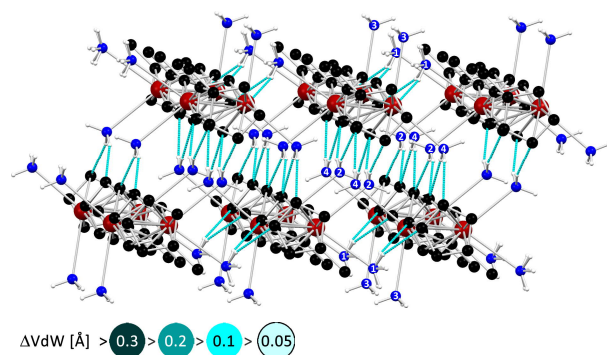


Figure 72: Packing plot of **17** and NH- π interactions between strands of **17**. The ammonia molecules of N2 and N4 connect two strands, N1 connect this pair of strands to the next one. Strands above and below that pattern do not interact.

The ammonia molecules of N1, N2, and N4 interact with the adjacent anions in the same way as in **12** and **16**. The hydrogen atoms of N2 and N4 bridge the anions of adjacent rubidocene fragments. Each disordered moiety of the ammonia molecule of N1 interacts with one anion. The contact distances range from

2.758(6) Å to 2.771(9) Å ($\Delta\text{VdW} = 0.142(6) \text{ \AA} - 0.129(9) \text{ \AA}$). The ammonia molecule of N3 is blocked for this interaction and bent away from the ammonia molecule of N2 by the methyl groups of the own strand and the adjacent strand. It lies within a pocket of four methyl groups in similar distance (Figure 73). The same effect causes also the non-linear coordination of the ammonia molecule of N1. The hydrogen atoms of the two disordered moieties are tilted by 30.7° from the ideal position toward the rubidium cation. Two methyl groups within the same strand hinder the molecule from the ideal position.

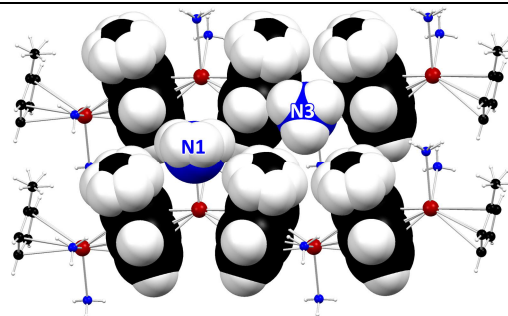


Figure 73: Two neighbored strands of **17** with partly depicted in a spacefill model. Sterical restraint of the methyl groups causes bending of the hydrogen atoms of the ammonia molecule of N1 and the bending of the whole ammonia molecule of N3.

The structural features of **17** place it between **13** and **16**. The coordination sphere of the rubidium cations is filled by coordination of Cp' and two molecules of ammonia as in **16** and no side-on interaction as in **13** is present. Whereas in **13**, layers are formed that do not interact by NH- π interactions with each other, the strands of **17** form a 2-dimensional pattern by NH- π interactions of the ammonia molecule of N1. Two of these 2-dimensional patterns are interconnected by the NH- π interactions of the ammonia molecules of N2 and N4. In this double-layered arrangement, the methyl groups point toward the next layer and hinder any interaction of the ammonia molecule of N3.

3.4.3. (Ind)Rb(NH₃)₂ (**18**): A 2-dimensional Coordination Polymer

(Ind)Rb(NH₃)₂ (**18**) was synthesized by condensation of ammonia to a solution of Rb(hmds) and indene in Et₂O at -78°C . The white precipitation was dissolved over night at -45°C and crystallization took place at -76°C . **18** crystallizes in the monoclinic space group $P2_1/c$ with two indenyl anions, two rubidium cations, and four molecules of ammonia in the asymmetric unit. The two cations are bridged by two molecules of ammonia and each cation is

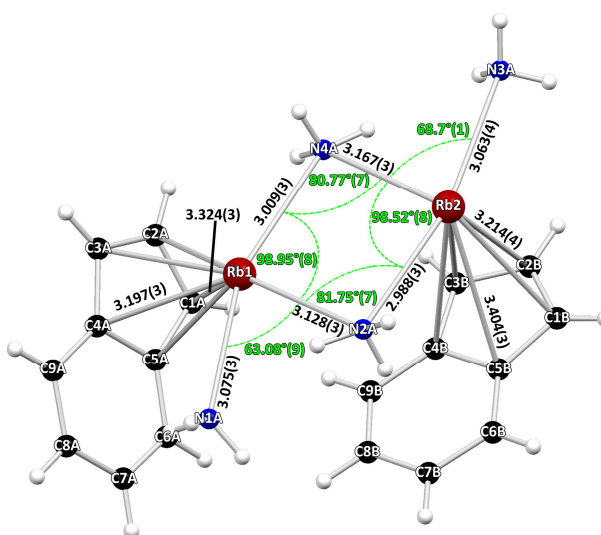


Figure 74: Asymmetric unit of (Ind)Rb(NH₃)₂ (**18**). The whole structure is disordered by 5.9(2)%. The minor disordered moiety has not been depicted for clarity. Bond distances are given in [Å].

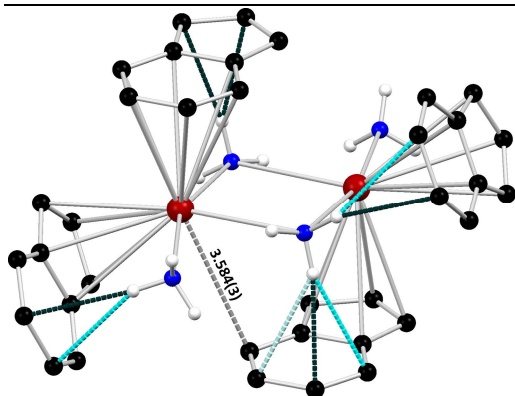


Figure 75: Building block of the 2-dimensional layer of **18**, a $\text{Rb}_2(\text{NH}_3)_2(\text{NH}_3)_2$ fragment surrounded by four indenyl anions and NH- π interactions. Distances are given in [Å].

single-coordinated by another molecule of ammonia (Figure 74). The indenyl anions coordinate to the cations with the five-membered ring. The whole structure is disordered on a second position by 5.9(2)%, which will not be included into the following discussion. The $\text{Rb}_2(\mu\text{-NH}_3)_2(\text{NH}_3)_2$ -unit is very similar to corresponding fragment in $(\text{Flu})\text{K}(\text{NH}_3)_2$ (**15**). The bridging ammonia molecule of N2A coordinates Rb1 with a distance of 3.124(3) Å and Rb2 with a distance of 2.993(2) Å. The Rb1–N2A–Rb2-

angle is 81.73°(7). The corresponding values for N4A are 3.015(3) Å for Rb1, 3.160(3) Å for Rb2, and the Rb1–N2A–Rb2-angle is 80.80°(7). The distances of the single-coordinated ammonia molecules lies between the values of the 'bridging' with 3.073(3) Å for Rb1–N1A and 3.064(4) Å for Rb2–N3A.

The packing plot gives a similar picture. Around the central $\text{Rb}_2(\mu\text{-NH}_3)_2(\text{NH}_3)_2$ -moiety, four indenyl anions are arranged (Figure 75). Each cation coordinates two of the rubidium cations. Rb1 coordinates the indenyl anions of C1A–C9A at the five-membered ring (C1A–C5A) and the anion of C1B–C9B at the six-membered ring (C4B–C9B). Rb2 coordinates both anions at the five-membered ring. The distances from the ring planes range from 3.020(8) Å to 3.086(8) Å. The rubidium cations are not sitting perfectly upon the ring centres, but shift in various directions. The Rb–C-distances range from 3.197(3) Å to 3.444(3) Å for both η^5 - and η^6 -coordination and vary for every single coordination in a range from 0.127 Å to 0.222 Å. Additional side-on coordination is only present for Rb1, which has a short contact to C9B of an adjacent six-membered ring with a distance of 3.548(4) Å.

NH- π -interactions are present for all ammonia molecules except the one of N3A. The ammonia molecules of N1A and N4A interact with one adjacent anion and the ammonia molecule of N2A with two anions as previously observed in the case of **15**, where the additional six-membered ring of the fluorenyl anion provides more possibilities for NH- π interaction. The present contacts of the hydrogen atoms of the ammonia molecules to the closest carbon atoms of the interacting anions are very short lying between 2.49(2) Å and 2.57(2) Å ($\Delta\text{VdW} = 0.41(2)$ Å–0.33(2) Å).

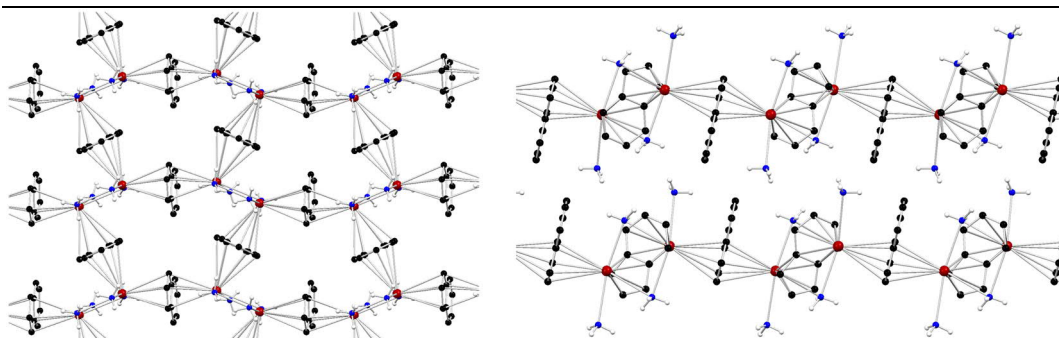


Figure 76: Packing plots of **18**. Left: Single layer of **18** viewed from above. Right: Stacking of the layers of **18**.

In the crystal packing, 2-dimensional coordination polymers are formed similar to **15** (Figure 76). Main differences are the presence of only one Rb–ind side-on interaction instead of two K–flu side-on interactions in **15**, and the absence of NH– π interactions for the ammonia molecule of N3A. Both differences are caused by the lack of an additional six-membered ring of the indenyl anion compared to the fluorenyl anion.

3.4.4. (Flu)Rb(NH₃)₂·THF (**19**): An Intercalation Compound

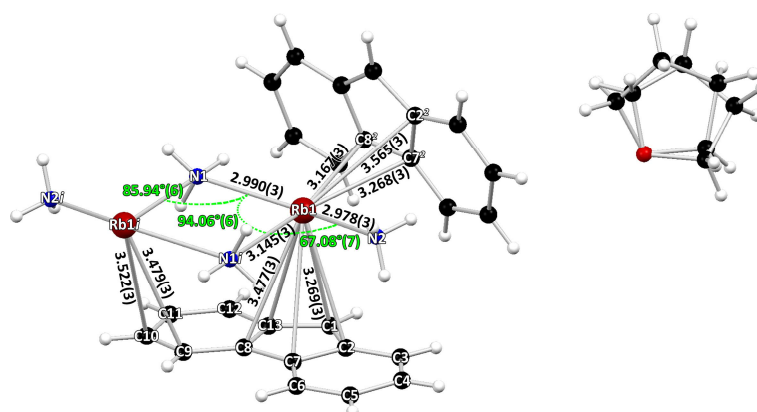


Figure 77: Section of the crystal structure of (Flu)Rb(NH₃)₂·THF (**19**). Distances are given in [Å]. Label ‘i’ and ‘2’ indicates symmetry generation by inversion and a twofold axis, respectively. The other labelled atoms are part of the asymmetric unit. The thf molecule (including oxygen) is disordered by 28.0(7)%

(Flu)Rb(NH₃)₂·THF (**19**) was synthesized by saturating a solution of Rb(hmds) and fluorene in THF with gaseous ammonia at -15°C . Subsequent crystallization at -76°C gives **19** in the orthorhombic space group *Pbca* with a fluorenyl anion, coordinated to the five-membered ring by a rubidium cation, two molecules of ammonia attached to the cation, and a lattice molecule of THF (Figure 77). The structural motif is very similar to **15**. A Rb₂(μ -NH₃)₂(NH₃)₂-unit is corralled by four fluorenyl anions (Figure 78). Different to **15**, the rubidium cations coordinate the anions only at the five-membered rings with distanc-

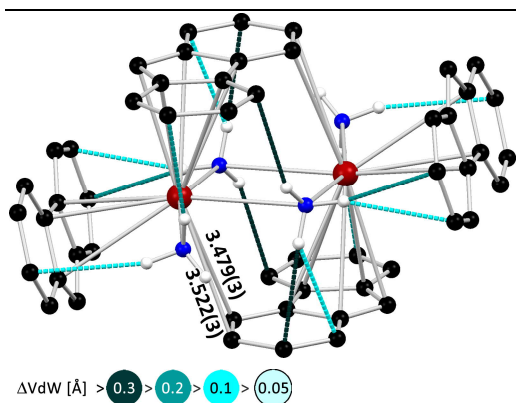


Figure 78: Building block of the 2-dimensional layer of **19**, a $\text{Rb}_2(\text{NH}_3)_2(\text{NH}_3)_2$ fragment surrounded by four fluorenyl anions and $\text{NH}-\pi$ interactions. Distances are given in [Å].

es to the ring planes of 3.108(5) Å and 3.141(5) Å. The rubidium cation coordinates the two five-membered rings differently. To one anion the cation is shifted towards C1 with a distance of 3.269(3) Å and away from C7 and C8 with distances of 3.472(3) Å and 3.478(3) Å and to the other anion it is strongly shifted towards C7 and C8 with distances of 3.268(3) Å and 3.167(3) Å. The distance to C1 of 3.646(3) Å is much longer and can only be regarded as a very weak interaction, since the distance is only 0.05 Å shorter than the sum of the Van-der-Waals

radii. The rubidium cation has also a side-on coordination to a six-membered ring of a third adjacent anion with distances to C9 and C10 of 3.479(3) Å and 3.522(3) Å.

The ammonia molecules are involved in $\text{NH}-\pi$ interaction. The bridging ammonia molecule of N1, with a distance to Rb1 of 2.989(3) Å and a distance of 3.145(3) Å to the symmetry equivalent, interacts with three adjacent anions. The contacts of the involved hydrogen atoms to the closest carbon atoms are short with distances ranging from 2.59(2) Å to 2.64(2) Å. The single coordinated ammonia molecule of N2 has a distance to the rubidium cation of 2.978(3) Å and interacts with two adjacent anion planes. The distances to the closest carbon atoms are 2.76(2) Å and 2.64(2) Å.

The 2-dimensional layered structure of **19** looks again similar to the layers of **15** and **18**, differing in the occurrence of the THF molecules between the layers (Figure 79). This type of co-crystallization has only been observed in $\text{Cp}^*\text{Na}(\text{NH}_3)_3 \cdot (\text{HN}(\text{SiMe}_3)_2)_{0.8}$ (**9**), where $\text{HN}(\text{SiMe}_3)_2$ occupied the central void formed by six $\text{Cp}^*\text{Na}(\text{NH}_3)_3$ -strands in a hexagonal

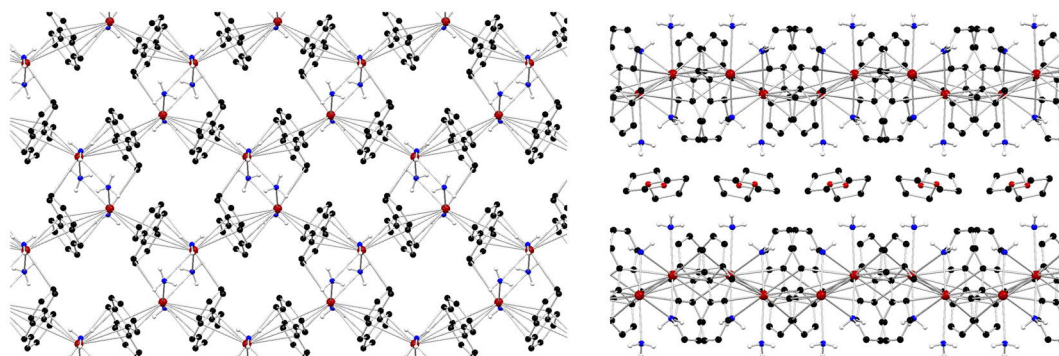


Figure 79: Packing plots of **19**. Left: Single layer of **19** viewed from above. Right: Stacking of the layers of **18** with thf intercalated between the layers.

arrangement.

The THF molecules are not lying with their hydrocarbon backbone upright between the layers, but bend into the gap between the layers of (Flu)Rb(NH₃)₂. Both the sterical restraint from the layers and the NH–O and CH–O interactions keep them in their position (Figure 80). The hydrogen interactions are

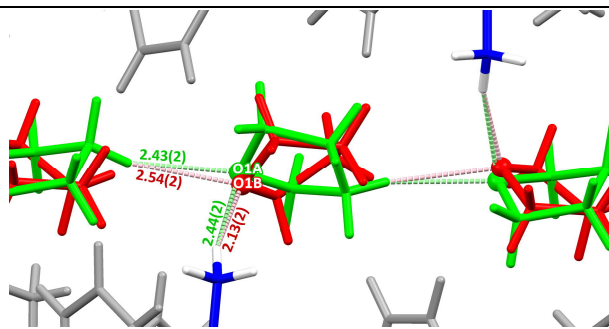


Figure 80: Interactions of the two disordered moieties of thf with the environment. The green fraction is occupied by 82(7)%, the red fraction is occupied by 28(7)%.

different for each disordered moiety. Both fractions of THF interact with the ammonia molecule of N₂. The minor red fraction has a strong interaction (O–HN: 2.13(2) Å) and the major green fraction has a weaker interaction (O–HN: 2.44(2) Å). The weaker O–HN interaction is countered with a stronger O–HC interaction (2.43(2) Å) to an adjacent THF molecule. The corresponding interaction with the red fraction is weaker with 2.54(2) Å. Only the mayor green fraction provides a CH-hydrogen atom for this kind of interaction. The use of Et₂O in **18** and mtbe in **15** did not lead to that kind of intercalation, probably due to their higher steric bulk.

3.5. Caesium Derivatives

3.5.1. $\text{CpCs}(\text{NH}_3)$ (**20**): Between coordination polymer and unsolvated CsCp

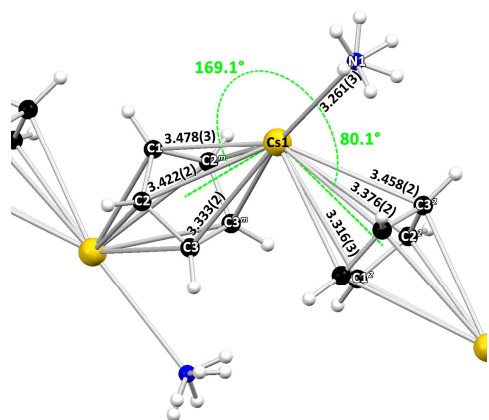


Figure 81: Crystal structure of $\text{CpCs}(\text{NH}_3)$ (**20**). The labels 'm' and '2' indicate symmetry equivalence by mirror planes and twofold axes, respectively. The other labels are part of the asymmetric unit. The ammonia molecule of N1 is disordered by symmetry. Bond distances are given in Å.

$\text{CpCs}(\text{NH}_3)$ (**20**) has been synthesized by condensation of ammonia to previously synthesized and dried CsCp . The reaction mixture has been warmed up to -33°C and the solution turned clear. Crystallization took place at -76°C . **20** crystallizes in the orthorhombic space group $Pnma$ with half of a Cp-anion, a caesium cation, and one molecule of ammonia in the asymmetric unit (Figure 81). The ring-carbon atom C1, the caesium cation Cs1, and the nitrogen atom N1 are lying on a mirror plane. The hydrogen atoms of the ammonia molecule are symmetry-site disordered along the

mirror plane. The whole Cp-ring is completed by symmetry operation along the mirror. The whole structure consists of a zig zag -shaped 1-dimensional coordination polymer, but different to the potassium- and rubidium-equivalents of **12** and **16**, only one molecule of ammonia is coordinated to the caesium cation with a distance of $3.261(3)$ Å (Figure 82). Compared to potassium and rubidium, the coordination of the Lewis-hard ammonia to the Lewis-soft caesium cation is much weaker. The result is a much less dominant influence of the ammonia molecule as in the previously observed structures. The distance of

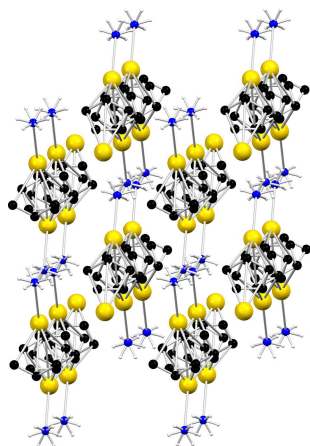


Figure 82: Packing plot of **20**. CH-hydrogen atoms have been omitted for clarity.

the caesium cation to both planes of the two coordinating Cp-anions is $3.171(2)$ Å. The angle between the two planes is $77.26^\circ(7)$. The cation is η^5 -coordinated to both rings with Cs–C-distances between $3.316(3)$ Å and $3.478(3)$ Å. Cs1 is slightly shifted towards the open side of the angle. The coordination of the ammonia molecule to the caesium cation is unconventional. The angles between N1, Cs1, and the centroids of the two coordinating Cp-anions are 169.1° and 80.1° . The ammonia molecule is not bending transversal to the direction of the 1-dimensional coordination polymer, but is bending into the direction of propagation.

The coordination polymers in **20** are more densely packed than in the potassium- and rubidium-derivatives **12** and **16**, where each polymeric strand is surrounded by six others. The direction of propagation in **12** and **16** is the *b*-axis and by calculating the distances of Cp-centroids, the distance of the polymeric chains can be obtained. The Cp-anions are lying in one plane along the *b*-axis and their centre is also the centre of the polymeric chain along the *b*-axis. The distances range from 6.286 Å to 6.482 Å in **12** and from 6.400 Å to 6.552 Å in **16**. The distance of the polymeric chains in **20** with is 5.727 Å. The distance comes close to solvent free CsCp with a distance of 5.275 Å.

In CsCp the interaction between the polymeric chains are dominated by electrostatic side-on interaction of the cation to Cp-rings of adjacent CsCp-strands.^[33b] The distances to the closest interacting carbon atoms are 3.765 Å and 3.773 Å. A similar configuration can be found in **20** (Figure 83). The Cp-rings of the adjacent polymeric chains are not arranged in a clear side-on fashion as in CsCp, where the caesium cation lies about 0.4 Å outside the anion planes of the two interacting Cp-anions. In **20**, the caesium cation shifts about 2.004(2) Å out of the anion plane of the two interacting anions. However, the distance to the closest carbon atom is even closer with a distance of 3.710(2) Å to C3. The structure could be therefore seen as a insertion of ammonia into the solid state structure of CsCp rather than solvated polymer chains as in the case of potassium and rubidium. But the ammonia molecule is not just filling up a gap in the crystal structure but also actively shapes it. Although the hydrogen atoms appear to be disordered, NH- π interactions are present (Figure 84).

In each of its two configurations, the ammonia molecule interacts with Cp-anions in close proximity. All three hydrogen atoms have rather weak interactions, but interact from three directions with the anion.

Besides the steric repulsion of the two side-on-interacting Cp-anions, the NH- π interactions help to understand the strange orientation of the ammonia

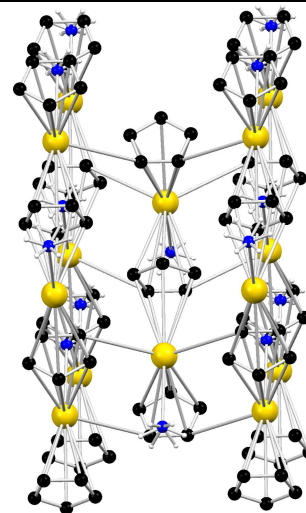
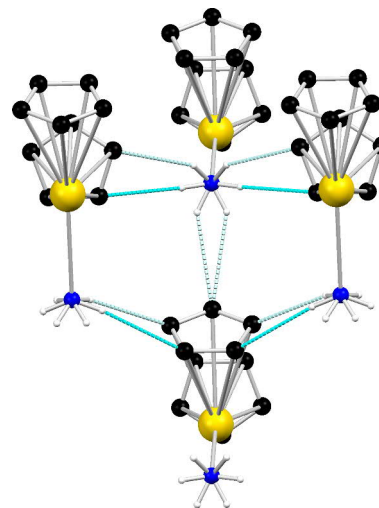


Figure 83: Side-on interactions of caesium with adjacent Cp-anions with a Cs–C distance of 3.720(2) Å.



Δvdw [Å] > 0.3 > 0.2 > 0.1 > 0.05

Figure 84: NH- π interactions of the disordered ammonia molecule with the environment.

molecule in the crystal structure as well as the strong bending of the anions within the zig zag -arrangement. Each caesium cation coordinates two Cp-anions and a NH₃-molecule directly. The closer environment of the cation consists of two side-on interacting Cp-anions and a NH₃-molecule from an adjacent strand (Figure 82). The NH₃-molecule interacting with one of the directly coordinated Cp-anions. The Cp-anions are somewhat 'pushed and pulled' together by the environment.

3.5.2. Cp'Cs(NH₃) (21): Between Cp'K(NH₃) and Cp'Rb(NH₃)₂

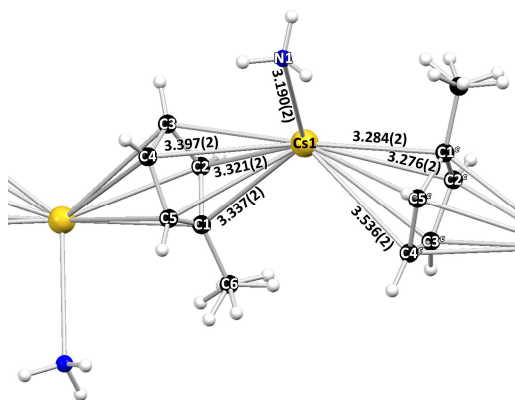


Figure 85: Crystal structure of Cp'Cs(NH₃) (21). The label 'c' indicates symmetry equivalence by a c-glide plane. The other labels are part of the asymmetric unit. Distances are given in Å. The methyl-group is disordered by 48(4)%.

Cp'Cs(NH₃) (21) has been synthesized by condensation of ammonia to previously synthesized and dried CsCp'. The reaction mixture was warmed up to -33°C and the solution turned clear. Subsequent crystallization at -76°C gave 21 in the monoclinic space group *P*2₁/*c* with one Cp'-anion, a caesium cation, and one molecule of ammonia within the asymmetric unit (Figure 85). The hydrogen atoms of the methyl-group are disordered by 48(4)%. 21 forms 1-dimensional coordination-polymers in a zig zag -arrangement with the methyl group pointing in alternating direction along the strand (Figure 86).

The caesium cation coordinates both anions in a η⁵-fashion with distances to the ring planes of 3.150(2) Å and 3.136(2) Å and a distance range to the coordinating carbon atoms of 3.276(2) Å to 3.536(2) Å. The angle between two anions is with 34.76°(4) far less bended

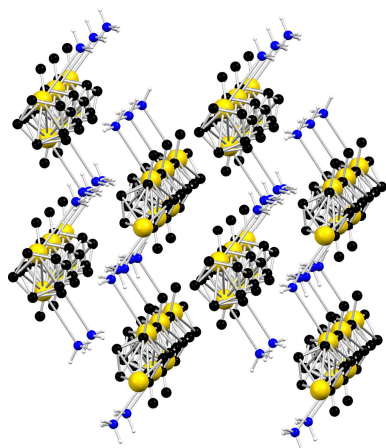


Figure 86: Packing plot of 21.

than in 20. Only one molecule of ammonia is coordinating the caesium cation with a distance of 3.190(2) Å. The absence of a second molecule of ammonia once more reflects the weak coordination of a Lewis-hard ligand like ammonia to a Lewis-soft caesium-cation. At the position where a second ammonia molecule would have been anticipated, a Cp'-anion of an adjacent coordination-polymer strand is present. Similar to 20, a side-on coordination is formed between the caesium cation to C3 of an adjacent strand with a distance of 3.756(2) Å of. The distance is close to the distances of

3.765 Å and 3.773 Å in CsCp and longer than the distance of 3.710(2) Å in **20**. The caesium cation is not in plane with the side-on coordinating anion, but 1.465(3) Å above its ring plane.

The rest of the environment of caesium is filled with another ammonia molecule from a neighbored strand and a methyl-group. NH- π interactions of the ammonia molecule with an adjacent Cp-ring are present with distances of 2.769(9) Å and 2.821(5) Å.

The polymeric strands are interacting from one side via Cs-Cp side-on and from the other side via NH- π (Figure 87). The pattern

has similarities and significant differences to the corresponding potassium derivative **13** and the rubidium derivative **17**. In **13**, the coordination polymer strands form only K-Cp side-on interactions, **17** forms only NH- π , **21** combines both. In **13** the strands form a 2-dimensional layer without corresponding to each other, in **17** the strand form double layers, solely connected by NH- π , and also do not interact with the next double-layer. In both cases the methyl groups and ammonia point out of the plane of the layer and create steric restraint for interaction. In **21** NH- π also form some sort of a double layer. Those double layers are interconnected by Cs-Cp side-on.

3.5.3. (Ind)Cs(NH₃) (**22**): A 2-Dimensional Coordination Polymer

(Ind)Cs(NH₃) (**22**) has been synthesized by condensation of ammonia to a mixture of indene and Cs(hmds) at -78°C. Subsequent crystallization took place at -76°C and gave **22** in the monoclinic space group *C2/c* with two half-occupied indenyl-anions, a caesium cation and a molecule of ammonia in the asymmetric unit. Both anions show symmetry-site disorder. The indenyl anion of C1-C9 is placed on a twofold axis and the anion of C10-C18 is placed on an inversion centre (Figure 88). The effect of both symmetry elements is the interchange of the five- and the six-membered ring. In the crystal packing **22** forms a 2-dimensional coordination polymer as the rubidium-indenyl structure **18** and the potassium- and rubidium-fluorenyl structures **14** and **19** (Figure 90). Each anion is coordinated from one side at the five-membered ring and from the other side at the six-membered ring. The distance of the caesium cation to the ring plane ranges from 3.160(4) Å to

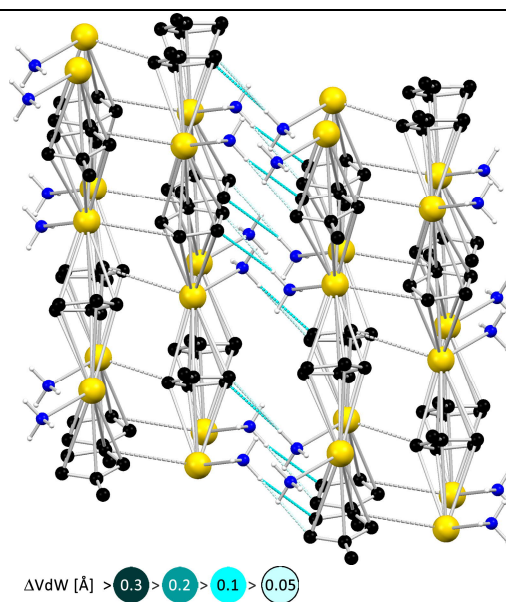


Figure 87: NH- π interactions and Cs-Cp' side-on interactions of the coordination polymer strands of **21**.

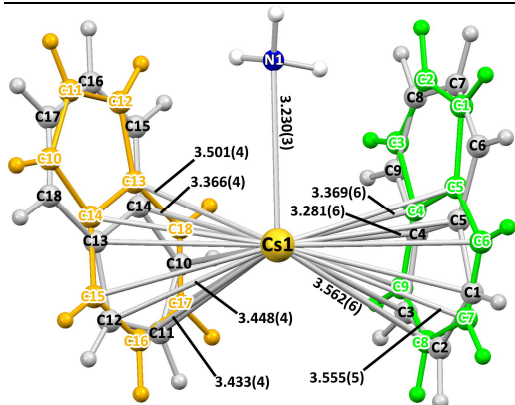


Figure 88: Asymmetric unit of $(\text{Ind})\text{Cs}(\text{NH}_3)$ (**22**) including the symmetry site disorder of the indenyl anions. The orange moiety indicates disorder by inversion, the green moiety disorder by a twofold axis. For each Cs–ind interaction the shortest and longest distance is depicted. Bond distances are given in Å.

Cs1 has either a short contact to the five membered ring at C10 with a distance of 3.523(4) Å or to the six-membered ring with distances of 3.480(4) Å to C17 and 3.719(4) Å to C18. The bridging ammonia-molecule is also involved in NH- π interactions with short contacts ranging from 2.567 Å to 2.722 Å.

As is the previously discussed caesium-structures **20** and **21**, an anticipated second molecule of ammonia is absent. In **22** the caesium cation is uncoordinated from one side, leaving a vacant position. Instead of an additional molecule of ammonia, an anion of the next layer is occupying the position. Nonetheless, a single-coordinating ammonia-molecule couldn't be incorporated in any NH- π interaction. The central motif of the layer, a $\text{Cs}_2(\mu\text{-NH}_3)_2^{(2+)}$ -unit surrounded by four

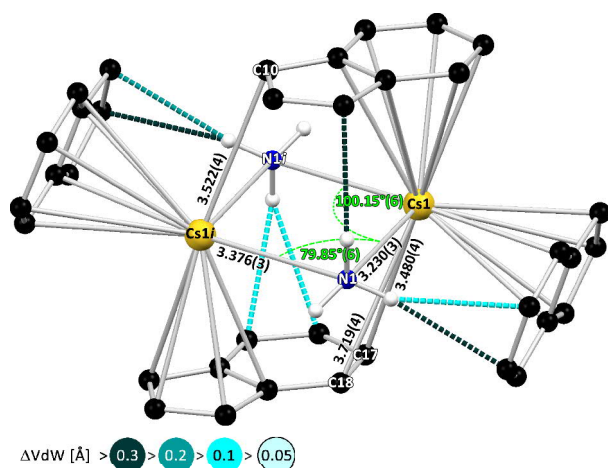


Figure 89: Building block of the 2-dimensional pattern of **22**. A $\text{Cs}_2(\text{NH}_3)_2$ -fragment is surrounded by four indenyl anions. Sites of the anions have been chosen to depict all present interactions. Bond distances are given in Å.

3.240(5) Å and the distances to the carbon atoms of the ring range from 3.2814(6) Å to 3.563(6) Å.

The ammonia molecule of N1 bridges two caesium cations within the $\text{Cs}_2(\mu\text{-NH}_3)_2^{(2+)}$ -fragment. It is coordinated to Cs1 with a distance of 3.230(3) Å and to its symmetry equivalent with 3.376(2) Å. The Cs1–N1–Cs1-angle is 79.85°(6) (Figure 89). Similar to the previously observed 2-dimensional layers, the caesium cation coordinates a third anion (C10–C18) as well. Since there are always two possible directions of the anion, Cs1 has either a short contact to the five

membered ring at C10 with a distance of 3.523(4) Å or to the six-membered ring with distances of 3.480(4) Å to C17 and 3.719(4) Å to C18. The bridging ammonia-molecule is also involved in NH- π interactions with short contacts ranging from 2.567 Å to 2.722 Å. As is the previously discussed caesium-structures **20** and **21**, an anticipated second molecule of ammonia is absent. In **22** the caesium cation is uncoordinated from one side, leaving a vacant position. Instead of an additional molecule of ammonia, an anion of the next layer is occupying the position. Nonetheless, a single-coordinating ammonia-molecule couldn't be incorporated in any NH- π interaction. The central motif of the layer, a $\text{Cs}_2(\mu\text{-NH}_3)_2^{(2+)}$ -unit surrounded by four anions, is built in a very space efficient way. The $\text{Cs}_2(\mu\text{-NH}_3)_2^{(2+)}$ -unit is perfectly covered within the layer and incorporates the ammonia molecules in moderately strong interactions with the anions. A single coordinating NH_3 -molecule would have no possibility to interact with an anion. If single coordinating NH_3 -molecules were present, the layers would be pushed further apart and the space in between would not be sufficiently filled, leav-

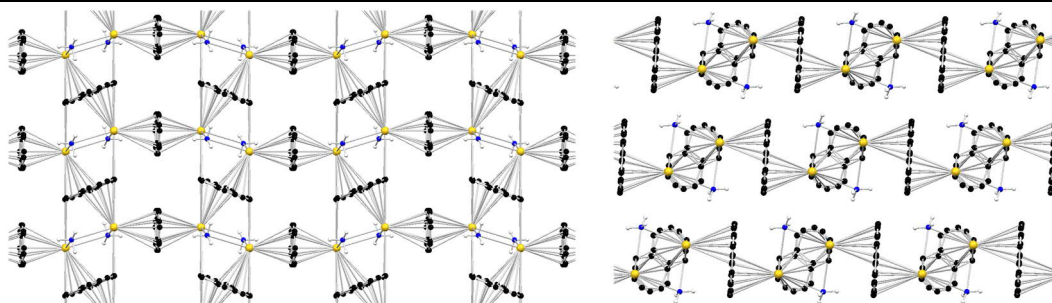


Figure 90: Packing plot of **22**. Left: A single 2-dimensional coordination polymer viewed from above. Right: Stacking of the 2-dimensional coordination polymers.

ing empty voids. In the analogue rubidium-containing structure of **18** the arrangement of the anion manages to incorporate as many ammonia-molecules in hydrogen bonding as possible, but one molecule of ammonia is left without any NH- π -interactions. Due to the weak coordination of ammonia to caesium, the single coordinating ammonia molecules are abandoned for the gain of a more efficient packing.

3.5.4. (Ind)Cs(NH₃)(THF) (**23**): 2-Dimensional Coordination Polymer

(Ind)Cs(NH₃)(THF) (**23**) has been synthesized by condensation of ammonia to a solution of indene and Cs(hmds) in THF at -78°C . Subsequent crystallization at -76°C gave crystals in the triclinic space group $P\bar{1}$ with two half-occupied indenyl-anions, a caesium cation and a molecule of ammonia and THF each in the asymmetric unit. The structure appears to be similar built to **22** with an additional molecule of THF occupying the vacant position at the caesium cation (Figure 91). The indenyl anions both show positional disorder and symmetry site disorder. Both anions are placed on inversion centres, leading to an interchange of the five- and six-membered rings as in **22**.

The anion of C1A-C9A is disordered on a second position by 37(2)% and the anion of C1B-C9B on a second position by 23(2)%.

Therefore four positions of each anion are possible (Figure 92). Also the THF-molecule is disordered on a second position by 49.1(8)%. The disorder of the anions however does not

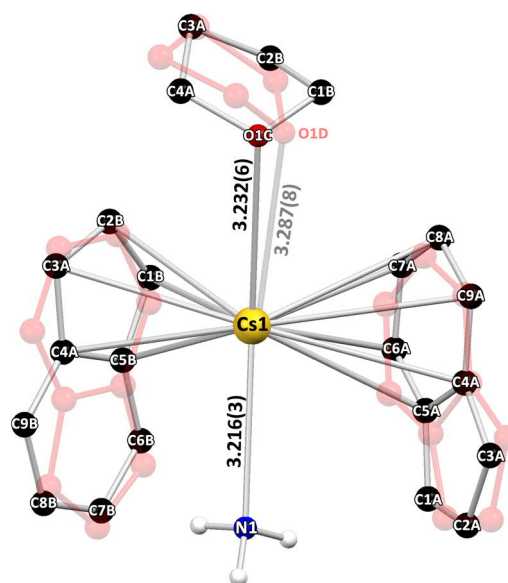


Figure 91: Asymmetric unit of (Ind)Cs(NH₃)(THF) (**23**). Both anions show positional disorder (red/transparent; occupancy: C1A-C9A 75(2)%, C1B-C9B: 64(2)%,) and are symmetry site disordered by inversion (not depicted). The thf molecule is disordered by 49.1(8)%. Bond distances are given in Å. Cs-C contact distances (all configurations) range from 3.28(2) Å to 3.638(9) Å.

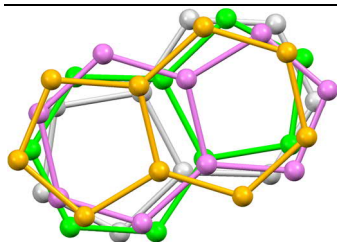


Figure 92: Indenyl anion C1B-C9B in all possible position regarding symmetry site and positional disorder.

change the picture of the coordination. As in **22**, the anions are coordinated from one side at the five-membered ring and from the other side at the six-membered ring. The distances of the caesium cation to the anion-planes range from 3.17(2) Å to 3.256(7) Å. The distance range of 3.28(2) Å to 3.638(9) Å for the coordinating carbon atoms is slightly broader than in **22**. Coordination to a third anion is gained as well with a distance range of 3.453 Å to 3.622 Å for the four possible positions. The ammonia molecule is coordinated to Cs1 with a distance of 3.216(3) Å and to its symmetry equivalent with a distance of 3.300(3) Å. NH- π contacts range from 2.546(8) Å to 2.84(2) Å and are similar to those in **22**.

The THF-molecule coordinates the cation with a distance to the oxygen atom of 3.231(6) Å (O1C) and 3.291(7) Å (O1D) and it is bended towards the 2-dimensional layer. A reason why THF coordinates the vacant position of the caesium cation in **23** and ammonia in **22** not, may be the more efficient packing. THF “intercalates” between the layers by filling the space more efficiently than ammonia could probably do. The bending of the molecules is induced by steric restraint of the surrounding indenyl-anions (Figure 93). The indenyl anions also force the THF molecule on one of the two positions by blocking the position between the two. The close distance of the hydrocarbon backbone of the red moiety in Figure 93 explains the almost 1:1 ratio of the disorder. The combination of a red and a green moiety is the combination with least steric strain. Two green fractions would also be disadvantageous because the green fraction has closer distances to the environment and is therefore less favourable than the red fragment.

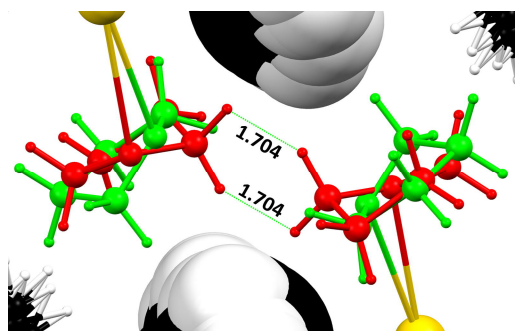


Figure 93: Disorder of the thf molecule as a combined results of steric restraint between thf itself and the indenyl anions depicted in a spacefill model. Red and green indicate the two almost 1:1 fractions of disordered thf. Distances are given in Å.

The packing of **23** (Figure 94) is very much the same as in **22** besides the intercalation of THF. The positional disorder of the indenyl anions does not have a visible effect on the whole pattern. However, the coordination of THF brings the 2-dimensional coordination polymers further apart. Their mutual steric repulsion seems to have an ordering effect on the indenyl anions in **22**, which gets lost in **23** with the result of the positional disorder of the anions.

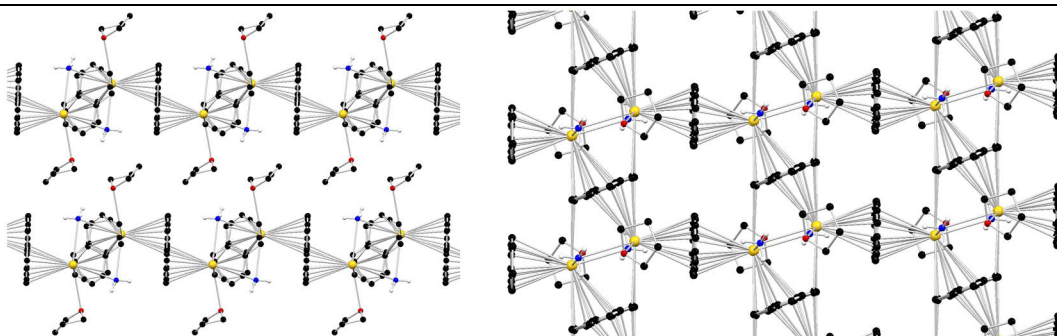


Figure 94: Packing plot of **23**. Minor disordered fractions have been omitted. Left: Stacking of the 2-dimensional coordination polymers of **23**. Right: 2-dimensional coordination polymer of **23** viewed from above.

3.5.5. (Flu)Cs(NH₃)₂ (**24**): A 2-dimensional coordination Polymer as well

(Flu)Cs(NH₃)₂ (**24**) has been synthesized by condensation of ammonia to a mixture of fluorene and Cs(hmds) in THF at -78°C . Crystallization at -76°C gave **24** in the triclinic space group $P\bar{1}$ with two fluorenyl-anions, one caesium cation, and two molecules of ammonia in the asymmetric unit. The fluorenyl anions are placed on inversion centres and show symmetry induced disorder (Figure 95). No interchange between the positions of the five- and six-membered ring is present as in **22** and **23**. Instead, the

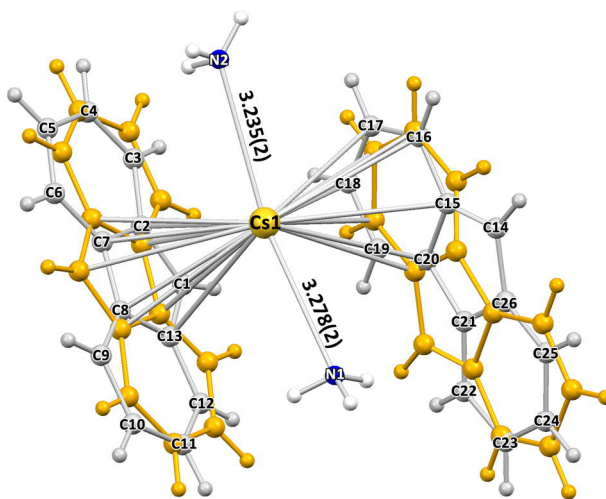


Figure 95: Asymmetric unit of (Flu)Cs(NH₃)₂ (**24**) including the symmetry site disorder of the fluorenyl anions. The anions in orange are symmetry related by inversion. The depicted Cs–C contacts range from 3.283(9) Å to 3.670(5) Å. Bond distances are given in Å.

orientation of the anion changes with the five-membered rings pointing in opposing directions. The structure of **24** is similar to the potassium- and rubidium-containing structures **15** and **19**, a Cs₂(μ-NH₃)₂(NH₃)₂⁽²⁺⁾-moiety surrounded by four anions. In contrast to **15** and **19**, the anions within the layers are not equally coordinated.

In **24** two different types of coordinated anions are present. The anion of C1-C13 is solely coordinated from both sides at the five-membered ring whereas the anion of C14-C26 is coordinated solely at the six-membered rings. The two six-membered rings are coordinated from different sides by one cation only. The distances of the cations to the planes of the anions are slightly different with 3.201(5) Å and 3.208(5) Å to the five-membered ring and

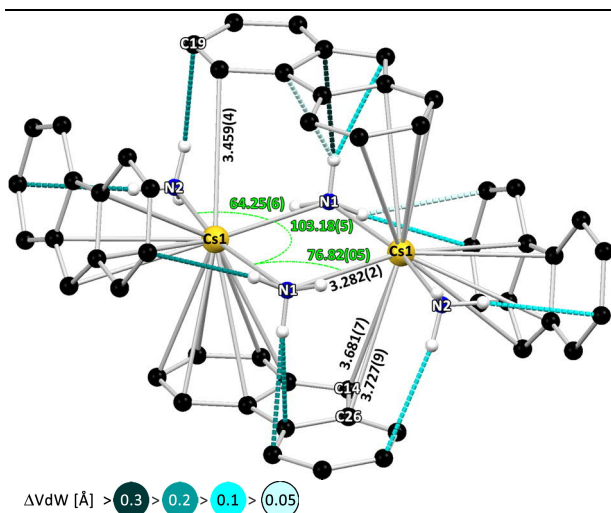


Figure 96: NH- π interaction in a building block of a $\text{Cs}_2(\mu\text{-NH}_3)_2(\text{NH}_3)_2$ -fragment surrounded by four fluorenyl anions. The site of the anions has been chosen to visualize all present interactions. Distances are given in Å.

potassium- and rubidium containing structures **15** and **19**. In contrast to the caesium-indenyl structures **22** and **23**, a single coordinated molecule of ammonia is attached to the caesium cation. The additional six-membered ring integrates the additional molecule of ammonia by NH- π interaction.

3.285(4) Å and 3.29(5) Å for the six membered rings. The Cs-C-contact distances range from 3.284(8) Å to 3.670(5) Å. Coordination to a third anion is present with distances between 3.460 Å and 3.727 Å. The distances of the bridging ammonia molecule to the caesium cations are 3.278(2) Å and 3.282(2) Å. The distance to the single-coordinated ammonia-molecule is 3.235(2) Å.

The pattern of NH- π interaction (Figure 96) and the crystal packing (Figure 97) are very similar to the

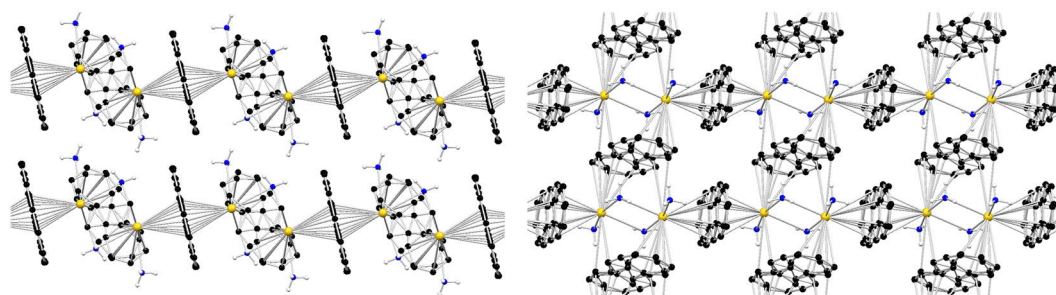
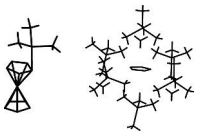
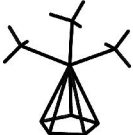
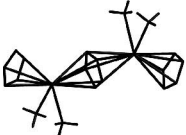
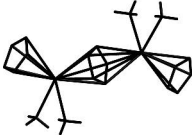
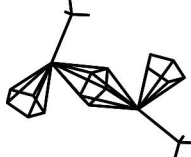
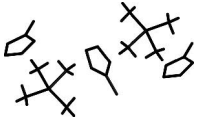

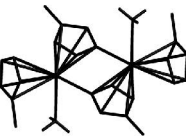

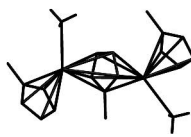


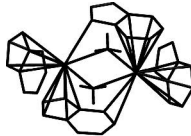
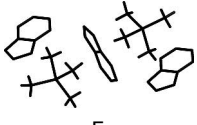
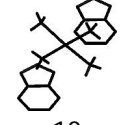


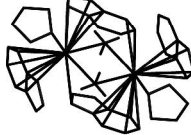
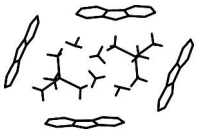

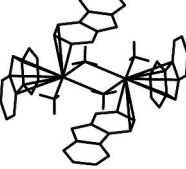

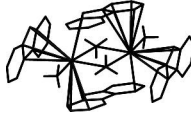


Figure 97: Packing plot of **24**. Left: Stacking of the 2-dimensional coordination polymers. Right: View on a single 2-dimensional coordination polymer.

3.6. Compound Overview

| Lithium | Sodium | Potassium | Rubidium | Caesium |
|--|--|--|---|---|
|  1 (l) 2 (r) CIP, SSIP |  7 CIP |  12 1-D Pol. |  16 1-D Pol. |  20 1-D Pol. |
|  3 SSIP |  8 CIP |  13 2-D Pol. |  17 1-D Pol. |  21 1-D Pol. |
|  4 CIP/SSIP |  9 CIP | | |  22 (o) 23 (u) 2-D Pol. |
|  5 SSIP |  10 CIP/SSIP |  14 1-D Pol. |  18 2-D Pol. |  22 (o) 23 (u) 2-D Pol. |
|  6 SSIP |  11 SSIP |  15 2-D Pol. |  19 2-D Pol. |  24 2-D Pol. |

4. Discussion

4.1. Lithium Ammoniacates

Comparing the Li-ammoniacates 1–6, one straightforward observation is the high rate of solvent separation under formation of the tetrahedral $\text{Li}(\text{NH}_3)_4^+$ -cation. All structures except 1 are solvent-separated. Besides the lithocene derivative of Cp^*_2Li^- , the counterions in the structures are naked anions. The dominant factors in

the organization of the structures are NH- π interaction and solvent separation under formation of the $\text{Li}(\text{NH}_3)_4^+$ -cation. Lithium has the smallest ionic radius of the alkali metal ions and has the strongest interactions with the ammonia molecules. The Li–N distances in 1–6 range between 2.03 Å and 2.09 Å, whereas the Na–N distances of the sodium ammoniacates 7, 8, and 10 range between 2.44 Å and 2.50 Å (excluding 9 and 11, which is due to the disorder of the ammonia molecules). This strong interaction leads to the rigid tetrahedral coordination of lithium. The calculations described in section 3.2.5 show that the deformation energy from tetrahedral to square planar conformation is 2–3 times higher for the $\text{Li}(\text{NH}_3)_4^+$ -cation than for the $\text{Na}(\text{NH}_3)_4^+$ -cation. The highest deviation from the ideal tetrahedral arrangement is the cation in 4 with one N–Li–N angle stretched to 133.2°(2).

The lithium ion is effectively shielded from interacting with the anions and therefore NH- π interactions play the crucial role in the assembly of cation and anion within the crystal structures. The cationic complex provides three hydrogen atoms per tetrahedral face for interaction (Figure 98). The triangular arrangement of the hydrogen atoms fits the size of the aromatic π -system of the anions. Therefore the anions are likely to interact with the tetrahedral faces with their three hydrogen atoms as in the structures 3–6 (to a lesser extent in the case of 5). The hydrogen atoms of the cations do not significantly shift from the conformation depicted in Figure 98 by interactions with anions.

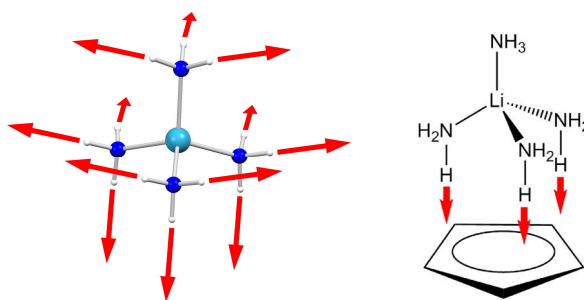


Figure 98: Idealized $\text{Li}(\text{NH}_3)_4^+$ -cation and their dominant mode of interaction with Cp-derivatives.



Figure 99: Zig zag arrangement of $\text{Li}(\text{NH}_3)_4^+$ and Cp derivatives.

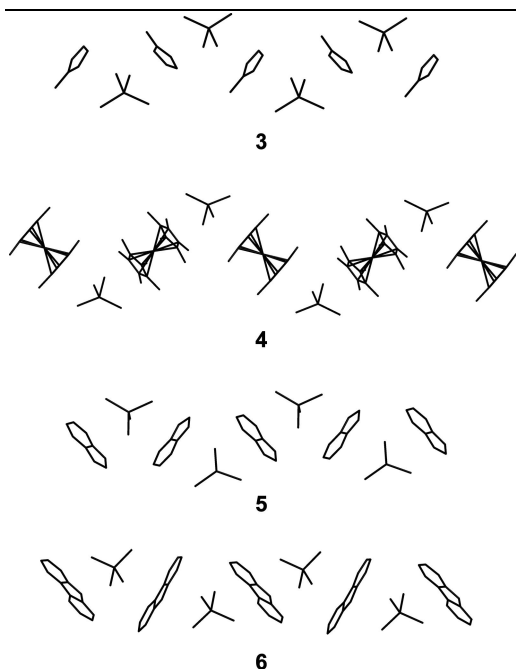


Figure 100: Zig zag patterns of the structures 3-6.

The tetrahedral shape of the cation and the interaction of both sides of the anion result in a linear zig zag arrangement (Figure 99). Cp', indenyl, fluorenyl, and also the lithocene derivative Cp*₂Li form this kind of arrangement in the structures 3–6 (Figure 100). This effect is remarkable, since the anions are very different in shape and electronic properties. Cp' is a small anion with a high charge concentration in the π-system. Cp*₂Li is very voluminous with charge enriched π-systems, overcompensated by the lithium cation. Indenyl and fluorenyl have enlarged π-systems with lower charge concentration.

The repeating observation of the zig zag pattern allows it to discuss the structures 3–6 in terms of crystal engineering. Crystal engineering engages in the design of crystalline materials with specific chemical, electrical, or mechanical properties through molecular self-assembly. To obtain the desired framework, the building blocks of a specific geometry assemble mostly via ligand-to-metal coordination and hydrogen bonding (for more information, see section 1.4). To classify the specific intermolecular interactions viable for crystal engineering, Gautam Desiraju marked the term “supermolecular synthon”, lend from the term “synthon” in organic chemistry to describe building blocks in retrosynthesis.^[124a, 124b] A supermolecular synthon in crystal engineering is an intermolecular interaction between specific functional groups,

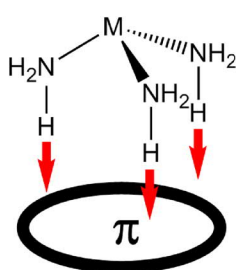


Figure 101: A supermolecular synthon of an M(NH₃)₃-fragment (M = any metal) connected to an aromatic π-system by NH-π interaction.

which can be used in supermolecular structures and frameworks. The identifiable supermolecular synthon in the structures 3–6 are three ammonia molecules coordinated to a metal ion, interacting with an aromatic π-system (Figure 101). This linear interaction in combination with the tetrahedral shape of the Li(NH₃)₄⁺-building block results in the observed zig zag pattern. It should be noted that the linearity of the patterns is not necessarily a result of the shape of the building blocks. A helical arrangement is also imaginable, but disadvantages in packing efficiency are likely to be expected.

The Cp' anion in 3 is the smallest anion within 3–6. Together with structure 1 and 4 it has the strongest NH-π interactions with an

average H–C interaction distance of 2.58 Å compared to 2.54 Å in **1** and 2.57 Å in **4** (Table 15). The structures **5** and **6** have significantly weaker NH- π interaction with average 2.70 Å for the indenyl and 2.65 Å for the fluorenyl compound. Whether these differences stem from electronic or steric effects cannot be judged straightforwardly. One potential explanation for the weaker interaction in **5** and **6** is the dilution of the negative charge in the π -systems of indenyl and fluorenyl. On the other hand, strong NH- π interaction takes place with lithocene derivatives in **1** and **4**, where the sandwiched lithium cation compensates the negative charge of the anions Cp and Cp*. The stronger interaction in **3** is therefore more likely a result of the crystal packing. Also indenyl and fluorenyl have more available locations for NH- π interaction than Cp' and Cp*, allowing the cations to arrange more flexibly.

The structure of **3** demonstrates the preference of solvent separation in the presented lithium ammoniacates. The solvent-separated ion-pair [Li(NH₃)₄][Cp'] (**3**) has been synthesized similarly to **1** by saturating the solution of Cp'Li in thf with gaseous ammonia. Instead of forming a CIP, a SSIP is formed. The sterical impact of the methyl group clearly determines the formation of the SSIP, hindering the formation of analogue Cp-structures of **1** and **2**.

Table 15: NH- π interactions in lithium ammoniacates

| | 1 | 2 | 3 | 4 | 5 | 6 |
|--|-------------|---------------|---------------|-------------|-------------|--------------|
| Ratio of NH ₃ hydrogen atoms involved in NH- π interactions per NH ₃ hydrogen atom | 3/9 33% | 16/30 53% | 13/24 54% | 6/12 50% | 7/12 58% | 19/36 53% |
| Average lengths of NH- π interactions [Å] | 2.54 | 2.76 | 2.58 | 2.57 | 2.70 | 2.65 |
| Ratio of NH- π interactions per aromatic carbon atom | 3/10 30% | 16/10 160% | 13/10 130% | 6/10 60% | 7/9 78% | 19/26 73% |

With the use of the Cp*-ligand, also solvent separation under formation of a Li(NH₃)₄⁺-complex takes place. The counterion is not a free Cp*-anion but a Cp*-lithocene. This indicates that the Cp*-anion cannot be sufficiently stabilized as a naked anion by NH- π interactions. The five methyl groups allow interactions only directly above/underneath the anion plane, whereas the Cp and Cp' can be approached from NH₃ from various directions. But also with that steric restraint, stabilization of a free Cp* is imaginable, since the present NH- π interactions are strong with three molecules of ammonia interacting with each anion. Additionally to the less beneficial packing properties of Cp*, the five methyl groups also contribute charge density to the π -system, making it more attractive to cations. In **4** the distance of the lithium cation to the ring plane of 1.900(2) Å is significantly shorter compared to average 1.98 Å in [Li(diglyme)₂][LiCp₂].^[47a] These two properties of the Cp*-anion lead to the observed structure. Different to the structures **3**, **4**, and **5**, the zig zag strains are not entirely arranged parallel. The strains are parallel in the direc-

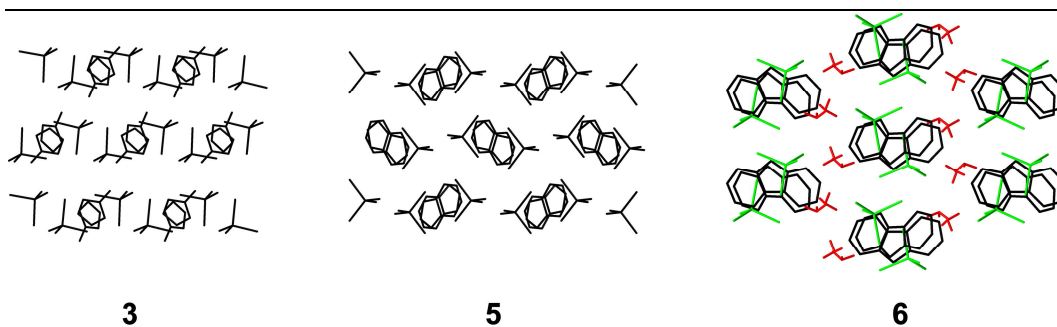


Figure 102: View along the zig zag strains for structures 3, 5, and 6. Hydrogen atoms except for lattice ammonia have been omitted. Cations and lattice ammonia in 6 are highlighted by color.

tion of the *a*- and *b*-axis, but change their orientation along the *c*-axis. The size of anions and cations does not fit that well as in the other structures, where all strains are ordered parallel. The Cp^*_2Li -anion is massively enlarged in width and length compared to the other anion and does not allow a similar compact arrangement as in 3, 4, and 5. The results are voids filled by lattice ammonia with an occupation of 87%. The partly occupation is a peculiar observation, since the ammonia molecule is incorporated in the lattice by NH–N interactions. Therefore, the interaction is a side-effect of filling the void. The creation of the void in 4 emphasizes the preference and stability of the zig zag arrangement, since voids are thermodynamically unfavorable and in this case only partially filled with ammonia.

The pattern of the indenyl ammoniacate 5 is very similar to the structure of the Cp' ammoniacate 3 (Figure 102). Cations and anions have similar positions along the strains. The cations are framing both Cp' and indenyl in the view along the *c*-axis. Both anions fit the size of one cationic tetrahedral face very well. The size difference of a methyl group and a six-membered ring does not seem to have a big impact in relation to the $\text{Li}(\text{NH}_3)_4^+$ -cation. Both anions provide sufficient π -density for NH– π interaction. That said, as the indenyl anion provides more possibilities for NH– π interactions, a more relaxed arrangement and weaker interactions are observed. The N–Li–N angles range between 104.2° to 121.2° in 5 and between 98.2° and 125.8° in 3.

The view along the *b*-axis of the fluorenyl ammoniacate 6 gives a slightly different picture. Whereas the anions in 3 and 5 have alternating directions, the fluorenyl anions in 6 are pointing into the same direction. The $\text{Li}(\text{NH}_3)_4^+$ -cations are also more integrated between the anions and are not located above or underneath the anions in contrast to 3 and 5. This is a result of the larger size and accessibility of the fluorenyl anion for NH– π interactions. In the view along the *a*-axis in 6, the lattice ammonia appears to be “intercalated” between rows of zig zag strains. In fact, the lattice ammonia is filling up the space left from the $\text{Li}(\text{NH}_3)_4^+$ -cations. The zig zag strains in 6 undergo a shift compared to 3 and 5

(Figure 103). Whereas the strands in **3** and **5** are almost plainly stacked upon each other, the strains in **6** shift in a way that two open angles of a flu-Li(NH₃)₄-flu element are facing each other. This shift gives room for the lattice ammonia, which glues together these adjacent rows. The pattern creates additional NH-N and NH- π interactions, interconnecting all strands in all directions. The result is a channel structure with Li(NH₃)₄⁺-cations and lattice ammonia en-framed by fluorenyl anions. The incorporation of lattice ammonia into the pattern of zig zag strands, which was a side-effect in **4** with its bulky Cp*₂Li-anions, becomes a driving force in the construction of the pattern in **6**.

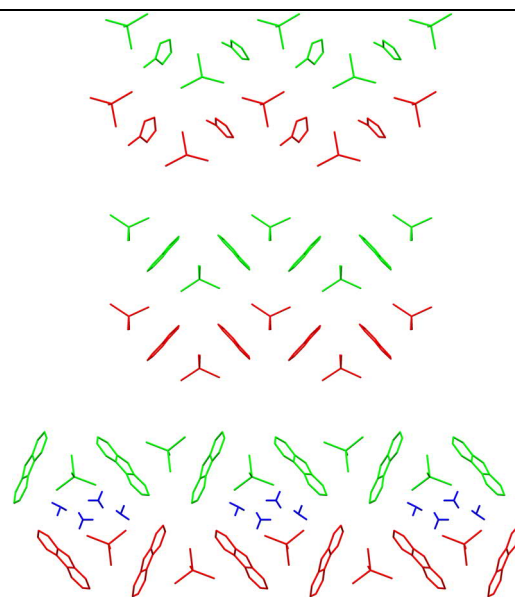


Figure 103: Stacking of the zig zag rows in **3**, **5**, and **6**.

In contrast to the structures of the lithium ammoniacates presented in this work, the two Cp-containing literature structures **1** and **2** (Figure 104) deviate substantially from the zig zag pattern. The two structures were part of the preceding diploma thesis “Cyclopentadienyllithium – Vom Ammoniakat zum Lithocen” and were the first two observed ammoniacates of alkali metals and aromatic carbanions.^[143, 155] The formation of the two structures haven't been fully understood by then and will therefore be included in this discussion to further illuminate the role of anions, cations, and interaction in the patterns of the lithium ammoniacates.

Structure **1** is not a SSIP and structure **2** has no zig zag arrangement. Both distinctions have to do with the shape of the Cp-anion as a compact disc compared to the more bulky derivatives presented so far. It is smaller and more regular than indenyl and fluorenyl and its access to NH- π interactions is not hindered by methyl groups. The disc shape of Cp has in general a significant effect on the crystal packing of unsolvated alkali metal cyclopentadienyl compounds, which explains the formation of the exceptional structure of **1**, a distorted lithocene anion, co-coordinated by a Li(NH₃)₃⁺ fragment.

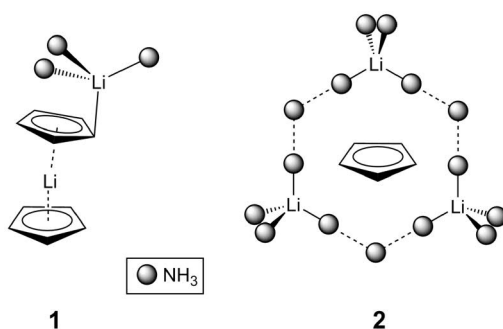


Figure 104: Exceptions from the zig zag arrangement: **1** and **2**.

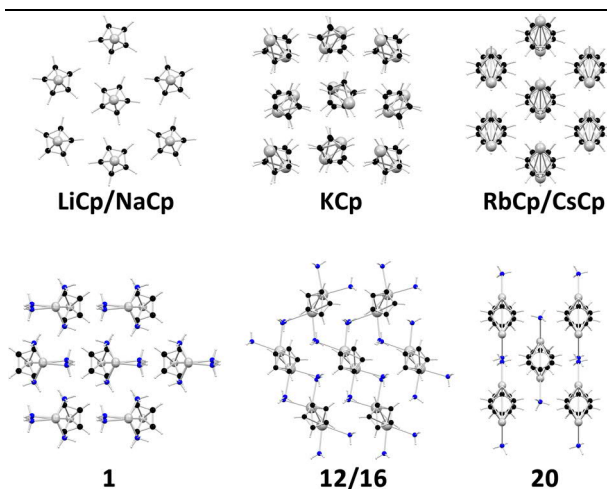


Figure 105: View along various strings of unsolvated and ammonia solvated polymeric alkali metal cyclopentadienyl compounds and the CIP **1**. Two motives are present: one string is surrounded either by four (KCp, **20**) or six other strings.

Unsolvated alkali metal cyclopentadienyl compounds have linear arrangements with one coordination polymer strand surrounded by six others in most cases. This is the case in LiCp, NaCp, RbCp, and CsCp, whereas KCp is surrounded by four strands due to strong mutual interactions (Figure 105).^[33a, 33b] The geometry of the packing is not of crystallographic nature, but a result of efficient packing of cylindrical-shaped coordination polymers. The pattern can therefore be described

as a pseudo-sixfold arrangement and does not form with other Cp-derivatives or bulky donorbases. KCp' is helical in contrast to KCp and coordination of TMEDA to NaCp creates a helical coordination polymer with cation–anion bending in contrast to straight linear NaCp.^[39, 85b] The pseudo-sixfold arrangement can even be found in the ammonia solvated isostructural CpK(NH₃)₂ (**12**) and CpRb(NH₃)₂ (**16**). In CpCs(NH₃) (**20**) one polymer strand is surrounded by four other strands instead, driven by Cs–Cp side-on interactions in analogy to KCp.

Structure **1** has a very similar pseudo-sixfold arrangement (Figure 105, Figure 107). It does not form polymeric chains, but the Cp₂Li₂(NH₃)₃ molecules are stacked upon each other

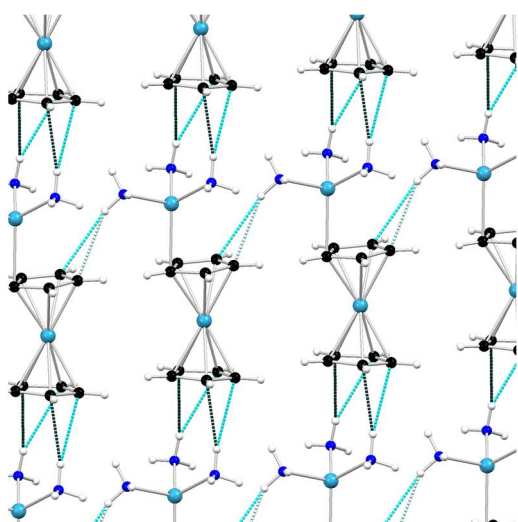


Figure 106: Arrangement of **1** within the crystal structure.

by strong NH- π interactions (Figure 106, Table 15). The interactions resemble the interactions in the previously described lithium ammoniacates and reflects the hence derived supermolecular synthon. Weak NH- π interaction also takes place between molecules outside the linear arrangement, but interlink the strands only in one direction. The preference of the dense pseudo-sixfold arrangement explains some of the features of **1**, like the formation of co-coordinated lithocene, its syn-arrangement, the tilt of the

lithocene fragment, and the η^1 -coordination of the $\text{Li}(\text{NH}_3)_3$ -moiety.

The shift of the $\text{Li}(\text{NH}_3)_3$ -moiety has two consequences: two molecules of ammonia can strongly interact with the next anion within the linear arrangement and the $\text{Li}(\text{NH}_3)_3$ -moieties fit between the four adjacent LiCp_2 -moieties (Figure 107). It also enables weak interaction between the "strands" in one direction. The bending within the LiCp_2 -moiety is a result of this shift.

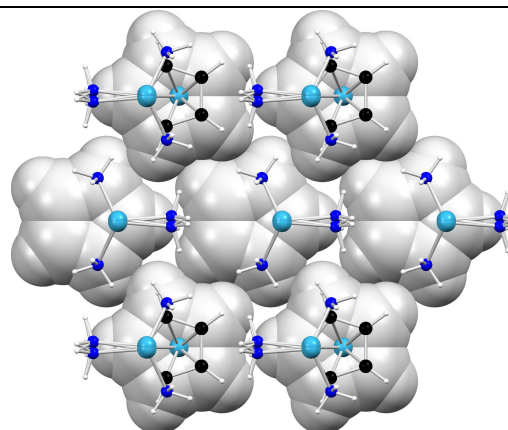


Figure 107: Six molecules of **1**. The Cp anions on a similar level are highlighted in a grey spacefilling depiction.

The question evokes why lithium does not form a piano-stool-type complex like the sodium ammoniacate **7**. With the use of the three-dentate ligand *pmdeta* and CpLi , such complex is formed. The lithium- π distance is significantly larger than with other ligands like *dme* or *tmeda*. However, the hydrocarbon backbone of the ligand hinders an optimized coordination of the cation. Therefore free coordination of ammonia is even more able to weaken the $\text{Li}-\pi$ interaction and to shift the cation from the ring centre. But there is a limit in the shift for the anion, since the anion still prefers η^5 -coordination. A shift to the η^1 -position necessary for the pseudo sixfold arrangement is not possible. In **1** the $\text{Li}(\text{NH}_3)_3^+$ -coordinated anion is also coordinated by another LiCp fragment to form lithocene. This weakens the attraction to the $\text{Li}(\text{NH}_3)_3$ -moiety significantly and allows it to shift to the ring periphery. The lithocene fragment also fits well into the pseudo-sixfold arrangement.

Discussion

Lithium Ammoniacates

A whole new structure emerges with more equivalents of ammonia and lower crystallization temperature. Instead of a CIP, a SSIP with naked anions are formed in **2**. Anion and cations do not form a zig zag arrangement as well. The apparent structure is a linear channel formed of $\text{Li}(\text{NH}_3)_4^+$ and lattice ammonia fused together by NH–N interactions and filled with naked anions (Figure 108). The formation of structure **2** is now entirely determined by NH- π interaction. The feature of the channel structure of **2** is the very high amount of NH- π interactions. The two anions in the asymmetric unit interact with 16 hydrogen atoms of adjacent ammonia molecules. This is the highest ratio of NH- π interaction per carbon atom for all the discussed structures (Table 15). The interactions are weaker than those of **1** or **3** because no cation is facing an anion directly with one tetrahedral side, which allows stronger interactions in the zig zag arranged structures. The $\text{M}(\text{NH}_3)_3\text{-}\pi$ synthon is not present. Each anion in **2** is directly surrounded by three lattice ammonia molecules and three cations in their front and back, respectively. This way, the amount of NH- π interactions is maximized and all molecules of the structure are inter-linked with each other in all directions. The disc shape of the anion enables NH- π interactions from various directions. Cp' and Cp* are limited in this regard because of the steric repulsion of the methyl groups. Fluorenyl and indenyl allow NH- π interactions from almost all directions as well, but their bulky structure and their lower charge concentration lead to the adaption of the zig zag arrangement. The structure of **2** displays the inverted structure of **6**. Instead of a channel of anions filled with cation and lattice ammonia, cations and lattice ammonia form channels filled with anions.

These two structures lead to the conclusion, that for the basic unsubstituted Cp-anion, from which all other anions derived, the simple zig zag rule does not apply. Efficient packing and maximization of NH- π bonding are creating two entirely different patterns, whereas one methyl group or two anellated rings lead to the same crystal pattern.

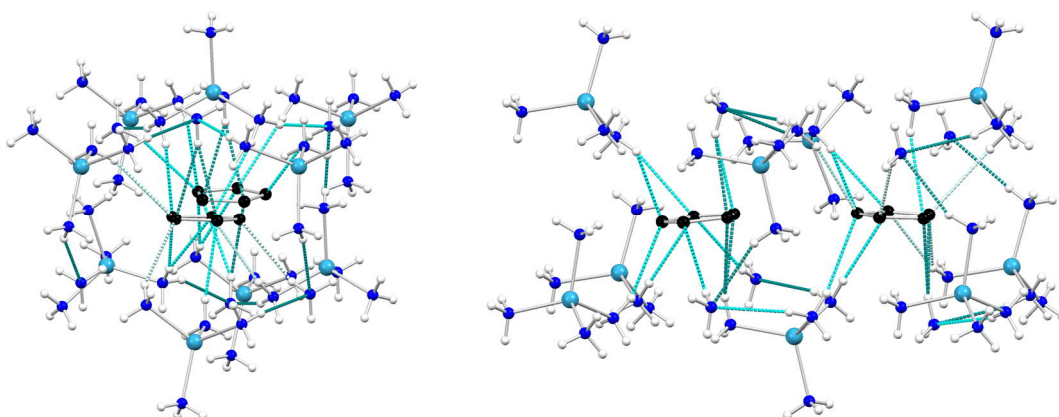


Figure 108: Channel structure within **2** viewed from two directions. $\text{Li}(\text{NH}_3)_4^+$ cations and lattice ammonia form a cavity in which Cp is fixed by NH- π interactions.

4.2. Sodium Ammoniacates

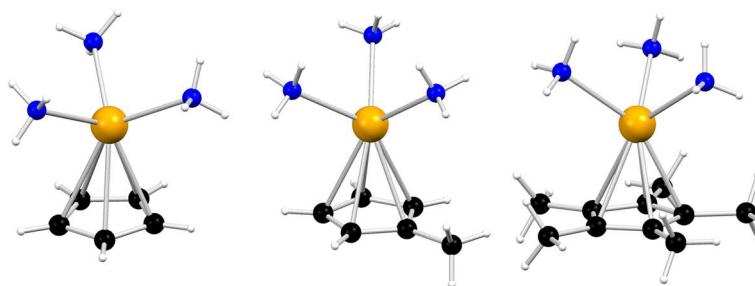


Figure 109: The three piano-stool complexes $\text{CpNa}(\text{NH}_3)_3$ (7), $\text{Cp}'\text{Na}(\text{NH}_3)_3$ (8), and $\text{Cp}^*\text{Na}(\text{NH}_3)_3$ (9)

Sodium has a larger ionic radius than lithium, resulting in larger metal–ammonia distances and a higher preference for interaction with the π -density of the aromatic carbanions than lithium. Therefore the sodium ammoniacates have a different shape compared to the analogue lithium structures. Cp, Cp', and Cp* form CIPs (Figure 109). The indenyl ammoniacate is at the boundary of solvent separation and only the fluorenyl ammoniacate is fully solvent-separated. NH- π interactions play also an important role in the shape of the complexes and in the arrangement within the crystal packing.

The three monocyclic Cp-derivatives of Cp, Cp', and Cp* form 'piano-stool' contact-ion pairs. A sodium cation is η^5 -coordinated by the anion and is itself coordinated by three molecules of ammonia. They have also similar patterns in their crystal structures. The complexes are stacked upon each other with the ammonia molecules interacting with the next anion (Figure 110). This theme is similar to the interaction of the $\text{Li}(\text{NH}_3)_4^+$ -cations with Cp', Cp*, indenyl, and fluorenyl as well as the interaction of the $\text{Li}(\text{NH}_3)_3$ -moiety in **1** with the next lithocene fragment. The supermolecular synthon derived from the lithium structures (Figure 101) can therefore be applied here as well. The $\text{Na}(\text{NH}_3)_3$ -umbrellas are

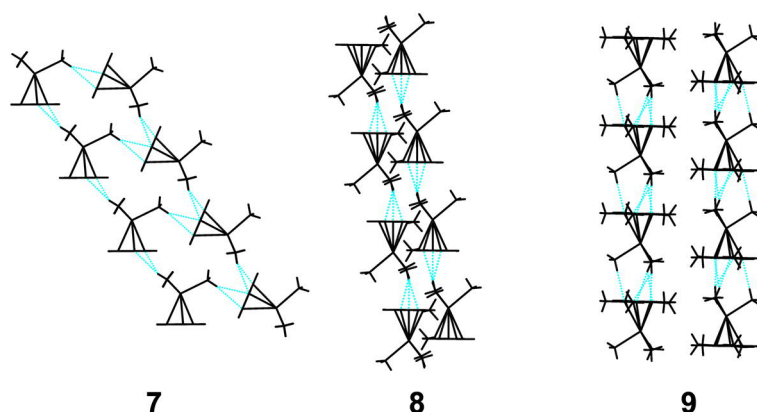


Figure 110: Linear arrangement of the piano-stool complexes in the respective crystal structure.

Discussion

Sodium Ammoniacates

very similar in their size to the tetrahedral faces of $\text{Li}(\text{NH}_3)_4^+$, despite the longer Na–N distances compared to the Li–N distances. The distances between the nitrogen atoms in the different ammonia molecules vary from 3.10 Å to 3.78 Å in the lithium structures, from 3.76 Å to 3.84 Å in **7**, and from 3.36 Å to 3.60 Å in **8**. The corresponding distances of **9** are not included into the comparison due to the high amount of disorder.

In their linear arrangement forged by NH- π interaction, the crystal structures of **7**, **8**, and **9** shift toward each other to a different extent. The complexes in **7** are highly shifted, the complexes in **8** are slightly shifted, and the complexes in **9** are not shifted at (Figure 110). This correlates strongly with the fitting of the synthon. The synthon is poorly reflected in **7**, reasonably reflected in **8**, and fits perfectly in the case of **9**. The reason for the poor reflection in **7** is similar to the previously discussed structure $[\text{Li}(\text{NH}_3)_4][\text{Cp}]\cdot\text{NH}_3$ (**2**). The anion is unhindered by methyl-groups, which enables more interactions with surrounding ammonia molecules. In **7**, five out of nine ammonia hydrogen atoms are involved in NH- π interaction in contrast to two in **8** and three in **9**. That means each Cp is involved in five interactions as well. This can only be achieved by the stair-like arrangement, which exposes the complex to its neighbors. The adaption of the synthon is therefore outweighed by the favorable maximization of NH- π interactions.

The methyl group in **8** prohibits the interaction with its other neighbors and forces the coordinated ion pairs to form a less complex pattern. This has been already observed in the case of **3**, where the methyl group leads to the formation of the common zig zag arrangement. What has also been observed in the structure of **3** is the strong interaction of two hydrogen atoms of a tetrahedral face and one weaker interaction. This is the case in **8** as well with two ammonia molecules being highly involved in interactions and the third one having no significant interaction. NH- π interactions in **8** are stronger with NH–C-distances ranging from 2.50 Å to 2.85 Å compared to 2.68 Å to 2.85 Å in **7**.

The perfectly linear alignment of the complexes in **9** is caused by the large size of the Cp*-anion and its regular disc shape. The one methyl group of Cp' in **8** effectively hinders interactions alongside, above, and underneath the complexes. They adapt to it in forming straighter linear strands. The remaining shift in the strands is caused by the need of efficient packing and maximization of two out of three possible NH- π interactions. The five methyl groups of Cp* in **9** push the strand into perfect alignment. The strands form tubes with bulges (Cp*) and notches (Na), arranging with each other like tongue and groove. The result is a sixfold arrangement of the strands with a significant void in the center of six of these strands. The disorder of the anions shows that the orientation of the anion within the strands is not important. All ammonia molecules are equally involved in NH- π

interactions, making **9** the perfect paradigm for the presented synthon. The void that is created is filled with $\text{HNSi}(\text{SiMe}_3)_2$, but it is likely that the void can be filled by various other guest molecules.

With the use of indenyl, the character of the structure shifts from ‘piano-stool’-type complexes toward solvent separation. $[\text{Na}(\text{NH}_3)_4][\text{Ind}]$ (**10**) is a structure between a CIP and a SSIP, reflected in the exceptional square-planar shape of the $\text{Na}(\text{NH}_3)_4^+$ -cation. The $\text{M}(\text{NH}_3)_3\text{-}\pi$ synthon ($\text{M} = \text{any metal}$) does not apply here. The structure is driven by the preferred octahedral coordination of sodium and $\text{NH}\text{-}\pi$ interactions. Besides the

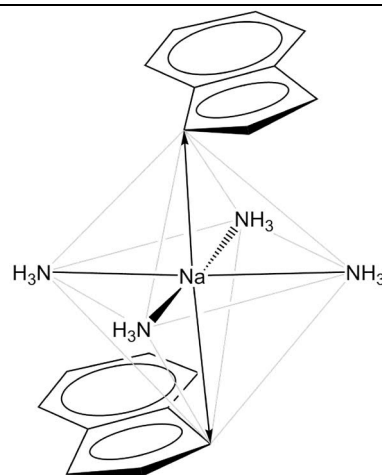


Figure 11: Octahedral coordination of the sodium cation in **10**.

four ammonia molecules, the sodium cation interacts with the periphery of the five-membered ring, the area of the highest local charge concentration within the anion (Figure 11). However, with distances of 3.05 Å and 3.24 Å the interactions are pretty weak. Each anion interacts with six NH_3 -hydrogen atoms and one of the four ammonia molecules is not even involved in any of the $\text{NH}\text{-}\pi$ interactions.

The square planar configuration fits very well to the shape of the indenyl anions. The two rings of indenyl cover the sodium cation with two cis-arranged ammonia molecules very well. The theoretical calculation of an isolated $\text{ind}^-\text{-Na}^+\text{-ind}^-$ fragment shows that this configuration is stable. The square planar $\text{Na}(\text{NH}_3)_4^+$ -complex only shifts slightly from the position in the crystal to incorporate also the fourth NH_3 -molecule in $\text{NH}\text{-}\pi$ interactions. For that purpose, the sodium cation even shifts further away from the positions of C1 and C3.

The configuration of indenyl and the coordinated sodium cation resembles the coordinated lithium cation in **1**, where a lithium ion coordinates the outskirts of a Cp-anion. Like indenyl, the attraction of the Cp-ring to Li^+ in **1** is decreased by coordination of a lithium cation from the other side of the anion. In both cases the configurations are supported by $\text{NH}\text{-}\pi$ interactions. The cation **1** is pyramidal-coordinated by ammonia because of its small ionic radius. The ammonia mol-

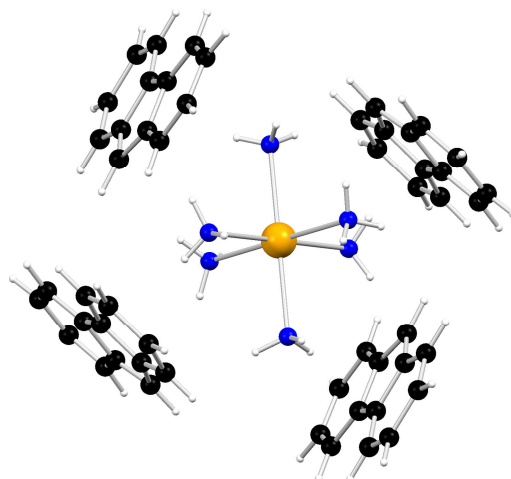


Figure 12: A $\text{Na}(\text{NH}_3)_6^+$ -complex surrounded by four fluorenyl anions in **11**.

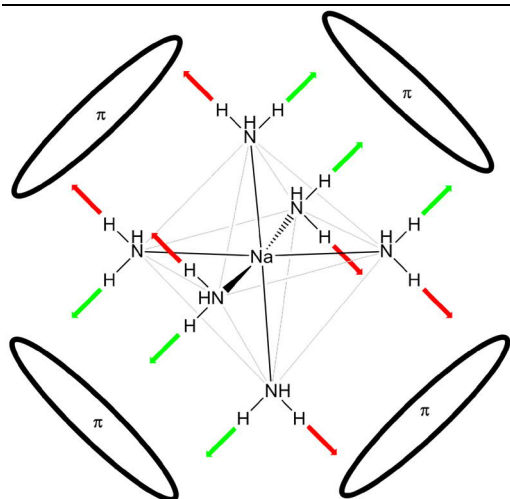


Figure 113: NH- π interaction of the $\text{Na}(\text{NH}_3)_6^+$ cation with the surrounding anions in **11** according to the $\text{M}(\text{NH}_3)_3$ - π synthon.

The sodium cation is shielded from any interactions with the fluorenyl anions like $\text{Li}(\text{NH}_3)_4^+$ in the lithium compounds. As in the lithium-fluorenyl compound **6**, the fluorenyl anions in **11** form channels, fitting to the octahedral geometry of the $\text{Na}(\text{NH}_3)_6^+$ -complex (Figure 113).

Structure **11** does not form a square planar configuration like **10**, although the anion would be capable of doing so. The anions could coordinate the sodium cation with the top of the five-membered ring, the point of the highest charge concentration, and would give enough space for NH- π interaction. However, in the case of **11** the NH- π interactions are the only factor at play. This is due to the fact that the $\text{M}(\text{NH}_3)_3$ - π synthon is applied here in an efficient way. The octahedral complex has eight faces, each capable of interacting with an anion. Four of these faces are actually involved in this interaction (Figure 113). The other four octahedral faces are directed toward the channel and the other complexes. The anions arrange according to the geometry of the interacting octahedral faces. This setup also explains the modulation. The six fused rings of the fluorenyl anions are directed

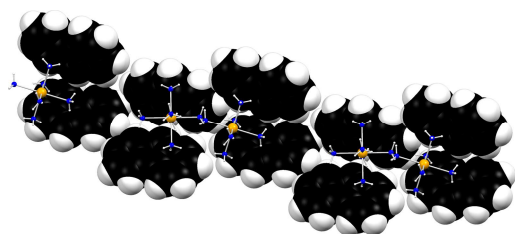


Figure 114: Arrangement of the fluorenyl anions on one side of the channel.

ecules interact with Cp-anions above and in front of the $\text{Li}(\text{NH}_3)_3^+$ -moiety. The sodium cation in **10** is able to shift to the position at the outskirts of the five-membered ring of indenyl where the local charge concentration is the highest.

The picture changes again with the use of fluorene. Although the structure could not be successfully refined because of the modulation, the important features are visible. $[\text{Na}(\text{NH}_3)_{4/6}][\text{Flu}]$ (**11**) is a solvent-separated ion pair (Figure 112). The sodium-cations are mainly sixfold-coordinated, but also fourfold-coordinated in a tetrahedral configura-

tion. The sodium cation is shielded from any interactions with the fluorenyl anions like $\text{Li}(\text{NH}_3)_4^+$ in the lithium compounds. As in the lithium-fluorenyl compound **6** already demonstrates the many possibilities of NH- π interaction with the anion. The anions in **11** have alternating orientations along the channel. The five-membered ring points either up or down.

There are little gaps between the anions, but generally, π -density is continuously present along the channel. The complexes can therefore occupy many equivalent positions. Also the presence of a minor fraction of $\text{Na}(\text{NH}_3)_4^+$ -complexes shows the flexibility of the system.

4.3. Cp- and Cp'-Ammoniacates of the Higher Alkali Metal Cations

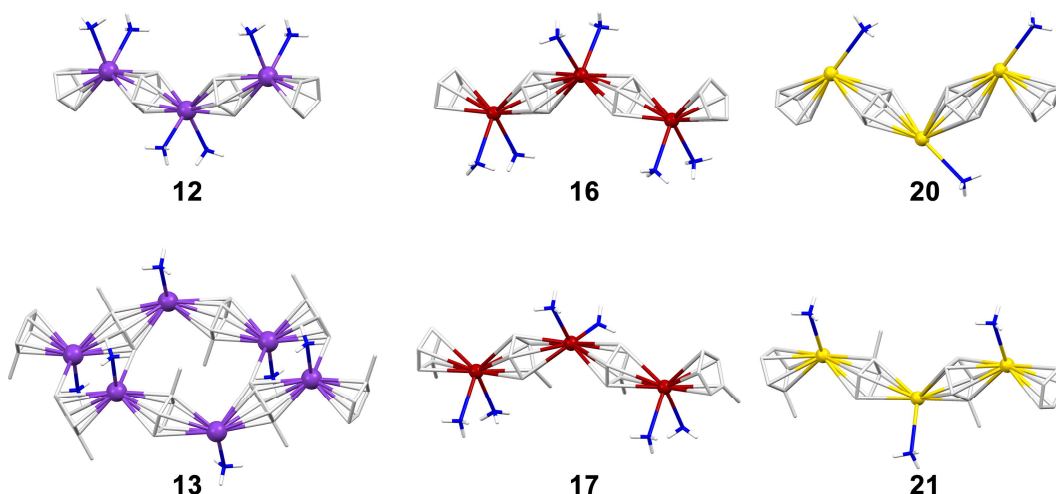


Figure 115: From left to right: the Cp- (upper row) and Cp'-compounds (lower row) of potassium, rubidium and caesium

The ammoniacates of the higher alkali metal cations with Cp and Cp' consist mostly of linear 1-dimensional coordination polymers (Figure 115). The cations are η^5 -coordinated by two anions in a bent arrangement, leading to a rippled coordination polymer. Besides this major similarity between the structures, they differ in their number of coordinated ammonia molecules, the geometry of ammonia coordination, and their stacking in the crystal.

The crystal structures of $\text{CpK}(\text{NH}_3)_2$ (**12**) and $\text{CpRb}(\text{NH}_3)_2$ (**16**) are isostructural. Cell parameters, space group and crystal structure are almost identical. In both structures the cations are twofold-coordinated by ammonia. The structure of $\text{CpCs}(\text{NH}_3)$ (**20**) is different to those of **12** and **16**. Only one molecule of ammonia coordinates the cation. It bends along the direction of propagation, and the Cp–Cs–Cp angle is very narrow. The structure of $\text{Cp}'\text{K}(\text{NH}_3)$ (**13**) is more of a two-dimensional coordination polymer composed of 1-dimensional coordination polymers interconnected by K–Cp side-on interactions. The rubidium structure $\text{Cp}'\text{Rb}(\text{NH}_3)_2$ (**17**) is built correspondent to the structures **12** and **16**. The cations are also twofold-coordinated by ammonia, but with one narrow and one widened N–Rb–N angle. The caesium structure $\text{Cp}'\text{Cs}(\text{NH}_3)$ (**21**) corresponds again to the caesium structure **20**, with one coordinated molecule of ammonia, but this time bent across the direction of propagation.

As briefly mentioned in section 4.1, the structures of **12** and **16** embody a pseudo sixfold-arrangement. One 1-dimensional coordination polymer is surrounded by six others (Figure 116). All the anions and $\text{K}(\text{NH}_3)_2$ -moieties of neighboring strands are strictly parallel.

Cp- and Cp'-Ammoniacates of the Higher Alkali Metal Cations

Using the centroids of the anions, the pseudo-sixfold arrangement can be well-described. The lengths of the edges of the hexagon in Figure 116 and the distances from the centre of the hexagon to the edges range from 6.29 Å to 6.48 Å, diverging less than 3%. With the disc shape of the Cp-anion, the '2-dimensional' sphere packing is the most efficient way for the arrangement. The 1-dimensional coordination polymers can be seen as tubes (in analogy to spheres) with a hexagonal packing in analogy to the sphere packing in one layer. This pattern is repeated in the arrangement of the ammonia molecules as

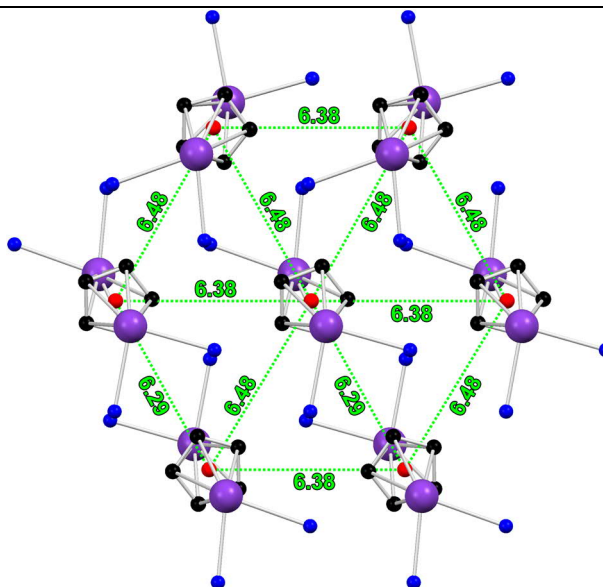


Figure 116: Section from the crystal structure of CpK(NH₃)₂ (**12**) depicting the pseudo-sixfold arrangement of the 1-dimensional coordination polymers. Distances between centroids (red) are given in Å. All centroids lie in a plane. Hydrogen atoms are omitted.

well (Figure 117). The planes perpendicular to the direction of propagation is completely filled with Cp-anions of K(NH₃)₂-moieties. The space around each potassium cation, besides the two NH₃-molecules attached to each cation, is filled with four ammonia molecules from neighboring 1-dimensional coordination polymers. The six ammonia molecules form a slightly distorted hexagon around the two cations with edges ranging from 3.52 Å to 3.84 Å, varying by 8.3%. The values for CpRb(NH₃)₂ (**16**) range from 6.40 Å to 6.55 Å (varying about 2.3 Å) for Cp-centroids and 3.64 Å to 3.96 Å (varying about 8.8%) for the ammonia molecules.

In contrast to the similarity of the Cp-derivatives **12** and **16**, the Cp'-ammoniacates Cp'K(NH₃) (**13**) and Cp'Rb(NH₃)₂ (**17**) look very different. **13** is a 2-dimensional coordination polymer with 1-dimensional coordination polymers fused together by K–Cp side-on interactions and **17** is a 1-dimensional coordination polymer build analogue to **12** and **16**. The particular arrangement in **13** is based on the stronger attraction of potassium to π -density. This effect is demonstrated in the solvent-free structure of KCp in comparison to RbCp and CsCp. All three structures consist of bent metallocene strands and in all structures the cations are involved in side-on interactions with adjacent anions. Due to the smaller ionic radius of K⁺, the shortest distance to the next anion outside the strand is 3.33 Å, whereas the distance is 3.73 Å in RbCp and 3.77 Å in CsCp. RbCp and CsCp also have the previously mentioned 'pseudo-sixfold' arrangement (Figure 105), whereas KCp

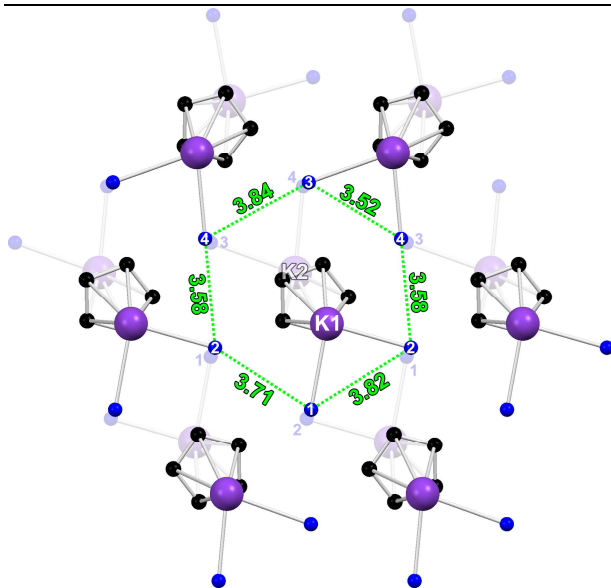


Figure 117: Section from the crystal structure of **12** highlighting the pseudo-sixfold symmetry of the ammonia molecules surrounding the potassium cations. Hydrogen atoms are omitted and the $\text{K}(\text{NH}_3)_2$ -fragments in the back are depicted transparently. The numbers equate to the atomic labelling. Distances between nitrogen atoms are given in Å. All nitrogen atoms lie in one plane.

3.28 Å even shorter than in KCp . The methyl groups point out of the plane as well as the ammonia molecules, which are not involved in any $\text{NH}-\pi$ interaction in contrast to all other ammoniacate structures presented in this work. The methyl groups and ammonia molecules of one layer fit together with those of the next layer and fill the space between the layers efficiently, which is reminiscent of biological membranes consisting of lipids with hydrophobic tails and hydrophilic heads (Figure 118).

These side-on interactions are absent in **17** and the rubidium cation prefers the coordination of two ammonia molecules. However, another version of a layer formation can be observed here. This time the polymeric strands form a 'soft' double layer in contrast to the 'hard' 2-dimensional coordination polymer of **12**. Within the layer the strands are not connected by side-on coordination but by much weaker $\text{NH}-\pi$ interactions. Two of these

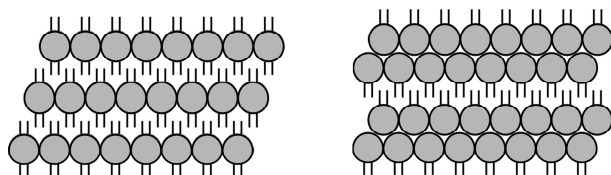


Figure 118: Scheme of the layers of **13** and **17**. The grey spheres represent the CpK -coordination polymer strands, the lines represent methyl-groups and ammonia molecules.

forms more of a square grid. In terms of efficient packing, the square grid is less favourable than the 'pseudo-sixfold' packing and it is forced into this arrangement by the stronger side-on interactions. The same effect comes into play in **13**. The methyl group obviously does not allow a 'pseudo-sixfold' packing due to the steric hindrance and less spherical shape of the anion. To gain an efficient packing, the cation in **13** prefers side-on coordination to Cp' before coordination of ammonia in order to form dense 2-dimensional layers. The distance of potassium to the next side-on-coordinated carbon atom is with

layers are connected via $\text{NH}-\pi$ interaction as well. The methyl groups and the non-interacting ammonia molecules (one of the four different NH_3 -molecules is not involved in any $\text{NH}-\pi$ interactions) point out of only one side of a layer.

Cp- and Cp'-Ammoniacates of the Higher Alkali Metal Cations

The caesium compounds of Cp and Cp' have significantly different features compared to those of potassium and rubidium. In both cases, only one ammonia molecule coordinates the caesium cation. Due to the large radius of caesium, the Cs–NH₃ coordination is the weakest and leads to the abandoning of one additional molecule of ammonia in preference of Cs–Cp side-on interactions.

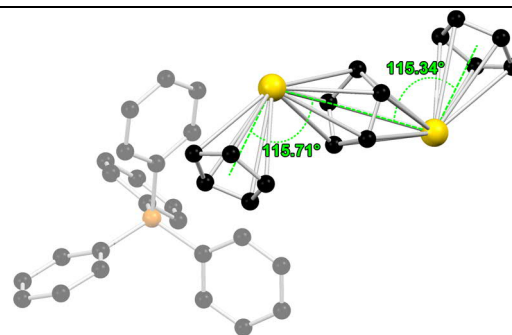


Figure 119: The triple-decker anion [Ph₄P][Cs₂Cp₃] published by *Harder and Prosenč*.^[156]

The consequence of the large cationic radius

is visible in Cs(Cp)(NH₃) (**20**). The Cp–Cs–Cp angle (calculated with the centroids of the Cp-anions) is bent to 110.76° (Table 16), the smallest angle in the compound class of Cp-containing coordination polymers. In all other similar compounds listed in Table 16, the Cp–M–Cp angles range between 128.70° (**13**) and 145.24° (KCp(Et₂O)). The two Cp-anions are pushed together to maximize the coordination of the Cs-cation. The narrow angle demonstrates the flexibility of the Cp–M–Cp fragment. A strong bending was observed previously in the ‘triple-decker’ anion of [Ph₄P][Cs₂Cp₃] (Figure 119) with a bending angle of 115.6°, forced by intermolecular Cs–Cp interactions.^[156]

Table 16: Cp–M distances (measured by planes) and Cp–M–Cp angles (measured by centroids) of various coordination polymers of the CpM-type (M = K, Rb, Cs).

| Compound | Cp–M [Å] | Cp–M–Cp | Compound-nr./CSD |
|--|-----------|-----------------|----------------------------------|
| <i>CpK</i> (NH ₃) ₂ | 2.88/2.89 | 138.31°/141.38° | 12 |
| <i>CpRb</i> (NH ₃) ₂ | 3.01/3.02 | 136.30°/137.85° | 16 |
| <i>CpCs</i> (NH ₃) | 3.17 | 110.76° | 20 |
| <i>Cp'K</i> (NH ₃) | 2.82/2.84 | 128.70 | 13 |
| <i>Cp'Rb</i> (NH ₃) ₂ | 3.00/3.01 | 141.31°/144.23° | 17 |
| <i>Cp'Cs</i> (NH ₃) | 3.14/3.15 | 140.96° | 21 |
| <i>KCp</i> | 2.82 | 137.95° | NIBSOG ^[33a] |
| <i>RbCp</i> | 2.97 | 131.35° | TIQKEJ ^[33c] |
| <i>RbCp</i> | 2.95/2.99 | 123.49°/136.53° | TIQKEJ01 ^[33c] |
| <i>CsCp</i> | 3.16 | 129.71° | RAVHUR ^[33b] |
| <i>KCp</i> (Et ₂ O) | 2.77 | 145.24° | NAGSUJ ^[101] |
| <i>KCp</i> (DME)(THF) ₂ | 2.81/2.85 | 136.12°/137.02° | XUMKEW ^[102] |

Additionally to the two Cp-anions and the ammonia molecule, the cation has two side-on interactions with adjacent coordination polymer strands. This fivefold interaction is not only reflected in the strongly bent Cp–Cs–Cp angle, but also in the strongly bent coordination of the ammonia molecule, which does not bend away from the Cp-anion, but toward it along the direction of propagation. The Cp_{centroid}–Cs–NH₃ angle is only 80.1°. The

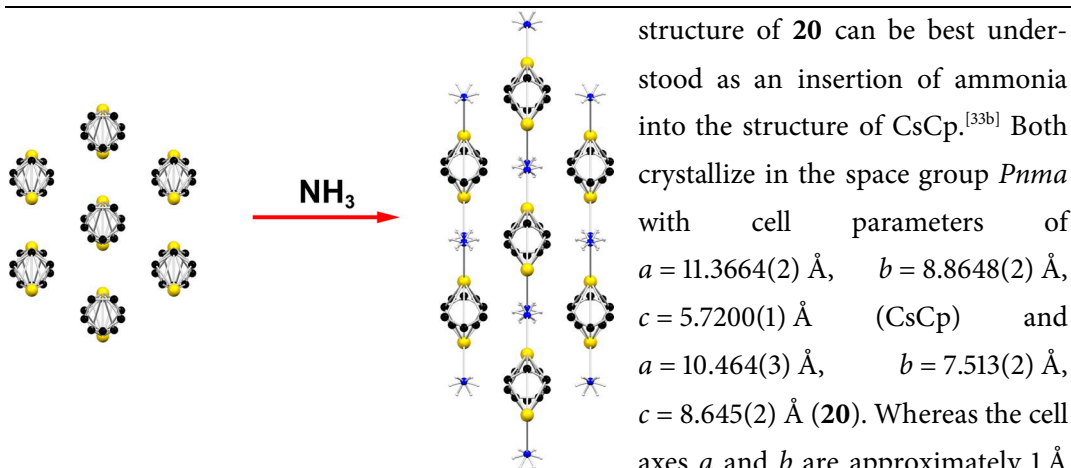


Figure 120: Stretching of the CsCp-structure along the c -axis by insertion of ammonia.

structure of **20** can be best understood as an insertion of ammonia into the structure of CsCp.^[33b] Both crystallize in the space group $Pnma$ with cell parameters of $a = 11.3664(2) \text{ \AA}$, $b = 8.8648(2) \text{ \AA}$, $c = 5.7200(1) \text{ \AA}$ (CsCp) and $a = 10.464(3) \text{ \AA}$, $b = 7.513(2) \text{ \AA}$, $c = 8.645(2) \text{ \AA}$ (**20**). Whereas the cell axes a and b are approximately 1 \AA shorter in **20**, the c -axis is approximately 3 \AA longer. The pseudo six-

fold arrangement in CsCp is therefore stretched along the c -axis (Figure 120). The pseudo sixfold arrangement of CsCp also gets squeezed together, causing the reduction of the a -axis and, as already mentioned, the strands itself are more compact due to the narrow Cp–Cs–Cp angle, causing the reduction of the b -axis. In this way, the caesium cation keeps the side-on interaction to the adjacent Cp-anions.

The structure of CsCp'(NH₃) (**21**) shares a similar feature with **20**, the side-on interaction. The methyl group of the Cp'-anion hinders the side-on coordination to two adjacent anions. The solid state structure of CsCp' is unknown and can therefore not be compared to **21**. Structure **21** has a layer type arrangement like the Cp' ammoniacates of potassium (**13**) and rubidium (**17**). The coordination polymers within the layers do not interact with each other, because the methyl groups are not pointing out of the layer, but are held within the layer, in contrast to **13** and **17**. That steric repulsion blocks any interaction. Each layer is connected to the adjacent layer by either NH- π interaction from one side or Cs–Cp' side-on coordination from the other side. The feature of the methyl groups within the layer can be attributed to the size of the caesium cation, which allows a much more flexible arrangement of Cp' and NH₃.

4.4. Indenyl and Fluorenyl Ammoniacates of Potassium, Rubidium and Caesium

The indenyl- and fluorenyl-anions show a distinctively different behaviour for the lower (Li, Na) and higher (K, Rb, Cs) alkali metal ions. The lower charge concentration of the indenyl anion compared to Cp and stabilization by NH- π interaction leads to solvent separation in the case of

[Li(NH₃)₄][Ind] (**5**). The sodium compound [Na(NH₃)₄][Ind] (**10**) forms an almost solvent-separated ion pair between two anions with weak interactions of sodium to the periphery of five-membered rings. The fluorenyl-anion leads in to the formation of channel-like structures both in the case of [Li(NH₃)₄][Flu]·(NH₃)₂ (**6**) and [Li(NH₃)_{4/6}][Flu] (**11**).

Ammoniacates of the higher alkali metal ions are looking different to their lower alkali metal equivalents. With sodium on the edge of solvent separation from the indenyl anions, the higher alkali metal cations coordinate both the five- and the six-membered rings and form 1- and 2-dimensional coordination polymers.

A new supermolecular synthon emerges in the indenyl structures of rubidium (**18**) and caesium (**22**, **23**), as well as in the fluorenyl structures of potassium (**15**), rubidium (**19**), and caesium (**24**). All structures are remarkably similarly built 2-dimensional coordination polymers. In most cases, a M₂(μ -NH₃)₂(NH₃)₂-moiety (M = K, Rb, Cs) is surrounded by four anions (Figure 121).

The structure of (Ind)Cs(NH₃) (**22**) does not entirely fit into that picture. In **22** only the two bridging NH₃-molecules are present, the single coordinated molecules are absent. In (Ind)Cs(NH₃)(THF) (**23**) the (absent) single-coordinated NH₃-molecules are replaced by thf. Otherwise, the geometry and the pattern of the coordination polymer is virtually the same. This is also true for **23**. The indenyl structure **14** does not fit into this pattern. It is a 1-dimensional helical coordination polymer, but it gives some hint to the formation of the 2-dimensional patterns.

First, the indenyl structures will be discussed and compared to (Ind)K(NH₃)₂ (**14**) and the Cp-based coordination polymers to elucidate the formation of the 2-dimensional coordination polymers. The fluorenyl structures will be discussed afterwards in the same context.

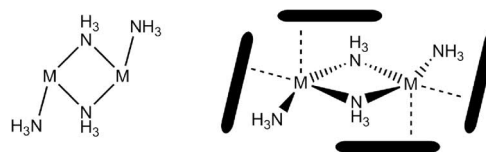


Figure 121: Supermolecular synthon of an M₂(m-NH₃)₂(NH₃)₂-moiety (left) (M = any metal), surrounded by four planar aromatic carbanions (right).

Discussion

Indenyl and Fluorenyl Ammoniacates of Potassium, Rubidium and Caesium

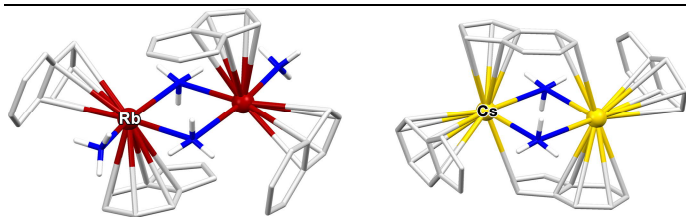


Figure 122: (Ind)Rb(NH₃)₂ (**18**) (left) and (Ind)Cs(NH₃)₂ (**22**) (right) resembling the supermolecular synthon of the 2-dimensional structures.

The rubidium structure (Ind)Rb(NH₃)₂ (**18**) is built of a Rb₂(μ-NH₃)₂(NH₃)₂-fragment corralled by four indenyl anions. Three indenyl anions coordinate the rubidium cations of the Rb₂(μ-NH₃)₂(NH₃)₂-fragment with

the five-membered ring (Figure 122). One indenyl anion coordinates with the six-membered ring. All but one ammonia molecules are incorporated in NH-π interaction. The fourth molecule simply fills up the coordination sphere of one rubidium cation.

In the caesium structure (Ind)Cs(NH₃)₂ (**22**) the pattern shifts significantly. Because of the larger ionic radius, the cation is more affine to the six-membered ring and less affine to ammonia. Although the anions show symmetry-induced disorder, each anion is coordinated from one side at the five-membered ring and from the other side at the six-membered ring. This arrangement leads to a more compact layer compared to **18** (Figure 123). The caesium also profits from more side-on interactions within the arrangement than rubidium. The thickness of the layer is reduced at the cost of available π-density for single-coordinated ammonia. The thf-molecule in **23** coordinates the caesium cation, because it intercalates between the layers and fills the space between them. The ammonia molecule is much smaller and would not be able to fill the space efficiently, thus creating significant voids.

A view on the two compounds from a different perspective outside the synthon is even more insightful. The two structures can also be understood as single 1-dimensional coordination polymers fused together by the bridging ammonia molecules (Figure 124). This way, the structures can be compared to the other 1-dimensional coordination polymers.

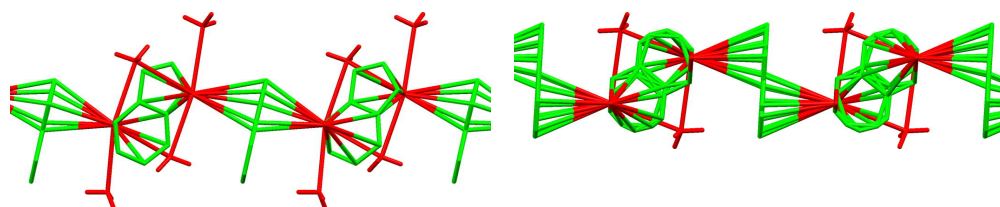


Figure 123: The layers of **18** (left) and **22** (right).

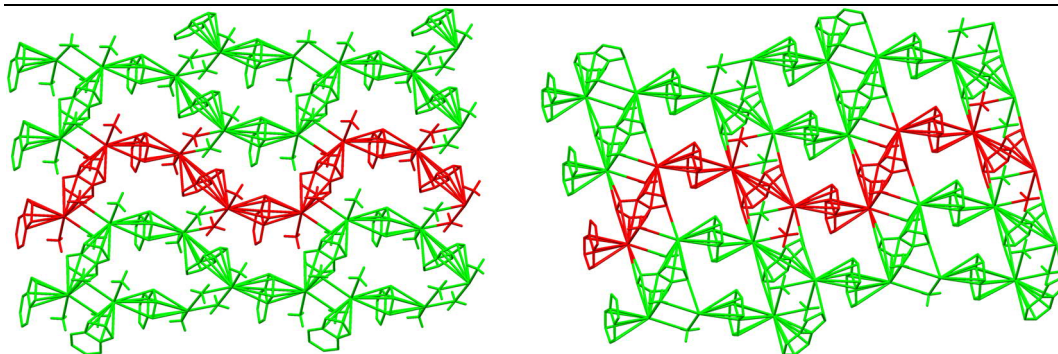


Figure 124: The 2-dimensional layers of **18** (left) and **22** (right) as a composition of 1-dimensional coordination polymers linked together by bridging ammonia.

In **18**, the substructure is a meandering 1-dimensional coordination polymer. Within this strand, the anions coordinate the rubidium cations in two ways. The uncoordinated rings are either in *trans*-position or in *cis*-position for each respective cation. The strands are linked together by the bridging ammonia molecules. The *cis/trans*-pattern has been observed before in the structure of (Ind)K(NH₃)₂ (**14**) (Figure 125). It is a 1-dimensional helical coordination polymer with the cations exclusively coordinated to the five-membered ring. Within this helical arrangement the six-membered rings are either in *cis*-position around the cation or in *trans*-position (Figure 125). The strands themselves are not interlinked by bridging ammonia.

In **18** the strands are interconnected, where one Rb(NH₃)₂-fragment of one strand faces a fragment of another strand. In this context, a *cis*-arranged fragments are always bridged with a *trans*-arranged fragment and vice versa. In **14** the K(NH₃)₂-fragments come close to each other as well, but they do not interconnect. The *cis*-arranged K(NH₃)₂-fragments face *cis*-arranged fragments of a neighboring strand and *trans*-arranged fragments face other *trans*-arranged fragments, but not of the same strand. In **18**, the Rb–Rb distance of the Rb₂(μ-NH₃)₂(NH₃)₂-moiety is 4.00 Å. The intermolecular K–K distances in **14** are

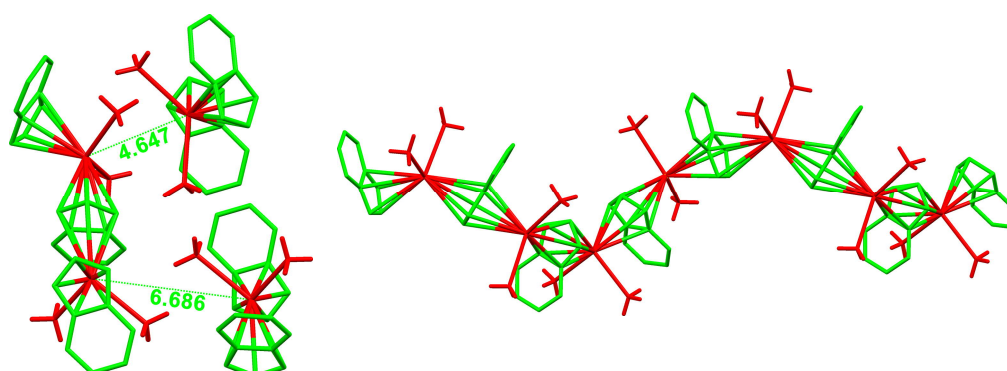


Figure 125: Left: K–K distances between neighboured strands of (Ind)K(NH₃)₂ (**14**) in Å. Right: Helical strand of **14**.

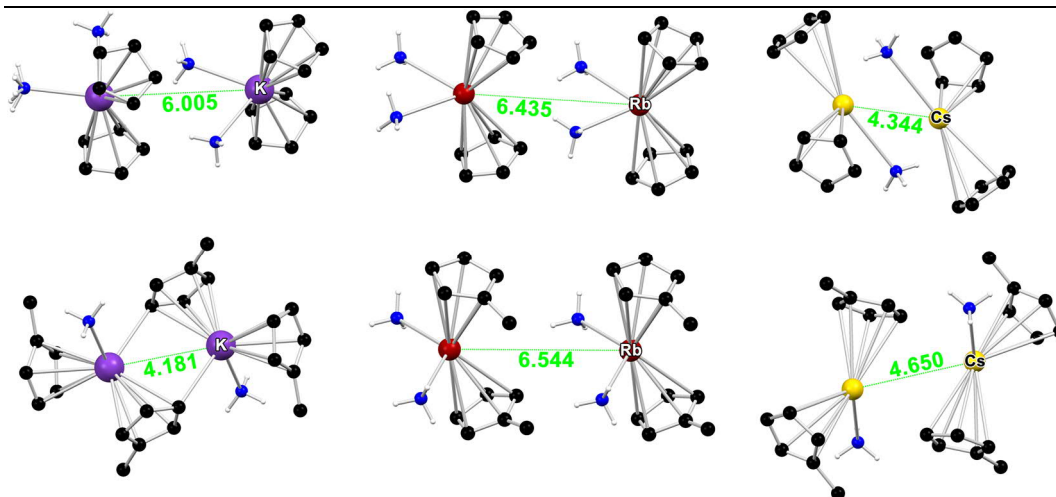


Figure 126: M–M distances (M = K, Rb, Cs) in Å for the Cp-compounds of potassium, rubidium, and caesium (upper tier) and the respective Cp'-compounds (lower tier).

4.65 Å for the *trans*-fragment and 6.69 Å for the *cis*-fragment. In both cases the ammonia molecules are in positions which almost look like 'proto-states' of interconnecting. This is especially true for the *trans*-arranged moieties. The higher affinity of potassium to the five-membered ring hinders the formation of a 2-dimensional layer. The higher ionic radius of rubidium on the other side has more flexibility in coordination and can therefore form a more complex pattern of interaction.

In the case of **22**, the pattern differs from **18** in the way that no more *cis/trans*-arrangements are present in the 1-dimensional substructure, but only *cis*-arranged moieties. The same meandering pattern is present as in **18** and the connection between the strands is additionally enforced by side-on interactions. From the helical arrangement in **14** to the interconnected meandering strands in **18** and the more compact form in **22**, a stepwise compression of the patterns is observed. The compression is driven by the growing affinity of the cations to the π -density of the indenyl anions.

Looking back to previously discussed Cp- and Cp'-structures of the higher alkali metal compounds, it appears that in all structures the $M(\text{NH}_3)_2^-$ or $M(\text{NH}_3)$ -moieties (M = K, Rb, Cs) come close to each other to a certain extent (Figure 126). This is less true in $\text{CpK}(\text{NH}_3)_2$ (**12**), $\text{CpRb}(\text{NH}_3)_2$ (**16**), and $\text{Cp}'\text{Rb}(\text{NH}_3)_2$ (**17**). Compared to the Rb–Rb distance of 4.00 Å in **18**, the M–M distances are more than 2 Å longer (Figure 126). In $\text{Cp}'\text{K}(\text{NH}_3)$ (**13**), $\text{CpCs}(\text{NH}_3)$ (**20**), and $\text{Cp}'\text{Cs}(\text{NH}_3)$ (**21**), the M–M distances are not much longer. In these compounds significant side-on interactions between cations and anions are present, which exist in all of the 2-dimensional polymers of the indenyl- and fluorenyl-type. The side-on interactions bring the strands closer to each other. In the 2-

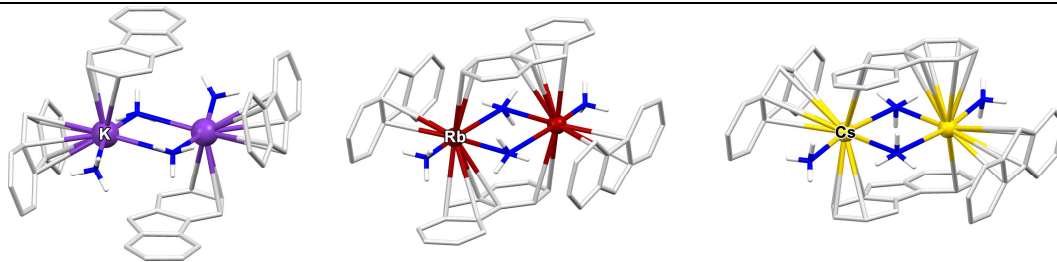


Figure 127: Sections of the fluorenyl compounds of potassium (15), rubidium (19), and caesium (24) representing the supermolecular synthon of the 2-dimensional coordination polymers.

dimensional coordination polymers, the two $M(\text{NH}_3)_2$ - or $M(\text{NH}_3)$ -moieties finally snap together.

The supermolecular synthon derived from the indenyl structures applies well for the fluorenyl structures (Figure 127). All fluorenyl structures with potassium, rubidium, and caesium form the same pattern, a $M_2(\mu\text{-NH}_3)_2(\text{NH}_3)_2$ -moiety ($M = \text{K, Rb, Cs}$) corralled by four fluorenyl anions very similar to the indenyl structures 18, 22, and 23. The only differences are the coordination patterns within these building blocks. Potassium coordinates a five-membered ring, the periphery of the six-membered ring, and forms an additional interaction with the top of another five-membered ring (not depicted in Figure 128). Rubidium coordinates two five-membered rings and forms a side-on coordination to a six-membered ring. Caesium coordinates like potassium a five- and a six-membered ring and also forms side-on coordination to either the top of another five-membered ring or to a six-membered ring. The caesium cation also has single-coordinated ammonia molecules in 24, which are absent in the indenyl precursor 22. With the additional six-membered rings, these molecules can now be integrated into the structure by $\text{NH}\text{-}\pi$ interaction.

The 2-dimensional patterns of the fluorenyl compounds are structured in the same principle as the indenyl structures. They consist of 1-dimensional strands as substructures, fused together by bridging ammonia (Figure 128). One difference is very striking: the 1-dimensional strands in all three structures are not meandering but straight. The additional coordination sites provided by the added six-membered ring are countered by an increased steric strain, allowing the anions only to arrange erect within the layer.

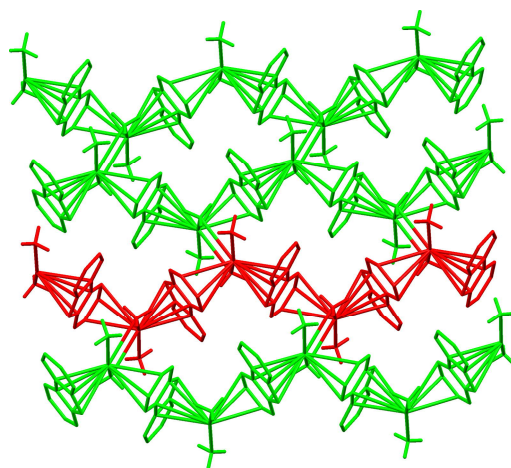


Figure 128: The 2-dimensional coordination polymer of $(\text{Flu})\text{K}(\text{NH}_3)_2$ (15) composed of 1-dimensional coordination polymers as a substructure.

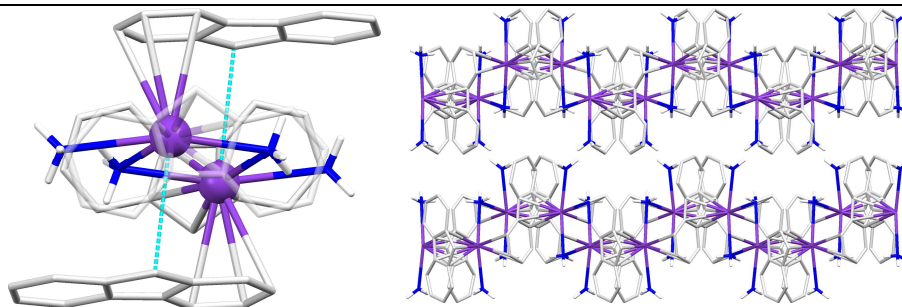


Figure 129: Left: the central building block of **15** with the interactions of K^+ with the top of the five-membered ring highlighted in cyan. The fluorenyl anion in the front is depicted transparently. Right: the pleated 2-dimensional layers of **15**.

This lack of flexibility results in the straight pattern of the 1-dimensional substructure.

The size of the anion also explains the formation of $(Flu)K(NH_3)_2$ (**15**). Unlike the structures **19** and **24**, it has no precursor in the indenyl structures. **15** forms a 1-dimensional helical coordination polymer, which is packed like tongue and groove. The additional six-membered ring clearly does not allow a similar helical arrangement as in the respective indenyl structure **14**.

Another difference of **15** compared to **19** and **24** is the pleated nature of the 2-dimensional layer (Figure 129). The layers in **19** and **24** are flat. A flat pattern seems to be more beneficial for the packing. For that reason $(Ind)Cs(NH_3)$ (**22**) gets rid of the single-coordinated ammonia molecules, which are still present in the rubidium analogue **18**, but not entirely incorporated in $NH-\pi$ interaction. The reason for the coordination of ammonia in **18** lies in the higher affinity of Rb^+ to ammonia due to the smaller radius. The same effect can play a role in **15**. The potassium cation interacts strongly with the top of the five-membered ring of an additional fluorenyl anion with distances of 3.420 Å and 3.552 Å. At the top of the five-membered ring, the highest charge accumulation is present. For the same reason main-group metals form σ -bonds with the top of the five membered ring and solvated alkali metals like lithium coordinate around that area as in $Li(flu)(thf)_3$, $Li(flu)(Et_2O)_2$, and $Li(flu)(quinuclidin)_2$.^[55-57] Potassium as the hardest of the latter alkali metal cations therefore has the highest affinity to that position, which overcomes the tendency to form smooth flat layers. The structure defining preference for side-on coordination has been previously demonstrated in KCp and $Cp'K(NH_3)$.

The role of ammonia in the formation of the 2-dimensional coordination polymers with the $M_2(\mu-NH_3)_2(NH_3)_2$ -synthon is clearly not the same as in the lithium and sodium containing structures. As in the Cp- and Cp'-compounds of the higher alkali metal compounds, metal- π interactions play a much greater role. Besides the basic coordination within the 1-dimensional substructures, side-on coordination plays a significant role in

Indenyl and Fluorenyl Ammoniacates of Potassium, Rubidium and Caesium

fusing them together. NH- π interactions have not been thoroughly discussed for the indenyl and fluorenyl structures. Their role in the formation of the 2-dimensional layers is difficult to determine. Probably they work well together with another key aspect of ammonia, its size and donor strength. The small size allows the fusion of the 1-dimensional substructures to 2-dimensional layers by bridging two cations of neighboring strands. Donor solvents like thf could fulfil this task too, but they would create a less compact layer. Thf could also, at least partly, replace the single-coordinated ammonia molecules. Structure **23** has proven that it is possible. NH- π interactions therefore provide an additional benefit. They interact with the vacant π -density of the anions and add additional glue, strengthening the interaction between the strands.

5. Summary

Looking back on the major results, ammonia has proved to be a very efficient donor solvent for complexes of alkali metals and cyclopentadienyl derivatives. The insolubility of these pure salt-like compounds increases with the alkali metal's ionic radius and constitutes a challenge in chemical synthesis. Ammonia has shown to be able to dissolve all components with the exceptions of Cp*K, Cp*Rb, and Cp*Cs, where the anions effectively shield the cations. The measurement of the obtained crystals via X-ray diffraction turned out to be infeasible using standard crystal-cooling techniques due to the high volatility of ammonia in the crystal. New techniques were developed to provide a continuous cooling chain at very low temperatures ($-78\text{ }^{\circ}\text{C}$ down to $-196\text{ }^{\circ}\text{C}$) from the reaction vessel to the diffractometer.

The degree of aggregation in the presented ammonia-solvated complexes of alkali metals and cyclopentadienyl derivatives is strongly related to the size of the cation. Lithium as the smallest cation has the strongest attraction to ammonia and, in almost all cases, nearly complete stabilization of individual ions is observed. All studied ammonia compounds containing lithium form SSIPs with the exception of $\text{Cp}_2\text{Li}_2(\text{NH}_3)_3$ (**1**). Most of the SSIPs consist of a $\text{Li}(\text{NH}_3)_4^+$ -cation and a naked anion stabilized by $\text{NH}\cdots\pi$ hydrogen bonding. In $[\text{Li}(\text{NH}_3)_4][\text{Cp}^*_2\text{Li}]$, the methyl groups of the Cp* anion sterically hinder an efficient stabilization by hydrogen bonding. Sodium has a larger ionic radius and, compared with lithium, the cation– NH_3 attraction is weakened and the cation–anion attraction is consequently enhanced. Cp, Cp', and Cp* form CIPs in the form of piano-stool complexes, which are the smallest representatives ever found of their kind. The dilution of the negative charge in indenyl and fluorenyl also weakens the cation–anion interactions. $[\text{Na}(\text{NH}_3)_4][\text{Ind}]$ (**10**) has properties at the boundary of a CIP and a SSIP. The anions are located on top and at the bottom of an unprecedented square planar $\text{Na}(\text{NH}_3)_4^+$ cation. Complete solvent separation takes place in $[\text{Li}(\text{NH}_3)_{4/6}][\text{Flu}]$. In the ammonia-solvated compounds containing potassium, rubidium, and caesium, the cation–anion interactions dominate the aggregation due to the larger radius of these cations. The anions Cp and Cp' form linear, zig-zag shaped 1-dimensional coordination polymers with all three of these cations. $\text{Cp}'\text{K}(\text{NH}_3)$ (**12**) is a 2-dimensional coordination polymer due to strong cation–anion side-on interactions. Indenyl and fluorenyl form almost identical 2-dimensional coordination polymers with the higher alkali metals. Only $(\text{Ind})\text{K}(\text{NH}_3)_2$ (**13**) remains a 1-dimensional coordination polymer. The ammonia–caesium attraction is the weakest of all, resulting only in single coordination of ammonia with Cp, Cp', and the indenyl anion.

All 2-dimensional coordination polymers are made up of 1-dimensional strands fused together by cation–anion side-on interactions and/or bridging ammonia molecules.

Hydrogen bonding is a common theme which plays a major role in the formation of the crystal patterns. It is the driving force in stabilizing the naked anions of the lithium ammoniacates. Anions and cations of these compounds are arranged in the same zig-zag pattern regardless of size and shape of the anions. This led to the discovery of a new supramolecular synthon: a pyramidal $M(\text{NH}_3)_3$ moiety interacting with the π -system of an anion via $\text{NH}-\pi$ hydrogen bonding. This intermolecular organization principle can also be found in the linear arrangement of the sodium-containing piano-stool complexes and in the dynamic channel structure of $[\text{Na}(\text{NH}_3)_{4/6}][\text{Flu}]$ (**11**). The influence of hydrogen bonding was intensely studied in $[\text{Na}(\text{NH}_3)_4][\text{Ind}]$ (**10**) and identified as powerful enough to enable the exceptional square planar configuration of the $\text{Na}(\text{NH}_3)_4^+$ cation. Hydrogen bonding is only of secondary importance in the Cp- and Cp'-compounds of the higher alkali metals, where the π -systems are more shielded by the cations. However, hydrogen bonds also play a crucial role in the formation of the 2-dimensional coordination polymers, where they support the crosslinks through bridging ammonia of the substructural 1-dimensional polymer strands.

6. Experimental Section

6.1. General procedures

All reactions are sensitive to air and moisture and were carried out under modified *Schlenk*-conditions.^[157] Argon and nitrogen were used as protective gas. Before usage the gases were deoxygenized with a copper-catalyst and dried with P_4O_{10} . The inert gas first passes a heated column filled with pellets of the catalyst and subsequently three other columns filled with roughly granulated P_4O_{10} , P_4O_{10} on silica with a moisture indicator, and molecular sieve. Solvents were dried using standard laboratory procedures and were freshly distilled from Na/K-alloy (Et_2O , mtbe, *n*-pentane) and potassium (THF). All chemicals are commercially available or have been synthesized according to the literature as for Rb(hmds) and Cs(hmds).^[158] CpH and Cp'H were obtained by cracking and subsequent distillation of dicyclopentadiene and dimethyldicyclopentadiene under *Schlenk*-conditions. Stored at 4°C, CpH and Cp'H were used within two weeks. The ammonia-gas has been pre-dried by two columns filled with KOH and NaOH. Before condensation into the flask, the ammonia-gas was condensed in a *Schlenk*-tube with a piece of sodium (Figure 130). From the occurring blue solution ammonia was evaporated and re-condensed into the reaction vessel. For condensation of ammonia a cooling bath of dry ice/acetone (or isopropyl alcohol) was used.

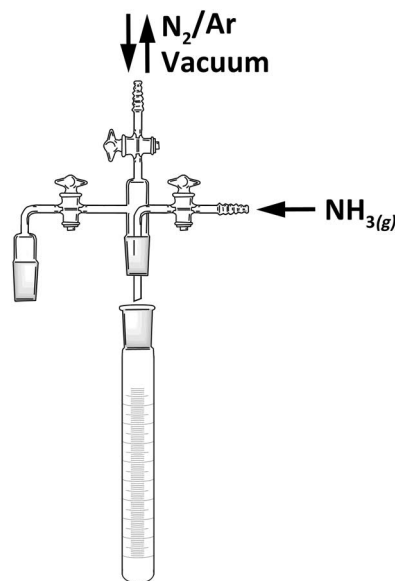


Figure 130: *Schlenk*-apparatus for liquidification of and subsequent evaporation of ammonia.

6.2. Synthesis

6.2.1. $[Li(NH_3)_4][Cp']$ (3)

Cp'Li has been previously synthesized by slowly adding a 1.2 M-solution of *n*-butyllithium in hexane (52.2 mL, 70.4 mmol) to a solution of freshly distilled Cp'H (5.0 mL, 58.7 mmol) in Et_2O (150 mL) at 0°C, stirred for 1 h at room temperature. After filtration, washing with Et_2O (40 mL) and pentane (40 mL), and drying under reduced pressure, the white granulated solid was stored in an argon dry box. Cp'Li (0.40 g, 4.6 mmol) was solved in THF (20 mL) and the reaction mixture was cooled to -15°C. In a flux of frequent small bubbles, gaseous ammonia was fed into the solution over a cannula for 15 min. The

Experimental Section

Synthesis

clear and pale yellow solution was stored for crystallization at -87°C . **3** formed colorless needle-shaped crystals.

6.2.2. $[\text{Li}(\text{NH}_3)_4][\text{Cp}^*_2\text{Li}]\cdot(\text{NH}_3)_{0.87}$ (**4**)

$\text{Li}(\text{hmds})\cdot\text{Et}_2\text{O}$ (0.27 g, 1.13 mmol) was solved in liquid ammonia (12 mL) at -78°C . Cp^*H (0.2 mL, 1.2 mmol) was added and the reaction mixture and instantly formed a white solid. The reaction mixture was slowly warmed up to -33°C and the white solid melted. The reaction mixture was stirred until the evolved droplets disappeared and subsequently cooled down to -78°C . The clear and colourless solution was stored for crystallization at -45°C . **4** crystallized in elongated colorless blocks.

6.2.3. $[\text{Li}(\text{NH}_3)_4][\text{Ind}]$ (**5**)

Indene (0.8 mL, 6.9 mmol) was added dropwise into a solution of $\text{Li}(\text{hmds})$ (1.04 g, 6.21 mmol) in a mixture of Et_2O (12 mL) and THF (10 mL) at -15°C . In a flux of frequent small bubbles, gaseous ammonia was fed into the solution over a cannula for 10 min. A white precipitation was formed and removed by filtration over celite. The clear and pale green solution was stored for crystallization at -16°C . **5** crystallizes as colorless needle-shaped crystals.

6.2.4. $[\text{Li}(\text{NH}_3)_4][\text{Flu}](\text{NH}_3)_2$ (**6**)

Fluorene (0.40 g, 2.4 mmol) was solved in mtbe (10 mL) and a solution of *n*-butyllithium in hexane (0.45 mL, 2.4 mmol, 5.4 M) was added dropwise at 0°C . The reaction mixture turned orange and was stirred for 20 min. At -78°C ammonia was condensed into the reaction mixture under formation of a yellow precipitation. The reaction mixture was stirred and ammonia was subsequently condensed into the reaction mixture until the solution turned clear. The clear and orange-colored solution was stored for crystallization at -76°C . **6** formed orange block-shaped crystals.

6.2.5. $\text{CpNa}(\text{NH}_3)_3$ (**7**)

CpH (0.2 mL, 2.5 mmol) was added dropwise into a solution of $\text{Na}(\text{hmds})$ (0.45 g, 2.44 mmol) in THF (15 mL) at 0°C . The reaction mixture was stirred for 1 h at room temperature. At -15°C gaseous ammonia was fed into the solution over a cannula in a flux of frequent small bubbles for 10 min. The clear and pale violet solution was stored for crystallisation at -30°C . **7** formed colourless block-shaped crystals.

6.2.6. ***Cp*^{*}*Na*(NH₃)₃ (**8**)**

Cp^{*}H (0.7 mL, 8.3 mmol) was added dropwise to a solution of Na(hmds) (0.94 g, 8.31 mmol) in THF (25 mL) at room temperature. The reaction mixture was stirred for another 10 min and cooled down to –15°C afterwards. In a flux of frequent small bubbles, gaseous ammonia was fed into the solution over a cannula for 15 min. The clear and pale green solution was stored for crystallisation at –45°C. **8** formed colorless thin plate-shaped crystals.

6.2.7. ***Cp*^{*}*Na*(NH₃)₃·(*HN*(SiMe₃)₂)_{0.4} (**9**)**

Na(hmds) (0.23 g, 1.25 mmol) was solved in liquid ammonia (12 mL) at –78°C. *Cp*^{*}H (0.22 mL, 1.38 mmol) was added and the reaction mixture instantly formed a white solid. The reaction mixture was slowly warmed up to –33°C and the white solid melted. The reaction mixture was stirred until the evolved droplets disappeared and subsequently cooled down to –78°C. The clear and pale green solution was stored for crystallization at –76°C. **9** formed needle-shaped crystals.

6.2.8. **[Na(NH₃)₄][*Ind*] (**10**)**

Indene (0.37 mL, 3.14 mmol) was added dropwise to a solution of Na(hmds) (0.48 g, 2.62 mmol) in Et₂O (20 mL) at room temperature. The reaction mixture was stirred for another 10 min and cooled down to –15°C afterwards. In a flux of frequent small bubbles, gaseous ammonia was fed into the solution over a cannula for 18 min. The clear and pale green solution was stored for crystallisation at –16°C. **10** formed colorless plate-shaped crystals.

6.2.9. **[Na(NH₃)_{4/6}][*Flu*] (**11**)**

Fluorene (0.19 g, 1.15 mmol) and Na(hmds) (0.21 g, 1.15 mmol) were solved in mtbe (10 mL). The reaction mixture turned orange and was stirred for 10 min. At –78°C ammonia was condensed into the reaction mixture under formation of a yellow precipitation. The reaction mixture was stirred and ammonia was subsequently condensed into the reaction mixture until the solution turned clear again. The clear and orange-colored solution was stored for crystallization at –76°C. **11** formed orange block-shaped crystals.

6.2.10. ***Cp*K(NH₃)₂ (**12**)**

Ammonia was condensed to a mixture of K(hmds) (0.46 g, 2.36 mmol) and *Cp*H (0.22 mL, 2.36 mmol) at –78°C until the solution turned clear. The clear and colorless solution was stored for crystallisation at –45°C. **12** formed colorless block-shaped crystals.

6.2.11. ***Cp'K(NH₃) (13)***

Cp'H (0.33 mL, 3.92 mmol) was slowly added to a solution of K(hmds) (0.50 g, 2.51 mmol) in Et₂O (20 mL) at room temperature. The reaction mixture was stirred for another 10 min and subsequently cooled down to -15°C. In a flux of frequent small bubbles, gaseous ammonia was fed into the solution over a cannula for 16 min. The clear and colorless solution was stored for crystallisation at -45°C. **13** formed colorless block-shaped crystals.

6.2.12. ***(Ind)K(NH₃)₂ (14)***

Indene (0.44 mL, 3.73 mmol) was slowly added to a solution of K(hmds) (0.62 g, 3.14 mmol) in Et₂O (20 mL) at room temperature. The reaction mixture was stirred for another 10 min and subsequently cooled down to -15°C. In a flux of frequent small bubbles, gaseous ammonia was fed into the solution over a cannula for 17 min. The clear and colorless solution was stored for crystallisation at -45°C. **13** formed colorless block-shaped crystals.

6.2.13. ***(Flu)K(NH₃)₂ (15)***

Fluorene (0.77 g, 4.61 mmol) and K(hmds) were solved in mtbe (20 mL). The reaction mixture turned orange and was stirred for 20 min. At -78°C ammonia was condensed into the reaction mixture under formation of a yellow precipitation. The reaction mixture was stirred and ammonia was subsequently condensed into the reaction mixture until the solution turned clear. The clear and orange-coloured solution was stored for crystallization at -76°C. **15** formed orange plate-shaped crystals.

6.2.14. ***CpRb(NH₃)₂ (16)***

CpH (0.07 g, 1.1 mmol) was slowly added to a solution of Rb(hmds) (0.24 g, 1.0 mmol) in Et₂O (5 mL) at room temperature. The reaction mixture was stirred for 30 min and all volatile substances were subsequently removed under reduced pressure. At -78°C ammonia was condensed to the white solid while stirring until the solution turned clear. The clear and colourless solution was stored for crystallisation at -76°C. **16** formed colourless block-shaped crystals.

6.2.15. ***Cp'Rb(NH₃)₂ (17)***

Cp'H (0.08 g, 1.0 mmol) was slowly added to a solution of Rb(hmds) (0.22 g, 0.9 mmol) in Et₂O (5 mL) at room temperature. The reaction mixture was stirred for 30 min and all volatile substances were subsequently removed under reduced pressure. At -78°C ammonia (28 mL) was condensed to the white solid. The reaction mixture was warmed up to

-45°C and the solution turned clear. The clear and colourless solution was stored for crystallisation at -76°C . **17** formed colourless block-shaped crystals.

6.2.16. **(Ind)Rb(NH₃)₂ (18)**

Indene (0.14 g, 1.2 mmol) was slowly added to a solution of Rb(hmds) (0.29 g, 1.2 mmol) in Et₂O (5 mL) at room temperature. The reaction mixture was stirred for 30 min and the reaction mixture was cooled down to -78°C . Ammonia (19.2 mL) was condensed to the solution and a white precipitation was formed. The reaction mixture was warmed up to -45°C and the solution turned clear after 1 d. The clear and colourless solution was stored for crystallisation at -76°C . **18** formed colourless block-shaped crystals.

6.2.17. **(Flu)Rb(NH₃)·THF (19)**

Rb(hmds) (0.50 g, 2.03 mmol) and fluorene (0.34 g, 2.03 mmol) were solved in THF (20 mL) and stirred at room temperature for 1.5 h. The reaction mixture turned orange and was cooled down to -15°C . In a flux of frequent small bubbles, gaseous ammonia was fed into the solution over a cannula for 15 min. The clear and colorless solution was stored for crystallisation at -76°C . **19** formed orange block-shaped crystals.

6.2.18. **CpCs(NH₃) (20)**

CpH (0.05 mL, 0.61 mmol) was slowly added to a solution of Cs(hmds) (0.16 g, 0.55 mmol) in THF (10 mL) at room temperature. The reaction mixture was stirred for 30 min and all volatile substances were subsequently removed under reduced pressure. At -78°C ammonia (11 mL) was condensed to the white solid. The reaction mixture was warmed up to -33°C and stirred until the solution turned clear. The clear and colourless solution was stored for crystallisation at -76°C . **20** formed colourless needle-shaped crystals.

6.2.19. **Cp'Cs(NH₃) (21)**

Cp'H (0.30 g, 3.7 mmol) was slowly added to a solution of Cs(hmds) (1.0 g, 3.4 mmol) in THF (10 mL) at room temperature. The reaction mixture was stirred for 30 min and all volatile substances were subsequently removed under reduced pressure. At -78°C ammonia (16 mL) was condensed to the white solid. The reaction mixture was warmed up to -33°C and stirred until the solution turned clear. The clear and colourless solution was stored for crystallisation at -76°C . **21** formed colourless needle-shaped crystals.

6.2.20. **(Ind)Cs(NH₃) (22)**

Ammonia was condensed to a mixture of Cs(hmds) (0.39 g, 1.33 mmol) and indene (0.16 mL, 1.33 mmol) at -78°C until the solution turned clear. The clear and colorless solution was stored for crystallisation at -76°C . **22** formed colorless block-shaped crystals.

6.2.21. **(Ind)Cs(NH₃)(THF) (23)**

Indene (0.16 mL, 1.33 mmol) was slowly added to a solution of Cs(hmds) (0.39 g, 1.33 mmol) in THF (10 mL) at room temperature. The reaction mixture was stirred for 30 min. At -78°C ammonia (15 mL) was condensed to the reaction mixture. The reaction mixture was warmed up to -33°C and stirred until the solution turned clear. The clear solution was stored for crystallisation at -76°C . **23** formed colourless needle-shaped crystals.

6.2.22. **(Flu)Cs(NH₃)₂ (24)**

Fluorene (0.57 g, 2.03 mmol) was added to a solution of Cs(hmds) (1.0 g, 3.4 mmol) in THF (10 mL) at room temperature. The reaction mixture was stirred for 30 min and all volatile substances were subsequently removed under reduced pressure. At -78°C ammonia (15 mL) was condensed to the white solid. The reaction mixture was warmed up to -33°C and stirred until the solution turned clear. The clear and colourless solution was stored for crystallisation at -76°C . **16** formed colourless block-shaped crystals.

7. Crystal Structure Determination

7.1. Crystal Selection

The crystal selection and mounting of the compounds presented in this work was challenging due to the rapid decomposition of the crystals outside the mother liquor. The crystals are not only highly sensitive to air and moisture as almost any other alkali-organometallic compound, but also suffer from evaporation of ammonia out of the crystal lattice. The decomposition happened to be so rapidly, that additional measures to the procedures for sensitive crystals had to be taken. The new developed techniques are described in the following.

7.1.1. *Special Requirements in Treatment of Highly Sensitive Crystals*

Decomposition of crystals during sample preparation is a problem many crystallographers have to deal with. The two main problems are decomposition of air- and moisture sensitive compounds when exposed to air and evaporation of lattice solvent after removing crystals out of the mother liquor. These two problems can be dealt with by exclusion of air and cooling of the sample. One possibility is the mounting of crystals in capillaries. The disadvantage of the capillary-method is the high effort and the limited range of compounds. A more efficient way is to prepare the sample in inert oil, which is cooled and sufficiently protected from air by a stream of evaporated nitrogen. For this purpose *Stalke et al.* developed the X-Temp2-device in which two heating elements evaporate liquid nitrogen from a dewar-flask and regulate the temperature of the gas-flow in the nozzle.^[159] By regulating the impressed voltage of the heating elements both the flow rate of the stream and its temperature (-100°C to $+25^{\circ}\text{C}$) can be regulated and adapted to the specific task. The nozzle is placed close to object slide on the microscope. The used inert oil is perfluorated-polyether oil. Different viscosities can be mixed to obtain the right viscosity at a specific temperature. The oil protects the crystals from air during preparation, helps separating and cleaning the crystals, leaves behind a protecting film of the crystal to survive the way from the microscope to the goniometer, and, shock-cooled on the goniometer by the crystal-cooling device, forms a protecting glass around the crystal.

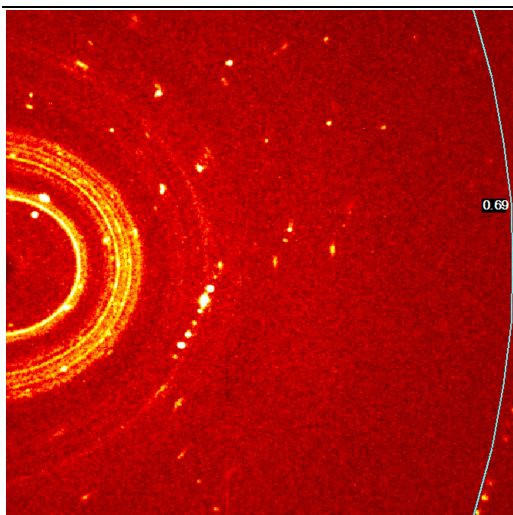


Figure 131: Frame of compound **2** on a BRUKER APEX2 Quazar, equipped with an Incoated $I\mu S$, Mo- K_{α} radiation.

The compounds presented in this work push the limit of this method. Even at the lowest possible temperature of the gas-flow, once the crystals are taken out of the mother liquor the crystals decompose within seconds under release of ammonia. Figure 131 shows a diffraction-frame of a successful measurement of $[\text{Li}(\text{NH}_3)_4][\text{Cp}]\cdot\text{NH}_3$ (**2**). Crystals were taken out of the mother liquor and instantly started to decompose. Without further inspection one crystal was mounted on the tip of a MiTeGen©MicroMount and rapidly moved to the goniometer. Powder rings of the instant decomposition a clearly

visible. A large block-shaped crystal was selected and, which turned white on the surface and was highly fragmented. An intact crystal domain couldn't be visually identified. This affected the data quality, giving a relatively high R_{int} (5.42 %), large scale variations of the reflection-intensities, and high R -values for the refinement. However, the data quality was sufficient enough to yield an R_1 -value of 3.98% ($I > 2\sigma$) and a wR_2 -value of 11.33% (all data). Only the large size of the crystal allowed a measurement, crystals of smaller size or plate- or needle-shaped crystals are accessible to that method.

7.1.2. A Copper Block for Crystal Cooling

The limit to the temperature was set by the fact, that the object slide for sample preparation was placed on a glass-plate at the foot of the microscope. The glass-plate transports heat to the object slide and compensates the cooling effect of the X-Temp2 at a certain point. Therefore the object slide needed to be further and constantly cooled while at the same time being able to enlighten the sample for selection and preparation. To accomplish it, a plate of copper ($8.5 \times 8.3 \times 1.0 \text{ cm}^3$) (Figure 132) was developed, which could be cooled by liquid nitrogen and dry ice and placed on the microscope.

Copper has been chosen for its high thermal conductivity ($401 \text{ Wm}^{-1}\text{K}^{-1}$ at 27°C).^[134] Two recesses of have been milled into the plate: a small recess ($27 \text{ mm} \times 77 \text{ mm} \times 1 \text{ mm}$) for the object slide and a bigger recess ($40 \text{ mm} \times 77 \text{ mm} \times 1 \text{ mm}$) for a cooling agent like dry ice, which has been used in all experiments. To enlighten the sample with the light source underneath the foot of the microscope, a hole of 20 mm in diameter was milled into the centre of the small recess. The hole was sealed from the other side by a glass plate

(26 mm × 26 mm), which was cut off an object slide and glued into a recess of 27 mm × 27 mm × 1 mm) with a low-temperature stable silicone. The glass of the object slide is of homogeneous fabric, which is important for the use of the polarisation filter in the optic of the microscope. During sample preparation the hole is filled with a fluid, that does not freeze at 77 K (EtOH, *i*-PrOH), to cool of the sample and prevent ice-formation. The object slide is clamped by two clips made of spring steel sheet, which are fixed by two screws in tapped holes. The plate has been galvanized with nickel to prevent oxidation of the surface. To insulate the copper-plate from the glass plate in the foot of the microscope, a thin layer of Styrofoam was used.

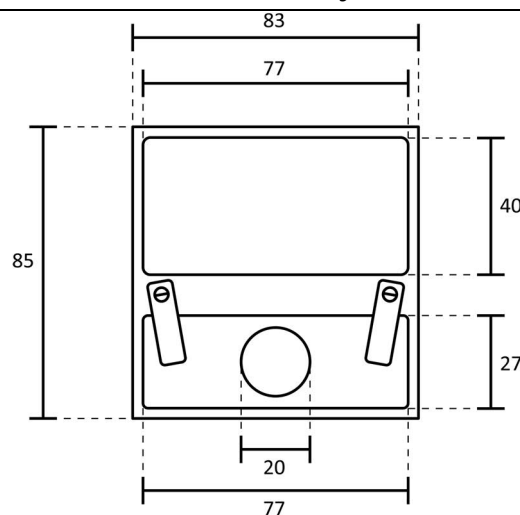


Figure 132: Dimensions [mm] of the copper plate used for crystal cooling during sample preparation.

7.1.3. Sample Preparation

The copper plate is cooled in liquid nitrogen and moved with a pincer to the microscope. With cotton gloves the plate can be aligned on the insulator and to the right position on the microscope. The hole in the recess for the object slide is filled with a fluid and the slide is fixed with the clips. On the other recess a block of dry ice is placed to keep the block cool for a long period of time. After aligning the cooling stream of the X-Temp2 to the object slide, a drop of inert oil with a very low viscosity is put on the slide (Figure 133).

The *Schlenck*-flask with the crystals in mother liquor is placed close to the object slide in a cooling bath. Crystals are transferred at reverse flow of protective gas from the *Schlenck*-flask into the oil. This has to happen very fast. Even very sensitive crystals survive a short exposure to air. To pick up a sufficient crystal, the pin equipped with a MiTeGen©MicroMount is put on a handle with a magnetic head. This allows to directly dipping the crystal into liquid nitrogen after selection. This whole procedure needs to be

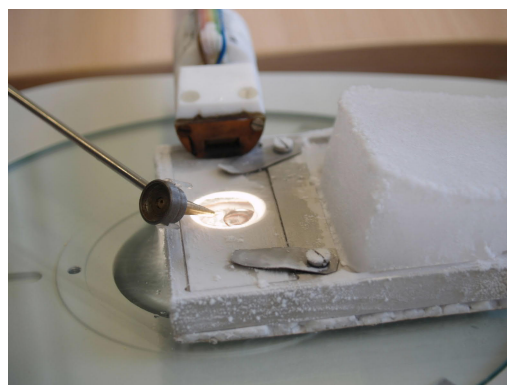


Figure 133: Sample preparation under a microscope using the N₂(l)-cooled copper block with an additional block of dry ice and the XTemp2.

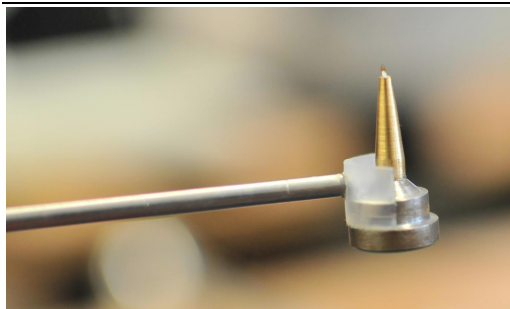


Figure 134: Cutted section of a protection cap from a mounting pin attached to a handle. The device allows quick and precise handling of the sample.

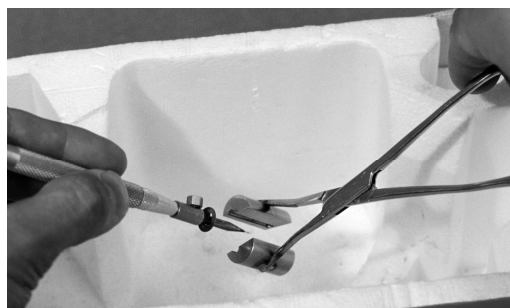


Figure 135: Cold-transfer tong for cooling a mounting pin in liquid nitrogen.

pursued in a concentrated but swift manner and requires some training.

Different methods to transfer the crystal from the Dewar flask of liquid nitrogen to the goniometer head can be used. In this work a section of a pin-cap was cut out and fixed to a handle (Figure 134). A pin-cap is a sealed cylinder of plastic with a magnetic ring to protect a sample for storage and/or transportation. With the pin on the handle the crystals could be picked up, dipped into liquid nitrogen, and moved from liquid nitrogen to the goniometer head. A Dewar flask with a handle was used to get as close as possible to the goniometer head to put the pin on it in a quick move. Another method is the 'cold-transfer tong', which is basically a tong with two halves of a cylinder at the top that enclose the pin (Figure 135).

The pin is transferred from a handle to the tong in liquid nitrogen.

7.1.4. *Advantages of the Procedure*

The described method is very efficient for diffraction experiments of very sensitive and rapidly decomposing crystals. Basic elements are sample cooling at very low and enduring temperatures by the copper block and X-Temp2 during sample preparation and sample transportation in liquid nitrogen. Exposure to air is minimized by quickly moving the sample from the flask to the block, into $N_{2(l)}$, and to the head of the goniometer, where it is finally protected by the cooling device. Even crystals that decompose very fast even on the copper-block like $CpCs(NH_3)$ (**20**) and $Cp'Cs(NH_3)$ (**21**) survive those short-time exposures. The space for sample preparation is limited and icing occurs over time, but does not pose a challenge to sample preparation with the necessary skillset. This method is very efficient, does not require further elaborate setup, and made a broad range of hypersensitive compounds accessible, which could not be prepared otherwise. The crystal quality does not suffer from the preparation method and yielded good datasets throughout.

7.2. Data Acquisition and Processing

The data collections were carried out on Bruker APEX2 Ultra or Quazar diffractometers equipped with Bruker TXS Mo, Incoatec λ Mo or Incoatec λ Ag sources. The data were collected in ω -scan mode and the collection strategy was calculated with the APEX plugin COSMO^[160] or entered by hand.

The unit cell was indexed with the tools in the Bruker APEX2 software suite.^[161] The intensities on the raw frames were integrated with SAINT 8.34a.^[161] The orientation matrix was refined in several integration runs and the maximum resolution was adjusted so that only useable data with a maximum R_{int} of 0.20 were integrated.

The software SADABS 2014/5^[162] was used for absorption correction and scaling. TWINABS 2012/1^[163] was utilized in the cases of non-merohedral twins. XPREP in various versions up to 2013/1 was used for the examination of data statistics and preliminary space group determination.^[164] The program SHELXT 2014/4^[154] was used to create a structure solution which was refined using SHELXL-2014/7^[165] within the SHELXL-GUI.^[166]

All non-hydrogen-atoms were refined with anisotropic displacement parameters (ADPs). The C-bonded hydrogen atoms were set on calculated positions and refined isotropically using a riding model with their U_{iso} values constrained to 1.5 times the U_{eq} of their pivot atoms for terminal sp^3 carbon atoms and 1.2 times for all other carbon atoms. The N-bonded hydrogen atom coordinates were refined from the residual density map and constrained to 1.5 U_{eq} of their pivot nitrogen atom. The N-H distances were restrained on 0.91 Å.

7.3. General Remarks on Disorder Refinement

Disorder is a repeatedly recurring phenomenon in small molecule X-Ray diffraction.^[167] In this section, the treatment of disorder will be described referring to both ammoniacate structures and structures determined in collaboration with other workgroups.

In an ideal crystal all atoms in the unit cell are in the same position along the crystal. In reality, many if not most crystals are affected by each impurity, disorder, modulation, or twinning. Disorder is the randomly displacement of an atom, a functional group, or the whole molecule from unit cell to unit cell. The electron density map obtained by X-Ray diffraction is by nature only a spacial and time average of the electron density of all unit cells within the crystal. Disorder itself is caused by low energy barriers for rotation or shift of functional groups. Disorder can be dynamic or static. Dynamic disorder involves flexible atoms, molecules or functional groups and can be minimized by sample cooling. Static disorder is an inherent property of the crystal.

Crystal Structure Determination

General Remarks on Disorder Refinement

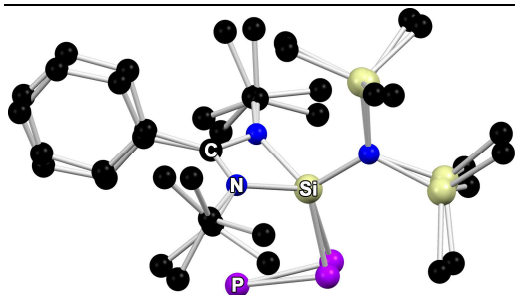


Figure 136: Asymmetric unit of $(\text{PhC}(\text{N}^i\text{Bu})_2\text{N}(\text{SiMe}_3)_2\text{Si})_2\text{P}_4$ (RM_SK500_b) showing librational disorder of the Bz-group and a phosphorous atom as well as librational/rotational disorder of the ^iBu - and SiMe_3 -groups.

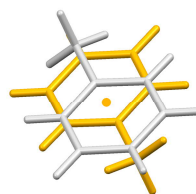


Figure 137: Toluene placed on an inversion centre indicated by orange spheres. The two colours represent the two symmetry related orientations.

The three main types of disorder are substitutional disorder, positional disorder, and symmetry induced disorder. Substitutional disorder is the occupation of the same position in the crystal structure by two or more sorts of atoms/molecules. It is static disorder and depends mostly on substance purity during crystallization. Examples are two different metal ions at a coordination site, two types of solvent molecules occupying a void in the crystal lattice, or two similar anions like Cl^-/Br^- as counteranions. The most frequent type of disorder is positional disorder. Affected are often ^iBu -, ^iPr -, and SiMe_3 -groups by rotation or Bz-groups by libration as shown in Figure 136. Symmetry induced disorder takes place, when a molecule is placed on a symmetry element higher than the symmetry of the molecule itself. Lattice toluene is often located on an inversion centre (Figure 137). Toluene itself has no inversion symmetry and appears half occupied in two inverted orientations around the centre of symmetry.

There are three main indicators for disorder. The most obvious one is high residual electron density close to the atomic positions in the $F_o - F_c$ residual density map. Other indicators of disorder are size and shape of the isotropic and anisotropic displacement parameters (Figure 138).

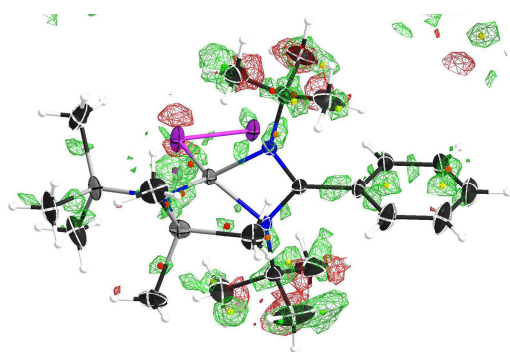


Figure 138: Anisotropic refinement of the asymmetric unit of RM_SK500_b without treatment of disorder. Lattice toluene has been omitted. Q-peaks, residual density, and elliptic U_{ij} -values indicate disorder.

tors of disorder are size and shape of the isotropic and anisotropic displacement parameters (Figure 138). Oversized U_{iso} -values compared to most other atoms indicate disorder, because the refinement program tries to compensate the missing electron density from the reduced occupancy through increased thermal motion. Cigar shaped ellipsoids are a clear warning sign of disorder. A more subtle indication for disorder are

meaningless bond lengths and angles are often but not always visible.

Disorder means spreading of charge density of otherwise discrete atomic positions only affected by thermal motion. The accuracy of the atomic positions suffers greatly from disorder and has to be supported by restraints and constraints for atomic positions and anisotropic displacement parameters. Restraints are additional structural informations implemented into the refinement and are treated like additional experimental observation by SHELXL. They increase the number of refinable parameters. Constraints are exact mathematical relationships that reduce the number of free parameters in a model. They are applied on most hydrogen atoms, especially those attached to carbon. In the case of positional disorder on two sites, the site occupancy of the second moiety is constrained to 1-sof (site occupation factor). Without restraints as additional structural information, the refinement program cannot distinguish both position and thermal motion in a meaningful way. Therefore restraints have to be seen as mandatory and need to be applied from the very beginning. Commonly used restraint for atomic positions are SADI, DFIX, SAME, and FLAT. Restraints for anisotropic displacement are RIGU, SIMU, ISOR, and the outdated DELU. SADI (same distance) restrains the distances between two or more pairs of atoms to an equal value (Figure 139). Constraints of atomic positions and thermal motion of disordered moieties are helpful in the case of weak disorder or poor data quality.

Since both the refinement of the atomic position and the anisotropic displacement refinement compete for the same available charge density, restraints have to be placed on the U_{ij} -parameters as well (Figure 140). The site occupation factor and the anisotropic displacement parameters are correlated and need to be adequately distributed to the two or more positions of the disordered atoms. The DELU instruction is a rigid-bond restraint that equalizes the U_{ij} -component along the bond. It has been largely replaced by the RIGU instruction, which does not only restraint the U_{ij} -component along the bond, but expands the restraint to U_{ij} -components perpendicular to the bond direction. The RIGU instruction created more restraints, but reflects the nature of the anisotropic displacement more accurately. The SIMU instruction restrains all components of the U_{ij} -parameters to be

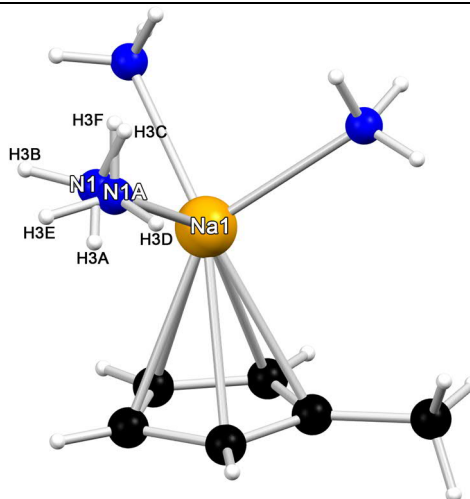


Figure 139: Treatment of disorder in $\text{Cp}^*\text{Na}(\text{NH}_3)_3$ (**8**). SADI instructions equalize N–Na bond length and 1,3-H,H-distances. The DFIX instruction set all N–H-bonds to 0.91 Å.

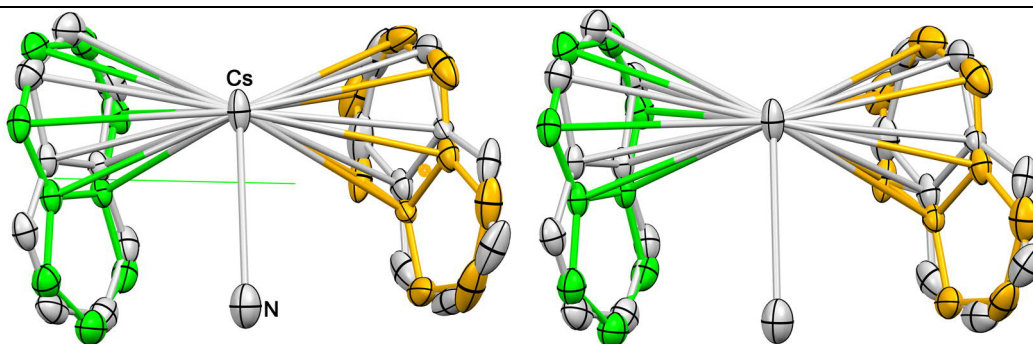


Figure 140: Disorder treatment in $\{\text{IndCs}(\mu\text{-NH}_3)_3\}$ (**22**). Both anions are disordered around symmetry elements: the orange sphere as an inversion centre and the green line as a twofold axis. The orange/green atoms are symmetry generated. Atoms on the left are treated without APD-restraints, atoms on the right are treated with RIGU and SIMU.

similar. This is not a physically accurate description, but a helpful tool at low resolution data or disorder and therefore has a higher default standard deviation. Like positional restraints have to be applied at the very beginning of anisotropic refinement.

In some cases the amount of disorder is below 10% and can be overlooked or visibly appears only after anisotropic refinement and the anisotropic displacement parameters are not affected by the disorder. This is the case in $[\text{Li}(\text{NH}_3)_4][\text{Flu}]\cdot(\text{NH}_3)_2$ (**6**) (Figure 141). The anion on the left is disordered by roughly 7% and the anion on the right by roughly 3%. The amount of charge density is therefore very low and totally insufficient to describe either atomic positions or thermal displacement. In this case the right strategy is to use available Q-peaks and atomic positions of the major fraction to model the second fraction. SAME instructions give the fraction the right shape and RIGU and SIMU instructions provide reasonable ADPs. It is also justifiable to use constraints like EADP to fix the U_{ij} -parameters to another atom if the ADPs of an atom if the amount of disorder is very low.

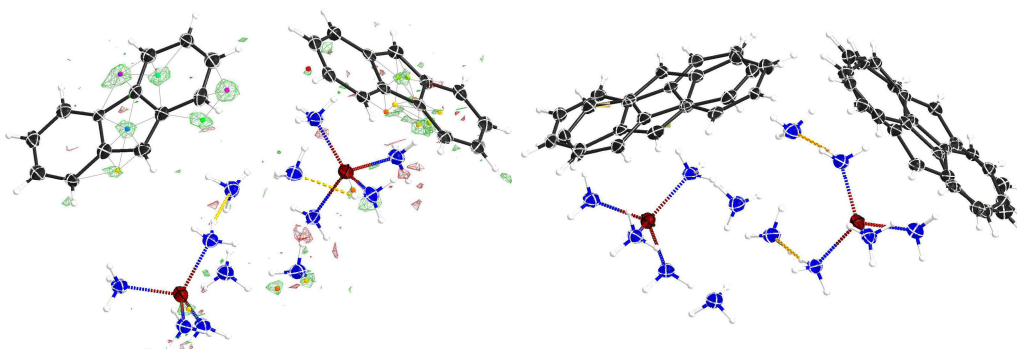


Figure 141: Minor disorder in $[\text{Li}(\text{NH}_3)_4][\text{Flu}]\cdot(\text{NH}_3)_2$ (**6**) represented by residual charge density and Q-peaks with the highest intensity of 0.26 (pink) and the subsequent disorder refinement.

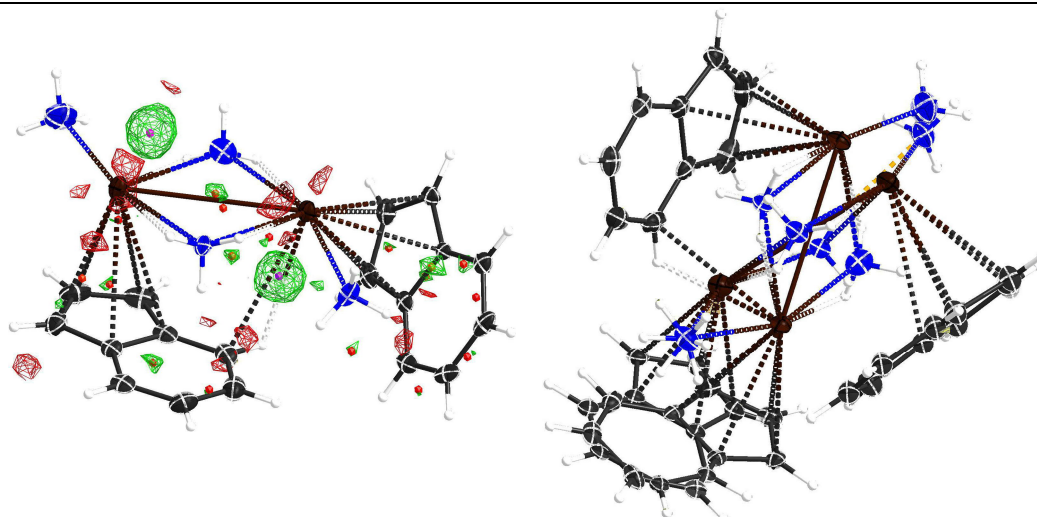


Figure 142: Disorder in $(\text{Ind})\text{Rb}(\text{NH}_3)_2$ (**18**). Left: the 6%-disorder is visually dominated in the second positions of the rubidium cations. Right: subsequent refinement revealed disorder of the entire content of the asymmetric unit.

Things can be more complicated when the structure shows minor disorder and a heavy atom is involved. This is the case in $(\text{Ind})\text{Rb}(\text{NH}_3)_2$ (**18**) (Figure 142). The whole content of the asymmetric unit is disordered by roughly 6%. Some crystallographers might ignore or oversee this low amount of disorder when only light atoms are involved, because the quality of the structure is only slightly affected. Heavy atoms create two problems: minor occupancy still creates significant peaks in the residual density map and they dominate the structure factors. The first point requires dealing with it and the second point makes it more difficult, because lighter atoms appear to be less accurately resolved when a heavy atom is present. The indenyl anions are not challenging, because a system of nine atoms is less variable in its position than single ammonia molecules. Their position is much vaguer and required a sophisticated set of positional restraints. The positions of the attached hydrogen atoms are basically created out of thin air and can not be attributed to actual positions.

Another great challenge in disorder refinement are solvent molecules in structures of large sized molecules. These molecules often form large voids, because their spatial geometry does not allow a compact crystal packing. One example is displayed in Figure 143. The molecule consists of a P_4 -chain with silicon at both ends, each coordinated by two $\text{N}(\text{TMS})_2^-$ ligands and a $\text{C}(\text{N}^i\text{Bu}_2)_2(\text{Ph})$ ligands. The dumbbell shape leads to large voids around the P_4 -chains, which is filled with disordered toluene. After identifying six positions, residual density is still present, but no additional position could successfully be refined. Because of the vague distribution of charge density, the occupancies did not refine stable and were fixed to a specific value.

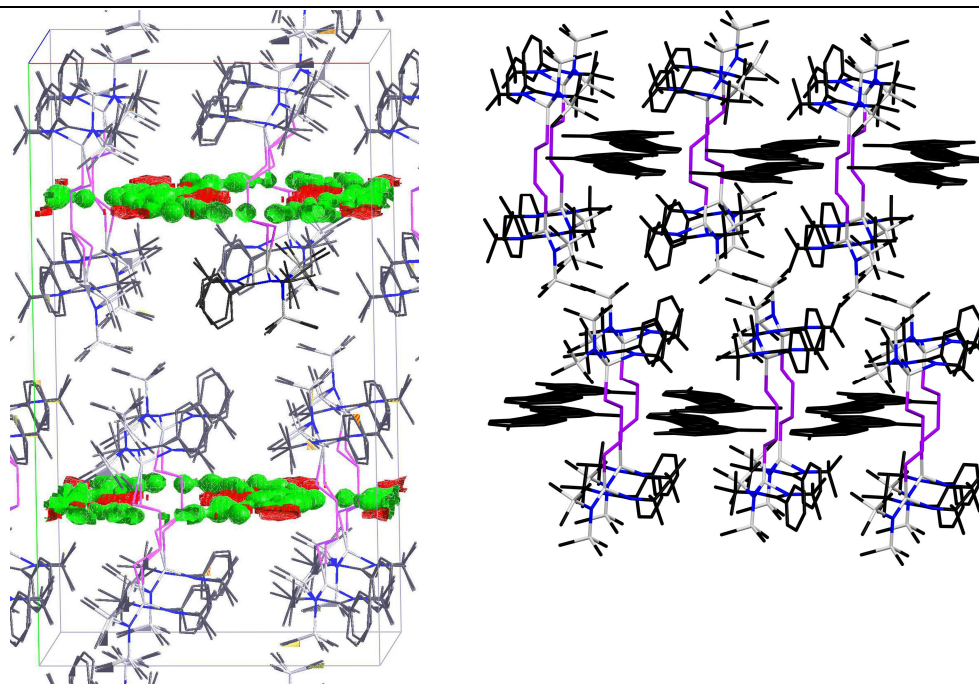


Figure 143: Strings of disordered toluene inside channel voids in $P_4((Si(N(TMS)_2)(C(N^iBu_2)(Ph))_2$ (see RM_SK500b). The picture on the left shows amorphous electron density with the voids left by the main molecule. The picture on the right shows the resulting refinement of the lattice toluene (disorder of the main molecule has been omitted).

The previously described methods can reach a boundary when the structure is large and allows large quantities of lattice solvent to co-crystallize. Figure 144 depicts a cage structure of four large bidentate ligands connected by two Pd^{2+} -cations. The structure contains besides the BF_4^- -counteranions a vast amount of highly disordered lattice-dichlorobenzene. The disorder could be successfully refined, but in similar cases with

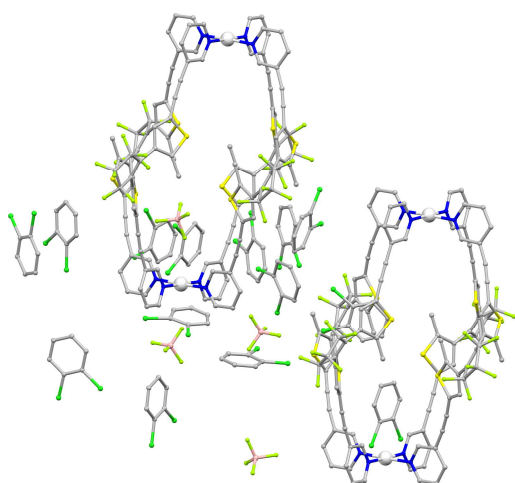


Figure 144: Dichlorobenzene as lattice solvent and BF_4^- anions between large size cage structures (see MX00). Disordered moieties have been removed for clarity.

poor data quality, the SQUEEZE function in PLATON^[168] can be an alternative treatment. SQUEEZE creates a new hkl-file with corrected structure factors omitting undesired electron density. It has been applied to a similar cage structure (see 7.12.1 RM_FS65), in which strands of amorphous electron density of unresolved lattice acetone proved to be untreatable. The R_1 -value dropped from 22.11% to 11.15%, proving this treatment to be a powerful alternative in the case of amorphous electron density combined with poor data quality.

7.4. Treatment of the Modulated Structures 9 and 11

Incommensurately modulated structures together with quasicrystals and composite crystals belong to the class of aperiodic crystals.^[150] Modulation can be understood as a loss of periodicity in three dimensions and the atoms become d -dimensional domains rather than fixed points in the 3-dimensional space. In practice, the atoms incrementally shift their position from unit cell to unit cell in a periodic fashion. This can be understood as ordered (or periodic) disorder. The additional periodicity creates additional Bragg-reflections, which are aligned around the main hkl -reflections (Figure 145). The orientation of the additional Bragg-reflections for integration is given as the so called q -vector. It contains the orientation of the satellite reflections relative to the main reflections. The additional dimension(s) of the structure leads to additional symmetry and therefore expanded point groups. These reflections are much weaker than the main reflections, but they can be integrated by SAINT 8.34a. Treatment of this data is not possible with the ShelX program package but the modulation function can be eventually refined in JANA 2006.^[153]

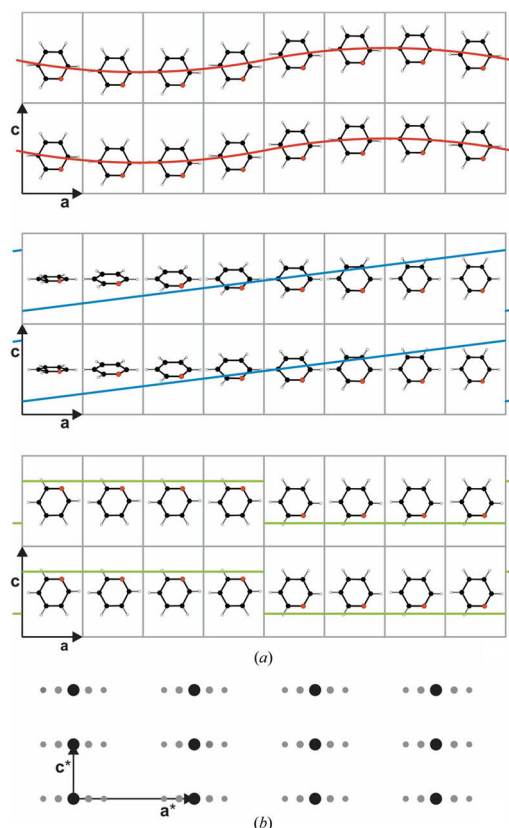
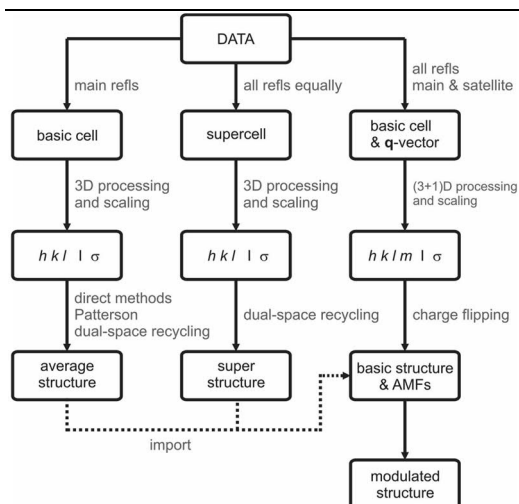


Figure 145: Sinusoidal, sawtooth-, or crenel-type modulation along the a-axis and resulting satellite reflections. Graphics were taken from [150].

Solvation and refinement of the structures $\text{Cp}^*\text{Na}(\text{NH}_3)_3 \cdot ((\text{HN}(\text{SiMe}_3)_2)_{0.4})$ (**9**) and $[\text{Na}(\text{NH}_3)_{4/6}][\text{Flu}]$ (**11**) using modulation functions in JANA 2006 was conducted in collaboration with *Dr. Andreas Schönleber* from the university of Bayreuth, an expert in modulation of both inorganic compounds and small molecules. Unfortunately, the combined efforts did not lead to a successful refinement of both structures and an alternative route for structure solution was chosen. Scheme 14 describes the path for treatment of modulated structures. For both structures the first two routes have been chosen: the route over the main reflections to obtain the average structure and the supercell approach to obtain the superstructure. The route over all reflections and q -vectors to obtain the modulated structure has been unsuccessful in the two cases. The route over the basic cell and neglecting the

Crystal Structure Determination Treatment of the Modulated Structures 9 and 11



Scheme 14: Different approaches for solution and refinement of modulated structures.

reflect the different positions of that atoms and molecules due to modulation. Missing and



Figure 146: The basic cell approach neglecting the satellite reflections leads to an averaging of the content and large displacement parameters and unusual bond length. Graphics were taken from [150].

Both approaches definitely show the crystal content, but finer details of the structures cannot be discussed. In the case of $\text{Cp}^*\text{Na}(\text{NH}_3)_3 \cdot (\text{HN}(\text{SiMe}_3)_2)_{0.4}$ (**9**), the presence of piano chair CIPs is obvious, but bending angles or hydrogen bonding cannot be discussed accurately. In the case of $[\text{Li}(\text{NH}_3)_{4/6}][\text{Flu}]$ (**11**) the presence of SSIPs is obvious, including $\text{Li}(\text{NH}_3)_6^+$ - and $\text{Li}(\text{NH}_3)_4^+$ -cations.

Table 17 presents some crystallographic data regarding both approaches. Whereas **9** as a commensurate modulated structure performs well in both approaches with $R_1 = 4.36\%$ (basic cell) and $R_1 = 5.33\%$ (supercell), the incommensurate modulated structure **11** (estimated q-vector: 0.8; 0; -0.4) performs poorly in both approaches with $R_1 = 15.55\%$ (basic cell) and $R_1 = 45.08\%$ (supercell). In all cases but the supercell approach

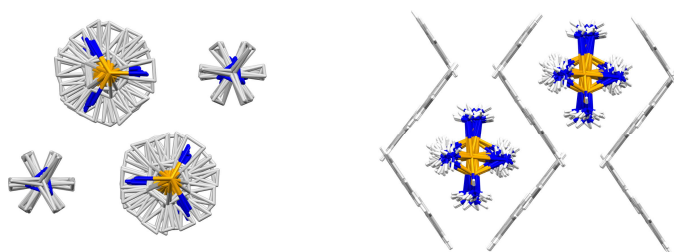


Figure 147: Modulation along the strings of $\text{Cp}^*\text{Na}(\text{NH}_3)_3$ in **9** and along the fluorenyl channels in **11**.

satellite reflections basically ignores the modulation and the periodical displacement of the atoms. The periodical displacement is averaged, resulting in large ADPs and likely to unrealistic bond lengths and angles (Figure 146). However, determination of the cell content is possible and can be further used for a subsequent refinement that involves the description of the modulation.

In the supercell approach all reflections are taken as main reflections, resulting in a much larger unit cell. The large amount of atoms and molecules within that unit cell

reflect the different positions of that atoms and molecules due to modulation. Missing and weak satellite reflections lead to a low data to parameter ratio and an unstable refinement.

Both approaches definitely show the crystal content, but finer details of the structures cannot be discussed. In the case of $\text{Cp}^*\text{Na}(\text{NH}_3)_3 \cdot (\text{HN}(\text{SiMe}_3)_2)_{0.4}$ (**9**), the presence of piano chair CIPs is obvious, but bending angles or hydrogen bonding cannot be discussed accurately.

In all cases but the supercell approach of **11**, the data to parameter ratio is way under the desired 10:1 ratio. The better ratio in the supercell approach of **11** surely does not help in the refinement.

Crystal Structure Determination
Treatment of the Modulated Structures 9 and 11

Generally, the whole structure is affected by modulation, not just parts of it (Figure 147). In **9** the modulation occurs mainly along the c-axis, which is the direction of the Cp*Na(NH₃)₃-strands. The modulation mainly affects the orientation of the CIPs perpendicular to the direction of the strands. In the case of **11**, modulation takes place long the direction of the fluorenyl channels. The fluorenyl anions are much less affected by modulation an unproblematic to refine. The Na(NH₃)₆⁺ and Na(NH₃)₄-cations however are very difficult to refine and seem to occupy a continuum.

Table 17: Selected crystallographic information of Cp*(Na(NH₃)₃·(HNSiMe₃)₂)_{0.4} (**9**) and [Li(NH₃)_{4/6}][Flu] (**11**) in the basic cell approach and the supercell approach.

| | Cp*Na(NH ₃) ₃ ·(HN(SiMe ₃) ₂) _{0.4} (9) | [Li(NH ₃) _{4/6}][flu] (11) |
|--|--|---|
| basic cell | | |
| <i>a</i> | 12.337(2) | 22.184(2) |
| <i>b</i> | 12.337(2) | 11.5435(6) |
| <i>c</i> | 7.0334(6) | 14.9147(8) |
| β | 90 | 121.225(2) |
| Crystal system | Trigonal | Monoclinic |
| space group | <i>P</i> $\bar{3}$ 1 <i>c</i> | <i>C</i> 2/ <i>c</i> |
| Z | 4 | 8 |
| Data/parameter/restraints | 340/196/485 | 2328/427/1421 |
| <i>R</i> ₁ (<i>I</i> > 2σ(<i>I</i>)) | 4.36% | 15.55% |
| <i>wR</i> ₂ (all data) | 12.42% | 49.67% |
| max. diff. peak/hole [e Å ⁻³] | 0.204/−0.328 | 2.013/−1048 |
| supercell | | |
| <i>a</i> | 21.362(2) | 11.537(2) |
| <i>b</i> | 21.362(2) | 14.370(3) |
| <i>c</i> | 35.160(2) | 53.057(7) |
| α | 90 | 91.008(9) |
| β | 90 | 90.205(6) |
| γ | 120 | 113.658(7) |
| Crystal system | trigonal | triclinic |
| space group | <i>P</i> 3 <i>c</i> 1 | <i>P</i> 1 |
| Z | 30 | 20 |
| Data/parameter/restraints | 9694/1688/13171 | 22104/1473/95168 |
| <i>R</i> ₁ (<i>I</i> > 2σ(<i>I</i>)) | 5.33% | 45.08% |
| <i>wR</i> ₂ (all data) | 16.27% | 80.02% |
| max. diff. peak/hole [e Å ⁻³] | 0.219/−0.206 | 2.719/−2.618 |

7.5. Treatment of the Twinned Structure CpK(NH₃)₂ (12)

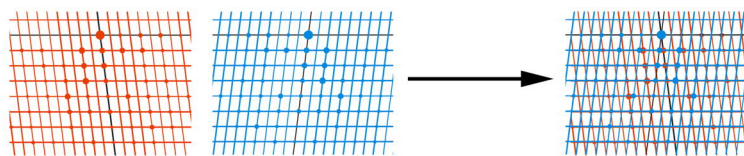


Figure 148: Exact overlap, partial overlap, and non overlap of the reflection in nonmerohedral twinning.

Twinning occurs when two or more crystal domains of the same species are joined together in a defined mutual orientation, expressed by the twin law.^[169] These domains can be visible under the microscope, but in many cases the twinned crystal appears homogeneous. The following case of CpK(NH₃)₂ (12) is a so-called non-merohedral twin in contrast to merohedral twins, reticular twins, or pseudo-merohedral twins. The twin operator in nonmerohedral twins is arbitrary, but often rotation around 180°. In non-merohedral twins the reflections show exact overlap, partial overlap, and non-overlap (Figure 148). For integration of non-merohedral with SAINT v.8.34a, the two or more domains have to be identified in reciprocal space plots.

Figure 149 depicts the three domains in the reciprocal space of compound 12. The crystal system is orthorhombic with cell edges of $a = 22.279(5)$ Å, $b = 10.843(3)$ Å, and $c = 6.381(2)$ Å. The major domain is depicted in grey with a share of 53%, the second largest domain is depicted in green with a share of 41%, and a minor domain depicted in red

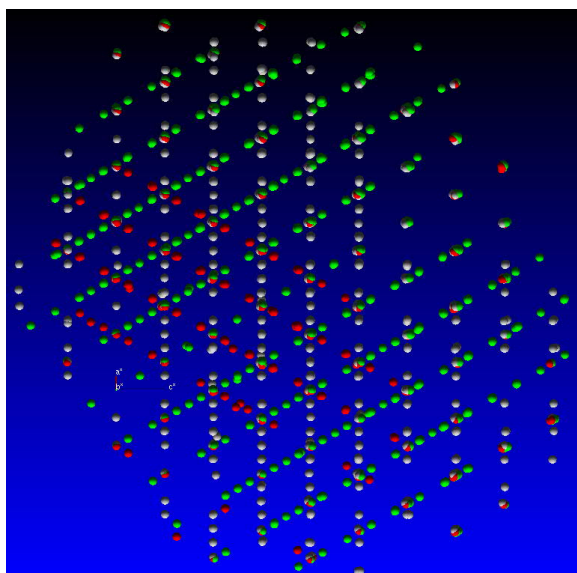


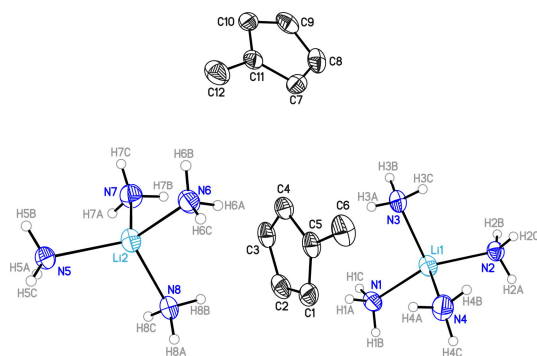
Figure 149: Three domains in the twinned crystal of CpK(NH₃)₂ (12) in the reciprocal space. The largest domain is depicted in grey, the second largest in green, and the third in red.

with a share of 6%. The integration of all three domains proved to be difficult. The different domains of non-merohedral twins are integrated by SAINT v.7.68. The R_{int} -value is relatively poor for the integration of all three fractions with values between 9–11% ($I > 3\sigma$). Refinement of the structures results in R_1 -values around 5.6% and high residual density peaks. Omitting the shallow third fraction of the integration resulted in a better R_{int} -value of 5.66% ($I > 3\sigma$), but the ignored third fraction negatively affected the refinement and resulted in only marginal improvement of the R_1 -value.

In order to deal with the problems of including and omitting the third fraction, an approach has been undertaken to profit from the beneficial integration of the two major domains and to assign the composite reflection later on additionally to the third domain in the *hkl*-file. The two major domains were integrated together in SAINT v.8.34a and scaled and corrected for absorption in TWINABS 2012/1. A detwinned *hkl*-file was created for initial structure solution and refinement. For a more accurate refinement using the twin-data, an *hkl*-file with the information of the twin components was created. The twin laws of the two twin fractions result only in exact and non-overlap. A third domain was additionally assigned to the overlapping reflections in the *hkl*-file according to the twin laws. The contributions of each domain were determined using badge scale factors (BASF) in ShelXL and are mentioned above. The twin-refinement resulted in an improved R_1 -value of 3.52%, a significant improvement towards the previously mentioned approaches with R_1 -values around 5.6%.

7.6. Lithium Ammoniacates

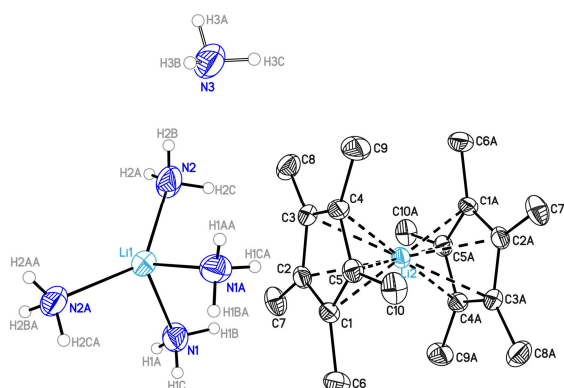
7.6.1. $[Li(NH_3)_4][Cp']$ (3)



Graphical representation of the structural motif. Non-ammonia hydrogen atoms have been omitted.

| | | | |
|---------------------------------------|--|--|------------------|
| Structure code | twin5t | Z | 4 |
| Empirical formula | C ₆ H ₁₉ N ₄ Li | Crystal dimensions [mm ³] | 0.2 x 0.15 x 0.1 |
| Formula weight [g mol ⁻¹] | 154.19 | $\rho_{\text{calcd.}}$ [g cm ⁻³] | 0.976 |
| Sample temperature [K] | 100 (2) | μ [mm ⁻¹] | 0.062 |
| Wavelength [Å] | 0.71073 | $F(000)$ | 344 |
| Crystal system | Triclinic | θ range [°] | 1.564 – 25.361 |
| Space group | $P\bar{1}$ | Reflections collected | 10891 |
| Unit cell dimensions [Å] | | Unique reflections | 3789 |
| | a = 6.961(2) | R_{int} | 0.0206 |
| | b = 11.596(2) | Completeness to θ_{max} | 98.4 % |
| | c = 13.322(3) | restraints/parameters | 552/274 |
| | $\alpha = 94.82(2)^\circ$ | GooF | 1.062 |
| | $\beta = 100.95(3)^\circ$ | R_1 ($I > 2\sigma(I)$) | 0.0359 |
| | $\gamma = 92.76(2)^\circ$ | wR_2 (all data) | 0.0973 |
| Volume [Å ³] | 1049.9(4) | max. diff. peak/hole [e Å ⁻³] | 0.758/–0.663 |
| Extinction coefficient | - | Absolute structure parameter | - |

7.6.2. $[Li(NH_3)_4][Cp^*Li] \cdot (NH_3)_{0.87}$ (4)



Graphical representation of the structural motif. Non-ammonia hydrogen atoms have been omitted. Non-hydrogen atoms labeled with the letter A are symmetry generated. The lattice ammonia molecule has a reduced occupation of 86.7(6)%. The ammonia molecule containing N2 is disordered on two sites by 50(2)%. All hydrogen atoms of the methyl groups are disordered.

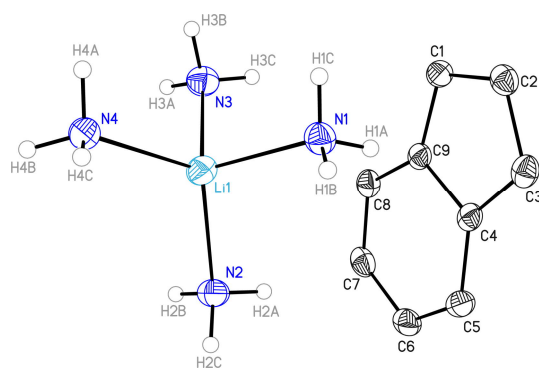
The hydrogen atoms of all ammonia molecules show is symmetry site disorder along a mirror plane.

| | | | |
|---------------------------------------|-------------------------------|---|------------------|
| Structure code | pccn | Z | 4 |
| Empirical formula | $C_{20}H_{44.55}N_{4.85}Li_2$ | Crystal dimensions [mm^3] | 0.1 x 0.1 x 0.03 |
| Formula weight [$g\ mol^{-1}$] | 366.97 | $\rho_{\text{calcd.}}$ [$g\ cm^{-3}$] | 1.973 |
| Sample temperature [K] | 100 (2) | μ [mm^{-1}] | 0.057 |
| Wavelength [\AA] | 0.71073 | $F(000)$ | 818 |
| Crystal system | Orthorhombic | θ range [$^\circ$] | 2.317 – 30.522 |
| Space group | <i>Pccn</i> | Reflections collected | 47481 |
| Unit cell dimensions [\AA] | | Unique reflections | 3836 |
| | a = 8.769(2) | R_{int} | 0.0254 |
| | b = 16.256(2) | Completeness to θ_{max} | 99.9 % |
| | c = 17.578(3) | restraints/parameters | 78/176 |
| | | GooF | 1.059 |
| | | R_1 ($I > 2\sigma(I)$) | 0.0458 |
| | | wR_2 (all data) | 0.1443 |
| Volume [\AA^3] | 2505.7(8) | max. diff. peak/hole [$e\ \text{\AA}^{-3}$] | 0.382/−0.168 |
| Extinction coefficient | - | Absolute structure parameter | - |

Crystal Structure Determination

Lithium Ammoniacates

7.6.3. $[\text{Li}(\text{NH}_3)_4][\text{Ind}]$ (5)



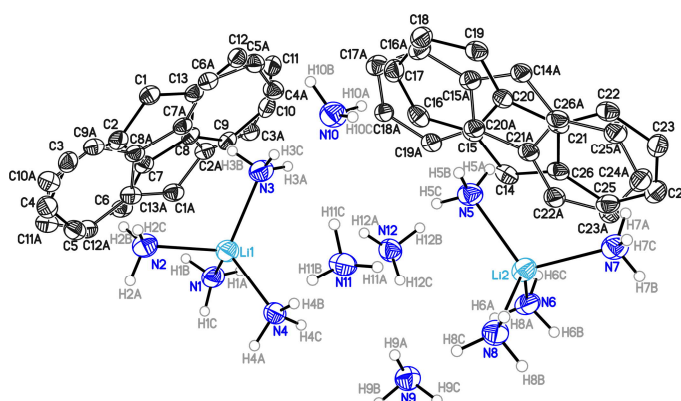
Graphical representation of the structural motif. Non-ammonia hydrogen atoms have been omitted.

This structure has been published in:

R. Michel, T. Nack, R. Neufeld, J. M. Dieterich, R. A. Mata, D. Stalke, *Angew. Chem. Ind. Ed.* **2013**, 52, 734-738.

| | | | |
|--|--|---|------------------|
| Structure code | sad | Z | 4 |
| Empirical formula | $\text{C}_9\text{H}_{19}\text{N}_4\text{Li}$ | Crystal dimensions [mm^3] | 0.15 x 0.1 x 0.1 |
| Formula weight [g mol^{-1}] | 190.22 | $\rho_{\text{calcd.}}$ [g cm^{-3}] | 1.078 |
| Sample temperature [K] | 100 (2) | μ [mm^{-1}] | 0.067 |
| Wavelength [\AA] | 0.71073 | $F(000)$ | 416 |
| Crystal system | Orthorhombic | θ range [$^\circ$] | 2.50 – 34.35 |
| Space group | $P2_12_12_1$ | Reflections collected | 20621 |
| Unit cell dimensions [\AA] | | Unique reflections | 4836 |
| | a = 8.492(4) | R_{int} | 0.0238 |
| | b = 10.262(3) | Completeness to θ_{max} | 99.1 % |
| | c = 13.445(6) | restraints/parameters | 132/167 |
| | | GooF | 1.082 |
| | | R_1 ($I > 2\sigma(I)$) | 0.0344 |
| | | w R_2 (all data) | 0.0917 |
| Volume [\AA^3] | 1171.7(8) | max. diff. peak/hole [e \AA^{-3}] | 0.327/–0.153 |
| Extinction coefficient | - | Absolute structure parameter | 0.3(11) |

7.6.4. $[Li(NH_3)][Flu] \cdot (NH_3)_2$ (6)

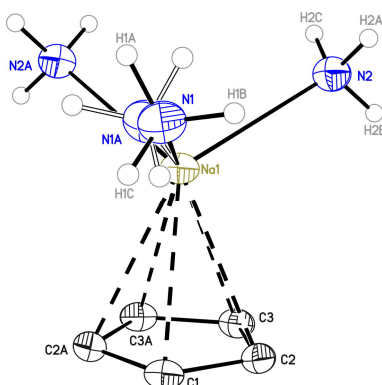


Graphical representation of the structural motif. Non-ammonia hydrogen atoms have been omitted. The fluorenyl anion C1-C13 is disordered by 3(4)% and the fluorenyl anion C14-C26 is disordered by 7(3)%.

| | | | |
|---------------------------------------|---------------------------|--|-----------------|
| Structure code | pn | Z | 4 |
| Empirical formula | $C_{13}H_{27}N_6Li$ | Crystal dimensions [mm ³] | 0.1 x 0.1 x 0.1 |
| Formula weight [g mol ⁻¹] | 274.34 | $\rho_{\text{calcd.}}$ [g cm ⁻³] | 1.089 |
| Sample temperature [K] | 100 (2) | μ [mm ⁻¹] | 0.044 |
| Wavelength [Å] | 0.56086 | $F(000)$ | 600 |
| Crystal system | Monoclinic | θ range [°] | 1.639 – 19.537 |
| Space group | Pn | Reflections collected | 29533 |
| Unit cell dimensions [Å] | | Unique reflections | 5840 |
| | a = 15.812(2) | R_{int} | 0.0451 |
| | b = 6.358(2) | Completeness to θ_{max} | 97.9 % |
| | c = 17.464(3) | restraints/parameters | 5056/675 |
| | $\beta = 1674.0(7)^\circ$ | Goof | 1.060 |
| | | R_1 ($I > 2\sigma(I)$) | 0.0335 |
| Volume [Å ³] | 1674.0(7) | w R_2 (all data) | 0.0777 |
| Extinction coefficient | - | max. diff. peak/hole [e Å ⁻³] | 0.147/-0.118 |
| | | Absolute structure parameter | -1.8(10) |

7.7. Sodium Ammoniacates

7.7.1. $CpNa(NH_3)_3$ (7)



Graphical representation of the whole molecule. Non-ammonia hydrogen atoms have been omitted. Non-hydrogen atoms labeled with the letter A are symmetry generated. The ammonia molecule of N1 shows symmetry site disorder along a mirror plane.

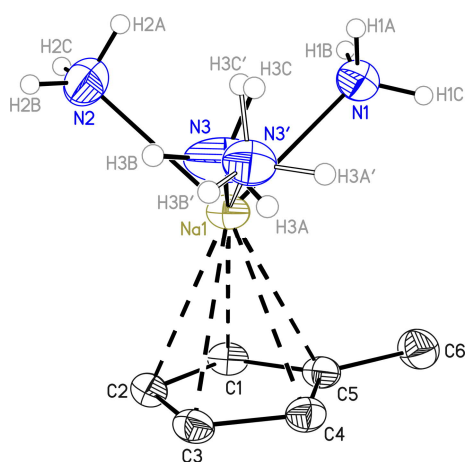
Published in:

J. Hey, D. M. Andrada, R. Michel, R. A. Mata, D. Stalke, *Angew. Chem. Int. Ed.* **2013**, 52, 10365-10369

(In the publication a high resolution experiment has been done to get access to charge density studies, therefore crystallographic information differ to this work)

| | | | |
|---------------------------------------|--|--|-----------------|
| Structure code | pnma | Z | 4 |
| Empirical formula | C ₅ H ₁₄ N ₃ Na | Crystal dimensions [mm ³] | 0.1 x 0.1 x 0.1 |
| Formula weight [g mol ⁻¹] | 139.18 | $\rho_{\text{calcd.}}$ [g cm ⁻³] | 1.075 |
| Sample temperature [K] | 100 (2) | μ [mm ⁻¹] | 0.112 |
| Wavelength [Å] | 0.71073 | F(000) | 304 |
| Crystal system | Orthorhombic | θ range [°] | 3.340 – 30.503 |
| Space group | <i>Pnma</i> | Reflections collected | 15239 |
| Unit cell dimensions [Å] | | Unique reflections | 1359 |
| | a = 11.685(3) | R _{int} | 0.0245 |
| | b = 10.295(2) | Completeness to θ_{max} | 100.0 % |
| | c = 7.151(2) | restraints/parameters | 75/67 |
| | | GooF | 1.141 |
| | | R ₁ (I > 2 σ (I)) | 0.0316 |
| | | wR ₂ (all data) | 0.0908 |
| Volume [Å ³] | 860.3(4) | max. diff. peak/hole [e Å ⁻³] | 0.363/−0.123 |
| Extinction coefficient | - | Absolute structure parameter | - |

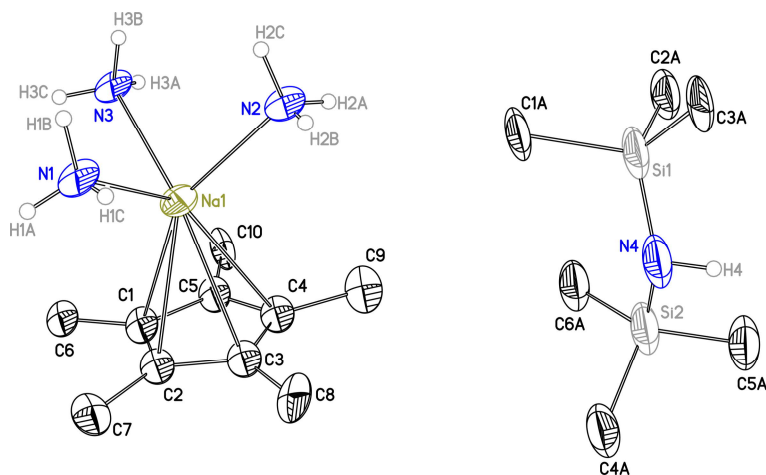
7.7.2. *Cp*'Na(NH₃)₃ (**8**)



Graphical representation of the structural motif. Non-ammonia hydrogen atoms have been omitted. The ammonia molecule containing N3 is disordered by 40(2)%.

| | | | |
|---------------------------------------|--|---|-------------------|
| Structure code | twin5t | Z | 4 |
| Empirical formula | C ₆ H ₁₉ N ₄ Na | Crystal dimensions [mm ³] | 0.2 x 0.15 x 0.02 |
| Formula weight [g mol ⁻¹] | 153.21 | $\rho_{\text{calcd.}}$ [g cm ⁻³] | 1.060 |
| Sample temperature [K] | 100 (2) | μ [mm ⁻¹] | 0.106 |
| Wavelength [Å] | 0.71073 | <i>F</i> (000) | 168 |
| Crystal system | Triclinic | θ range [°] | 1.773 – 28.302 |
| Space group | <i>P</i> $\bar{1}$ | Reflections collected | 13867 |
| Unit cell dimensions [Å] | | Unique reflections | 2381 |
| | a = 6.199(2) | <i>R</i> _{int} | 0.0556 |
| | b = 7.162(2) | Completeness to θ_{max} | 99.9 % |
| | c = 11.647(3) | restraints/parameters | 133/138 |
| | α = 82.60(3)° | GooF | 1.067 |
| | β = 81.91(2)° | <i>R</i> ₁ (<i>I</i> > 2 σ (<i>I</i>)) | 0.0417 |
| | γ = 70.20(2)° | w <i>R</i> ₂ (all data) | 0.1197 |
| Volume [Å ³] | 479.8(2) | max. diff. peak/hole [e Å ⁻³] | 0.318/–0.318 |
| Extinction coefficient | - | Absolute structure parameter | - |

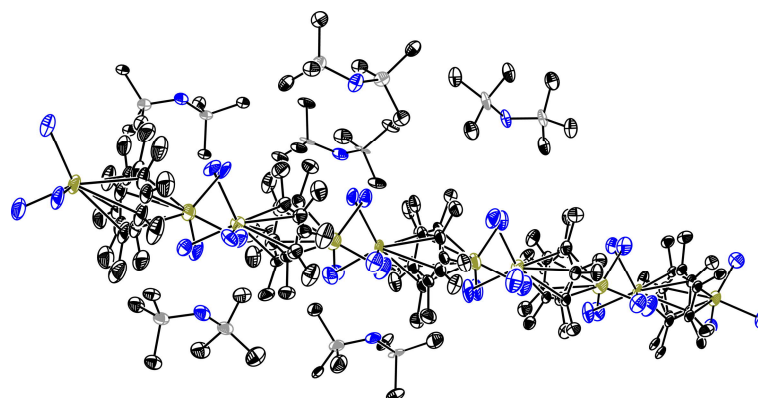
7.7.3. $Cp^*Na(NH_3)_3 \cdot (HN(SiMe_3)_2)_{0.4}$ (9) (Basic Cell)



Graphical representation of the structural motif. C-bonded hydrogen atoms have been omitted. $Cp^*Na(NH_3)_3$ and $HN(SiMe_3)_2$ are disordered by symmetry, which involves a threefold and three perpendicular twofold axis.

| | | | |
|---------------------------------------|-------------------------------------|--|------------------|
| Structure code | twin5t | Z | 4 |
| Empirical formula | $C_{12.4}H_{31.6}N_{3.4}NaSi_{0.8}$ | Crystal dimensions [mm ³] | 0.2 x 0.1 x 0.02 |
| Formula weight [g mol ⁻¹] | 273.87 | $\rho_{\text{calcd.}}$ [g cm ⁻³] | 1.962 |
| Sample temperature [K] | 100 (2) | μ [mm ⁻¹] | 0.145 |
| Wavelength [Å] | 0.56086 | $F(000)$ | 608 |
| Crystal system | Trigonal | θ range [°] | 1.504 – 16.415 |
| Space group | $P\bar{3}1c$ | Reflections collected | 3055 |
| Unit cell dimensions [Å] | | Unique reflections | 304 |
| | a = 12.337(2) | R_{int} | 0.0249 |
| | b = 12.337(2) | Completeness to θ_{max} | 60.0 % |
| | c = 7.033(2) | restraints/parameters | 485/196 |
| | | GooF | 1.110 |
| | | R_1 ($I > 2\sigma(I)$) | 0.0436 |
| Volume [Å ³] | 927.1(2) | w R_2 (all data) | 0.1290 |
| Extinction coefficient | - | max. diff. peak/hole [e Å ⁻³] | 0.206/−0.328 |
| | | Absolute structure parameter | - |

7.7.4. $Cp^*Na(NH_3)_3 \cdot (HN(SiMe_3)_2)_{0.4}$ (9) (Supercell)



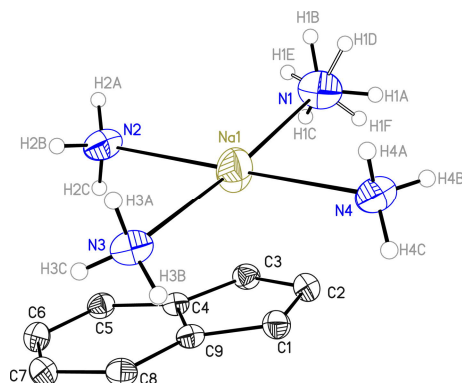
Graphical representation of the structural motif. Hydrogen atoms have been omitted. Each $Cp^*Na(NH_3)_3$ unit is disordered on two positions, which have been refined with fixed occupations of 50%. The $HN(SiMe_3)_2$ units are disordered by symmetry around a threefold axis.

| | | | |
|---------------------------------------|-------------------------------------|--|-----------------|
| Structure code | rh_b_neu | Z | 30 |
| Empirical formula | $C_{12.4}H_{31.6}N_{3.4}NaSi_{0.8}$ | Crystal dimensions [mm ³] | 0.2 x 0.1 x 0.2 |
| Formula weight [g mol ⁻¹] | 273.87 | $\rho_{\text{calcd.}}$ [g cm ⁻³] | 0.982 |
| Sample temperature [K] | 100 (2) | μ [mm ⁻¹] | 0.073 |
| Wavelength [Å] | 0.56086 | $F(000)$ | 4560 |
| Crystal system | Trigonal | θ range [°] | 1.261 – 16.284 |
| Space group | $P31c$ | Reflections collected | 38268 |
| Unit cell dimensions [Å] | | Unique reflections | 9694 |
| | a = 21.362(2) | R_{int} | 0.0556 |
| | b = 21.362(2) | Completeness to θ_{max} | 57.8 % |
| | c = 35.160(2) | restraints/parameters | 13171/1688 |
| | | GooF | 1.056 |
| | | R_1 ($I > 2\sigma(I)$) | 0.0533 |
| | | w R_2 (all data) | 0.1627 |
| Volume [Å ³] | 13894.9(2) | max. diff. peak/hole [e Å ⁻³] | 0.219/–0.206 |
| Extinction coefficient | - | Absolute structure parameter | 0.4(5) |

Crystal Structure Determination

Sodium Ammoniacates

7.7.5. $[Na(NH_3)_4][Ind]$ (10)



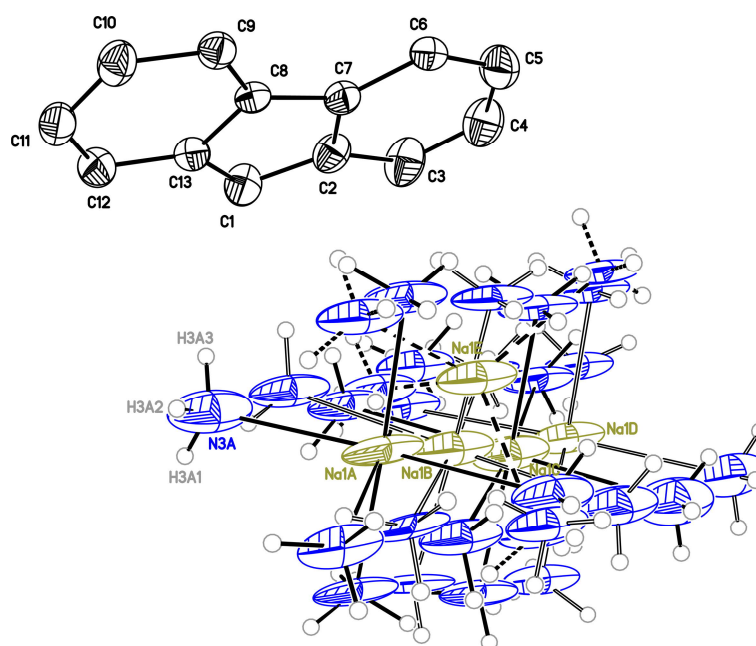
Graphical representation of the structural motif. Non-ammonia hydrogen atoms have been omitted. The hydrogen atoms of the ammonia molecule containing N1 are disordered by 36(4)%.

This structure has been published in:

R. Michel, T. Nack, R. Neufeld, J. M. Dieterich, R. A. Mata, D. Stalke, *Angew. Chem. Int. Ed.* **2013**, *52*, 734-738.

| | | | |
|---------------------------------------|---------------------------|---|------------------|
| Structure code | twin4 | Z | 2 |
| Empirical formula | $C_9H_{19}N_4Na$ | Crystal dimensions [mm^3] | 0.2 x 0.1 x 0.01 |
| Formula weight [$g\ mol^{-1}$] | 206.27 | $\rho_{calcd.}$ [$g\ cm^{-3}$] | 1.124 |
| Sample temperature [K] | 100 (2) | μ [mm^{-1}] | 0.102 |
| Wavelength [\AA] | 0.71073 | $F(000)$ | 224 |
| Crystal system | Monoclinic | θ range [$^\circ$] | 2.83 – 30.05 |
| Space group | $P2_1$ | Reflections collected | 29185 |
| Unit cell dimensions [\AA] | | Unique reflections | 1858 |
| | a = 6.865(2) | R_{int} | 0.0353 |
| | b = 14.391(3) | Completeness to θ_{max} | 100.0 % |
| | c = 6.966(2) | restraints/parameters | 211/177 |
| | $\beta = 117.70(2)^\circ$ | GooF | 1.072 |
| | | R_1 ($I > 2\sigma(I)$) | 0.0298 |
| | | w R_2 (all data) | 0.0827 |
| Volume [\AA^3] | 609.3(3) | max. diff. peak/hole [$e\ \text{\AA}^{-3}$] | 0.313/–0.158 |
| Extinction coefficient | - | Absolute structure parameter | 0.2(3) |

7.7.6. $[Na(NH_3)_{4/6}][Flu]$ (11) (Basic Cell)



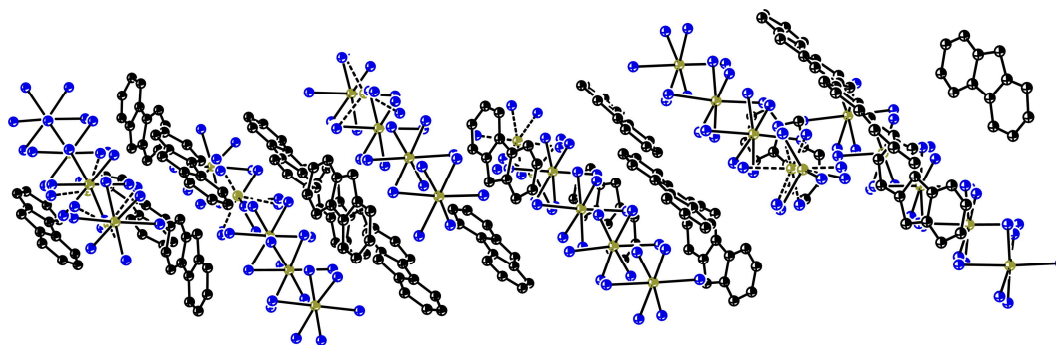
Graphical representation of the structural motif. Non-ammonia hydrogen atoms have been omitted. The ammonia molecule containing N3 is disordered by 40(2)%. The $Na(NH_3)_6^+$ -complexes (in the order A-D) have occupations of 22.1(6)%, 25.7(6)%, 20.9(7)%, and 5.0(6)%. The $Na(NH_3)_4^+$ -complex has an occupation of 16.2(5)%.

| | | | |
|---------------------------------------|---------------------------|---|-----------------|
| Structure code | c2c | Z | 30 |
| Empirical formula | $C_{13}H_{23.6}N_{5.7}Na$ | Crystal dimensions [mm^3] | 0.2 x 0.2 x 0.3 |
| Formula weight [$g\ mol^{-1}$] | 282.84 | $\rho_{calcd.}$ [$g\ cm^{-3}$] | 1.150 |
| Sample temperature [K] | 100 (2) | μ [mm^{-1}] | 0.096 |
| Wavelength [\AA] | 0.71073 | $F(000)$ | 1220 |
| Crystal system | Monoclinic | θ range [$^\circ$] | 2.065 – 23.293 |
| Space group | $C2/c$ | Reflections collected | 15194 |
| Unit cell dimensions [\AA] | | Unique reflections | 2328 |
| | a = 22.184(2) | R_{int} | 0.0276 |
| | b = 11.544(2) | Completeness to θ_{max} | 79.1 % |
| | c = 14.915(2) | restraints/parameters | 1427/427 |
| | β = 121.23(2) | GooF | 2.814 |
| | | R_1 ($I > 2\sigma(I)$) | 0.1532 |
| | | w R_2 (all data) | 0.4992 |
| Volume [\AA^3] | 3266.1(3) | max. diff. peak/hole [$e\ \text{\AA}^{-3}$] | 1.953/–1.046 |
| Extinction coefficient | - | Absolute structure parameter | - |

Crystal Structure Determination

Sodium Ammoniacates

7.7.7. $[Na(NH_3)_{4/6}][Flu]$ (11) (Supercell)

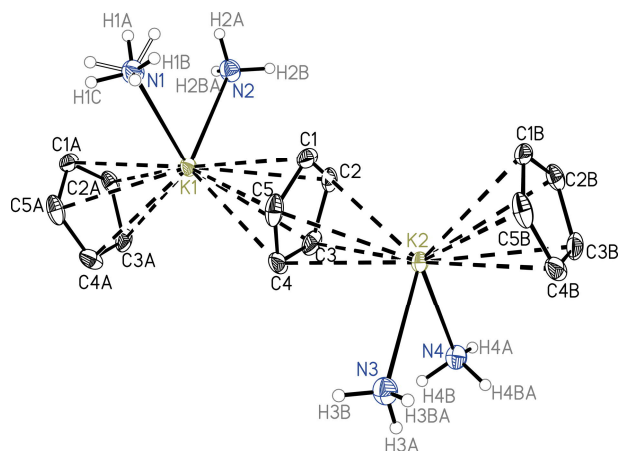


Graphical representation of the structural motif. Hydrogen atoms have been omitted.

| | | | |
|---------------------------------------|---------------------------|--|-----------------|
| Structure code | p1_test | Z | 20 |
| Empirical formula | $C_{13}H_{26.2}N_{5.7}Na$ | Crystal dimensions [mm ³] | 0.2 x 0.2 x 0.3 |
| Formula weight [g mol ⁻¹] | 285.87 | $\rho_{\text{calcd.}}$ [g cm ⁻³] | 1.178 |
| Sample temperature [K] | 100 (2) | μ [mm ⁻¹] | 0.098 |
| Wavelength [Å] | 0.71073 | $F(000)$ | 3106 |
| Crystal system | Triclinic | θ range [°] | 1.152 – 23.257 |
| Space group | <i>P</i> 1 | Reflections collected | 66977 |
| Unit cell dimensions [Å] | | Unique reflections | 40352 |
| | $a = 11.537(2)$ | R_{int} | 0.0756 |
| | $b = 14.370(3)$ | Completeness to θ_{max} | 75.9 % |
| | $c = 53.057(7)$ | restraints/parameters | 27466/1472 |
| | $\alpha = 91.008(9)$ | Goof | 2.059 |
| | $\beta = 90.205(6)$ | R_1 ($I > 2\sigma(I)$) | 0.2849 |
| | $\gamma = 113.658(7)$ | wR_2 (all data) | 0.6315 |
| Volume [Å ³] | 8055(2) | max. diff. peak/hole [e Å ⁻³] | 2.764/–3.063 |
| Extinction coefficient | - | Absolute structure parameter | not determined |

7.8. Potassium Ammoniacates

7.8.1. $CpK(NH_3)_2$ (**12**)



Graphical representation of the structural motif. Non-ammonia hydrogen atoms have been omitted. Non-hydrogen atoms labeled with the letter A and B are symmetry generated. The hydrogen atoms of the ammonia molecule containing N1 are symmetry site disordered.

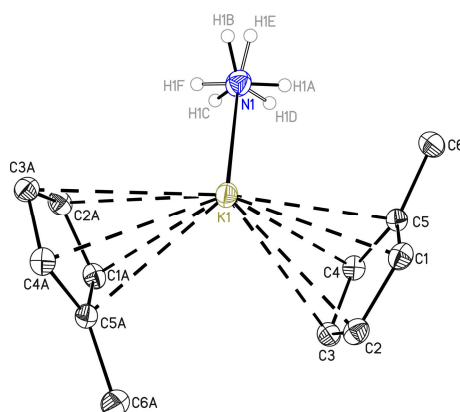
The crystal is a threefold twin. The treatment of the dataset is described in section 0.

| | | | |
|---------------------------------------|-----------------|---|-----------------|
| Structure code | twin5t | Z | 8 |
| Empirical formula | $C_5H_{11}N_2K$ | Crystal dimensions [mm^3] | 0.1 x 0.1 x 0.1 |
| Formula weight [$g\ mol^{-1}$] | 138.26 | $\rho_{calcd.}$ [$g\ cm^{-3}$] | 1.192 |
| Sample temperature [K] | 100 (2) | μ [mm^{-1}] | 0.311 |
| Wavelength [\AA] | 0.56086 | $F(000)$ | 592 |
| Crystal system | Orthorhombic | θ range [°] | 1.443 – 20.656 |
| Space group | <i>Pnma</i> | Reflections collected | 68914 |
| Unit cell dimensions [\AA] | | Unique reflections | 3296 |
| | a = 22.279(5) | R_{int} | 0.0612 |
| | b = 10.843(3) | Completeness to θ_{max} | 100.0 % |
| | c = 6.381(2) | restraints/parameters | 132/120 |
| | | GooF | 1.146 |
| | | R_1 ($I > 2\sigma(I)$) | 0.0354 |
| | | wR_2 (all data) | 0.1027 |
| Volume [\AA^3] | 1541.3(7) | max. diff. peak/hole [$e\ \text{\AA}^{-3}$] | 0.368/−0.217 |
| Extinction coefficient | - | Absolute structure parameter | - |

Crystal Structure Determination

Potassium Ammoniacates

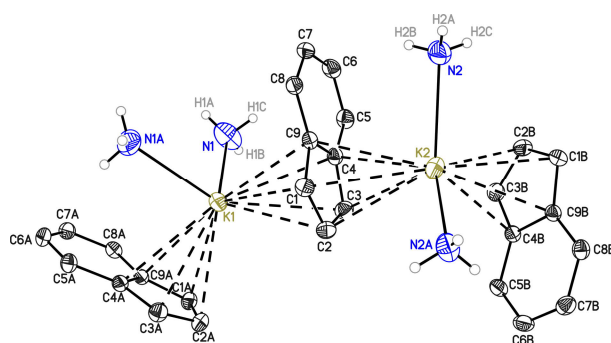
7.8.2. *Cp*'K(NH₃) (13)



Graphical representation of the structural motif. Non-ammonia hydrogen atoms have been omitted. Non-hydrogen atoms labeled with the letter A are symmetry generated. The hydrogen atoms of the ammonia molecule are disordered by 49(5)%. The hydrogen atoms (hidden) of the methyl are disordered by 29(11)%.

| | | | |
|---------------------------------------|------------------------------------|---|------------------|
| Structure code | p21c | Z | 4 |
| Empirical formula | C ₆ H ₁₀ NK | Crystal dimensions [mm ³] | 0.1 x 0.1 x 0.03 |
| Formula weight [g mol ⁻¹] | 135.25 | $\rho_{\text{calcd.}}$ [g cm ⁻³] | 1.247 |
| Sample temperature [K] | 100 (2) | μ [mm ⁻¹] | 0.636 |
| Wavelength [Å] | 0.71073 | <i>F</i> (000) | 288 |
| Crystal system | Monoclinic | θ range [°] | 12.741 – 35.001 |
| Space group | <i>P</i> 2 ₁ / <i>c</i> | Reflections collected | 19843 |
| Unit cell dimensions [Å] | | Unique reflections | 3159 |
| | <i>a</i> = 6.511(2) | <i>R</i> _{int} | 0.0342 |
| | <i>b</i> = 10.222(2) | Completeness to θ_{max} | 100.0 % |
| | <i>c</i> = 10.877(3) | restraints/parameters | 30/95 |
| | β = 95.74(2)° | Goof | 1.046 |
| | | <i>R</i> ₁ (<i>I</i> > 2 σ (<i>I</i>)) | 0.0259 |
| | | <i>wR</i> ₂ (all data) | 0.0677 |
| Volume [Å ³] | 720.3(3) | max. diff. peak/hole [e Å ⁻³] | 0.490/–0.297 |
| Extinction coefficient | 0.012(2) | Absolute structure parameter | - |

7.8.3. *(Ind)K(NH₃)₂* (14)



Graphical representation of the structural motif. Non-ammonia hydrogen atoms have been omitted.

This structure has been published in:

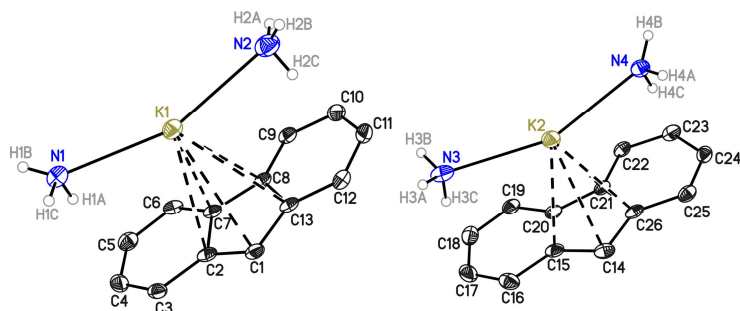
R. Michel, T. Nack, R. Neufeld, J. M. Dieterich, R. A. Mata, D. Stalke, *Angew. Chem. Int. Ed.* **2013**, *52*, 734-738.

| | | | |
|---------------------------------------|---|--|-----------------|
| Structure code | fddd | Z | 32 |
| Empirical formula | C ₉ H ₁₃ N ₂ K | Crystal dimensions [mm ³] | 0.1 x 0.1 x 0.1 |
| Formula weight [g mol ⁻¹] | 188.31 | $\rho_{\text{calcd.}}$ [g cm ⁻³] | 1.195 |
| Sample temperature [K] | 100 (2) | μ [mm ⁻¹] | 0.459 |
| Wavelength [Å] | 0.71073 | F(000) | 3200 |
| Crystal system | Orthorhombic | θ range [°] | 1.759 – 30.510 |
| Space group | Fddd | Reflections collected | 38900 |
| Unit cell dimensions [Å] | | Unique reflections | 3201 |
| | a = 18.318(2) | R _{int} | 0.0451 |
| | b = 19.172(2) | Completeness to θ_{max} | 100.0 % |
| | c = 23.841(3) | restraints/parameters | 30/128 |
| | | GooF | 1.056 |
| | | R ₁ (I > 2 σ (I)) | 0.0317 |
| | | wR ₂ (all data) | 0.0794 |
| Volume [Å ³] | 8372.8(16) | max. diff. peak/hole [e Å ⁻³] | 0.413/-0.205 |
| Extinction coefficient | - | Absolute structure parameter | - |

Crystal Structure Determination

Potassium Ammoniacates

7.8.4. (Flu)K(NH₃)₂ (15)

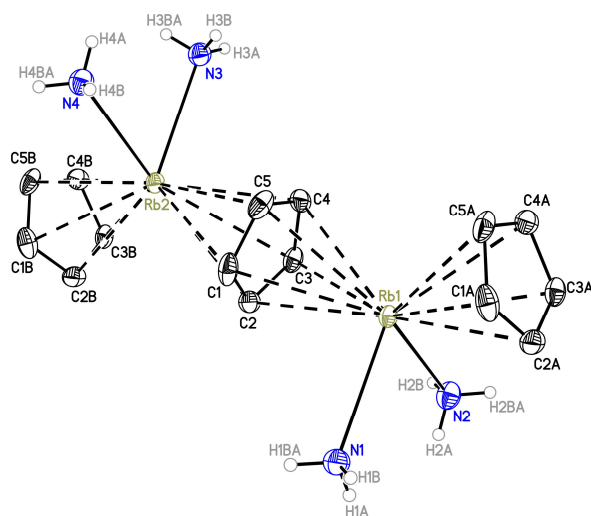


Graphical representation of the structural motif. Non-ammonia hydrogen atoms have been omitted.

| | | | |
|---------------------------------------|--|---|-----------------------|
| Structure code | p21c | Z | 8 |
| Empirical formula | C ₁₃ H ₁₅ N ₂ K | Crystal dimensions [mm ³] | 1.193 x 0.693 x 0.066 |
| Formula weight [g mol ⁻¹] | 238.37 | $\rho_{\text{calcd.}}$ [g cm ⁻³] | 1.315 |
| Sample temperature [K] | 100 (2) | μ [mm ⁻¹] | 0.220 |
| Wavelength [Å] | 0.56086 | <i>F</i> (000) | 1008 |
| Crystal system | Monoclinic | θ range [°] | 1.670 – 20.556 |
| Space group | <i>P</i> 2 ₁ / <i>c</i> | Reflections collected | 57524 |
| Unit cell dimensions [Å] | | Unique reflections | 4943 |
| | <i>a</i> = 19.970(3) | <i>R</i> _{int} | 0.0705 |
| | <i>b</i> = 10.866(2) | Completeness to θ_{max} | 99.8 % |
| | <i>c</i> = 11.515(2) | restraints/parameters | 132/325 |
| | β = 2408.7(7)° | Goof | 1.136 |
| Volume [Å ³] | 1674.0(7) | <i>R</i> ₁ (<i>I</i> > 2 σ (<i>I</i>)) | 0.0521 |
| Extinction coefficient | - | <i>wR</i> ₂ (all data) | 0.1313 |
| | | max. diff. peak/hole [e Å ⁻³] | 0.425/−0.331 |
| | | Absolute structure parameter | - |

7.9. Rubidium Ammoniacates

7.9.1. $CpRb(NH_3)_2$ (16)



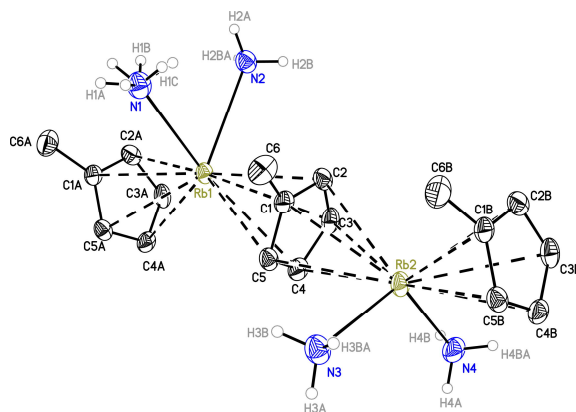
Graphical representation of the structural motif. Non-ammonia hydrogen atoms have been omitted. Non-hydrogen atoms labeled with the letter A and B are symmetry generated. Symmetry generated hydrogen atoms haven't been labeled. The hydrogen atoms of all ammonia molecules are symmetry site disordered.

| | | | |
|---------------------------------------|------------------|---|-----------------|
| Structure code | pnma | Z | 8 |
| Empirical formula | $C_5H_{11}N_2Rb$ | Crystal dimensions [mm^3] | 0.1 x 0.1 x 0.1 |
| Formula weight [$g\ mol^{-1}$] | 184.63 | $\rho_{calcd.}$ [$g\ cm^{-3}$] | 1.511 |
| Sample temperature [K] | 100 (2) | μ [mm^{-1}] | 3.247 |
| Wavelength [\AA] | 0.56086 | $F(000)$ | 736 |
| Crystal system | Orthorhombic | θ range [$^\circ$] | 1.424 – 27.759 |
| Space group | <i>Pnma</i> | Reflections collected | 70775 |
| Unit cell dimensions [\AA] | | Unique reflections | 3954 |
| | a = 22.570(6) | R_{int} | 0.0424 |
| | b = 11.234(3) | Completeness to θ_{max} | 100.0 % |
| | c = 6.400(2) | restraints/parameters | 132/118 |
| | | GooF | 1.146 |
| | | R_1 ($I > 2\sigma(I)$) | 0.0239 |
| | | wR_2 (all data) | 0.0484 |
| Volume [\AA^3] | 1622.9(8) | max. diff. peak/hole [$e\ \text{\AA}^{-3}$] | 0.518/–0.735 |
| Extinction coefficient | - | Absolute structure parameter | - |

Crystal Structure Determination

Rubidium Ammoniacates

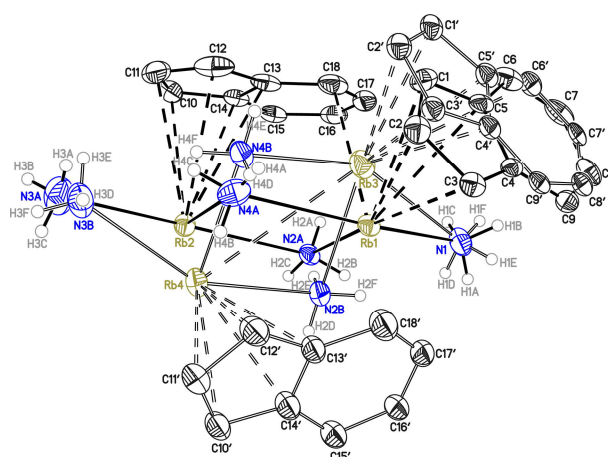
7.9.2. $Cp'Rb(NH_3)_2$ (17)



Graphical representation of the structural motif. Non-ammonia hydrogen atoms have been omitted. Non-hydrogen atoms labeled with the letter A and B are symmetry generated. Hydrogen atoms with four letters are symmetry generated as well. The hydrogen atoms of the ammonia molecules containing N1 are symmetry site disordered. The hidden hydrogen atoms of the methyl-group are disordered by 61(2)%.

| | | | |
|---------------------------------------|---------------------------|--|------------------|
| Structure code | p21m | Z | 4 |
| Empirical formula | $C_6H_{13}NRb$ | Crystal dimensions [mm ³] | 0.1 x 0.1 x 0.03 |
| Formula weight [g mol ⁻¹] | 198.65 | $\rho_{\text{calcd.}}$ [g cm ⁻³] | 1.477 |
| Sample temperature [K] | 100 (2) | μ [mm ⁻¹] | 5.469 |
| Wavelength [Å] | 0.71073 | $F(000)$ | 400 |
| Crystal system | Monoclinic | θ range [°] | 1.701 – 29.148 |
| Space group | $P2_1/m$ | Reflections collected | 50259 |
| Unit cell dimensions [Å] | | Unique reflections | 2508 |
| | a = 6.544(2) | R_{int} | 0.0381 |
| | b = 11.403(2) | Completeness to θ_{max} | 100.0 % |
| | c = 12.226(3) | restraints/parameters | 132/130 |
| | $\beta = 101.65(2)^\circ$ | GooF | 1.028 |
| | | R_1 ($I > 2\sigma(I)$) | 0.0191 |
| | | w R_2 (all data) | 0.0404 |
| Volume [Å ³] | 893.5(4) | max. diff. peak/hole [e Å ⁻³] | 0.333/–0.267 |
| Extinction coefficient | 0.009(3) | Absolute structure parameter | - |

7.9.3. (*Ind*)Rb(NH₃)₂ (**18**)



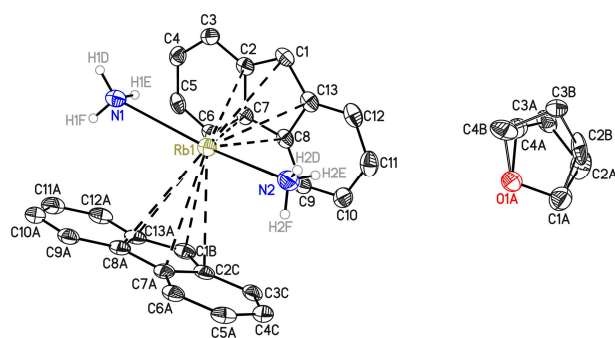
Graphical representation of the structural motif. Non-ammonia hydrogen atoms have been omitted. The whole Ind₂Rb₂(NH₃)₄ (containing Rb3, Rb4, NXB CXX') unit is disordered by 5.9(1)%. The atom N1 has not been included into the disorder refinement.

| | | | |
|---------------------------------------|--|--|-----------------|
| Structure code | p21c | Z | 8 |
| Empirical formula | C ₉ H ₁₃ N ₂ Rb | Crystal dimensions [mm ³] | 0.1 x 0.1 x 0.1 |
| Formula weight [g mol ⁻¹] | 234.68 | $\rho_{\text{calcd.}}$ [g cm ⁻³] | 1.509 |
| Sample temperature [K] | 100 (2) | μ [mm ⁻¹] | 4.743 |
| Wavelength [Å] | 0.71073 | $F(000)$ | 944 |
| Crystal system | Monoclinic | θ range [°] | 1.283 – 30.036 |
| Space group | $P2_1/c$ | Reflections collected | 60831 |
| Unit cell dimensions [Å] | | Unique reflections | 6035 |
| | a = 17.057(3) | R_{int} | 0.0553 |
| | b = 6.912(2) | Completeness to θ_{max} | 99.8 % |
| | c = 18.841(3) | restraints/parameters | 1895/498 |
| | β = 111.53(2)° | Goof | 1.194 |
| | | R_1 ($I > 2\sigma(I)$) | 0.0395 |
| | | w R_2 (all data) | 0.0828 |
| Volume [Å ³] | 2066.5(8) | max. diff. peak/hole [e Å ⁻³] | 0.728/–0.998 |
| Extinction coefficient | 0.00186(12) | Absolute structure parameter | - |

Crystal Structure Determination

Rubidium Ammoniacates

7.9.4. (Flu)Rb(NH₃)₂·THF (19)

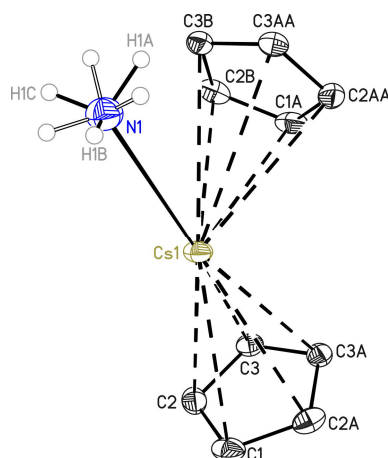


Graphical representation of the structural motif. Non-ammonia hydrogen atoms have been omitted. Fluorenyl atoms labeled with the letter A are symmetry generated. The THF-molecule is disordered by 18.0(6)%.

| | | | |
|---------------------------------------|--|--|-----------------|
| Structure code | p21c | Z | 8 |
| Empirical formula | C ₁₇ H ₂₃ N ₂ ORb | Crystal dimensions [mm ³] | 0.1 x 0.1 x 0.1 |
| Formula weight [g mol ⁻¹] | 356.84 | $\rho_{\text{calcd.}}$ [g cm ⁻³] | 1.397 |
| Sample temperature [K] | 100 (2) | μ [mm ⁻¹] | 2.919 |
| Wavelength [Å] | 0.71073 | $F(000)$ | 1472 |
| Crystal system | Orthorhombic | θ range [°] | 1.656 – 26.364 |
| Space group | <i>Pbca</i> | Reflections collected | 63166 |
| Unit cell dimensions [Å] | | Unique reflections | 3460 |
| | a = 11.136(2) | R_{int} | 0.0597 |
| | b = 12.386(3) | Completeness to θ_{max} | 99.9 % |
| | c = 24.599(5) | restraints/parameters | 239/236 |
| | | GooF | 1.254 |
| | | R_1 ($I > 2\sigma(I)$) | 0.0326 |
| | | w R_2 : (all data) | 0.0779 |
| Volume [Å ³] | 3393.0(12) | max. diff. peak/hole [e Å ⁻³] | 0.415/–0.387 |
| Extinction coefficient | - | Absolute structure parameter | - |

7.10. Caesium Ammoniacates

7.10.1. $CpCs(NH_3)$ (20)



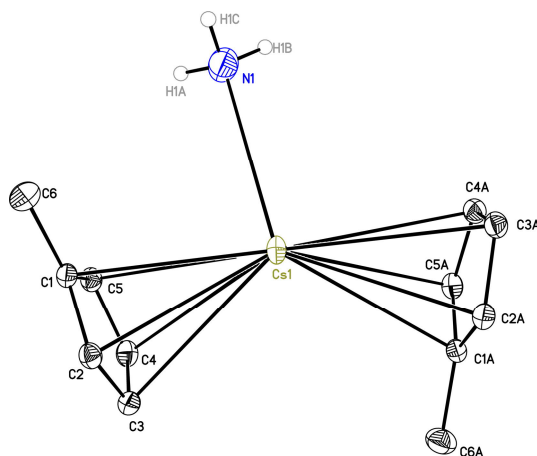
Graphical representation of the structural motif. Non-ammonia hydrogen atoms have been omitted. Non-hydrogen atoms labeled with the letter A are symmetry generated. The hydrogen atoms of the ammonia molecule are symmetry site disordered.

| | | | |
|---------------------------------------|---------------|---|-----------------|
| Structure code | pnma | Z | 4 |
| Empirical formula | C_5H_8NCs | Crystal dimensions [mm^3] | 2.1 x 0.2 x 0.2 |
| Formula weight [$g\ mol^{-1}$] | 215.03 | $\rho_{calcd.}$ [$g\ cm^{-3}$] | 1.192 |
| Sample temperature [K] | 100 (2) | μ [mm^{-1}] | 5.332 |
| Wavelength [\AA] | 0.71073 | $F(000)$ | 400 |
| Crystal system | Orthorhombic | θ range [$^\circ$] | 3.056 – 30.500 |
| Space group | <i>Pnma</i> | Reflections collected | 8023 |
| Unit cell dimensions [\AA] | | Unique reflections | 1086 |
| | a = 10.464(3) | R_{int} | 0.0454 |
| | b = 7.512(2) | Completeness to θ_{max} | 99.9 % |
| | c = 8.647(2) | restraints/parameters | 9/47 |
| | | GooF | 1.134 |
| | | R_1 ($I > 2\sigma(I)$) | 0.0180 |
| | | wR_2 (all data) | 0.0391 |
| Volume [\AA^3] | 679.8(3) | max. diff. peak/hole [$e\ \text{\AA}^{-3}$] | 0.758/−0.663 |
| Extinction coefficient | 0.0047(4) | Absolute structure parameter | - |

Crystal Structure Determination

Caesium Ammoniacates

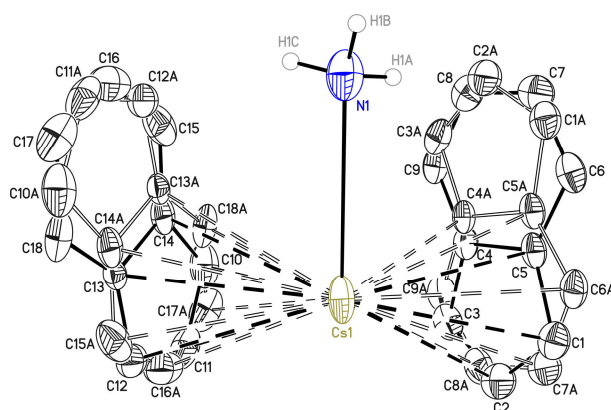
7.10.2. *Cp'Cs(NH₃) (21)*



Graphical representation of the structural motif. Non-ammonia hydrogen atoms have been omitted. Non-hydrogen atoms labeled with the letter A are symmetry generated.

| | | | |
|---------------------------------------|------------------------------------|---|-----------------|
| Structure code | pnma | Z | 4 |
| Empirical formula | C ₆ H ₁₀ NCs | Crystal dimensions [mm ³] | 1.0 x 0.2 x 0.2 |
| Formula weight [g mol ⁻¹] | 229.06 | $\rho_{\text{calcd.}}$ [g cm ⁻³] | 1.906 |
| Sample temperature [K] | 100 (2) | μ [mm ⁻¹] | 4.547 |
| Wavelength [Å] | 0.71073 | <i>F</i> (000) | 432 |
| Crystal system | Monoclinic | θ range [°] | 2.268 – 36.327 |
| Space group | <i>P</i> 2 ₁ / <i>c</i> | Reflections collected | 43787 |
| Unit cell dimensions [Å] | | Unique reflections | 3863 |
| | a = 9.370(3) | <i>R</i> _{int} | 0.0434 |
| | b = 7.480(2) | Completeness to θ_{max} | 99.9 % |
| | c = 11.885(2) | restraints/parameters | 6/85 |
| | β = 106.60(2) | GooF | 1.162 |
| | | <i>R</i> ₁ (<i>I</i> > 2 σ (<i>I</i>)) | 0.0150 |
| | | w <i>R</i> ₂ (all data) | 0.0358 |
| Volume [Å ³] | 798.3(3) | max. diff. peak/hole [e Å ⁻³] | 0.593/–0.637 |
| Extinction coefficient | - | Absolute structure parameter | - |

7.10.3. *(Ind)Cs(NH₃)* (22)



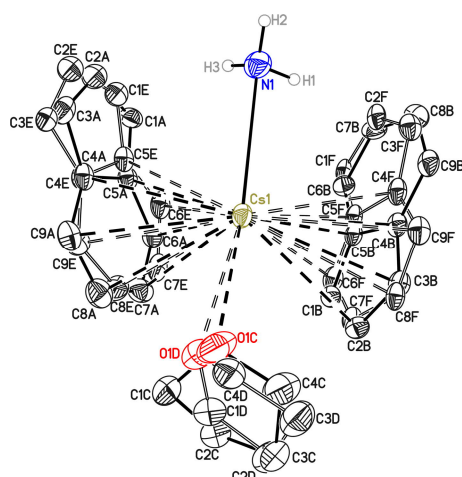
Graphical representation of the structural motif. Non-ammonia hydrogen atoms have been omitted. Non-hydrogen atoms labeled with the letter A are symmetry generated. Both indenyl anions are symmetry site disordered.

| | | | |
|---------------------------------------|------------------------------------|--|-----------------|
| Structure code | c2c | Z | 8 |
| Empirical formula | C ₉ H ₁₀ NCs | Crystal dimensions [mm ³] | 0.1 x 0.1 x 0.1 |
| Formula weight [g mol ⁻¹] | 265.09 | $\rho_{\text{calcd.}}$ [g cm ⁻³] | 1.913 |
| Sample temperature [K] | 100 (2) | μ [mm ⁻¹] | 2.101 |
| Wavelength [Å] | 0.56086 | F(000) | 1008 |
| Crystal system | Monoclinic | θ range [°] | 1.746 – 25.232 |
| Space group | C2/c | Reflections collected | 38946 |
| Unit cell dimensions [Å] | | Unique reflections | 3372 |
| | a = 14.523(3) | R _{int} | 0.0448 |
| | b = 6.883(2) | Completeness to θ_{max} | 100.0 % |
| | c = 19.381(3) | restraints/parameters | 761/190 |
| | β = 108.19(2)° | GooF | 1.091 |
| | | R ₁ (I > 2 σ (I)) | 0.0214 |
| | | wR ₂ (all data) | 0.0475 |
| Volume [Å ³] | 1840.6(7) | max. diff. peak/hole [e Å ⁻³] | 0.872/–2.157 |
| Extinction coefficient | - | Absolute structure parameter | - |

Crystal Structure Determination

Caesium Ammoniacates

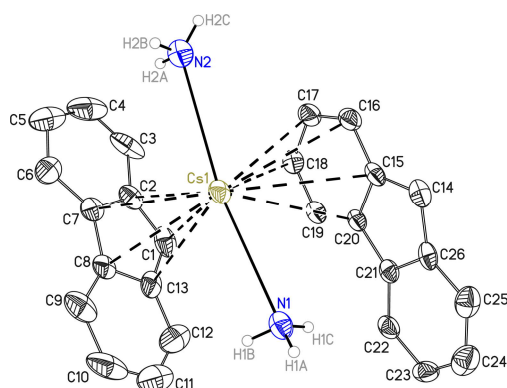
7.10.4. (Ind)Cs(NH₃)(THF) (23)



Graphical representation of the structural motif. Non-ammonia hydrogen atoms have been omitted. The indenyl anion C1A-C9A is disordered by 37(2)% and the indenyl anion C1B-C9B is disordered by 23(2)%. Additionally to the positional disorder, all indenyl moieties are symmetry site disordered as well, which is not depicted. The THF molecule is disordered by 49.1(7)%.

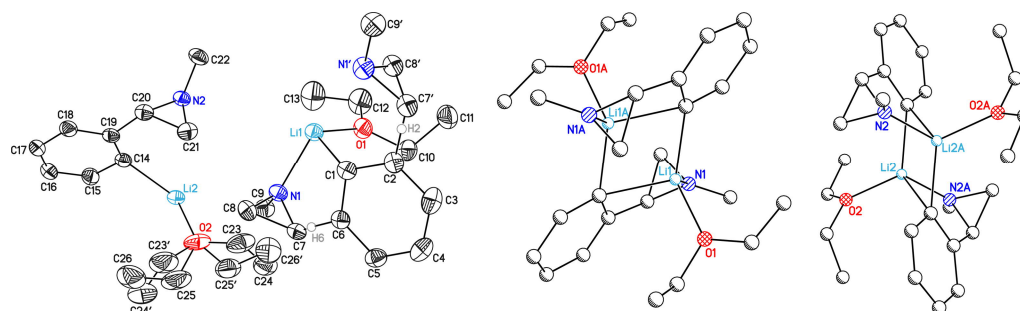
| | | | |
|---------------------------------------|--------------------------------------|--|-----------------|
| Structure code | c2c | Z | 2 |
| Empirical formula | C ₁₃ H ₁₈ NOCs | Crystal dimensions [mm ³] | 0.1 x 0.1 x 0.1 |
| Formula weight [g mol ⁻¹] | 337.19 | $\rho_{\text{calcd.}}$ [g cm ⁻³] | 1.622 |
| Sample temperature [K] | 100 (2) | μ [mm ⁻¹] | 2.662 |
| Wavelength [Å] | 0.71073 | F(000) | 332 |
| Crystal system | Triclinic | θ range [°] | 1.961 – 30.525 |
| Space group | $P\bar{1}$ | Reflections collected | 35339 |
| Unit cell dimensions [Å] | | Unique reflections | 4202 |
| | a = 6.881(2) | R _{int} | 0.0304 |
| | b = 9.695(2) | Completeness to θ_{max} | 100.0 % |
| | c = 10.918(3) | restraints/parameters | 2687/446 |
| | α = 85.19(2)° | GooF | 1.269 |
| | β = 72.38(2)° | R ₁ (I > 2 σ (I)) | 0.0189 |
| | γ = 85.30(3)° | wR ₂ (all data) | 0.0474 |
| Volume [Å ³] | 690.5(3) | max. diff. peak/hole [e Å ⁻³] | 0.750/−0.858 |
| Extinction coefficient | - | Absolute structure parameter | - |

7.10.5. *(Flu)Cs(NH₃)₂* (24)



Graphical representation of the structural motif. Non-ammonia hydrogen atoms have been omitted. Both fluorenyl anions are symmetry site disordered.

| | | | |
|---------------------------------------|---|---|-----------------|
| Structure code | p-1 | Z | 2 |
| Empirical formula | C ₁₃ H ₁₅ N ₂ Cs | Crystal dimensions [mm ³] | 0.1 x 0.1 x 0.1 |
| Formula weight [g mol ⁻¹] | 332.18 | $\rho_{\text{calcd.}}$ [g cm ⁻³] | 1.692 |
| Sample temperature [K] | 100 (2) | μ [mm ⁻¹] | 1.496 |
| Wavelength [Å] | 0.56086 | <i>F</i> (000) | 324 |
| Crystal system | Triclinic | θ range [°] | 1.596 – 20.546 |
| Space group | <i>P</i> $\bar{1}$ | Reflections collected | 19284 |
| Unit cell dimensions [Å] | | Unique reflections | 2668 |
| | a = 7.233(2) | <i>R</i> _{int} | 0.0255 |
| | b = 9.427(2) | Completeness to θ_{max} | 100.0 % |
| | c = 10.077(3) | restraints/parameters | 1340/280 |
| | α = 91.16(2)° | Goof | 1.185 |
| | β = 91.51(2)° | <i>R</i> ₁ (<i>I</i> > 2 σ (<i>I</i>)) | 0.0358 |
| | γ = 108.22(2)° | w <i>R</i> ₂ (all data) | 0.0361 |
| Volume [Å ³] | 652.2(3) | max. diff. peak/hole [e Å ⁻³] | 0.505/−0.250 |
| Extinction coefficient | - | Absolute structure parameter | - |

7.11. Structures determined for Aurelia Falcichio (Prof. Dr. Vito Capriati)**7.11.1. AF3**

Left: Graphical representation of the asymmetric unit. Hydrogen atoms except H2 and H6 have been omitted. Right: The whole molecules consist of dimers of the displayed fragments. Disordered parts have been omitted and letter A indicates symmetry relation.

The methyl-aziridine group of N1 together with H2 is disordered with the methyl-aziridine group of N1' together with H6 by 4.2(4)%. The diethylether sidearms (O2) are disordered 9,8(7)%.

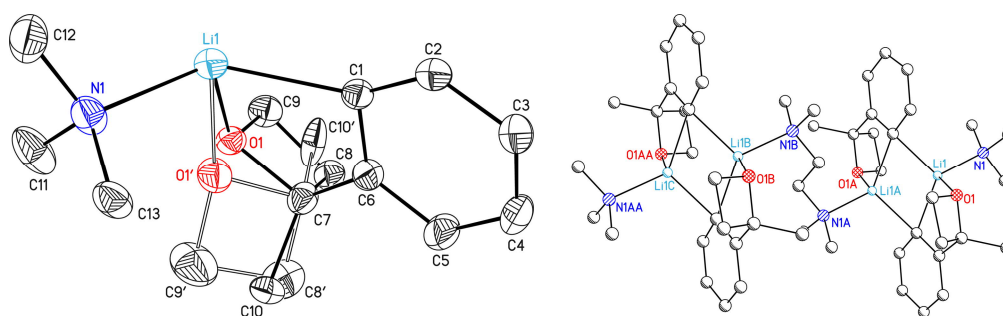
The sample is a twin crystal but the integration of both domains gives worse results than the exclusive integration of the main domain.

| | | | |
|---------------------------------------|---|--|-----------------|
| Structure code | AF3 | Z | 2 |
| Empirical formula | C ₂₆ H ₄₀ Li ₂ N ₂ O ₂ | Crystal dimensions [mm ³] | 0.1 x 0.1 x 0.1 |
| Formula weight [g mol ⁻¹] | 426.48 | $\rho_{\text{calcd.}}$ [g cm ⁻³] | 1.076 |
| Sample temperature [K] | 100 (2) | μ [mm ⁻¹] | 0.066 |
| Wavelength [Å] | 0.71073 | <i>F</i> (000) | 464 |
| Crystal system | Triclinic | θ range [°] | 1.486 – 25.376 |
| Space group | <i>P</i> $\bar{1}$ | Reflections collected | 19618 |
| Unit cell dimensions [Å] | | Unique reflections | 4747 |
| | a = 8.896(2) | R _{int} | 0.0339 |
| | b = 10.964(2) | Completeness to θ_{max} | 98.2 % |
| | c = 14.218(3) | restraints/parameters | 623/369 |
| | α = 77.28(3)° | GooF | 1.170 |
| | β = 79.15(2)° | R ₁ (I > 2 σ (I)) | 0.0702 |
| | γ = 80.10(2)° | wR ₂ (all data) | 0.1940 |
| Volume [Å ³] | 1316.3(5) | max. diff. peak/hole [e Å ⁻³] | 0.383/–0.407 |
| Extinction coefficient | - | Absolute structure parameter | - |

Crystal Structure Determination

Structures determined for Aurelia Falcichio (Prof. Dr. Vito Capriati)

7.11.2. AF4



Left: Graphical representation of the asymmetric unit. Right: The structure is a one dimensional coordination polymer build by dimers of lithiated 1,1-methylphenyloxacyclobutane bridged by TMEDA. Disordered parts have been omitted and letters A, B, C, AA indicate symmetry relation. Hydrogen atoms have been omitted.

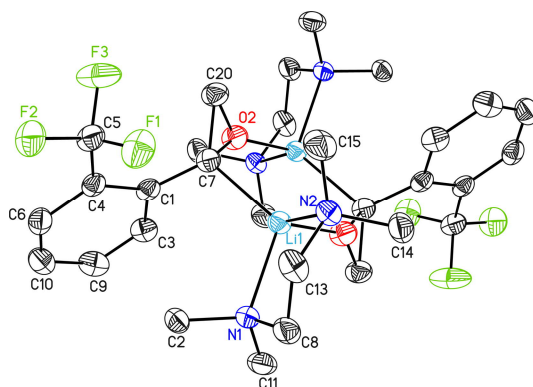
The methyl-oxacyclobutane fragment is disordered by 21.4(4)%.

| | | | |
|---------------------------------------|--------------------------------------|--|-----------------|
| Structure code | AF4 | Z | 2 |
| Empirical formula | C ₁₃ H ₁₉ LiNO | Crystal dimensions [mm ³] | 0.1 x 0.1 x 0.1 |
| Formula weight [g mol ⁻¹] | 212.23 | $\rho_{\text{calcd.}}$ [g cm ⁻³] | 1.141 |
| Sample temperature [K] | 100 (2) | μ [mm ⁻¹] | 0.070 |
| Wavelength [Å] | 0.71073 | $F(000)$ | 230 |
| Crystal system | Triclinic | θ range [°] | 2.195 – 25.493 |
| Space group | $P\bar{1}$ | Reflections collected | 12963 |
| Unit cell dimensions [Å] | | Unique reflections | 2290 |
| | a = 7.848(2) | R_{int} | 0.0383 |
| | b = 8.485(2) | Completeness to θ_{max} | 100 % |
| | c = 10.093(3) | restraints/parameters | 198/186 |
| | $\alpha = 69.97(2)^\circ$ | GooF | 1.096 |
| | $\beta = 78.47(2)^\circ$ | R_1 ($I > 2\sigma(I)$) | 0.0463 |
| | $\gamma = 89.12(3)^\circ$ | w R_2 (all data) | 0.1224 |
| Volume [Å ³] | 617(3) | max. diff. peak/hole [e Å ⁻³] | 0.221/−0.195 |
| Extinction coefficient | - | Absolute structure parameter | - |

Crystal Structure Determination

Structures determined for Aurelia Falcichio (Prof. Dr. Vito Capriati)

7.11.3. AF10



Graphical representation of the molecule. The atoms of the asymmetric unit are labeled. Hydrogen atoms have been omitted.

This structure has been published in:

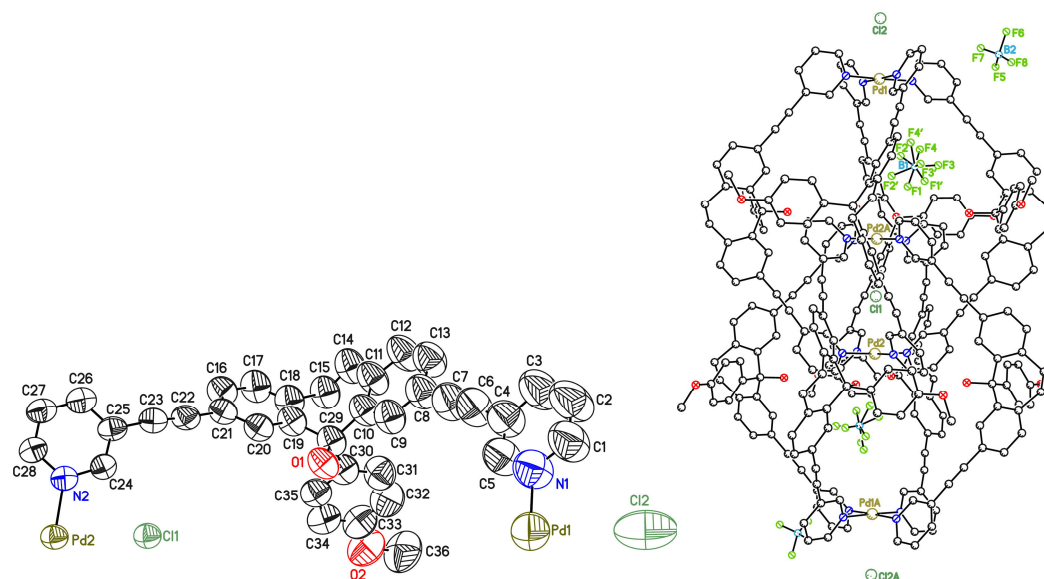
A. Salomone, F. M. Perna, A. Falcichio, S. O. Nilsson Lill, A. Moliterni, R. Michel, S. Florio, D. Stalke, V. Capriati *Chem. Sci* **2014**, *f*, 528-538.

CSD-Number 949695

| | | | |
|---------------------------------------|--|---|-----------------|
| Structure code | AF10 | Z | 2 |
| Empirical formula | C ₃₀ H ₄₄ F ₆ Li ₂ N ₄ O ₂ | Crystal dimensions [mm ³] | 0.1 x 0.1 x 0.1 |
| Formula weight [g mol ⁻¹] | 620.57 | $\rho_{\text{calcd.}}$ [g cm ⁻³] | 1.246 |
| Sample temperature [K] | 100 (2) | μ [mm ⁻¹] | 0.100 |
| Wavelength [Å] | 0.71073 | <i>F</i> (000) | 656 |
| Crystal system | Monoclinic | θ range [°] | 2.239 – 26.435 |
| Space group | <i>P</i> 2 ₁ / <i>c</i> | Reflections collected | 41883 |
| Unit cell dimensions [Å] | | Unique reflections | 3391 |
| | <i>a</i> = 9.593(2) | <i>R</i> _{int} | 0.0351 |
| | <i>b</i> = 11.372(2) | Completeness to θ_{max} | 99.9 % |
| | <i>c</i> = 15.779(3) | restraints/parameters | 0/203 |
| | β = 106.11(2)° | GooF | 1.042 |
| | | <i>R</i> ₁ (<i>I</i> > 2 σ (<i>I</i>)) | 0.0384 |
| | | <i>wR</i> ₂ (all data) | 0.1008 |
| Volume [Å ³] | 617(3) | max. diff. peak/hole [e Å ⁻³] | 0.281/−0.190 |
| Extinction coefficient | - | Absolute structure parameter | - |

7.12. Structures determined for the work group of Prof. Dr. Guido Clever

7.12.1. RM_FS65



Left: Graphical presentation of the asymmetric unit. BF_4^- -anions have been omitted. Right: The whole cage structure with chlorine and BF_4^- -anions in- an outside the boundaries of the cage structure. The (')-tag indicates positional disorder. Letter A indicates symmetry relation. Hydrogen atoms have been omitted.

The large cavities in- and outside the boundaries of the cage structure lead to a strong disorder of lattice acetonitrile molecules within the structure resulting in low resolution ($\theta_{\text{max}} = 17.26^\circ$). The amorphous electron density of the lattice solvent appears as strands in the cavities of the structure and cannot be described sufficiently. The structure factors have been recalculated by the SQUEEZE function within Platon (version:161012) and the $R_1 [I > 2s(I)]$ dropped from 22.11 % to 11.15 %.

The thermal motion of the BF_4^- -anions was refined isotropic due to disorder.

This structure has been published in:

S. Freye, R. Michel, D. Stalke, M. Pawliczek, H. Frauendorf, G. Clever, *J. Am. Chem. Soc.* **2013**, *135* (23), 8476-8479.

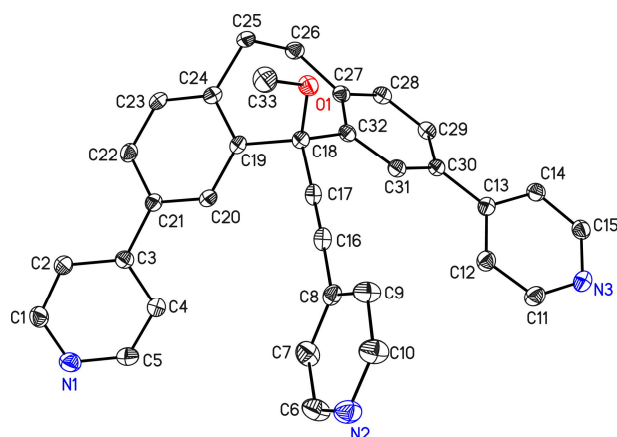
CCDC-No 954621

| | | | |
|---|--|--|----------------|
| Structure code | RM_FS65 | Z | 6 |
| Empirical formula | $\text{C}_{288}\text{H}_{200}\text{Cl}_{1.33}\text{B}_{6.67}\text{F}_{26.67}\text{N}_{16}\text{O}_{16}\text{Pd}_4$ | μ [mm^{-1}] | 0.243 |
| Formula weight [g mol^{-1}] | 5192.23 | $F(000)$ | 15888 |
| Sample temperature [K] | 100 (2) | θ range [$^\circ$] | 1.043 – 17.260 |
| Wavelength [\AA] | 0.71073 | Reflections collected | 270514 |
| Crystal system | Cubic | Unique reflections | 3048 |
| Space group | $Pn\bar{3}n$ | R_{int} | 0.0550 |
| Unit cell dimensions [\AA] | | Completeness to $\theta = 25.242^\circ$ | 33.9 % |
| | $a = 39.030(2)$ | restraints/parameters | 1565/418 |
| Volume [\AA^3] | 59456(9) | GooF | 3.012 |
| Extinction coefficient | - | $R_1 [I > 2\sigma(I)]$ | 0.1115 |
| Crystal dimensions [mm^3] | 0.2 x 0.2 x 0.08 | wR_2 (all data) | 0.3323 |
| $\rho_{\text{calcd.}}$ [g cm^{-3}] | 0.870 | max. diff. peak/hole [e \AA^{-3}] | 1.673/−0.376 |

Crystal Structure Determination

Structures determined for the work group of Prof. Dr. Guido Clever

7.12.2. RM_MX_T_Lig



Graphical representation of the molecule. The atoms of the asymmetric unit are labeled. Hydrogen atoms have been omitted.

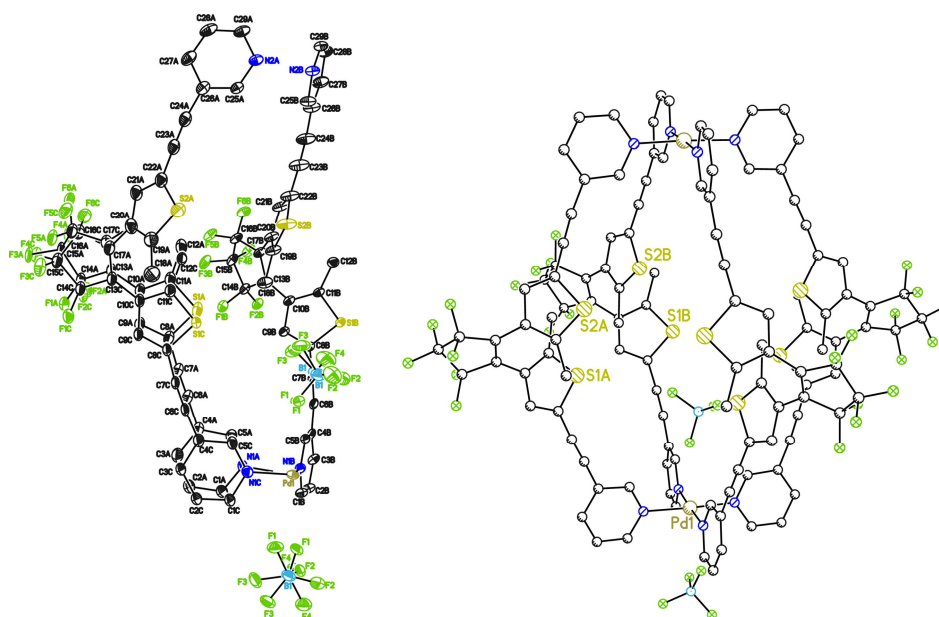
This structure has been published in:

M. Han, R. Michel, G. H. Clever, *Chem.-Eur. J.* **2014**, *20*, 10640.

CSD-Number 953531

| | | | |
|---------------------------------------|--|--|-----------------|
| Structure code | RM_MX_T_Lig | Z | 2 |
| Empirical formula | C ₃₃ H ₂₅ N ₃ O | Crystal dimensions [mm ³] | 0.1 x 0.1 x 0.1 |
| Formula weight [g mol ⁻¹] | 479.56 | $\rho_{\text{calcd.}}$ [g cm ⁻³] | 1.303 |
| Sample temperature [K] | 100 (2) | μ [mm ⁻¹] | 0.080 |
| Wavelength [Å] | 0.71073 | $F(000)$ | 506 |
| Crystal system | Triclinic | θ range [°] | 1.929 – 27.874 |
| Space group | $P\bar{1}$ | Reflections collected | 26776 |
| Unit cell dimensions [Å] | | Unique reflections | 5807 |
| | a = 10.424(2) | R_{int} | 0.0338 |
| | b = 11.196(2) | Completeness to θ_{max} | 99.9 % |
| | c = 12.161(3) | restraints/parameters | 0/203 |
| | $\alpha = 65.60(2)^\circ$ | GooF | 1.051 |
| | $\beta = 71.01(2)^\circ$ | R_1 ($I > 2\sigma(I)$) | 0.0447 |
| | $\gamma = 82.78(3)^\circ$ | w R_2 (all data) | 0.1129 |
| Volume [Å ³] | 1222.1(5) | max. diff. peak/hole [e Å ⁻³] | 0.334/−0.235 |
| Extinction coefficient | 0.0045(13) | Absolute structure parameter | - |

7.12.3. **MX00**



Left: Asymmetric unit with the lattice dichlorobenzene omitted. One sidearm together with the fluorocarbon backbone is disordered by 40.17(2)%. Right: Symmetry completed structure.

This structure has been published in:

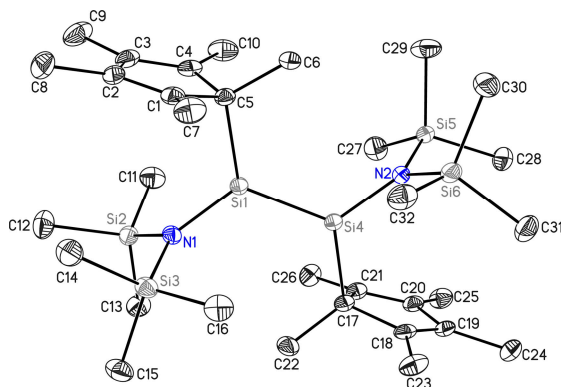
M. Han, R. Michel, B. He, Y.-S. Chen, D. Stalke, G. H. Clever, *Angew. Chem. Int. Ed.* **2013**, 52, 1319.

CSD-Number 900746

| | | | |
|---------------------------------------|---|--|-------------------|
| Structure code | MX00 | Z | 2 |
| Empirical formula | C ₂₀₆ H ₁₂₄ B ₄ Cl ₃₀ F ₄₀ N ₈ Pd ₂ S ₈ | Crystal dimensions [mm ³] | 0.1 x 0.08 x 0.01 |
| Formula weight [g mol ⁻¹] | 711.53 | $\rho_{\text{calcd.}}$ [g cm ⁻³] | 1.183 |
| Sample temperature [K] | 100 (2) | μ [mm ⁻¹] | 0.338 |
| Wavelength [Å] | 0.71073 | F(000) | 776 |
| Crystal system | Triclinic | θ range [°] | 1.32 – 20.87 |
| Space group | $P\bar{1}$ | Reflections collected | 21707 |
| Unit cell dimensions [Å] | | Unique reflections | 4202 |
| | a = 10.384(6) | R _{int} | 0.0657 |
| | b = 12.874(7) | Completeness to θ_{max} | 99.5 % |
| | c = 16.360(9) | restraints/parameters | 0/401 |
| | α = 72.12(2)° | Goof | 1.045 |
| | β = 78.51(2)° | R ₁ (I > 2 σ (I)) | 0.0430 |
| | γ = 75.56(2)° | wR ₂ (all data) | 0.1116 |
| Volume [Å ³] | 1997.8(19) | max. diff. peak/hole [e Å ⁻³] | 0.347/–0.365 |
| Extinction coefficient | 0 | Absolute structure parameter | - |

7.13. Structures determined for Shabana Khan (Prof. Dr. Herbert W. Roesky)

7.13.1. RM_SK20



Graphical representation of the molecule. The atoms of the asymmetric unit are labeled. Hydrogen atoms have been omitted.

This structure has been published in:

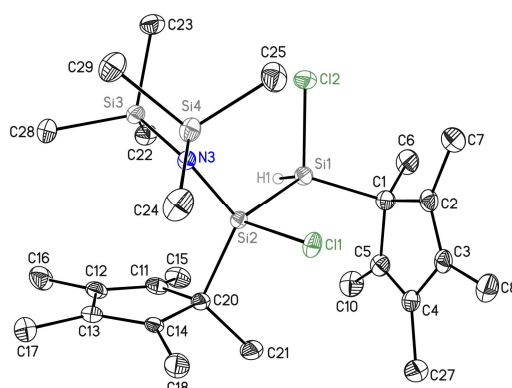
S. Khan, S. S. Sen, H. W. Roesky, D. Kratzert, R. Michel, D. Stalke, *Inorg Chem.*, **2010**, *49*, 9689.

CSD-Number 839822

| | | | |
|---------------------------------------|--|--|--------------------|
| Structure code | RM_SK20 | Z | 4 |
| Empirical formula | C ₃₂ H ₆₆ N ₂ Si ₆ | Crystal dimensions [mm ³] | 0.22 x 0.20 x 0.10 |
| Formula weight [g mol ⁻¹] | 647.41 | $\rho_{\text{calcd.}}$ [g cm ⁻³] | 1.096 |
| Sample temperature [K] | 100 (2) | μ [mm ⁻¹] | 0.235 |
| Wavelength [Å] | 0.71073 | $F(000)$ | 1424 |
| Crystal system | Monoclinic | θ range [°] | 1.26 – 27.88 |
| Space group | $P2_1/n$ | Reflections collected | 102129 |
| Unit cell dimensions [Å] | | Unique reflections | 9365 |
| | a = 17.655(2) | R_{int} | 0.0705 |
| | b = 10.1597(15) | Completeness to θ_{max} | 100.0 % |
| | c = 23.368(4) | restraints/parameters | 0/383 |
| | $\beta = 110.668(2)^\circ$ | GooF | 1.057 |
| | | R_1 ($I > 2\sigma(I)$) | 0.0404 |
| | | w R_2 (all data) | 0.1129 |
| Volume [Å ³] | 3921.9(10) | max. diff. peak/hole [e Å ⁻³] | 0.546/–0.324 |
| Extinction coefficient | 0 | Absolute structure parameter | - |

Crystal Structure Determination
Structures determined for Shabana Khan (Prof. Dr. Herbert W. Roesky)

7.13.2. *RM_SK20_2*



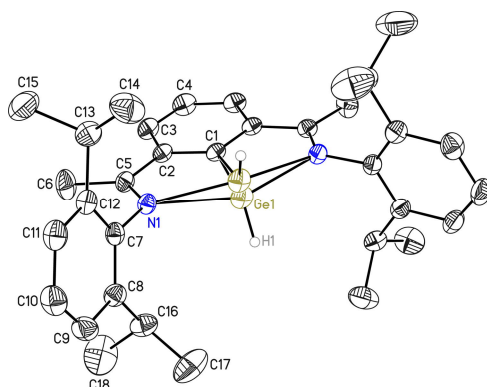
Graphical representation of the molecule. The atoms of the asymmetric unit are labeled. Hydrogen atoms have been omitted.

| | | | |
|---------------------------------------|--|---|-----------------|
| Structure code | RM_SK20_2 | Z | 2 |
| Empirical formula | C ₂₆ H ₄₉ Cl ₂ NSi ₄ | Crystal dimensions [mm ³] | 0.1 x 0.1 x 0.1 |
| Formula weight [g mol ⁻¹] | 558.92 | $\rho_{\text{calcd.}}$ [g cm ⁻³] | 1.188 |
| Sample temperature [K] | 100 (2) | μ [mm ⁻¹] | 0.377 |
| Wavelength [Å] | 0.71073 | <i>F</i> (000) | 604 |
| Crystal system | Triclinic | θ range [°] | 1.349 – 25.341 |
| Space group | <i>P</i> $\bar{1}$ | Reflections collected | 31932 |
| Unit cell dimensions [Å] | | Unique reflections | 5711 |
| | a = 9.693(2) | <i>R</i> _{int} | 0.0397 |
| | b = 10.840(2) | Completeness to θ_{max} | 100.0 % |
| | c = 15.716(3) | restraints/parameters | 0/318 |
| | α = 102.89(3)° | Goof | 1.031 |
| | β = 97.24(2)° | <i>R</i> ₁ (<i>I</i> > 2 σ (<i>I</i>)) | 0.0363 |
| | γ = 99.79(2)° | w <i>R</i> ₂ (all data) | 0.0920 |
| Volume [Å ³] | 1563.0(6) | max. diff. peak/hole [e Å ⁻³] | 0.729/–0.333 |
| Extinction coefficient | 0 | Absolute structure parameter | - |

Crystal Structure Determination

Structures determined for Shabana Khan (Prof. Dr. Herbert W. Roesky)

7.13.3. *RM_SK80b*



Graphical representation of the molecule. The atoms of the asymmetric unit are labeled. Hydrogen atoms have been omitted. The GeH-moiety is disordered by symmetry.

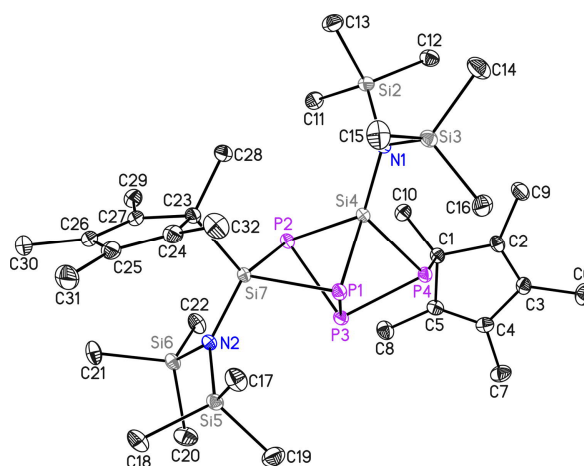
This structure has been published in:

S.Khan, P.P.Samuel, R.Michel, J.M.Dieterich, R.A.Mata, J.-P.Demers, A.Lange, H.W.Roesky, D.Stalke, *Chem. Commun.* **2012**, 48, 4890.

CSD-Number 863377

| | | | |
|---------------------------------------|--|---|------------------|
| Structure code | RM_SK80b | Z | 4 |
| Empirical formula | C ₃₄ H ₄₄ GeN ₂ | Crystal dimensions [mm ³] | 0.15 x 0.1 x 0.1 |
| Formula weight [g mol ⁻¹] | 558.92 | $\rho_{\text{calcd.}}$ [g cm ⁻³] | 1.175 |
| Sample temperature [K] | 100 (2) | μ [mm ⁻¹] | 1.002 |
| Wavelength [Å] | 0.71073 | <i>F</i> (000) | 1176 |
| Crystal system | Monoclinic | θ range [°] | 1.72 – 30.55 |
| Space group | <i>C2/c</i> | Reflections collected | 31743 |
| Unit cell dimensions [Å] | | Unique reflections | 4786 |
| | <i>a</i> = 15.509(2) | <i>R</i> _{int} | 0.0253 |
| | <i>b</i> = 8.506(2) | Completeness to θ_{max} | 99.6 % |
| | <i>c</i> = 24.339(3) | restraints/parameters | 1/182 |
| | β = 103.03(2)° | GooF | 1.041 |
| | | <i>R</i> ₁ (<i>I</i> > 2 σ (<i>I</i>)) | 0.0409 |
| | | <i>wR</i> ₂ (all data) | 0.1098 |
| Volume [Å ³] | 3128.1(9) | max. diff. peak/hole [e Å ⁻³] | 0.648/−0.324 |
| Extinction coefficient | 0.0007(2) | Absolute structure parameter | - |

7.13.4. **RM_SK200**



Graphical representation of the molecule. The atoms of the asymmetric unit are labeled. Hydrogen atoms have been omitted.

This structure has been published in:

S. Khan, R. Michel, S. S. Sen, H. W. Roesky, D. Stalke, *Inorg Chem.*, **2011**, *50*, 11786.

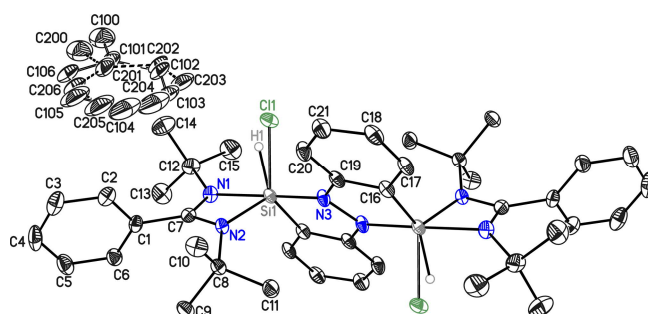
CSD-Number 835940

| | | | |
|---------------------------------------|---|--|------------------|
| Structure code | RM_SK200 | Z | 2 |
| Empirical formula | C ₃₂ H ₆₆ N ₂ P ₄ Si ₆ | Crystal dimensions [mm ³] | 0.2 x 0.15 x 0.1 |
| Formula weight [g mol ⁻¹] | 771.29 | $\rho_{\text{calcd.}}$ [g cm ⁻³] | 1.203 |
| Sample temperature [K] | 100 (2) | μ [mm ⁻¹] | 0.371 |
| Wavelength [Å] | 0.71073 | <i>F</i> (000) | 832 |
| Crystal system | Triclinic | θ range [°] | 0.97 – 29.15 |
| Space group | <i>P</i> $\bar{1}$ | Reflections collected | 50751 |
| Unit cell dimensions [Å] | | Unique reflections | 11473 |
| | a = 9.087(2) | R _{int} | 0.0378 |
| | b = 11.305(2) | Completeness to θ_{max} | 99.8 % |
| | c = 21.337(3) | restraints/parameters | 0/419 |
| | α = 82.12(2)° | Goof | 1.023 |
| | β = 84.01(2)° | R ₁ (I > 2 σ (I)) | 0.0316 |
| | γ = 79.70(2)° | wR ₂ (all data) | 0.0779 |
| Volume [Å ³] | 2129.1(7) | max. diff. peak/hole [e Å ⁻³] | 0.469/–0.289 |
| Extinction coefficient | 0 | Absolute structure parameter | - |

Crystal Structure Determination

Structures determined for Shabana Khan (Prof. Dr. Herbert W. Roesky)

7.13.5. RM_SK201



Graphical representation of the molecule. The atoms of the asymmetric unit are labeled. Hydrogen atoms except H1 have been omitted. H1 and Cl1 are disordered by 49.9(4)% and 50.1(4)%. The lattice-toluene molecule exhibits positional disorder by 39(2)% and additional disorder by symmetry.

This structure has been published in:

S. Khan, S. S. Sen, H. W. Roesky, D. Kratzert, R. Michel, D. Stalke, *Inorg Chem.*, **2010**, *49*, 9689.

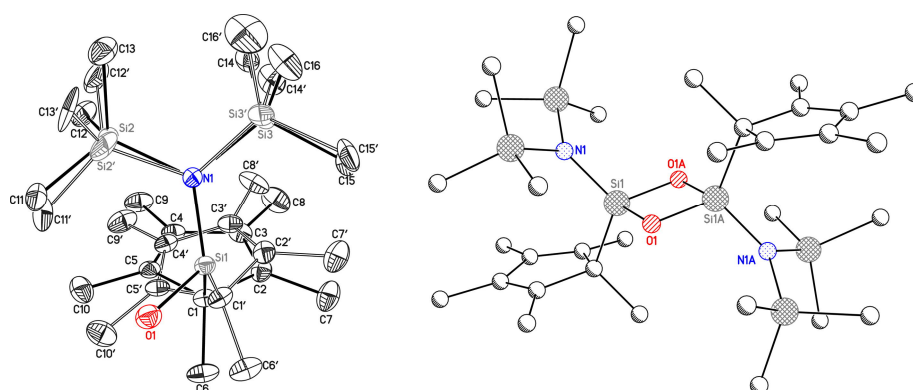
CSD-Number 839822

| | | | |
|---------------------------------------|--|---|-----------------|
| Structure code | RM_SK201 | Z | 1 |
| Empirical formula | C ₄₉ H ₆₃ ClN ₆ Si ₂ | Crystal dimensions [mm ³] | 0.2 x 0.2 x 0.1 |
| Formula weight [g mol ⁻¹] | 827.68 | $\rho_{\text{calcd.}}$ [g cm ⁻³] | 1.197 |
| Sample temperature [K] | 100 (2) | μ [mm ⁻¹] | 0.176 |
| Wavelength [Å] | 0.71073 | <i>F</i> (000) | 444 |
| Crystal system | Triclinic | θ range [°] | 1.67 – 26.47 |
| Space group | <i>P</i> $\bar{1}$ | Reflections collected | 27534 |
| Unit cell dimensions [Å] | | Unique reflections | 4737 |
| | a = 9.343(2) | <i>R</i> _{int} | 0.0348 |
| | b = 10.756(2) | Completeness to θ_{max} | 99.8 % |
| | c = 12.218(3) | restraints/parameters | 72/331 |
| | α = 94.31(2)° | GooF | 1.196 |
| | β = 97.30(2)° | <i>R</i> ₁ (<i>I</i> > 2 σ (<i>I</i>)) | 0.0611 |
| | γ = 108.20(2)° | w <i>R</i> ₂ (all data) | 0.1357 |
| Volume [Å ³] | 1148.4(5) | max. diff. peak/hole [e Å ⁻³] | 0.366/–0.305 |
| Extinction coefficient | 0 | Absolute structure parameter | - |

Crystal Structure Determination

Structures determined for Shabana Khan (Prof. Dr. Herbert W. Roesky)

7.13.6. RM_SK205



Left: Graphical representation of the asymmetric unit. Right: Graphical representation of the molecule. Hydrogen atoms have been omitted. The Cp* unit together with the two SiMe₃ units is disordered by 11.0(3)%.

This structure has been published in:

S.Khan, R.Michel, D.Koley, H.W.Roesky, D.Stalke, *Inorg. Chem.*, **2011**, 50, 10878.

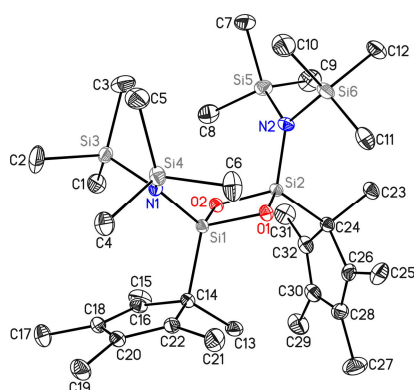
CSD-Number 832195

| | | | |
|---------------------------------------|---|--|-----------------|
| Structure code | RM_SK205 | Z | 2 |
| Empirical formula | C ₃₂ H ₆₆ N ₂ O ₂ Si ₆ | Crystal dimensions [mm ³] | 0.2 x 0.1 x 0.1 |
| Formula weight [g mol ⁻¹] | 679.41 | $\rho_{\text{calcd.}}$ [g cm ⁻³] | 1.152 |
| Sample temperature [K] | 100 (2) | μ [mm ⁻¹] | 0.242 |
| Wavelength [Å] | 0.71073 | <i>F</i> (000) | 744 |
| Crystal system | Monoclinic | θ range [°] | 1.98 – 26.36 |
| Space group | <i>P</i> 2 ₁ / <i>n</i> | Reflections collected | 18406 |
| Unit cell dimensions [Å] | | Unique reflections | 4007 |
| | a = 9.169(2) | R _{int} | 0.0468 |
| | b = 13.640(2) | Completeness to θ_{max} | 99.9 % |
| | c = 15.669(3) | restraints/parameters | 753/353 |
| | β = 90.73(2)° | Goof | 1.030 |
| Volume [Å ³] | 1959.5(6) | R ₁ (I > 2 σ (I)) | 0.0422 |
| Extinction coefficient | 0 | wR ₂ (all data) | 0.1121 |
| | | max. diff. peak/hole [e Å ⁻³] | 0.361/–0.278 |
| | | Absolute structure parameter | - |

Crystal Structure Determination

Structures determined for Shabana Khan (Prof. Dr. Herbert W. Roesky)

7.13.7. RM_SK205_cis



Graphical representation of the molecule. Hydrogen atoms have been omitted.

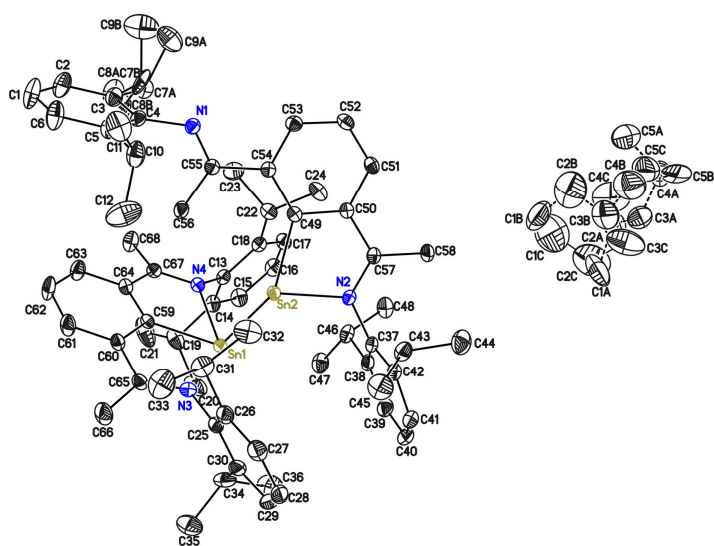
This structure has been published in:

S.Khan, R.Michel, D.Koley, H.W.Roesky, D.Stalke, *Inorg. Chem.*, **2011**, *50*, 10878.

CSD-Number 832194

| | | | |
|---------------------------------------|---|--|-------------------|
| Structure code | RM_SK205_cis | Z | 4 |
| Empirical formula | C ₃₂ H ₆₆ N ₂ O ₂ Si ₆ | Crystal dimensions [mm ³] | 0.2 x 0.05 x 0.03 |
| Formula weight [g mol ⁻¹] | 679.41 | $\rho_{\text{calcd.}}$ [g cm ⁻³] | 1.139 |
| Sample temperature [K] | 100 (2) | μ [mm ⁻¹] | 0.240 |
| Wavelength [Å] | 0.71073 | $F(000)$ | 1488 |
| Crystal system | Monoclinic | θ range [°] | 1.60 – 31.06 |
| Space group | $P2_1/n$ | Reflections collected | 84348 |
| Unit cell dimensions [Å] | | Unique reflections | 12685 |
| | a = 11.535(2) | R_{int} | 0.0274 |
| | b = 15.483(2) | Completeness to θ_{max} | 99.9 % |
| | c = 22.378(3) | restraints/parameters | 0/401 |
| | $\beta = 97.54(2)^\circ$ | GooF | 1.058 |
| | | R_1 ($I > 2\sigma(I)$) | 0.0346 |
| | | w R_2 (all data) | 0.0952 |
| Volume [Å ³] | 3962(9) | max. diff. peak/hole [e Å ⁻³] | 0.578/–0.283 |
| Extinction coefficient | 0 | Absolute structure parameter | - |

7.13.8. **RM_SK300**



Graphical representation of the molecule. Hydrogen atoms have been omitted. The ¹Pr-group is disordered by 28(2)%. The lattice pentane molecule is disordered on three sites with fractions of 72.2(3)%, 20.2(5)%, and 7.6(5)%.

This structure has been published in:

S.Khan, R.Michel, J.M.Dieterich, R.A.Mata, H.W.Roesky, J.-P.Demers, A.Lange, D.Stalke, *J. Am. Chem. Soc.* **2011**, *133*, 17889.

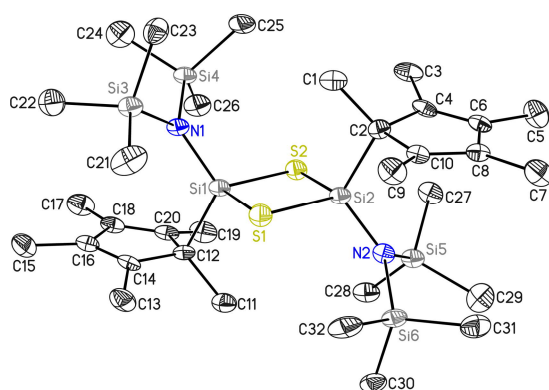
CSD-Number 833290

| | | | |
|---------------------------------------|--|--|-----------------|
| Structure code | RM_SK300 | Z | 4 |
| Empirical formula | C ₇₃ H ₉₈ N ₄ Sn ₂ | Crystal dimensions [mm ³] | 0.1 x 0.1 x 0.1 |
| Formula weight [g mol ⁻¹] | 1268.93 | $\rho_{\text{calcd.}}$ [g cm ⁻³] | 1.245 |
| Sample temperature [K] | 100 (2) | μ [mm ⁻¹] | 0.780 |
| Wavelength [Å] | 0.71073 | F(000) | 2656 |
| Crystal system | Monoclinic | θ range [°] | 1.24 – 27.86 |
| Space group | P2 ₁ /c | Reflections collected | 177456 |
| Unit cell dimensions [Å] | | Unique reflections | 16126 |
| | a = 16.411(6) | R _{int} | 0.0573 |
| | b = 16.426(6) | Completeness to θ_{max} | 99.9 % |
| | c = 25.192(9) | restraints/parameters | 361/851 |
| | β = 94.40(2)° | GooF | 1.042 |
| | | R ₁ (I > 2 σ (I)) | 0.0257 |
| | | wR ₂ (all data) | 0.0609 |
| Volume [Å ³] | 6771(4) | max. diff. peak/hole [e Å ⁻³] | 0.650/–0.487 |
| Extinction coefficient | 0 | Absolute structure parameter | - |

Crystal Structure Determination

Structures determined for Shabana Khan (Prof. Dr. Herbert W. Roesky)

7.13.9. RM_SK305_a



Graphical representation of the molecule. Hydrogen atoms have been omitted.

This structure has been published in:

S.Khan, R.Michel, D.Koley, H.W.Roesky, D.Stalke, *Inorg. Chem.*, **2011**, *50*, 10878.

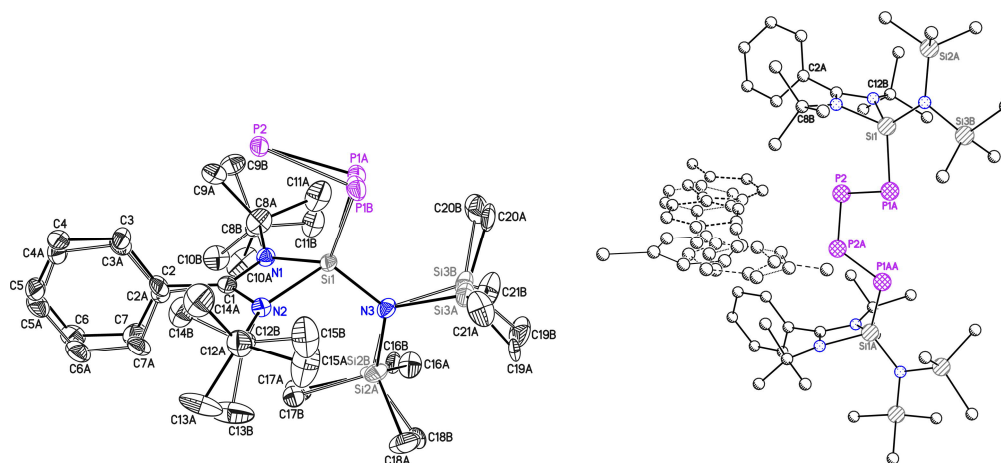
CSD-Number 832193

| | | | |
|---------------------------------------|---|---|-------------------|
| Structure code | RM_SK305_a | Z | 2 |
| Empirical formula | C ₃₂ H ₆₆ N ₂ S ₂ Si ₆ | Crystal dimensions [mm ³] | 0.1 x 0.08 x 0.01 |
| Formula weight [g mol ⁻¹] | 711.53 | $\rho_{\text{calcd.}}$ [g cm ⁻³] | 1.183 |
| Sample temperature [K] | 100 (2) | μ [mm ⁻¹] | 0.338 |
| Wavelength [Å] | 0.71073 | <i>F</i> (000) | 776 |
| Crystal system | Triclinic | θ range [°] | 1.32 – 20.87 |
| Space group | <i>P</i> $\bar{1}$ | Reflections collected | 21707 |
| Unit cell dimensions [Å] | | Unique reflections | 4202 |
| | a = 10.384(6) | <i>R</i> _{int} | 0.0657 |
| | b = 12.874(7) | Completeness to θ_{max} | 99.5 % |
| | c = 16.360(9) | restraints/parameters | 0/401 |
| | α = 72.12(2)° | GooF | 1.045 |
| | β = 78.51(2)° | <i>R</i> ₁ (<i>I</i> > 2 σ (<i>I</i>)) | 0.0430 |
| | γ = 75.56(2)° | w <i>R</i> ₂ (all data) | 0.1116 |
| Volume [Å ³] | 1997.8(19) | max. diff. peak/hole [e Å ⁻³] | 0.347/–0.365 |
| Extinction coefficient | 0 | Absolute structure parameter | - |

Crystal Structure Determination

Structures determined for Shabana Khan (Prof. Dr. Herbert W. Roesky)

7.13.11. RM_SK500_b



Left: Graphical presentation of the asymmetric unit with lattice toluene omitted. Right: Graphical presentation of the molecule including lattice toluene. The phenyl group is disordered by 45(3)%, the ^tBu-group containing C8A is disordered by 13.0(8)%, the ^tBu-group containing C12A is disordered by 33(2)%, the SiMe₃-group containing Si2A is disordered by 19(2)%. the SiMe₃-group containing Si3A is disordered by 10(2)%. And the P1A is disordered by 11(2)%. The six fractions of toluene are placed on a mirror plane and have been refined with fixed occupancies of 30%, 18%, 14%, 11%, 4%, and 3%, adding up to a summed toluene occupation of 80%.

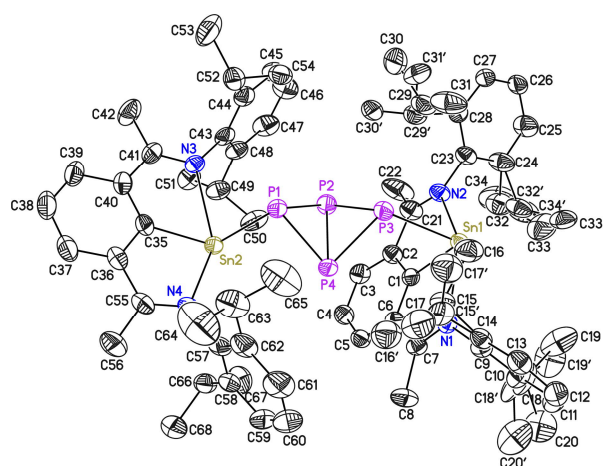
This structure has been published in:

S.Khan, R.Michel, S.S.Sen, H.W.Roesky, D.Stalke, *Angew. Chem., Int. Ed.* **2011**, *50*, 11786.

CSD-Number 835941

| | | | |
|---------------------------------------|---|--|------------------|
| Structure code | RM_SK500_b | Z | 4 |
| Empirical formula | C _{53.2} H _{94.8} N ₆ P ₄ Si ₆ | Crystal dimensions [mm ³] | 0.2 x 0.2 x 0.15 |
| Formula weight [g mol ⁻¹] | 1110.97 | $\rho_{\text{calcd.}}$ [g cm ⁻³] | 1.135 |
| Sample temperature [K] | 100 (2) | μ [mm ⁻¹] | 0.623 |
| Wavelength [Å] | 0.71073 | <i>F</i> (000) | 2400 |
| Crystal system | Orthorhombic | θ range [°] | 1.26 – 28.30 |
| Space group | <i>Pnma</i> | Reflections collected | 124628 |
| Unit cell dimensions [Å] | | Unique reflections | 8219 |
| | a = 18.145(2) | R _{int} | 0.0272 |
| | b = 32.364(3) | Completeness to θ_{max} | 99.9 % |
| | c = 11.070(2) | restraints/parameters | 3349/734 |
| | | GooF | 1.055 |
| | | R ₁ (<i>I</i> > 2 σ (<i>I</i>)) | 0.0354 |
| | | wR ₂ (all data) | 0.0989 |
| Volume [Å ³] | 6500(15) | max. diff. peak/hole [e Å ⁻³] | 0.558/–0.336 |
| Extinction coefficient | 0.00054(11) | Absolute structure parameter | - |

7.13.12. **RM_SK502**



Graphical representation of the molecule. The atoms of the asymmetric unit are labeled. Hydrogen atoms have been omitted. All ¹Pr-groups of the ligand on the right are disordered: the group containing C15 by 10.9(7)%, the group containing C18 by 19(3)%, the group containing C29 by 11.5(3)%, and the group containing C32 by 23(2)%.

This structure has been published in:

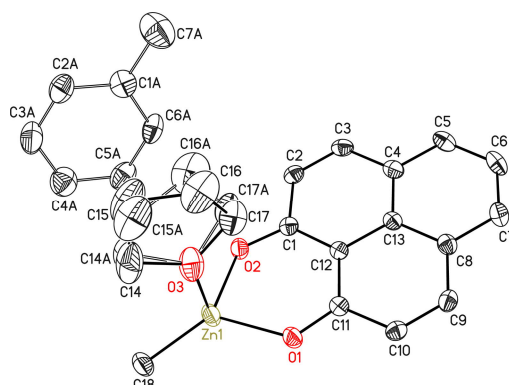
S.Khan, R.Michel, J.M.Dieterich, R.A.Mata, H.W.Roesky, J.-P.Demers, A.Lange, D.Stalke, *J. Am. Chem. Soc.* **2011**, *133*, 17889.

CSD-Number 833291

| | | | |
|---------------------------------------|---|---|--------------------|
| Structure code | RM_SK502 | Z | 2 |
| Empirical formula | C ₆₈ H ₈₆ N ₄ P ₄ Sn ₂ | Crystal dimensions [mm ³] | 0.25 x 0.2 x 0.007 |
| Formula weight [g mol ⁻¹] | 1320.67 | $\rho_{\text{calcd.}}$ [g cm ⁻³] | 1.332 |
| Sample temperature [K] | 100 (2) | μ [mm ⁻¹] | 0.897 |
| Wavelength [Å] | 0.71073 | <i>F</i> (000) | 2728 |
| Crystal system | Monoclinic | θ range [°] | 1.41 – 26.04 |
| Space group | <i>P</i> 2 ₁ / <i>c</i> | Reflections collected | 86017 |
| Unit cell dimensions [Å] | | Unique reflections | 12981 |
| | a = 14.644(2) | <i>R</i> _{int} | 0.0361 |
| | b = 17.463(2) | Completeness to θ_{max} | 99.8 % |
| | c = 26.602(2) | restraints/parameters | 512/827 |
| | β = 104.48(2)° | GooF | 1.072 |
| | | <i>R</i> ₁ (<i>I</i> > 2 σ (<i>I</i>)) | 0.0374 |
| | | w <i>R</i> ₂ (all data) | 0.0981 |
| Volume [Å ³] | 6586.8(13) | max. diff. peak/hole [e Å ⁻³] | 2.311/–0.857 |
| Extinction coefficient | 0 | Absolute structure parameter | - |

7.14. Structures determined for Tamal K. Sen

7.14.1. TKS_1_2



Graphical representation of the molecule. The atoms of the asymmetric unit are labeled. Hydrogen atoms have been omitted. The THF-molecule is disordered by 24(2)% and the lattice toluene is disordered by symmetry.

This structure has been published in:

K.V.Raman, A.M.Kamerbeek, A.Mukherjee, N.Atodiresei, T.K.Sen, P.Lazic, V.Caciuc, R.Michel, D.Stalke, S.K.Mandal, S.Blugel, M.Munzenberg, J.S.Moodera, *Nature* **2013**, 493, 509.

CSD-Number 859902

| | | | |
|---------------------------------------|---|--|--------------------|
| Structure code | TKS_1_2 | Z | 2 |
| Empirical formula | C _{21.5} H ₂₂ O ₃ Zn | Crystal dimensions [mm ³] | 0.29 x 0.14 x 0.12 |
| Formula weight [g mol ⁻¹] | 393.76 | $\rho_{\text{calcd.}}$ [g cm ⁻³] | 1.437 |
| Sample temperature [K] | 100 (2) | μ [mm ⁻¹] | 1.367 |
| Wavelength [Å] | 0.71073 | $F(000)$ | 410 |
| Crystal system | Triclinic | θ range [°] | 1.735 – 28.259 |
| Space group | $P\bar{1}$ | Reflections collected | 20.287 |
| Unit cell dimensions [Å] | | Unique reflections | 4482 |
| | a = 8.708(2) | R_{int} | 0.0236 |
| | b = 8.934(2) | Completeness to θ_{max} | 100.0 % |
| | c = 12.303(3) | restraints/parameters | 168/301 |
| | $\alpha = 105.93(2)^\circ$ | GooF | 1.095 |
| | $\beta = 95.62(3)^\circ$ | R_1 ($I > 2\sigma(I)$) | 0.0266 |
| | $\gamma = 94.67(2)^\circ$ | w R_2 (all data) | 0.0677 |
| Volume [Å ³] | 910.0(4) | max. diff. peak/hole [e Å ⁻³] | 0.442/−0.487 |
| Extinction coefficient | 0 | Absolute structure parameter | - |

8. Bibliography

- [1] a) W. Kaminsky, *Polyolefins: 50 years after Ziegler and Natta I - Polyethylene and Polypropylene*, Vol. 257, Springer-Verlag, Berlin Heidelberg, **2013**; b) W. Kaminsky, *Polyolefins: 50 years after Ziegler and Natta II - Polyolefins by Metallocenes and Other Single-Site Catalysts*, Vol. 258, Springer Verlag, Berlin Heidelberg, **2013**.
- [2] F. N. Tebbe, G. W. Parshall, G. S. Reddy, *J. Am. Chem. Soc.* **1978**, *100*, 3611-3613.
- [3] N. A. Petasis, E. I. Bzowej, *J. Am. Chem. Soc.* **1990**, *112*, 6392-6394.
- [4] D. W. Hart, J. Schwartz, *J. Am. Chem. Soc.* **1974**, *96*, 8115-8116.
- [5] P. M. Abeyasinghe, M. M. Harding, *J. Chem. Soc., Dalton Trans.* **2007**, 3474-3482.
- [6] C. Elschenbroich, *Organometallchemie*, 6 ed., Vieweg+Teubner Verlag, Wiesbaden, **2008**.
- [7] F. A. Carey, R. J. Sundberg, *Organische Chemie*, 1 ed., Wiley VCH, Weinheim, **1995**.
- [8] J. D. Fisher, P. H. M. Budzelaar, P. J. Shapiro, R. J. Staples, G. P. A. Yap, A. L. Rheingold, *Organometallics* **1997**, *16*, 871-879.
- [9] O. T. Beachley, T. D. Getman, R. U. Kirss, R. B. Hallock, W. E. Hunter, J. L. Atwood, *Organometallics* **1985**, *4*, 751-754.
- [10] V. I. Kulishov, N. G. Bokii, A. F. Prikhot'ko, Y. T. Struchkov, *Zh. Strukt. Khim.* **1975**, *16*, 252.
- [11] M. Birkhahn, P. Krommes, W. Massa, J. Lorberth, *J. Organomet. Chem.* **1981**, *208*, 161-167.
- [12] G. Bombieri, C. Panattoni, *Acta Cryst.* **1966**, *20*, 595.
- [13] J. Lorberth, W. Massa, S. Wocadlo, I. Sarraje, S. H. Shin, X. W. Li, *J. Organomet. Chem.* **1995**, *485*, 149-152.
- [14] H. E. Roscoe, S. F. R., *Eur. J. Org. Chem.* **1886**, *232*, 348-352.
- [15] G. Kraemer, A. Spilker, *Chem. Ber.* **1896**, *29*, 552-561.
- [16] J. Thiele, *Chem. Ber.* **1900**, *33*, 666-673.
- [17] J. Thiele, *Chem. Ber.* **1901**, *34*, 68-71.
- [18] T. J. Kealy, P. L. Pauson, *Nature* **1951**, *168*, 1039-1040.
- [19] a) G. Wilkinson, M. Rosenblum, M. C. Whiting, R. B. Woodward, *J. Am. Chem. Soc.* **1952**, *74*, 2125-2126; b) E. O. Fischer, W. Pfab, *Z. Naturforsch., B: Chem. Sci.* **1952**, *7*, 377.
- [20] C. R. Groom, I. J. Bruno, M. P. Lightfoot, S. C. Ward, *Acta Cryst. Sect. B* **2016**, *72*, 171-179.
- [21] N. Treitel, R. Shenhar, I. Aprahamian, T. Sheradsky, M. Rabinovitz, *PCCP* **2004**, *6*, 1113-1121.

- [22] *Römpp Lexikon Chemie*, 10 ed., Georg Thieme Verlag KG, Stuttgart, **1996-1999**.
- [23] E. V. Mutseneck, Z. A. Starikova, K. A. Lyssenko, P. V. Petrovskii, P. Zanello, M. Corsini, A. R. Kudinov, *Eur. J. Inorg. Chem.* **2006**, 2006, 4519-4527.
- [24] a) A. J. Hart-Davis, R. J. Mawby, *J. Chem. Soc. A* **1969**, 2403-2407; b) A. J. Hart-Davis, C. White, R. J. Mawby, *Inorg. Chim. Acta* **1970**, 4, 441-446; c) F. Basolo, *Coord. Chem. Rev.* **1982**, 43, 7-15; d) M. E. Rerek, L.-N. Ji, F. Basolo, *J. Chem. Soc., Chem. Commun.* **1983**, 1208-1209; e) M. E. Rerek, F. Basolo, *J. Am. Chem. Soc.* **1984**, 106, 5908-5912; f) L. F. Veiros, *Organometallics* **2000**, 19, 3127-3136; g) M. J. Calhorda, C. C. Romão, L. F. Veiros, *Chem. Eur. J.* **2002**, 8, 868-875.
- [25] a) S. Y. Knjazhanski, G. Cadenas, M. García, C. M. Pérez, I. E. Nifant'ev, I. A. Kashulin, P. V. Ivchenko, K. A. Lyssenko, *Organometallics* **2002**, 21, 3094-3099; b) A. Lapczuk-Krygier, L. Ponikiewski, J. Pikies, *Acta Cryst. Sect. E* **2011**, 67, m54.
- [26] a) A. Decken, A. J. MacKay, M. J. Brown, F. Bottomley, *Organometallics* **2002**, 21, 2006-2009; b) A. L. Mejdrich, T. W. Hanks, *Synth. React. Inorg. Met.-Org. Chem.* **1998**, 28, 953-973.
- [27] a) A. Raith, P. Altmann, M. Cokoja, W. A. Herrmann, F. E. Kühn, *Coord. Chem. Rev.* **2010**, 254, 608-634; b) R. D. Theys, M. E. Dudley, M. M. Hossain, *Coord. Chem. Rev.* **2009**, 253, 180-234; c) M. Sharma, M. S. Eisen, in *Organometallic and Coordination Chemistry of the Actinides* (Ed.: T. E. Albrecht-Schmitt), Springer Berlin Heidelberg, Berlin, Heidelberg, **2008**, pp. 1-85; d) M. Tamm, *Chem. Commun.* **2008**, 3089-3100.
- [28] S. Harder, *Coord. Chem. Rev.* **1998**, 176, 17-66.
- [29] a) C. Lambert, P. von Ragué Schleyer, *Angew. Chem.* **1994**, 106, 1187-1199; b) C. Lambert, P. von Ragué Schleyer, *Angew. Chem. Int. Ed.* **1994**, 33, 1129-1140.
- [30] a) H. P. Fritz, R. Schneider, *Chem. Ber.* **1960**, 93, 1171-1183; b) H. P. Fritz, L. Schäfer, *Chem. Ber.* **1964**, 97, 1829-1833.
- [31] a) R. H. Cox, H. W. Terry, L. W. Harrison, *J. Am. Chem. Soc.* **1971**, 93, 3297-3298; b) W. T. Ford, *J. Organomet. Chem.* **1971**, 32, 27-33; c) P. Fischer, J. Stadelhofer, J. Weidlein, *J. Organomet. Chem.* **1976**, 116, 65-73.
- [32] S. Alexandratos, A. Streitwieser, H. F. Schaefer, *J. Am. Chem. Soc.* **1976**, 98, 7959-7962.
- [33] a) R. E. Dinnebier, U. Behrens, F. Olbrich, *Organometallics* **1997**, 16, 3855-3858; b) R. E. Dinnebier, F. Olbrich, G. M. Bendele, *Acta Cryst. Sect. C* **1997**, 53, 699-701; c) R. E. Dinnebier, F. Olbrich, S. van Smaalen, P. W. Stephens, *Acta Cryst. Sect. B* **1997**, 53, 153-158.
- [34] R. E. Dinnebier, S. van Smaalen, F. Olbrich, S. Carlson, *Inorg. Chem.* **2005**, 44, 964-968.
- [35] R. Shannon, *Acta Cryst. Sect. A* **1976**, 32, 751-767.
- [36] W. J. Evans, T. J. Boyle, J. W. Ziller, *Organometallics* **1992**, 11, 3903-3907.
- [37] J. T. Foy, E. B. Wilkes, I. Aprahamian, *CrystEngComm* **2012**, 14, 6126-6128.

- [38] a) W.-P. Leung, F.-Q. Song, F. Xue, T. C. W. Mak, *J. Chem. Soc., Dalton Trans.* **1997**, 4307-4312; b) W. Nie, C. Qian, Y. Chen, J. Sun, *Organometallics* **2001**, *20*, 5780-5783; c) V. Kotov Vasily, G. Kehr, R. Fröhlich, G. Erker, *Z. Naturforsch., B: Chem. Sci.* **2006**, *61*, 1319.
- [39] Q. Bai, H. Roesky, P. Müller, *Bull. Pol. Acad. Sci., Chem.* **2002**, *50*, 1.
- [40] a) P. Jutzi, W. Leffers, B. Hampel, S. Pohl, W. Saak, *Angew. Chem.* **1987**, *99*, 563-564; b) P. Jutzi, W. Leffers, B. Hampel, S. Pohl, W. Saak, *Angew. Chem. Int. Ed.* **1987**, *26*, 583-584.
- [41] a) M. J. Harvey, T. P. Hanusa, M. Pink, *J. Chem. Soc., Dalton Trans.* **2001**, 1128-1130; b) S. Harder, C. Ruspic, *J. Organomet. Chem.* **2009**, *694*, 1180-1184.
- [42] S. Kheradmandan, H. W. Schmalle, H. Jacobsen, O. Blacque, T. Fox, H. Berke, M. Gross, S. Decurtins, *Chem. Eur. J.* **2002**, *8*, 2526-2533.
- [43] a) R. E. Dinnebier, M. Schneider, S. van Smaalen, F. Olbrich, U. Behrens, *Acta Cryst. Sect. B* **1999**, *55*, 35-44; b) C. Tedesco, R. E. Dinnebier, F. Olbrich, S. van Smaalen, *Acta Cryst. Sect. B* **2001**, *57*, 673-679; c) U. Behrens, R. E. Dinnebier, S. Neander, F. Olbrich, *Organometallics* **2008**, *27*, 5398-5400.
- [44] a) R. E. Dinnebier, S. Neander, U. Behrens, F. Olbrich, *Organometallics* **1999**, *18*, 2915-2918; b) C. Üffing, R. Köppe, H. Schnöckel, *Organometallics* **1998**, *17*, 3512-3515.
- [45] J.-L. Fauré, G. Erker, R. Fröhlich, K. Bergander, *Eur. J. Inorg. Chem.* **2000**, *2000*, 2603-2606.
- [46] a) P. Jutzi, E. Schlüter, C. Krüger, S. Pohl, *Angew. Chem.* **1983**, *95*, 1015-1016; b) P. Jutzi, E. Schlüter, C. Krüger, S. Pohl, *Angew. Chem. Int. Ed.* **1983**, *22*, 994-994; c) P. Jutzi, E. Schlüter, S. Pohl, W. Saak, *Chem. Ber.* **1985**, *118*, 1959-1967.
- [47] a) R. Michel, R. Herbst-Irmer, D. Stalke, *Organometallics* **2011**, *30*, 4379-4386; b) A. Hammel, W. Schwarz, J. Weidlein, *Acta Cryst. Sect. C* **1990**, *46*, 2337-2339; c) H. Chen, P. Jutzi, W. Leffers, M. M. Olmstead, P. P. Power, *Organometallics* **1991**, *10*, 1282-1286.
- [48] P. Jutzi, W. Leffers, S. Pohl, W. Saak, *Chem. Ber.* **1989**, *122*, 1449-1456.
- [49] F. Zaegel, J. C. Gallucci, P. Meunier, B. Gautheron, M. R. Sivik, L. A. Paquette, *J. Am. Chem. Soc.* **1994**, *116*, 6466-6467.
- [50] M. A. Edelman, P. B. Hitchcock, M. F. Lappert, D.-S. Liu, S. Tian, *J. Organomet. Chem.* **1998**, *550*, 397-408.
- [51] a) S. Harder, M. H. Prosenc, *Angew. Chem.* **1994**, *106*, 1830-1832; b) S. Harder, M. H. Prosenc, *Angew. Chem. Int. Ed.* **1994**, *33*, 1744-1746; c) W.-K. Wong, L. Zhang, W.-T. Wong, F. Xue, T. C. W. Mak, *Polyhedron* **1996**, *15*, 4593-4597; d) J. Wessel, E. Lork, R. Mews, *Angew. Chem.* **1995**, *107*, 2565-2567; e) J. Wessel, E. Lork, R. Mews, *Angew. Chem. Int. Ed.* **1995**, *34*, 2376-2378.
- [52] W. E. Rhine, G. D. Stucky, *J. Am. Chem. Soc.* **1975**, *97*, 737-743.

- [53] G. Boche, B. Ledig, M. Marsch, K. Harms, *Acta Cryst. Sect. E* **2001**, *57*, m570-m572.
- [54] M. Könemann, G. Erker, R. Fröhlich, E.-U. Würthwein, *J. Am. Chem. Soc.* **1997**, *119*, 11155-11164.
- [55] M. Håkansson, C.-H. Ottosson, A. Boman, D. Johnels, *Organometallics* **1998**, *17*, 1208-1214.
- [56] J. J. Brooks, W. Rhine, G. D. Stucky, *J. Am. Chem. Soc.* **1972**, *94*, 7339-7346.
- [57] F. Olbrich, *CSD Communication (Private Communication)* **2002**, CCDC 114095.
- [58] S. Neander, J. Körnich, F. Olbrich, *J. Organomet. Chem.* **2002**, *656*, 89-96.
- [59] a) S. Buchholz, K. Harms, M. Marsch, W. Massa, G. Boche, *Angew. Chem.* **1989**, *101*, 57-58; b) S. Buchholz, K. Harms, M. Marsch, W. Massa, G. Boche, *Angew. Chem. Int. Ed.* **1989**, *28*, 72-73.
- [60] M. Westerhausen, S. Schneiderbauer, N. Makropoulos, M. Warchhold, H. Nöth, H. Piotrowski, K. Karaghiosoff, *Organometallics* **2002**, *21*, 4335-4341.
- [61] G. R. Giesbrecht, J. C. Gordon, D. L. Clark, B. L. Scott, *J. Chem. Soc., Dalton Trans.* **2003**, 2658-2665.
- [62] A. Sekiguchi, Y. Sugai, K. Ebata, C. Kabuto, H. Sakurai, *J. Am. Chem. Soc.* **1993**, *115*, 1144-1146.
- [63] I. I. I. A. J. Arduengo, M. Tamm, J. C. Calabrese, F. Davidson, W. J. Marshall, *Chem. Lett.* **1999**, *28*, 1021-1022.
- [64] J. Bildmann Ulrich, M. Winkler, G. Müller Fachbereich, *Z. Naturforsch., B: Chem. Sci.* **2000**, *55*, 1005.
- [65] M. F. Lappert, A. Singh, L. M. Engelhardt, A. H. White, *J. Organomet. Chem.* **1984**, *262*, 271-278.
- [66] a) J. Paradies, G. Erker, R. Fröhlich, *Angew. Chem.* **2006**, *118*, 3150-3153; b) J. Paradies, G. Erker, R. Fröhlich, *Angew. Chem. Int. Ed.* **2006**, *45*, 3079-3082.
- [67] T. Nishinaga, D. Yamazaki, H. Stahr, A. Wakamiya, K. Komatsu, *J. Am. Chem. Soc.* **2003**, *125*, 7324-7335.
- [68] S. Burck, D. Gudat, M. Nieger, J. Tirree, *J. Chem. Soc., Dalton Trans.* **2007**, 1891-1897.
- [69] G. E. Herberich, A. Fischer, *Organometallics* **1996**, *15*, 58-67.
- [70] C. Dohmeier, E. Baum, A. Ecker, R. Köppe, H. Schnöckel, *Organometallics* **1996**, *15*, 4702-4706.
- [71] H. Wang, H. Wang, H.-W. Li, Z. Xie, *Organometallics* **2004**, *23*, 875-885.
- [72] G. E. Herberich, E. Barday, A. Fischer, *J. Organomet. Chem.* **1998**, *567*, 127-131.
- [73] J. N. Jones, A. H. Cowley, *Chem. Commun.* **2005**, 1300-1302.
- [74] H. Schumann, O. Stenzel, F. Girgsdies, R. L. Halterman, *Organometallics* **2001**, *20*, 1743-1751.

- [75] a) I. Hoppe, D. Hoppe, G. Boche, M. Marsch, K. Harms, *Angew. Chem.* **1995**, *107*, 2328-2330; b) I. Hoppe, M. Marsch, K. Harms, G. Boche, D. Hoppe, *Angew. Chem. Int. Ed.* **1995**, *34*, 2158-2160.
- [76] A. L. Spek, E. G. Ijpeji, G.-J. M. Gruter, *CSD Communication (Private Communication)* **2006**, CCDC 629601.
- [77] X. Pan, X. Wang, Y. Zhao, Y. Sui, X. Wang, *J. Am. Chem. Soc.* **2014**, *136*, 9834-9837.
- [78] a) R. Appel, E. Gaitzsch, F. Knoch, *Angew. Chem.* **1985**, *97*, 574-575; b) R. Appel, E. Gaitzsch, F. Knoch, *Angew. Chem. Int. Ed.* **1985**, *24*, 589-590.
- [79] E. Kirillov, L. Toupet, C. W. Lehmann, A. Razavi, J.-F. Carpentier, *Organometallics* **2003**, *22*, 4467-4479.
- [80] F. Feil, S. Harder, *Eur. J. Inorg. Chem.* **2003**, *2003*, 3401-3408.
- [81] X. Chen, X. Xue, L. Zhang, W.-H. Sun, *Inorg. Chem. Commun.* **2011**, *14*, 235-237.
- [82] M. L. Cole, C. Jones, P. C. Junk, *J. Chem. Soc., Dalton Trans.* **2002**, 896-905.
- [83] T. Kähler, F. Olbrich, *CSD Communication (Private Communication)* **2002**, CCDC 184336.
- [84] a) G. Rabe, H. W. Roesky, D. Stalke, F. Pauer, G. M. Sheldrick, *J. Organomet. Chem.* **1991**, *403*, 11-19; b) H. Bock, T. Hauck, C. Näther, Z. Havlas, *Z. Naturforsch., B: Chem. Sci.* **1997**, *52*, 524.
- [85] a) C. M. Widdifield, J. A. Tang, C. L. B. Macdonald, R. W. Schurko, *Magn. Reson. Chem.* **2007**, *45*, S116-S128; b) T. Aoyagi, H. M. M. Shearer, K. Wade, G. Whitehead, *J. Organomet. Chem.* **1979**, *175*, 21-31.
- [86] J. Z. Zhang Bin, Wang Yuling, Wei Gecheng, Chen Wenqi, *Chem. Res. Chinese U.* **1992**, *8*, 15-20.
- [87] T. Kähler, F. Olbrich, *CSD Communication (Private Communication)* **2002**, CCDC 185158.
- [88] a) S. Holl, H. Bock, K. Gharagozloo-Hubmann, *Acta Cryst. Sect. E* **2001**, *57*, m31-m32; b) H. Bock, T. Hauck, C. Näther, Z. Havlas, *Angew. Chem.* **1997**, *109*, 650-651; c) H. Bock, T. Hauck, C. Näther, Z. Havlas, *Angew. Chem. Int. Ed.* **1997**, *36*, 638-639.
- [89] S. Harder, M. H. Prosenec, U. Rief, *Organometallics* **1996**, *15*, 118-122.
- [90] F. Hung-Low, C. A. Bradley, *Inorg. Chem.* **2013**, *52*, 2446-2457.
- [91] a) H. Bock, A. John, C. Arad, C. Näther, Z. Havlas, *Angew. Chem.* **1994**, *106*, 931-934; b) H. Bock, C. Näther, Z. Havlas, A. John, C. Arad, *Angew. Chem. Int. Ed.* **1994**, *33*, 875-878; c) T. Kähler, F. Olbrich, *CSD Communication (Private Communication)* **2002**, CCDC 176072.
- [92] T. Kähler, U. Behrens, S. Neander, F. Olbrich, *J. Organomet. Chem.* **2002**, *649*, 50-54.
- [93] S. Corbelin, J. Kopf, E. Weiss, *Chem. Ber.* **1991**, *124*, 2417-2422.

- [94] C. Schade, P. von Ragué Schleyer, P. Gregory, H. Dietrich, W. Mahdi, *J. Organomet. Chem.* **1988**, *341*, 19-38.
- [95] J. C. Gallucci, O. Gobley, F. Zaegel, P. Meunier, B. Gautheron, H. Lange, R. Gleiter, N. Kozmina, L. A. Paquette, *Organometallics* **1998**, *17*, 111-113.
- [96] C. Nather, T. Hauck, H. Bock, *Acta Cryst. Sect. C* **1996**, *52*, 570-572.
- [97] C. M. Kotyk, M. R. MacDonald, J. W. Ziller, W. J. Evans, *Organometallics* **2015**, *34*, 2287-2295.
- [98] G. B. Deacon, F. Jaroschik, P. C. Junk, R. P. Kelly, *Organometallics* **2015**, *34*, 2369-2377.
- [99] a) S. Neander, F. E. Tio, R. Buschmann, U. Behrens, F. Olbrich, *J. Organomet. Chem.* **1999**, *582*, 58-65; b) C. B. Benda, M. Waibel, T. F. Fässler, *Angew. Chem.* **2015**, *127*, 373-373; c) C. B. Benda, M. Waibel, T. F. Fässler, *Angew. Chem. Int. Ed.* **2015**, *54*, 365-365; d) T. Kitagawa, K. Ogawa, K. Komatsu, *J. Am. Chem. Soc.* **2004**, *126*, 9930-9931; e) K. Ogawa, K. Komatsu, T. Kitagawa, *J. Org. Chem.* **2011**, *76*, 6095-6100; f) J. Lorberth, S.-H. Shin, S. Wocadlo, W. Massa, *Angew. Chem.* **1989**, *101*, 793-794; g) J. Lorberth, S.-H. Shin, S. Wocadlo, W. Massa, *Angew. Chem. Int. Ed.* **1989**, *28*, 735-736.
- [100] J. Paap, *Neuartige π -Organyle der schweren Alkalimetalle und des Magnesiums*, Doctoral Dissertation, Institut für Anorganische und Angewandte Chemie der Universität Hamburg, **2004**.
- [101] V. Jordan, U. Behrens, F. Olbrich, E. Weiss, *J. Organomet. Chem.* **1996**, *517*, 81-88.
- [102] K. Kunz, M. Bolte, H.-W. Lerner, M. Wagner, *Organometallics* **2009**, *28*, 3079-3087.
- [103] W. J. Evans, J. C. Brady, C. H. Fujimoto, D. G. Giarikos, J. W. Ziller, *J. Organomet. Chem.* **2002**, *649*, 252-257.
- [104] C. Kleeberg, *Z. Anorg. Allg. Chem.* **2011**, *637*, 1790-1794.
- [105] R. W. Seidel, C. Ganesamoorthy, S. Loerke, M. V. Winter, C. Gemel, R. A. Fischer, *Acta Cryst. Sect. C* **2013**, *69*, 573-576.
- [106] T. Yatabe, H. Nakai, K. Nozaki, T. Yamamura, K. Isobe, *Organometallics* **2010**, *29*, 2390-2393.
- [107] T. Yatabe, M. Karasawa, K. Isobe, S. Ogo, H. Nakai, *J. Chem. Soc., Dalton Trans.* **2012**, *41*, 354-356.
- [108] W. J. Evans, D. G. Giarikos, J. W. Ziller, *J. Organomet. Chem.* **2003**, *688*, 200-205.
- [109] H. Schumann, M. R. Keitsch, S. H. Mühle, *Z. Anorg. Allg. Chem.* **2002**, *628*, 1311-1318.
- [110] W. P. Schaefer, W. D. Cotter, J. E. Bercaw, *Acta Cryst. Sect. C* **1993**, *49*, 1489-1492.
- [111] P. Chadha, J. L. Dutton, P. J. Ragogna, *Can. J. Chem.* **2010**, *88*, 1213-1221.
- [112] F. Ortu, J. M. Fowler, M. Burton, A. Formanuk, D. P. Mills, *New J. Chem.* **2015**, *39*, 7633-7639.

- [113] A. Zaeni, *Synthese, Charakterisierung und Kristallstrukturuntersuchungen neuer Organometallverbindungen der Lanthanoide und der Alkalimetalle mit Fluoren und substituierten Fluorenylliganden*, Doctoral Dissertation, Fakultät für Verfahrens- und Systemtechnik der Otto-von-Guericke Universität Magdeburg **2004**.
- [114] C. Janiak, *Chem. Ber.* **1993**, *126*, 1603-1607.
- [115] U. Behrens, S. May, F. Olbrich, *Z. Kristallogr. - New Cryst. Struct.* **2007**, *222*, 307.
- [116] R. Zerger, W. Rhine, G. D. Stucky, *J. Am. Chem. Soc.* **1974**, *96*, 5441-5448.
- [117] B. Wilde, Diplomarbeit, Institut für Allgemeine und Anorganische Chemie der Universität Hamburg, **2002**.
- [118] B. Wilde, *Neuartige Organylverbindungen der Alkalimetalle*, Doctoral Dissertation, Institut für Anorganische und Angewandte Chemie der Universität Hamburg, **2007**.
- [119] a) S. Neander, U. Behrens, F. Olbrich, *J. Organomet. Chem.* **2000**, *604*, 59-67; b) S. Neander, *Synthese und Kristallstrukturuntersuchung von Organylen und Amiden der Alkalimetalle*, Doctoral Dissertation, Institut für Anorganische und Angewandte Chemie der Universität Hamburg, **1999**.
- [120] D. Hoffmann, F. Hampel, P. von Ragué Schleyer, *J. Organomet. Chem.* **1993**, *456*, 13-17.
- [121] U. Behrens, F. Olbrich, *CSD Communication (Private Communication)* **2008**, CCDC 687263.
- [122] W. Borchart-Ott, *Kristallographie: eine Einführung für Naturwissenschaftler*, 7 ed., Springer-Verlag, Berlin, **2008**.
- [123] G. R. Desiraju, *Crystal Engineering: The Design of Organic Solids*, Elsevier, Amsterdam, New York, **1989**.
- [124] a) G. R. Desiraju, *Angew. Chem.* **1995**, *107*, 2541-2558; b) G. R. Desiraju, *Angew. Chem. Int. Ed.* **1995**, *34*, 2311-2327; c) G. R. Desiraju, *Angew. Chem.* **2007**, *119*, 8492-8508; d) G. R. Desiraju, *Angew. Chem. Int. Ed.* **2007**, *46*, 8342-8356.
- [125] H. Li, M. Eddaoudi, M. O'Keeffe, O. M. Yaghi, *Nature* **1999**, *402*, 276-279.
- [126] K. E. Maly, E. Gagnon, T. Maris, J. D. Wuest, *J. Am. Chem. Soc.* **2007**, *129*, 4306-4322.
- [127] G. A. Jeffrey, *An Introduction to Hydrogen Bonding*, Oxford University Press, Oxford, **1997**.
- [128] a) T. Steiner, *Angew. Chem.* **2002**, *114*, 50-80; b) T. Steiner, *Angew. Chem. Int. Ed.* **2002**, *41*, 48-76.
- [129] S. S. Zumdahl, *Ammonia (NH₃)*, Encyclopædia Britannica Online, accessed 22.09.2016, <https://www.britannica.com/science/ammonia>.
- [130] a) H. Smil, *Enriching the Earth: Fritz Haber, Carl Bosch, and the Transformation of World Food Production.*, MIT Press, Cambridge, MA, **2004**; b) M. Appl, in

- Ullmann's Encyclopedia of Industrial Chemistry*, Wiley-VCH Verlag GmbH & Co. KGaA, **2000**.
- [131] *Ammoniak*, GESTIS-Stoffdatenbank, accessed 22.09.2016, [http://gestis.itrust.de/nxt/gateway.dll/gestis_de/001100.xml?f=templates\\$fn=default.htm\\$3.0](http://gestis.itrust.de/nxt/gateway.dll/gestis_de/001100.xml?f=templates$fn=default.htm$3.0).
- [132] M. K. Campbell, S. O. Farrel, *Biochemistry*, 7 ed., Cengage Learning, Boston, MA, **2007**.
- [133] *NIST Chemistry WebBook*, NIST - National Institute of Standards and Technology, accessed 22.06.2016, <http://webbook.nist.gov/chemistry/>.
- [134] W. M. Haynes, *CRC Handbook of Chemistry and Physics*, 96 ed., CRC Press/Taylor and Francis, Boca Raton, FL., **2016**.
- [135] A. F. Holleman, N. Wiberg, *Lehrbuch der Anorganischen Chemie*, 102 ed., de Gruyter, Berlin, Boston, **2008**.
- [136] F. G. Bordwell, *Acc. Chem. Res.* **1988**, *21*, 456-463.
- [137] M. B. Smith, J. March, *March's Advanced Organic Chemistry: Reactions, Mechanisms, and Structure*, 7 ed., John Wiley & Sons, Hoboken, NJ, **2013**.
- [138] *Ammoniak*, Linde AG, accessed 23-09.2016, http://www.linde-gas.de/de/products_and_supply/gase_a_x/gase.html.
- [139] National Center for Biotechnology Information. PubChem Compound Database, accessed 23.09.2016, <https://pubchem.ncbi.nlm.nih.gov/compound/222>.
- [140] P. G. T. Fogg, W. Gerrard, *Solubility of Gases and Liquids*, John Wiley & Sons, Inc., New York, **1991**.
- [141] R. den Besten, S. Harder, L. Brandsma, *J. Organomet. Chem.* **1990**, *385*, 153-159.
- [142] a) D. Stalke, *Angew. Chem.* **1994**, *106*, 2256-2259; b) D. Stalke, *Angew. Chem. Int. Ed.* **1994**, *33*, 2168-2171; c) P. Jutzi, N. Burford, *Chem. Rev.* **1999**, *99*, 969-990.
- [143] R. Michel, R. Herbst-Irmer, D. Stalke, *Organometallics* **2010**, *29*, 6169-6171.
- [144] M. M. Al-Ktaifani, P. B. Hitchcock, J. F. Nixon, *J. Organomet. Chem.* **2008**, *693*, 611-618.
- [145] a) H. Frumkin, G. Solomon, *Am. J. Ind. Med.* **1997**, *31*, 107-115; b) P. L. Pauson, in *Encyclopedia of Reagents for Organic Synthesis*, 2 ed., John Wiley & Sons, Ltd, Hoboken, NJ, **2001**; c) D. Seyferth, *Organometallics* **2003**, *22*, 2-20.
- [146] a) J. Hey, D. M. Andrada, R. Michel, R. A. Mata, D. Stalke, *Angew. Chem.* **2013**, *125*, 10555-10559; b) J. Hey, D. M. Andrada, R. Michel, R. A. Mata, D. Stalke, *Angew. Chem. Int. Ed.* **2013**, *52*, 10365-10369.
- [147] A. Madsen, *J. Appl. Crystallogr.* **2006**, *39*, 757-758.
- [148] C. Gatti, P. Macchi, *Modern Charge-Density Analysis*, 1 ed., Springer Netherlands, Dordrecht, **2012**.
- [149] C. Gatti, F. Cargnoni, L. Bertini, *J. Comput. Chem.* **2003**, *24*, 422-436.
- [150] T. Wagner, A. Schonleber, *Acta Cryst. Sect. B* **2009**, *65*, 249-268.

-
- [151] G. Sheldrick, *Acta Cryst. Sect. A* **2008**, *64*, 112-122.
- [152] a) R. Michel, T. Nack, R. Neufeld, J. M. Dieterich, R. A. Mata, D. Stalke, *Angew. Chem.* **2013**, *125*, 762-766; b) R. Michel, T. Nack, R. Neufeld, J. M. Dieterich, R. A. Mata, D. Stalke, *Angew. Chem. Int. Ed.* **2013**, *52*, 734-738.
- [153] V. Petříček, M. Dušek, L. Palatinus, in *Z. Kristallogr., Vol. 229*, **2014**, p. 345.
- [154] G. Sheldrick, *Acta Cryst. Sect. A* **2015**, *71*, 3-8.
- [155] R. Michel, *Cyclopentadienyllithium - Vom Ammoniakat zum Lithocen*, Diploma Thesis, Institut für Anorganische Chemie der Georg-August-Universität Göttingen, **2010**.
- [156] S. Harder, M. H. Prosenc, *Angew. Chem.* **1996**, *108*, 101-103.
- [157] C. M. Davis, K. A. Curran, *J. Chem. Educ.* **2007**, *84*, 1822.
- [158] S. Neander, U. Behrens, *Z. Anorg. Allg. Chem.* **1999**, *625*, 1429-1434.
- [159] a) T. Kottke, D. Stalke, *J. Appl. Crystallogr.* **1993**, *26*, 615-619; b) T. Kottke, R. J. Lagow, D. Stalke, *J. Appl. Crystallogr.* **1996**, *29*, 465-468; c) D. Stalke, *Chem. Soc. Rev.* **1998**, *27*, 171-178.
- [160] Bruker-AXS, **2011**, *COSMO*, Madison, Wisconsin, USA.
- [161] Bruker-AXS, **2014**, *APEX2*, Version 2014. 11-0, Madison, Wisconsin, USA.
- [162] L. Krause, R. Herbst-Irmer, G. M. Sheldrick, D. Stalke, *J. Appl. Crystallogr.* **2015**, *48*, 3-10.
- [163] G. M. Sheldrick, **2012**, *TWINABS*, Version 2012/1, Georg-August-Universität Göttingen, Göttingen.
- [164] G. M. Sheldrick, **2013**, *XPREP*, Version 2013/1, Madison, Wisconsin, USA.
- [165] G. Sheldrick, *Acta Cryst. Sect. C* **2015**, *71*, 3-8.
- [166] C. B. Hübschle, G. M. Sheldrick, B. Dittrich, *J. Appl. Crystallogr.* **2011**, *44*, 1281-1284.
- [167] P. Müller, *Crystallogr. Rev.* **2009**, *15*, 57-83.
- [168] A. L. Spek, **1980-2014**, *PLATON*, Version 191114, Utrecht University, Utrecht, Netherlands.
- [169] P. Müller, R. Herbst-Irmer, A. L. Spek, T. R. Schneider, M. R. Sawaya, *Crystal Structure Refinement - A Crystallographer's Guide to SHELXL*, Oxford University Press, Oxford, New York, **2006**.

Danksagung

Zuallerst danke ich meinem Doktorvater Prof. Dr. Dietmar Stalke für die Möglichkeit, auf einem neuen und herausfordernden Feld arbeiten zu können. Ich weiß ihr Vertrauen in mich sehr zu schätzen. Die Zeit im Arbeitskreis und auf Reisen haben mich um viele Erfahrungen und schöne Erinnerungen bereichert.

Bei Herrn Prof. Dr. Oliver Wenger bedanke ich mich für die freundliche Betreuung.

Bei Herrn Prof. Dr. Franc Meyer bedanke ich mich für die Übernahme des Korreferats.

Mein Dank gilt den weiteren Mitgliedern des Prüfungskomitees Dr. Heidrun Sowa, Prof. Dr. Thomas Waitz, Prof. Dr. Manuel Alcarazo und Prof. Dr. Konrad Koszinowski.

Großer Dank gebührt dem *Center for Materials Crystallography (CMC)* für die großzügige finanzielle Unterstützung in der Zeit meiner Promotion.

Dr. Regine Herbst-Irmer danke ich für die großartige und lehrreiche Unterstützung bei den unzähligen kristallographischen Problemen. Von den handgeschriebenen rosa Zetteln habe ich mehr über Kristallographie gelernt als aus allen Büchern.

Prof. Dr. Ricardo Mata und Dr. Johannes Dieterich danke ich für die umfangreichen theoretischen Rechnungen und die engagierte Mitarbeit an den Manuskripten. Meinen Kooperationspartnern danke ich für die vielen interessanten kristallographischen Probleme und die wertvollen Publikationserfahrungen.

Ich danke meinen Laborpraktikanten und Bachelorstudenten für ihre großartige Arbeit, die schöne Zeit miteinander und die wertvollen Erfahrungen in der Betreuung.

Meinem Arbeitskreis danke ich für die schöne gemeinsame Zeit, die entspannte freundschaftliche Atmosphäre und produktive Zusammenarbeit. Daniel Kratzert danke ich für die große Hilfe bei dem Videoprojekt. Bei Nils Finkelmeier und Conrad Weichbrodt bedanke ich mich für die schönen Samstagnachmittage (oft mit Verlängerung). Daniel Stern danke ich für die Einführung in den Arbeitskreis. Peter Stollberg möchte ich danken für die Hilfe mit den endlosen Nicklichkeiten am Ende der Arbeit. Mein größter Dank gilt Felix Engelhardt für die nimmermüde Hilfe bei Computerproblemen und bei der Korrektur meiner Arbeit.

Meinen Freunden Ulrich Reinders, Kord Ellermann, Adam Walli, Clara Landgraf, Jakob Hey, Eva Hey, Stefan Jackenkroll, Arne Wolpers und Bastian Ebeling danke ich für die schöne gemeinsame Zeit in Göttingen und die gegenseitige Unterstützung. Besonderer Dank gilt dabei Arne und Bastian für die großartige Hilfe bei der Korrektur.

Meiner Familie danke ich für die großartige Unterstützung, Liebe und Geduld.

Mein größter Dank gilt meiner Freundin Fei Luo. Danke für deine Liebe, dein Vertrauen, deine Hilfe in schwierigen Zeiten und deine positive Energie.

Curriculum vitae

Name: Reent Michel
Date of birth: 06.10.1982 in Wilhelmshaven
Nationality: German
Address: Zollweg 17, 26316 Zetel/Neuenburg
E-mail: reent.michel@gmail.com

Scientific career

- 04.2010 – 01.2017 Ph.D studies in the Gauss doctoral programme at the Georg August University Göttingen. Work on the doctoral thesis "Ammonia stabilized Carbanions" in the *Stalke* workgroup.
- 08.2009 – 03.2010 Work on the synthetic chemical graduation thesis "*Cyclopentadienyllithium – Vom Ammoniakat zum Lithocen*" in Prof. Dr. D. *Stalke's* workgroup at the Georg August University Göttingen.
- 04.2007 – 08.2007 Erasmus exchange to the Institute of Organic Chemistry at the University of Florence, workgroup Prof. Dr. Stefano Cicchi.
- 10.2003 – 03.2010 Chemistry studies at the Georg August University Göttingen.
- 06.2002 Abitur at *Lothar Meyer Gymnasium*, Varel.

Professional career

- 04.2006 – 2013 Scientific assistant (teaching): *Chemistry for students of medicine; Chemistry for students of biology; Advanced inorganic synthesis lab course; Lab course in catalytic chemistry; Modern methods in Inorganic Chemistry; Introduction to catalytic chemistry.*
- 09.2002 – 07.2003 Substitution service (*Zivildienst*) at the *Kinderhaus Collstede*, Zetel/Neuenburg.

Scientific Publications in Print

Thorben Schulte, Julian Holstein, Lennard Krause, Reent Michel, Dietmar Stalke, Eri Sakuda, Keisuke Umakoshi, Giovanna Longhi, Sergio Abbate, Guido Clever "A Chiral-at-Metal Phosphorescent Square-Planar Pt(II) Complex with Remarkable Chiroptical Properties" **2016**, submitted.

Roman Neufeld, Reent Michel, Regine Herbst-Irmer, Ralf Schöne, Dietmar Stalke "Introducing a Hydrogen Bond Donor into a Non Nucleophilic Brønsted Base: Alkali Metal Hexamethyldisilazide (HMDS, metal = Li, Na, K, Rb and Cs) with Ammonia" *Chemistry, A European Journal* **2016**, 22, 12340-12346.

Antonio Salomone, Filippo M. Perna, Aurelia Falcicchio, Sten O. Nilsson Lill, Anna Moliterni, Reent Michel, Saverio Florio, Dietmar Stalke, Vito Capriati "Direct Observation of a Lithiated Oxirane: A Synergistic Study Using Spectroscopic, Crystallographic, and Theoretical Methods on the Structure and Stereodynamics of Lithiated ortho-Trifluoromethyl Styrene Oxide", *Chemical Science* **2014**, 5, 528-538.

Reent Michel, Tobias Nack, Roman Neufeld, Johannes M. Dieterich, Ricardo A. Mata, Dietmar Stalke „Layered structure of $[Na(NH_3)_4][Ind]$, $Ind = C_9H_7$, containing a unprecedented square planar $Na(NH_3)_4^+$ cation", *Angewandte Chemie* **2013**, 125, 762-766; *Angewandte Chemie, International Edition* **2013**, 52, 734-738.

Muxin Han, Reent Michel, Bice He, Yu-Sheng Chen, Dietmar Stalke, Michael John, Guido H. Clever „Light-Triggered Guest Uptake and Release by a Photochromic Coordination Cage", *Angewandte Chemie* **2013**, 125, 1358-1362; *Angewandte Chemie, International Edition* **2013**, 52, 1319-1323.

Karthik V. Raman, Alexander M. Kamerbeek, Nicolae Atodiresei, Arup Mukherjee, Tamal K. Sen, Predrag Lazic, Vasile Caciuc, Reent Michel, Dietmar Stalke, Swadhin K. Mandal, Stefan Blügel, Markus Münzenberg, Jagadeesh S. Moodera „Interface-engineered templates for molecular spin memory devices", *Nature* **2013**, 493, 509-513.

Sabrina Freye, Reent Michel, Dietmar Stalke, Martin Pawliczek, Holm Frauendorf, Guido H. Clever „Template Control over Dimerization and Guest Selectivity of Interpenetrated Coordination Cages", *Journal of the American Chemical Society* **2013**, 135, 8476-8479.

Jakob Hey, Diego Andrada, Reent Michel, Ricardo A. Mata, Dietmar Stalke „Strong intermolecular interactions shaping a small piano stool complex", *Angewandte Chemie* **2013**, 125, 10555-10559; *Angewandte Chemie, International Edition* **2013**, 52, 10365-10369.

Shabana Khan, Prinson P. Samuel, Reent Michel, Johannes M. Dieterich, Ricardo A. Mata, Jean-Philippe Demers, Adam Lange, Herbert W. Roesky, Dietmar Stalke "Monomeric Sn(II) and Ge(II) hydrides supported by a tridentate pincer-based ligand", *Chemical Communications* **2012**, 48, 4890-4892.

Shabana Khan, Sakya S. Sen, Reent Michel, Daniel Kratzert, Herbert W. Roesky, Dietmar Stalke "Formation of a Unsymmetrical Complex via C-H Bond Activation of Diazobenzene by Stable N-Heterocyclic Chlorosilylene ($PhC(NtBu)_2SiCl$)", *Organometallics* **2011**, 30, 2643-2645.

Reent Michel, Regine Herbst-Irmer, Dietmar Stalke "Revealing coordination patterns in C_5 -cyclic lithiumorganics", *Organometallics* **2011**, 30, 4379-4386.

Shabana Khan, Reent Michel, Debasis Koley, Herbert W. Roesky, Dietmar Stalke "Reactivity Studies of a Disilene with N_2O and Elemental Sulfur", *Inorganic Chemistry* **2011**, *50*, 10878-10883.

Shabana Khan, Reent Michel, Johannes M. Dieterich, Ricardo A. Mata, Herbert W. Roesky, Jean-Philippe Demers, Adam Lange, Dietmar Stalke "Preparation of $R\text{Sn}(I)\text{-Sn}(I)R$ with Two Unsymmetrically Coordinated $\text{Sn}(I)$ Atoms and Subsequent Opening of the P_4 Tetrahedron", *Journal of the American Chemical Society* **2011**, *133*, 17889-17894.

Shabana Khan, Reent Michel, Sakya S. Sen, Herbert W. Roesky, Dietmar Stalke "A P_4 Chain and Cage from Silylene-Activated White Phosphorus", *Angewandte Chemie* **2011**, *123*, 11900-11993; *Angewandte Chemie, International Edition* **2011**, *50*, 11786-11789.

Shabana Khan, Sakya S. Sen, Herbert W. Roesky, Daniel Kratzert, Reent Michel, and Dietmar Stalke "One Pot Synthesis of Disilatricycloheptene Analogue and Jutzi's Disilene", *Inorganic Chemistry* **2010**, *49*, 9689-9693.

Reent Michel, Regine Herbst-Irmer, Dietmar Stalke "Unprecedented CpLi Ammoniacates ", *Organometallics (Communication)* **2010**, *29*, 6169-6171.

Presentations

Center for Materials Crystallography (CMC), Annual Meeting 2013, Arhus, Denmark; Oral Presentation.

Center for Materials Crystallography (CMC), 6th Workshop 2012, Göttingen; Oral Presentation.

Center for Materials Crystallography (CMC), 3th Workshop 2011, Arhus, Denmark; Oral Presentation.

27th European Crystallographic Meeting, Bergen, Norway 2012; Poster Presentation.

GDCh-Wissenschaftsforum Chemie 2011, Bremen; Poster Presentation.

1th Symposium on Industrial Organometallic Chemistry (SIOC) 2012, Goslar; Poster Presentation.